BOND PERFORMANCE BETWEEN PRECAST UHPC SUBSTRATES AND FIELD-CAST UHPC CONNECTIONS

Project No. BEC96

Final Report

Kingsley Lau
(Project initiated by David Garber)

Florida International University
10555 W. Flagler St.
Miami, FL 33174
Phone: 305) 348-6124
Email: kilau@fiu.edu

Project Manager
Christina Freeman
Olga Iatsko

Florida Department of Transportation
M.H. Ansley Structures Research Center
2007 E. Paul Dirac Dr.
Tallahassee FL 32310

June 2026

DISCLAIMER

The opinions, findings, and conclusions expressed in this publication are those of the authors and not necessarily those of the Florida Department of Transportation.

APPROXIMATE CONVERSIONS TO SI UNITS

SYMBOL	WHEN YOU KNOW	MULTIPLY BY	TO FIND	SYMBOL
LENGTH				
in	inches	25.4	millimeters	mm
mils	mils	25.4	micrometers	µm
ft	feet	0.305	meters	m
yd	yards	0.914	meters	m
mi	miles	1.61	kilometers	km

SYMBOL	WHEN YOU KNOW	MULTIPLY BY	TO FIND	SYMBOL
AREA				
in^2	square inches	645.2	square millimeters	mm^2
ft^2	square feet	0.093	square meters	m^2
yd^2	square yard	0.836	square meters	m^2
ac	acres	0.405	hectares	ha
mi^2	square miles	2.59	square kilometers	km^2

SYMBOL	WHEN YOU KNOW	MULTIPLY BY	TO FIND	SYMBOL
VOLUME				
fl oz	fluid ounces	29.57	milliliters	mL
gal	gallons	3.785	liters	L
ft^3	cubic feet	0.028	cubic meters	m^3
yd^3	cubic yards	0.765	cubic meters	m^3
NOTE: volumes greater than 1000 L shall be shown in m^3				

SYMBOL	WHEN YOU KNOW	MULTIPLY BY	TO FIND	SYMBOL
MASS				
oz	ounces	28.35	grams	g
lb	pounds	0.454	kilograms	kg
T	short tons (2000 lb)	0.907	megagrams (or "metric ton")	Mg (or "t")

SYMBOL	WHEN YOU KNOW	MULTIPLY BY	TO FIND	SYMBOL
TEMPERATURE (exact degrees)				
ºF	Fahrenheit	5 (F-32)/9 or (F-32)/1.8	Celsius	ºC
SYMBOL	**WHEN YOU KNOW**	**MULTIPLY BY**	**TO FIND**	**SYMBOL**
ILLUMINATION				
fc	foot-candles	10.76	lux	lx
fl	foot-Lamberts	3.426	candela/m^2	cd/m^2

SYMBOL	WHEN YOU KNOW	MULTIPLY BY	TO FIND	SYMBOL
FORCE and PRESSURE or STRESS				
lbf	poundforce	4.45	newtons	N
lbf/in^2	poundforce per square inch	6.89	kilopascals	kPa

APPROXIMATE CONVERSIONS TO CUSTOMARY UNITS

SYMBOL	WHEN YOU KNOW	MULTIPLY BY	TO FIND	SYMBOL
LENGTH				
mm	millimeters	0.039	inches	in
µm	micrometers	0.039	mils	mils
m	meters	3.28	feet	ft
m	meters	1.09	yards	yd
km	kilometers	0.621	miles	mi

SYMBOL	WHEN YOU KNOW	MULTIPLY BY	TO FIND	SYMBOL
AREA				
mm^2	square millimeters	0.0016	square inches	in^2
m^2	square meters	10.764	square feet	ft^2
m^2	square meters	1.195	square yards	yd^2
ha	hectares	2.47	acres	ac
km^2	square kilometers	0.386	square miles	mi^2

SYMBOL	WHEN YOU KNOW	MULTIPLY BY	TO FIND	SYMBOL
VOLUME				
mL	milliliters	0.034	fluid ounces	fl oz
L	liters	0.264	gallons	gal
m^3	cubic meters	35.314	cubic feet	ft^3
m^3	cubic meters	1.307	cubic yards	yd^3

SYMBOL	WHEN YOU KNOW	MULTIPLY BY	TO FIND	SYMBOL
MASS				
g	grams	0.035	ounces	oz
kg	kilograms	2.202	pounds	lb
Mg (or "t")	megagrams (or "metric ton")	1.103	short tons (2000 lb)	T

SYMBOL	WHEN YOU KNOW	MULTIPLY BY	TO FIND	SYMBOL
TEMPERATURE (exact degrees)				
°C	Celsius	1.8C+32	Fahrenheit	°F

SYMBOL	WHEN YOU KNOW	MULTIPLY BY	TO FIND	SYMBOL
ILLUMINATION				
lx	lux	0.0929	foot-candles	fc
cd/m^2	$candela/m^2$	0.2919	foot-Lamberts	fl

SYMBOL	WHEN YOU KNOW	MULTIPLY BY	TO FIND	SYMBOL
FORCE and PRESSURE or STRESS				
N	newtons	0.225	poundforce	lbf
kPa	kilopascals	0.145	poundforce per square inch	lbf/in^2

TECHNICAL REPORT DOCUMENTATION PAGE

1. Report No.	2. Government Accession No.	3. Recipient's Catalog No.

4. Title and Subtitle	5. Report Date
Bond Performance Between Precast UHPC Substrates and Field-Cast UHPC Connections	June 2026
	6. Performing Organization Code
7. Author(s) Kingsley Lau, Samanbar Permeh, and David Garber	8. Performing Organization Report No.
9. Performing Organization Name and Address Florida International University 10555 W. Flagler St. Miami, FL 33174	10. Work Unit No. (TRAIS) 11. Contract or Grant No. BEC96
12. Sponsoring Agency Name and Address Florida Department of Transportation 605 Suwannee St. MS 30 Tallahassee, FL 32399	13. Type of Report and Period Covered: Draft Final Report February 2022 – June 2026 14. Sponsoring Agency Code

15. Supplementary Notes

16. Abstract

Ultra-high performance concrete (UHPC) has been used in different applications and was explored to be used for precast elements; however, there was limited research and guidance on the connection between UHPC elements. General test methods to evaluate interface strength (e.g., direct tension pulloff, shear pushoff) can be used with the Mohr-Coulomb Friction Approach to determine the cohesion coefficient and coefficient of friction typically used to estimate interface shear strength. The test program here sought to explore the bond behavior of matchcast UHPC with various interface surface conditions, such as surface roughness (including smooth faces cast on plywood formwork, roughened surfaces created by casting on form liners) and exposed steel fibers at the interface (created by the use of paste retarders) in order to inform design provisions for matchcast UHPC. The effect of pre-corroded steel fibers and the surface wetting conditions were considered as well. Trends in interface shear behavior associated with surface conditions were identified. The most evident outcome from testing was that the presence of exposed steel fibers provided improved performance relative to only roughened surfaces. Roughened interfaces can improve the friction of the interface, but the presence of the exposed fibers improved both cohesive strength and provided improvement to the post-crack tensile strength. Additionally, there was improved cohesive bonding when prolonged wetting by burlap was made. Extended term ponding had reduced performance. Cohesion coefficient and friction factors for the various test conditions were assessed. Modification to interface shear strength provisions to include the effect of wetting conditions on cohesion was presented. The experimental work provided practical experiences that were translated into considerations for construction.

17. Key Word	18. Distribution Statement
UHPC, Interface Shear, Match, Cast, Fibers, Corrosion, Wetting, Bond	

19. Security Classif. (of this report)	20. Security Classif. (of this page)	21. No. of Pages	22. Price
unclassified	unclassified	170	

ACKNOWLEDGEMENTS

The work and assistance provided by the wonderful staff at the FDOT Ansley Structures Research Center (SRC) as well as the FDOT State Materials Office (SMO) is acknowledged and graciously recognized. Special thanks are given to Christina Freeman, Olga Iatsko, Steve Eudy, Mike Waters, Paul Tighe, Wade Johnson, Chris Schild, Clark Conyers, Miguel Ramirez and Ben Allen for which the completion of the research would not have been possible. Thanks are given to Richard DeLorenzo from SMO for support for flexural bond testing. Thanks to Mahyar Ramezani and Jayaramachandrasekhar Chandrasekhar Samudrala for assistance with direct tension, and Samanbar Permeh for corrosion testing and data curation.

EXECUTIVE SUMMARY

Ultra-high performance concrete (UHPC) has been used in different applications and was explored to be used for precast elements; however, there was limited research and guidance on the connection between UHPC elements. General test methods to evaluate interface strength based on the type of test were considered. Interface shear will often control the behavior of these joints. Standard test methods (e.g., direct tension pulloff, shear pushoff) can be used with the Mohr-Coulomb Friction Approach to determine the cohesion coefficient and coefficient of friction typically used to estimate interface shear strength. The test program here sought to explore the bond behavior of matchcast UHPC with various interface surface conditions, such as surface roughness (including smooth faces cast on plywood formwork, roughened surfaces created by casting on form liners) and exposed steel fibers at the interface (created by the use of paste retarders) in order to inform design provisions for matchcast UHPC. The effect of pre-corroded steel fibers and the surface wetting conditions were considered as well. In general, surface roughness would create a coarse anchor profile to facilitate better cohesive bond and provide greater friction that would facilitate interface shear strength. Surface moisture on the interface surface prior to casting would ideally facilitate cohesive bonding as the cementitious materials hydrate on the surface. The presence of exposed steel fibers ideally would also elevate interface shear capacity by increasing the post-crack tensile strength. The stochastic nature of concrete material testing creates undue variability. Adverse effects relating to air and moisture transport can create weak material on concrete surfaces that would affect interface bond but that would not necessarily affect bulk material behavior. Nevertheless, trends in interface shear behavior associated with surface conditions were identified.

The most evident outcome from testing was that the presence of exposed steel fibers provided improved performance relative to only roughened surfaces. Roughened interfaces can improve the friction of the interface, but the presence of the exposed fibers improved both cohesive strength and provided improvement to the post-crack tensile strength. The improved cohesion was thought related to local anchoring of hydrated cementitious materials onto fiber surfaces. The improvement to post-cracking behavior was consistent with expectations for fiber engagement creating additional clamping pressure. Even though the exposed fiber indicated elevated performance, pre-corroded fibers would negate those advantages. Additionally, there was improved cohesive bonding when prolonged wetting by burlap was made. Interestingly, long term ponding (shortly after demolding until casting) had reduced performance. It was thought that early prolonged and excessive interaction with water, although facilitating hydration) create heterogenous materials (ie differential strength, permeability, pore water content) at the interface that would affect how UHPC bonds to the substrate. Differential behavior due to different age substrate and matchcast were not clearly identified. Cohesion coefficient and friction factors for the various test conditions were assessed. Modification to interface shear strength provisions to include the effect of wetting conditions on cohesion as well as incorporating concepts to include the exposed fiber content on the post-crack clamping pressure was presented. The modified provision also provides a means to consider how exposed fibers can influence cohesion. Factors to incorporate the negative effect of corroded fibers were also introduced. The experimental work provided practical experiences that were translated into considerations for construction.

TABLE OF CONTENTS

LIST OF FIGURES

LIST OF TABLES

LIST OF PHOTOS

1. INTRODUCTION

Ultra-high performance concrete (UHPC) has been used in different applications for the past few decades. UHPC has been most widely used as a connection material between precast concrete components, as it allows for narrower joint widths, shorter development lengths, limited field-placed reinforcement (depending on application), good bond with conventional concrete precast elements, a more durable structure (due to the increased durability of UHPC), and accelerated construction.

As engineers, owners, and contractors are becoming more comfortable with UHPC, they are looking at using it for other applications. Another application is using UHPC to construct precast structural elements. One of the limiting factors for the use of UHPC for precast structural elements is the connection between these elements. The joints between precast elements are often constructed using UHPC. There are commonly accepted construction methods for achieving a satisfactory bond between conventional concrete precast members and the UHPC joint material. However, there has been limited research on the bond between a UHPC precast member and UHPC joint material. There is also a documented case of cracking at a similar UHPC-to-UHPC interface in the field [1]

This report summarizes literature related to UHPC, non-proprietary UHPC, interface and bond strength, quantifying surface roughness, and UHPC durability and corrosion resistance.

1.1 Ultra-High Performance Concrete (UHPC)

Ultra-high performance concrete (UHPC) is a cementitious composite material with high compressive strength, stiffness, and tensile strength and sustained post-cracking tensile strength and strain hardening response. Steel fibers are typically included in the mixture to provide the required post-cracking response. Pre-bagged commercial (or proprietary) UHPC products and non-proprietary UHPC mixtures are both available to achieve the necessary properties for various applications.

Some of the typical material properties for UHPC are summarized in Table 1.1.

Table 1.1. Typical range of mechanical properties for UHPC, from Graybeal [2], Shahrokhinasab and Garber [3] and Shahrokhinasab et al. [4]

Property	**Typical Range**
7-day Compressive Strength	14.5 to 19.5 ksi
14-day Compressive Strength	18 to 22 ksi
Direct Tensile Cracking Strength	0.8 to 1.2 ksi
Direct Tension Bond Test	0.35 to 0.6 ksi
Modulus of Elasticity	4,250 to 8,000 ksi
Long-term Drying Shrinkage	300 to 1,200 με
Long-term Autogenous Shrinkage	200 to 900 με
Initial setting time	4 to 10 hours
Final setting time	7 to 24 hours
Static flow	7.5 to 10 inches

Some additional definitions of UHPC are summarized in Table 1.2. The minimum compressive strength, tensile strength, and method for measuring tensile strength vary based on the organization or document providing the definition.

Table 1.2. Minimum definitions of UHPC, modified from Shahrokhinasab and Garber [3], and Tadros [5]

Document	**Ref.**	**Country**	**Min. f'_c (ksi)**	**Min. Tensile Strength (ksi)-**	**Other Criteria**
ACI 239R-18	[6]	USA	22.0	--	--
AFNOR NF P 18-470	[7]	France	18.8	0.87 (first crack, f_t)	Durability, ductility, and fire resistance
ASTM C1856-17	[8]	USA	17.0	--	--
CSA A23.1	[9]	Canada	17.4	0.58 (first crack, f_t)	Durability and ductility
FHWA	[10]	USA	21.7	0.72 (post crack, f_t)	Water to binder (w/b) ≤ 0.25
PCI	[5]	USA	18.0	1.50 (first crack, f_r), 2.00 (peak, f_r)	Durability and ductility
SIA 2052	[11]	Switz.	17.4	1.00 (first crack, f_t)	Ductility

An additional general requirement for UHPC is to keep the water-to-binder ratio (w/b) of UHPC less than 0.24 [3]. This low w/b leads to the desired mechanical properties. Additionally, dense particle packing of fine particles and low matrix porosity result in high durability of UHPC compared to conventional concretes. The high dosage of superplasticizer or high-range water-reducing admixture (HRWR) allows UHPC to flow by its weight and behave like a self-consolidating concrete even with low w/b.

1.1.1 UHPC Constituent Materials

The primary constituent materials in UHPC include cement, silica fume, additional supplementary cementitious materials (like fly ash, silica powder and slag), and fine aggregates. The proportions of these constituent materials depend on several factors including size, source, and reactive properties. Steel fibers are also typically included in UHPC usually between 1 and 6 percent by volume; steel fibers provide the post-cracking tensile behavior of the UHPC. The liquid component of UHPC mixtures includes water and superplasticizers or HRWRs. These are responsible for the hydration of cement and providing the flowability of the concrete. Other chemical admixtures like viscosity modifier admixture (VMA) can be also used if needed to stabilize heavier fibers [4]. A brief summary of each constituent material is provided in the following sections.

***Aggregate*:** UHPC mixtures can be made with a wide range of fine aggregate sizes and usually do not contain any coarse aggregate in their matrix. Although aggregates with an average size of 0.4 inches also are used for producing the UHPC mixtures, most successful mix designs are made using aggregate with a maximum size of 0.25 inches [12]. Many studies have shown a benefit when using multiple aggregate sizes by combining two different fine aggregates, which increases the density and improves the mechanical properties of UHPC mixture [13]-[17].

In addition to the average size of the aggregates, the source of particles and their shape also play an important role in the mechanical properties of UHPC. For low w/b concrete mixtures like UHPC, natural or rounded aggregates are generally more effective. These aggregates have lower water absorption and provide a better flow of concrete compared to angular, flaky, elongated and broken aggregates produced from natural stones. The effect of the shape of aggregate used in UHPC mixtures is a topic that could use further investigation.

Aggregates with different sources have been used for developing UHPC mixtures. The source of the aggregate affects its mechanical properties, which impacts the final properties of UHPC. Limestone is the most frequently reported source of aggregates used for producing non-proprietary UHPC mixtures. There have been some studies that used quartz particles produced from quartzite stone for developing UHPC mixtures; most of these studies were able to achieve more than 20 ksi compressive strength at 28 days. This is likely due to the higher stiffness and strength of quartz particles compared to limestone particles [18]-[21]

***Cement*:** Different cement types can be used in UHPC mixtures. One recommendation from previous literature related to general cement properties is to use cement with a maximum C_3A content of 8 percent and a blain fineness of less than 281228 in^2/lb; this has been shown to help minimize the workability challenges, including reducing heat generation and improving flow [22]. Past studies have used different types of cement successfully (Type I-White, Type III, and Type V), but Type I/II cement is the most frequently used because of cost and performance [16], [19], [22], [24]. It also has been reported that cement with high air content (e.g., masonry cement) cannot be used for UHPC, as it leads to the low compressive strength of around 11 ksi at 28 days [3].

Silica Fume**:** Silica fume is another recognized component of UHPC mixtures that plays an important role in filling the gaps between coarse particles and their pozzolanic reaction in the hydration process. Typical UHPC mixtures contain silica fume between 10 to 20 percent of cement weight [12]. Silica powder has been used instead of silica fume as well. Due to the higher water demand for silica powder and initially higher cost compared to silica fume, silica powder was not recommended for UHPC mixtures [25].

Other Supplemental Cementitious Materials**:** There have been several studies using different supplementary cementitious materials (SCMs) for developing UHPC mixtures. These additional materials were initially used to make concrete more economical, sustainable and impermeable [5], [12]. Fly ash, slag, and metakaolin are the most popular SCMs that have been used to date [26],[27].

There have been some studies that have reported using SCMs on a nanoscale. These studies generally reported a higher cost of production with minor improvements to mechanical properties and durability [28], [29], [30].

In general, most SCMs can be used for developing UHPC mixes based on their availability, but they need to be tested in trial batches before using in the field applications.

Fibers**:** The effect of fibers on the mechanical performance of UHPC depends on geometry, anchorage type, material, coating, chemical composition, weight, yield strength, volume fraction, dispersion, and orientation of the fibers [5]. In general, two different material fibers have been used in UHPC mixtures: metallic fibers, which typically are made of steel, and non-metallic, synthetic fibers. Regardless of the length and shape of fibers, metallic fibers have shown better performance in UHPC mixtures compared to non-metallic fibers due to their higher tensile capacity and stiffness [3]. Non-metallic fibers are more appropriate for architectural and landscaping elements like facades [31].

Fiber content can vary between 1 and 6 percent depending on the fiber type, application, and required tensile capacity, but the most common fiber content in the U.S. is 2 percent of total mixture volume [12]. Different fiber shapes have also been used, but the most commonly used steel fiber in UHPC is a brass-coated, straight, steel fiber with 0.008-inch diameter, 0.5-inch length, and a specified minimum tensile strength of 290 ksi [3].

Water**:** Like other cementitious materials, water is required to hydrate the cement. Because UHPC is a high-performance material, it is sensitive to the exact water content, quality, and temperature. All water quality and control requirements related to conventional concrete are applicable for UHPC mixtures as well [12]. As UHPC mixture has a very low water-to-binder ratio (w/b), it is important to prevent any water loss before and during the mixing process. Hence, for preventing water evaporation during the mixing process due to heat of hydration, it is recommended to use cold water or ice cubes where possible especially in severe hot climate conditions [5].

Additionally, due to low w/b ratios and high cement contents, UHPC has higher autogenous shrinkage than conventional concrete and high-performance concrete [32]. Several different methods have been used for controlling the shrinkage and self-desiccation of UHPC including control of hydration, addition of internal restraints, formation of expansive products, and replenishment of water through internal curing [32], [33]. Among all recognized methods, internal curing has been found to be the most effective method for controlling autogenous shrinkage. Internal curing can be provided using a material that absorbs water and releases it eventually during the hydration process; examples include porous aggregates, porous powder, superabsorbent polymer and cellulose fibers [33].

Chemical Admixtures**:** Different chemical admixtures can be used for developing UHPC mixtures. The most important is a high-range water reducer (HRWR) or superplasticizer. HRWRs are responsible for providing the required flowability of UHPC mixtures while they have a very low water-to-binder ratio. Most HRWRs are polycarboxylate-based, although Naftalin-based and lignosulfonate-based superplasticizers can also be used. There is limited information on the effect of the HRWR based on the mechanical properties of UHPC mixtures.

In addition to HRWR, other chemical admixtures can be used based on the application and required specification and specific purposes. For instance, chemical admixtures like viscosity-modifying admixtures (VMA) and corrosion-inhibiting admixtures can also be used in UHPC mixtures for specific actions [5]. VMA has been widely used for self-compacting concrete (SCC) with slump flows ranging from 26 to 31 inches and can be also used in UHPC to help prevent steel fiber segregation [3].

1.1.2 Non-Proprietary UHPC

There have been many previous research efforts that developed non-proprietary, or open-recipe, UHPC mixtures made with locally available materials in different regions of the U.S [3], [18]-[20], [23], [25], [34]-[37]. The properties achievable by researchers typically depend on the mechanical and chemical properties of the locally produced cement, SCMs, and fine aggregate. A summary of previous studies on non-proprietary UHPC mixtures is shown in Table 1.3.

Table 1.3. Previous research projects for developing non-proprietary UHPC mixes, from Shahrokhinasab and Garber [3]

Researcher	**Year**	**Location**	**Selected-UHPC Mix Parameters**						**Performance**	
			C: SF: SCM	*Other SCMs Used*	*w/c*	*w/b*	*Agg.:b*	*Fiber vol. fraction (%)*	*Flow (in.)*	*f'c (ksi)*
Tadros et al.[1]	2020	A	1.0: 0.25: 0.00	-	0.25	0.200	0.88	0 and 2	8-11	25.0
		B	1.0: 0.25: 0.11	LP	0.25	0.184	1.10	0 and 2	8.9, 9.2	23.4
		C	1.0: 0.25: 0.00	-	0.24	0.195	0.77	0 and 2	9.1	23.1
		D	1.0: 0.20: 0.18	LP	0.29	0.202	0.77	0 and 2	9.1	21.4
		E	1.0: 0.25: 0.00	-	0.23	0.188	1.10	0 and 2	8.9	23.6
Lawler et al.	2019	FL	1.0: 0.15: 0.15	FA (Class F)	0.23	0.170	1:0 to 2:0	1.5 and 2	8-10	18-19
Karim et al.[2]	2019	Iowa	1.0: 0.07: 0.00	-	0.20, 0.25	0.18, 0.2, 0.23	1.12, 1.3	2	8-9	10-17
Matos et al.	2019	Portugal	1.0: 0.54: 0.27	-	0.40	-	1.0	3	11.2-12.2	21-22
Looney et al.	2019	OK	1.0: 0.17: 0.50	S	0.18 to 0.22	0.18 to 0.23	0.75, 1.0	1 and 2	9-11	16-18.2
Berry et al.	2017	Montana	SF/FA = 0.75	FA	0.24	-	1.4 [3]	0 and 2	8-11	20-21
El-Tawil et al.	2016	Michigan	1.0: 0.25: 1.0	S	0.22	0.18	1.0	1.5	-	20.9-28.3
Graybeal	2013	WA, OR, ND, SD, NY, PA	1.0: 0.25: 0.25	FA	0.22 to 0.24	0.15 to 0.16	1.0	1 and 2	10.4-12.4	22.5-29
Tafraoui et al.	2009	France	1.0: 0.25: 0.25	Metakaolin	0.27	0.22	0.9, 1.18	0 and 2	-	15-27.5

c = cement; b = all cementitious materials; FA=fly ash; LP=limestone powder; S=slag or GGBS

[1]liquid portion of chemical admixtures was included in w:c and w:b calculations

[2]compressive strength was measured at 7 days

[3] sand to cement ratio

In addition to previous studies, a research effort was conducted by Florida International University and other partner universities at the Accelerated Bridge Construction University Transportation Center (ABC-UTC). The focus of the research was on developing a non-proprietary UHPC mix with locally available material [3], [4]. The mixture design developed at FIU was based on the materials summarized in Table 1,4.

Table 1.4. Material details and suppliers, from Shahrokhinasab and Garber [3]

Material	**Details**	**Sign**	**Supplier**
Fibers	Hiper Fiber	HF	Hiper Fiber
Cement	Type I-II	C	Titan America
Ground-Granulated Blast-Furnace Slag (GGBFS)	-	S	ARGOS USA Cement
Silica Fume	Master Life® SF 10	SF	BASF
Sand	Fine Masonry	FA	Titan America
Ultra-Fine Recovery Material	-	UFR	Titan America
High-Range Water Reducer	Glenium 7920	HRWR	BASF
Viscosity Modifying Admixture	VMA 358	VMA	BASF

Two mixture designs were developed based on the availability of ultra-fine recovery material (UFR), summarized in Table 1.5. UFR particles are recoverable fine materials coming from wastewater streams of aggregate plant system. The fine size of UFR (less than 150µm) has made it a conveyable and stackable material ideal for several industries [3].

These mixtures resulted in compressive strengths close to 18 ksi and modulus of rupture strengths above the 1.5-ksi first crack and 2.0-ksi peak minimum values used for UHPC [5].

Table 1.5. Non-proprietary mixture design developed by Shahrokhinasab and Garber [3]

Mix.	**Cement Type**	**W/B**	**Mix Proportions**						**Fiber**		**Admixtures**	
			ag/cm	*C*	*S*	*SF*	*FA*	*UFR*	*Type*	*Content (%)*	*HRWR (oz./cwt)*	*VMA (oz./cwt)*
1	Titan Type I/II	0.20	1.0	0.6	0.3	0.1	1.00	0.00	HF or OL	2.0	27.5	0
2	Titan Type I/II	0.20	1.0	0.6	0.3	0.1	0.70	0.30	HF or OL	2.0	29.5	0

Two Florida precasters also participated in the research conducted by Tadros et al. [5].

1.2 Interface Strength Evaluation Methods

Several different types of tests have been used to study the interface strength between two different concrete materials. Three of the primary categories of tests include: bending tests, tension tests (direct and indirect tension tests), and shear tests. Several different bending test setups used by previous researchers to test the strength of an interface are shown in Figure 1.1.

These setups have been used in the past to test the interface between different concrete materials including conventional concrete, lightweight concrete and UHPC.

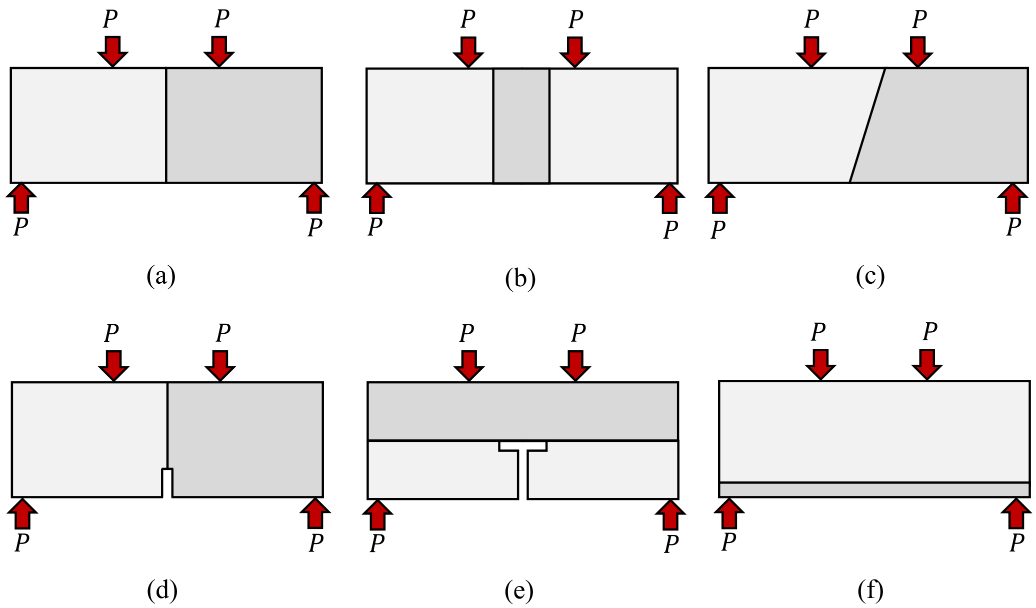

Figure 1.1. Different bending test setup for interface study proposed by (a) Ohama et al. [38], (b) Abu-Tair et al. [39], (c) Wall et al. [40], (d) Kunieda et al. [41], (e) Kamada and Li [42] and (f) Khayat and Valipour [43].

The tensile strength of interfaces can be tested using direct tension and indirect tension test methods. Direct tension tests are those where the testing procedure directly causes a perpendicular tensile stress across the interface. Direct tension tests, shown in Figure 1.2 (a), can be performed on specimens with different shapes (e.g., dogbones, rectangular prisms, cylinders). Another form of the direct tension test is the pulloff test, shown in Figure 1.2 (b), where the specimen provides the reaction for the tension pulloff force. Indirect tension tests are those where tension results across an interface from the spreading of stresses, such as split cylinder and splitting tests on cubic samples, shown in Figure 1.2 (c) and (d).

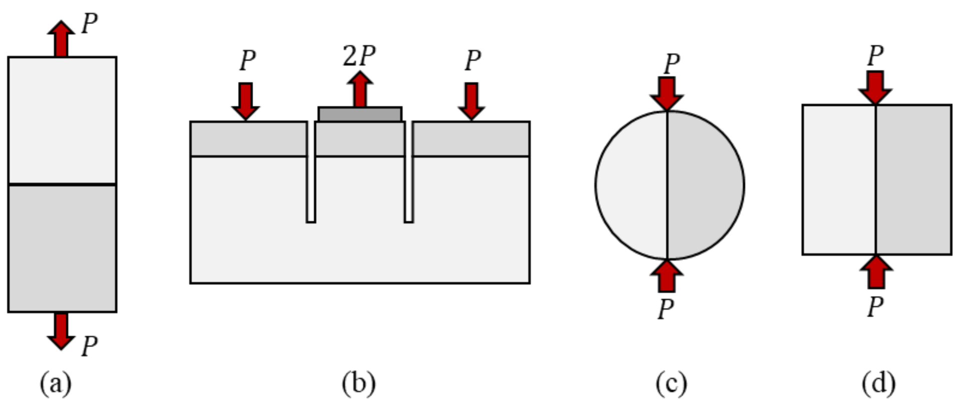

Figure 1.2. Tension tests: (a) direct tension test, (b) pulloff test (direct tension mechanism), (c) splitting tensile test on cylinder and (d) splitting tensile test on cube.

A list of previous studies that used different tension test setups are summarized in Table 1.6.

Table 1.6. List of studies using tension setups for evaluating the interface strength

Test Type	List of Studies	
Direct Tension	▪ Zanoti and Randl [44] ▪ Semendary et al. [44]	
Tension Pulloff	▪ Zanoti and Randl [44] ▪ Cairovic et al. [46] ▪ Julio et al. [47] ▪ Momayez et al. [48] ▪ Carbonell Munoz et al. [49]	▪ Graybeal [50] ▪ Harris et al. [51] ▪ Santos at al. [52] ▪ Semendary and Svecova [53] ▪ Harber et al. [54]
Splitting Tensile (cylinder)	▪ Espeche and Leon [55] ▪ Zanoti and Randl [44] ▪ Cairovic et al. [46]	▪ Tayeh et al. [56] ▪ Carbonell Munoz et al. [49] ▪ Graybeal [50]
Splitting Tensile (cube)	▪ Harris et al. [51]	▪ Momayez et al. [48]

The third category of tests for studying the interface strength is shear tests. There are many different types of tests that are used to determine the shear strength of an interface, shown in Figure 1.3. These tests either test shear directly with no normal force caused by loading (e.g., pushoff test) or test shear with a normal force across the interface caused by loading (e.g., bi-surface shear test).

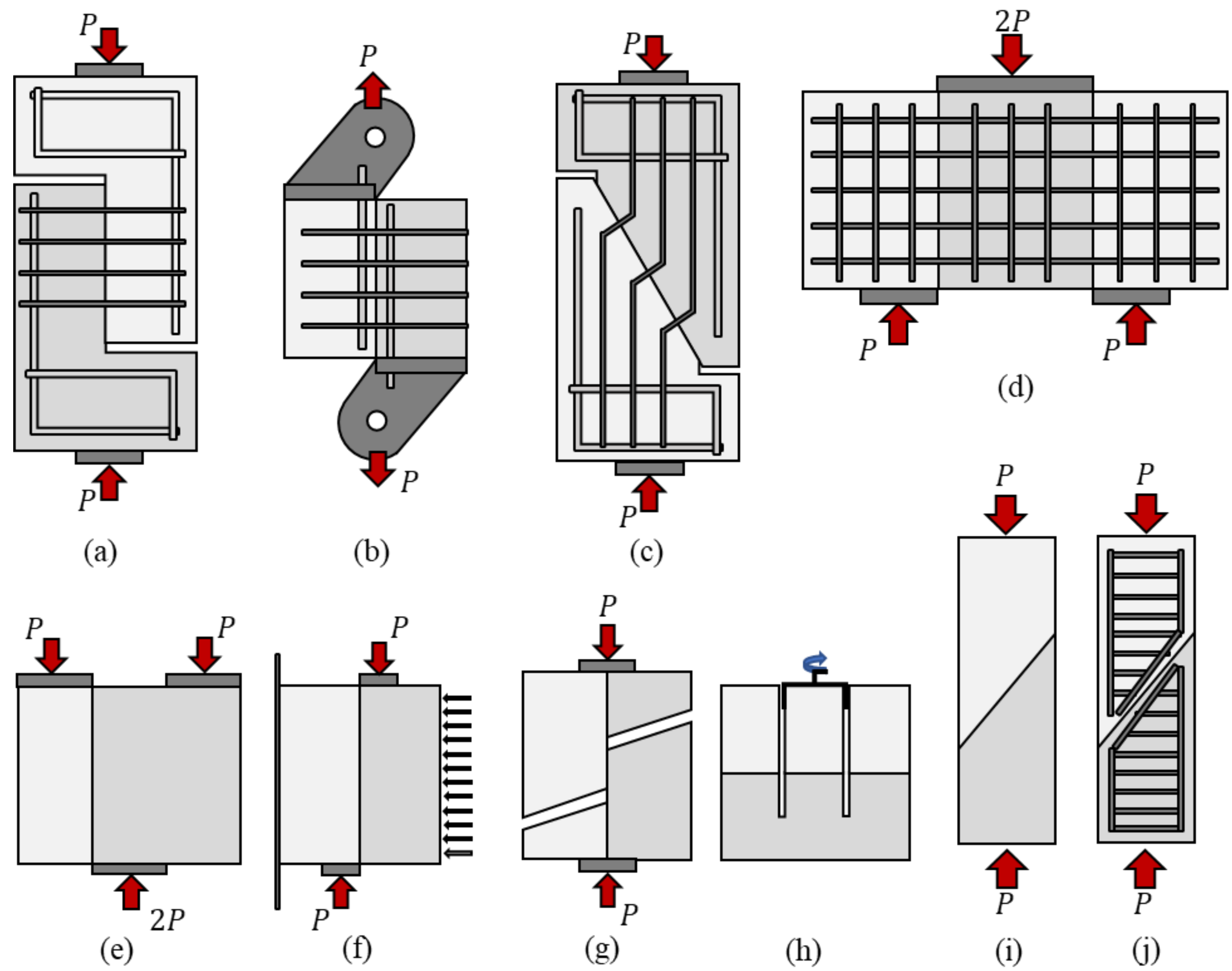

Figure 1.3. Different types of shear tests: (a) L-shape pushoff tests, (b) shear pulloff tests, (c) modified pushoff tests, (d) push-through tests, (e) bi-surface shear test, (f) pushoff tests (single shear plane), (g) Z-type test, (h) twist-off test, (i) slant shear test and (j) modified slant shear test.

Many different studies have been conducted to test the shear capacity of a variety of different interface planes with conventional concrete. A summary of these studies is provided in Table 1.7 Pushoff tests and slant shear tests are the most commonly used method for determining shear strength of an interface. There have been several studies that proposed angle modification and reinforcement conditions at the interfaces for slant shear tests [44], [57], [58].

Table 1.7. Primary test types for shear friction and list of studies using each type

Test Type	List of Studies	
Pushoff (L-shape)	▪ Bass et al. [59] ▪ Figueira et al. [60] ▪ Frenay [61] ▪ Hanson [62] ▪ Hofbeck et al. [63] ▪ Kahn [64] ▪ Mattock and Hawkins [65] ▪ Cairovic et al. [46]	▪ Mattock et al. [66] ▪ Mayers et al. [67] ▪ Mohamad et al. [68] ▪ Pruijssers and Lung [69] ▪ Walraven and Reinhardt [70] ▪ Walraven and Stroband [71] ▪ Xu et al. [72] ▪ Banta [73]
Shear Pulloff	▪ Mattock and Hawkins [65]	▪ Long and Murray [74]
Modified Pushoff	▪ Mattock and Hawkins [65]	
Push Through (out)	▪ Williams et al. [75] ▪ Zhang et al. [76]	▪ Zanoti and Randl [44]
Bi-Surface Shear	▪ Cairovic et al. [46] ▪ Semendary and Svecova [53]	▪ Farzad et al. [77] ▪ Valikhani [78]
Pushoff (Single Shear Plane)	▪ Nohamad and Ibrahim [79]	
Z-Type	▪ Cairovic et al. [80]	
Twist-Off	▪ Nader [81]	▪ Silfwerbrand [82]
Slant Shear	▪ Zanoti et al. [83] ▪ Zanoti and Randl [44] ▪ Semendary and Svecova [53] ▪ Tayeh et al. [56] ▪ Carbonell Munoz et al. [49]	▪ Harris et al. [51] ▪ Graybeal [50] ▪ Aelti and Sirtharan [84] ▪ Farzad et al. [77]
Modified Slant Shear	▪ Saldanha et al. [57]	

1.3 Shear Friction Equations

Many different shear friction equations have been proposed by different researchers based on results from different types of interface tests. These equations have ranged from simple linear equations to parabolic functions and more complex equations [85]. One of the more widely accepted shear friction hypotheses for explaining the mechanics of interface shear transfer was proposed by researchers in 1966 [86]. This shear friction hypothesis considers the roughened interface, applied normal force, and applied shear shown in Figure 1.4.

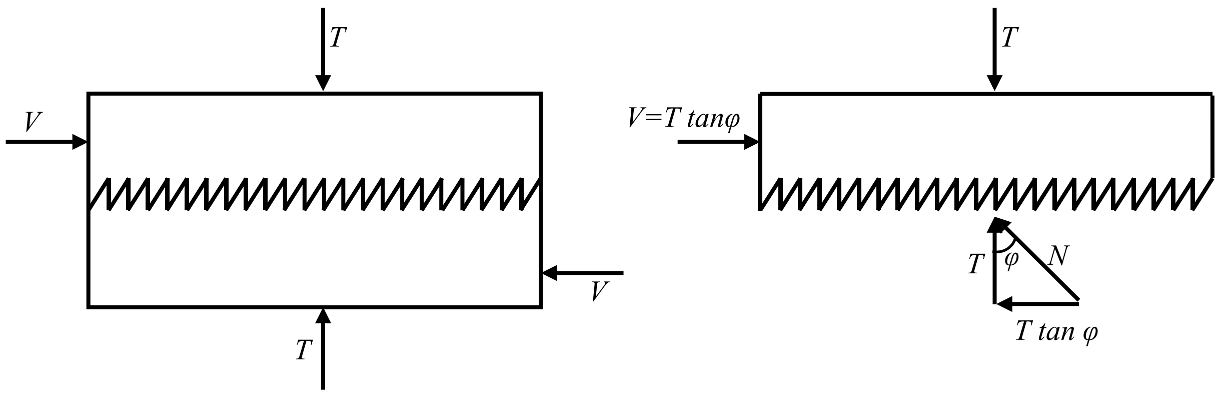

Figure 1.4. Shear friction theory proposed by Birkeland [86].

The shear strength of the interface can be determined based on the normal force and the coefficient of friction. The normal force can be determined based on the reinforcement crossing the interface. The reinforcement crossing the interface would be placed in tension as the interface slides, which would place a normal force on the surrounding concrete. The coefficient of friction, μ, can be determined based on the roughness of the interface. The interface shear strength can then be determined using Equation 1-2 for shear strength and Equation 1-2 for shear stress.

$$V_n = \mu A_s f_y \qquad \text{Equation 1-1}$$

$$v_n = \mu \rho_s f_y \qquad \text{Equation 1-2}$$

These equations have the basic form of the equations later adopted by ACI 318 and AASHTO LRFD Bridge Design Specification.

The current ACI 318 shear friction is essentially the same as the equation proposed by Birkeland [86], [87] :

$$V_n = \mu A_v f_y \qquad \text{Equation 1-3}$$

V_n shall not be taken as greater than the smaller of:

$$0.2A_{cv}f'_c \qquad (480 + 0.8f'_c)A_{cv} \qquad 1600A_{cv}$$

Where:

A_{vf} = area of steel crossing interface

μ = friction coefficient

f'_c = compressive concrete strength of the weaker concrete (ksi)

f_y = yield stress of steel

A_c = area of concrete contact across interface

The equations in AASHTO LRFD Bridge Design Specification (§5.7.4) [88] include an additional component that is based on the bond or cohesion (c) between the two sides of an interface. Theoretically, the cohesion (cA_{cv}) would resist a shear force first and then the friction component would resist shear once an interface crack forms. Test results have shown that it is conservative to combine these two terms, as shown in Equation 1-4; this is similar to what is typically done with V_c and V_s terms in one-way shear. An additional difference between Equation 1-1 and Equation 1-4 is the addition of an applied normal force (P_c) to the friction component.

$$V_{ni} = cA_{cv} + \mu(A_{vf}f_y + P_c)$$

Equation 1-4
AASHTO LRFD BDS 9th Ed. (5.7.4.3-3)

There are two limits placed on the nominal shear friction capacity, Equation 1-5 and Equation 1-6, based on the concrete compression strength (f'_c) and the area of the concrete interface plane (A_{cv}) found using Equation 1-7.

$$V_{ni} = K_1 f'_c A_{cv}$$

Equation 1-5
AASHTO LRFD BDS 9th Ed. (5.7.4.3-4)

$$V_{ni} = K_2 A_{cv}$$

Equation 1-6
AASHTO LRFD BDS 9th Ed. (5.7.4.3-5)

$$A_{cv} = b_{vi} L_{vi}$$

Equation 1-7
AASHTO LRFD BDS 9th Ed. (5.7.4.3-6)

Where:

b_{vi} = width of the interface considered to be involved in the shear transfer (in)

L_{vi} = length of the interface considered to be involved in the shear transfer (in)

c = cohesion factor (ksi)

μ = friction coefficient

P_c = compressive force perpendicular to the shear plane; if force is tensile, Pc = 0.0 (kip)

f'_c = compressive concrete strength of the weaker concrete (ksi)

K_1 = fraction of concrete strength available to resist the interface shear

K_2 = limiting interface shear resistance (ksi)

All the factors related to the above expressions are shown in Table 1.8.

Table 1.8. Factors to determine the interface shear capacity according to AASHTO [88]

<table>
<tr><th>Interface condition</th><th>c (ksi)</th><th>μ</th><th>K_1</th><th colspan="2">K_2 (ksi)</th></tr>
<tr><td rowspan="2">Cast-in-place concrete slab on clean concrete girder surfaces, free of laitance with surface roughened to an amplitude of 0.25in.</td><td rowspan="2">0.28</td><td rowspan="2">1.0</td><td rowspan="2">0.3</td><td>Normal weight concrete</td><td>1.8</td></tr>
<tr><td>Lightweight concrete</td><td>1.3</td></tr>
<tr><td>Normal weight concrete placed monolithically.</td><td>0.40</td><td>1.4</td><td>0.25</td><td colspan="2">1.5</td></tr>
<tr><td>Lightweight concrete placed monolithically, or placed against a clean concrete surface, free of laitance with surface intentionally roughened to an amplitude of 0.25 in.</td><td>0.24</td><td>1.0</td><td>0.25</td><td colspan="2">1.0</td></tr>
<tr><td>Normal weight concrete placed against a clean concrete surface, free of laitance, with surface intentionally roughened to an amplitude of 0.25in.</td><td>0.24</td><td>1.0</td><td>0.25</td><td colspan="2">1.5</td></tr>
<tr><td>Concrete placed against a clean concrete surface, free of laitance, but not intentionally roughened.</td><td>0.075</td><td>0.6</td><td>0.2</td><td colspan="2">0.8</td></tr>
<tr><td>Concrete anchored to as-rolled structural steel by headed studs or by reinforcing bars where all steel in contact with concrete is clean and free of paint.</td><td>0.025</td><td>0.7</td><td>0.2</td><td colspan="2">0.8</td></tr>
</table>

These values are based on research by several different researchers [63], [64], [85], [89], [90] using pushoff tests and horizontal shear beam tests.

The shear friction equations specified by the AASHTO LRFD Bridge Design Specification have been compared to experimental results by many other researchers [91]-[94]. Researchers have investigated the effect of different surface conditions, pre-existing cracks, presence of mechanical connectors, and the mechanical properties of substrate and new concrete and have generally found the AASHTO LRFD Bridge Design Specification provisions related to shear friction to be conservative [91], [93]. There have been some recent studies that have found the provisions to also be conservative for conventional concrete-to-UHPC interfaces [95].

Researchers have also investigated other factors, including the effect of dowel action of the reinforcement crossing the interface [63]. Dowel action is generally not separated out from the effect of the clamping force caused by elongation of the reinforcement crossing an interface. Past researchers [63] have commented that dowel action leads to stiffening and strengthening of the shear friction interface.

1.4 Measuring Cohesion and Friction Coefficients

There are several different methods for determining the cohesion and friction coefficients.

1.4.1 Mohr-Coulomb Friction Approach

Mohr-Coulomb's theory can be used to explain the concept of bond failure in which shear failure occurs. Cohesion and friction coefficients can be determined according to the Mohr-Coulomb friction approach, shown in Equation 1-8 through Equation 1-10. This approach assumes a linear relationship between the shear stress and normal stress across the interface. The normal stress (σ_n) can include applied normal stress (f_n) and the reinforcement crossing the friction plane ($\rho_v f_y$). The internal friction angle (ϕ) is related to the coefficient of friction and is determined using Equation 1-10 [96].

$$\tau_u = c + \mu\sigma_n \qquad \text{Equation 1-8}$$

$$\sigma_n = \rho_v f_y + f_n \qquad \text{Equation 1-9}$$

$$\mu = \tan\varphi \qquad \text{Equation 1-10}$$

Several different researchers [46], [53], [55], [76], [79], [83], [96]– [98] have used this approach to determine the cohesion (c), coefficient of friction (μ), and friction angle (ϕ). The cohesion is often found based on a direct tension of the interface. The coefficient of friction and friction angle are often found using slant shear, bi-shear, or direct shear tests, with applied normal stress across the shear plane.

The coefficient of friction can also be found using pushoff tests with reinforcement crossing the interface, similar to what was done by Crane [97]. A linear interpolation of the shear stress versus clamping force ($\rho_v f_y$) was performed for the test data where the intercept is equal to the cohesion and slope equal to the coefficient of friction, as shown in Figure 1.5.

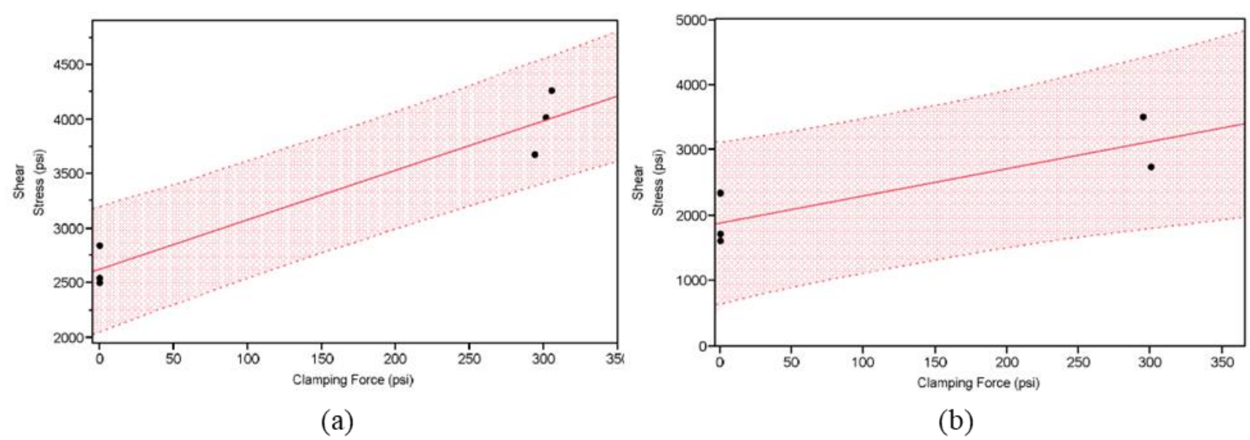

Figure 1.5. Linear regression analysis from Crane [97] monolithic UHPC pushoff specimens that were (a) uncracked and (b) pre-cracked.

The Mohr-Coulomb friction approach has been found to overestimate the shear strength in the tensile region [99].

1.4.2 Carol's Approach

An additional approach for finding the cohesion (c), coefficient of friction (μ), and friction angle (ϕ) is to use Carol's Approach [55], [99]. In this approach, as derived in [55], the shear strength and cohesion can be found using Equation 1-11 through Equation 1-13.

$$\tau_u = \sqrt{(c - \sigma_n \tan\varphi)^2 - (c - f_t \tan\varphi)^2} \qquad \text{Equation 1-11}$$

$$c = \left(\frac{2 - \sin\varphi}{\cos\varphi}\right) f_t, \qquad for\ \ \varphi > 30° \qquad \text{Equation 1-12}$$

$$c = \sqrt{3} \cdot f_t, \qquad for\ \ \varphi \leq 30° \qquad \text{Equation 1-13}$$

The cohesion is determined by using the tensile bond strength using Equation 1-12 or Equation 1-13 depending on the friction angle. The friction coefficient can be found using the linear approach (Equation 1-11) using either direct shear or slant shear test results.

Carol's Approach (Equation 1-11) was used and verified by other researchers and even was used for estimating the bond strength between normal concrete and fiber-reinforced material [83]. One example of the validation of Carol's Approach using fiber reinforced concrete is shown in Figure 1.6 [44].

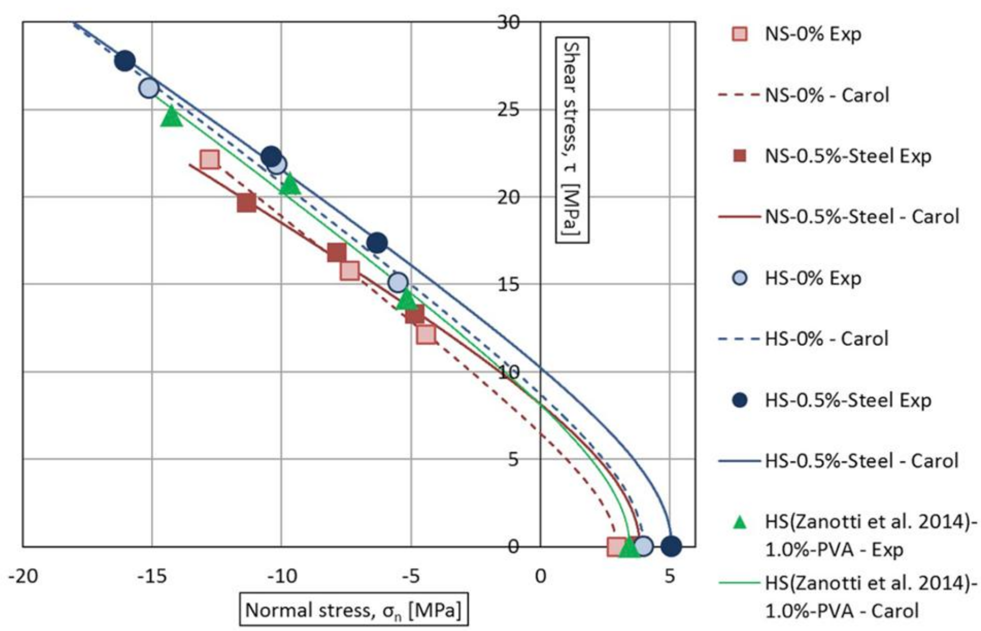

Figure 1.6. Experimental results of shear bond strength from slant shear tests and tensile splitting bond tests and failure envelopes obtained by fitting Carol's Approach, from Zanotti and Randl [44].

1.5 UHPC-to-Conventional Concrete Bond

There have been many previous studies [1], [49], [50], [54], [76]– [78], [95], [100], [101] looking at the bond between precast conventional concrete (CC) substrates and cast-in-place (CIP) UHPC. A summary of these studies, some of the variables investigated, test type used, and major findings are shown in Table 1.9. The common test types referenced in the table are shown in Figure 1.7.

Table 1.9. Summary of selected research on CC to UHPC bond

Researcher	**Year**	**Experimental Variables**	**Test Type**	**Significant Findings**
Aaleti and Sritharan [84]	2019	Compressive strength of CC, interface surface texture, curing condition, pouring sequence	Slant shear	Interface shear strength increased with increasing roughness and substrate concrete strength
Banta [73]	2005	Surface treatment, reinforcement ratio, aspect ratios; used lightweight concrete substrate	Pushoff test (with normal stress)	AASHTO LRFD BDS 3rd Edition [102] could be used to conservatively estimate interface shear strength
Farzad et al. [77]	2019	Wet/dry surface preparation of substrate	Flexural beam, slant shear, bi-surface shear	Developed numerical model for the interface
Graybeal [50]	2017	Precast surface preparation (roughness, interface moisture level, internal curing)	Flexural beam, splitting cylinder, direct tension pulloff	Direct tension pulloff best test for bond; best performance with prewetted, exposed aggregate finish
Graybeal [100] and Haber et al. [54]	2018	Scarification versus hydro demolition for UHPC overlays over existing CC substrate	Direct tension pulloff	Best performance for substrate prepared with hydro demolition
Harris et al. [51]	2015	Surface roughness, age and strength of concrete, interface angle (numerical)	Splitting tension, slant shear, direct tension pulloff	Current testing methods for bond can be difficult to properly implement consistently
Khayat and Valipour [43]	2014	One mix design was tested	Splitting tension (ASTM C1245 [103])	Failure occurred in substrate
Muñoz et al. [49]	2014	Surface treatments/roughness; also include freeze-thaw effects	Splitting tension, slant shear, pulloff	Could obtain bond strength greater than CC substrate with appropriate wetting of substrate. Roughness of substrate not critical factor.
Tayeh et al. [56]	2012	Surface roughness	Slant shear, splitting tension	Good bond between CC substrate and UHPC was observed with failure occurring in CC substrate
Valikhani et al. [101]	2020	Surface preparation (with and without sandblasting of substrate), with and without mechanical connectors and bonding agent	Bi-surface shear test	Bonding agent reduced bond strength by half; increasing surface roughness increases bond strength; used surface scanning to quantify surface roughness

Researcher	Year	Experimental Variables	Test Type	Significant Findings
Valikhani et al. [95]	2021	Surface roughness, reinforcement ratio	Modified pushoff shear test	AASHTO LRFD BDS 8th Edition [104] cohesion and friction coefficients are conservative; increased roughness increased shear strength; increased reinforcement increased shear strength and ductility
Zhang et al. [176]	2020	Strength of CC substrate and CIP UHPC at time of testing, curing, surface treatment, expansion agent in UHPC, transverse stress	Double-sided direct shear test	Increased strength of substrate, increased surface roughness, and transverse compression increased shear strength. Transverse tension and inclusion of expansion agent in UHPC decreased shear strength.

1.5.1 Common Test Methods

The most common test methods used to evaluate the interface between precast CC substrates and CIP UHPC are shown in Figure 1.7. The flexural strength of the interface is typically found using the flexural beam test, Figure 1.7 (a). The tensile strength has been typically found through direct tension pulloff, Figure 1.7 (b), or split cylinder test, Figure 1.7 (c). The shear strength has typically been found using slant shear tests, Figure 1.7 (d), bi-shear tests, Figure 1.7 (e), or modified pushoff tests, Figure 1.7 (f).

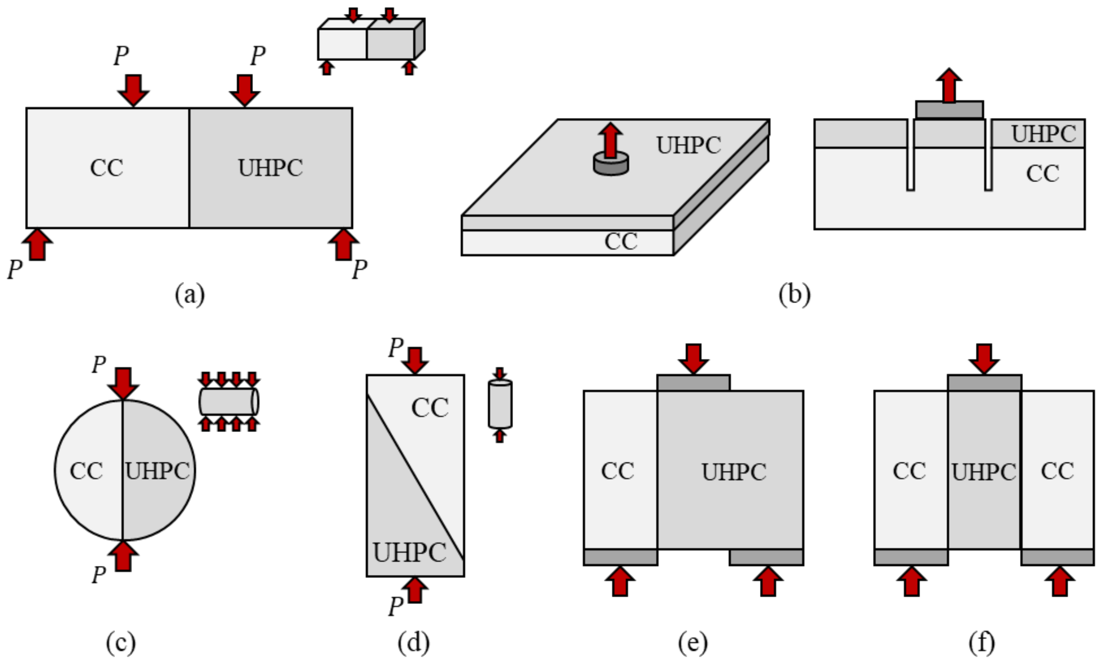

Figure 1.7. Common bond tests conducted on CC-to-UHPC specimens: (a) flexural beam test, (b) direct tension pulloff, (c) split cylinder test, (d) slant shear test, (e) bi-surface shear test, and (f) modified pushoff or push through test.

All of these tests, other than the direct tension pulloff tests, can be performed in a typical compression testing machine used to test conventional cylinders in compression.

1.5.2 Surface Roughness and Preparation

There have been many different surface roughnesses and surface preparations tested by these researchers. Some of the typical previously tested interfaces are summarized well by Munoz et al. [49]:

- Smooth: no surface preparation or lightly brushed or as cast against formwork
- Chipped: surface roughened using chipping hammer or drill
- Brushed: surface roughened by running rough brush over it during the finishing process
- Sandblasted: surface sandblasted after concrete hardens and formwork removed
- Grooved: surface grooved using saw or grinder to different depths
- Exposed aggregate: paste retarder applied to formwork prior to casting; pressure washer used to remove unhydrated paste within 24 hours of casting

Typical surface finishes achieved using these methods are shown in Figure 1.8.

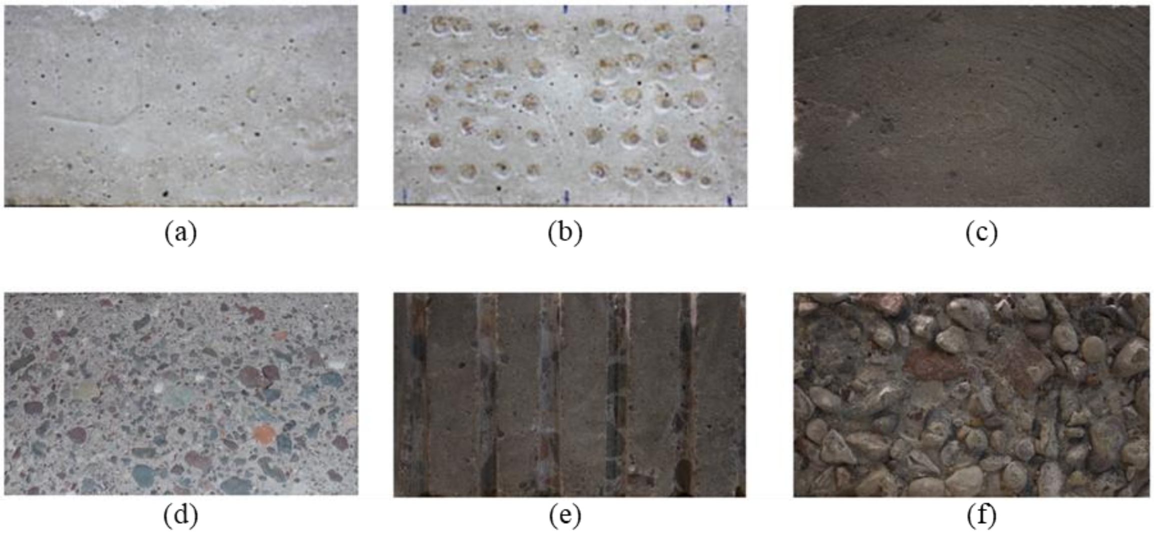

Figure 1.8. Typical surface finishes tested for CC-to-UHPC interfaces: (a) smooth, (b) chipped, (c) brushed, (d) sandblasted, (e) grooved, and (f) exposed aggregate, from Munoz et al. [49].

In general, a good bond between a CC substrate and CIP UHPC has been achieved with an exposed aggregate finish and proper surface preparation (i.e., saturated surface dry [SSD]) prior to casting of the CIP UHPC material. When these conditions are met, testing typically results in failure occurring in the substrate conventional concrete and not at the joint interface. A sample of the results from the literature is shown in Figure 1.9 from Graybeal [50] where failure occurred in the CC substrate material for exposed aggregate finish with wet burlap or SSD surface preparation.

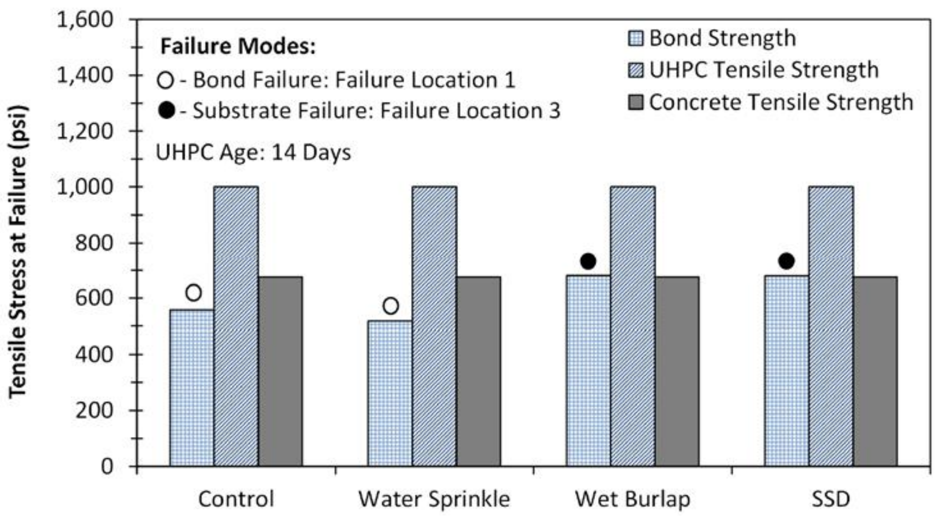

Figure 1.9. Sample result from Graybeal [50] for different interface surface preparations.

Aaleti and Sritharan [84] also investigated the use of several different formliners with various textures and mean texture depths, shown in Figure 1.10. They found that there was sufficient shear strength as long as the macro texture depth was greater than the 0.063 inches achieved by the 2/102 Parana formliner, which would be associated with the finishes shown in Figure 1.10 (c), (d), and (e).

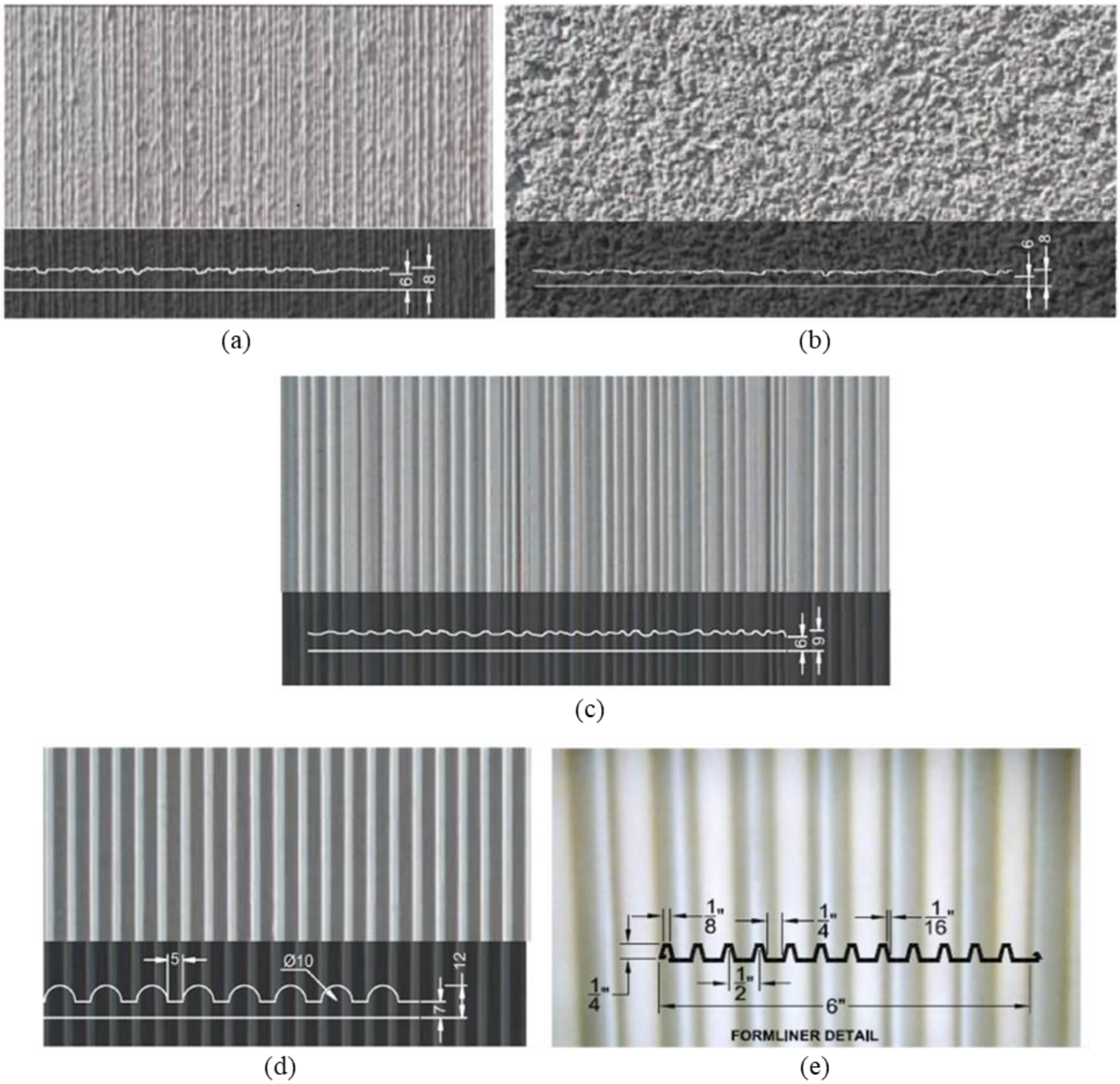

Figure 1.10. Different surface textures from Aaleti and Sritharan [84] using formliners with mean texture depths in parantheses: (a) 2/61 Thames (0.05 in.); (b) 2/102 Parana (0.063 in.); (c) Vltava (0.118 in.); (d) 2/63 Wisla (0.196 in.); and (e) fluted rib pattern (0.256 in).

1.5.3 Numerical Modeling of Interface

Numerical modeling of an interface between a substrate and CIP material typically requires modeling of the two materials themselves and then defining an interface layer (often with zero thickness) with different properties between the two materials. Most of the experimental studies on interfaces did not compare experimental results to numerical models.

Valikhani et al. [78] was one of the few studies that developed numerical modeling for the interface tests shown above. These researchers calibrated the compression, tension, and flexure stress-strain relationships for the base materials using experimental results. They calibrated the interface properties (e.g., cohesion, tensile strength, friction coefficient, interface stiffness) based on experimental test results from bi-shear testing. This process led to estimated results within about 1 percent of the experimental results.

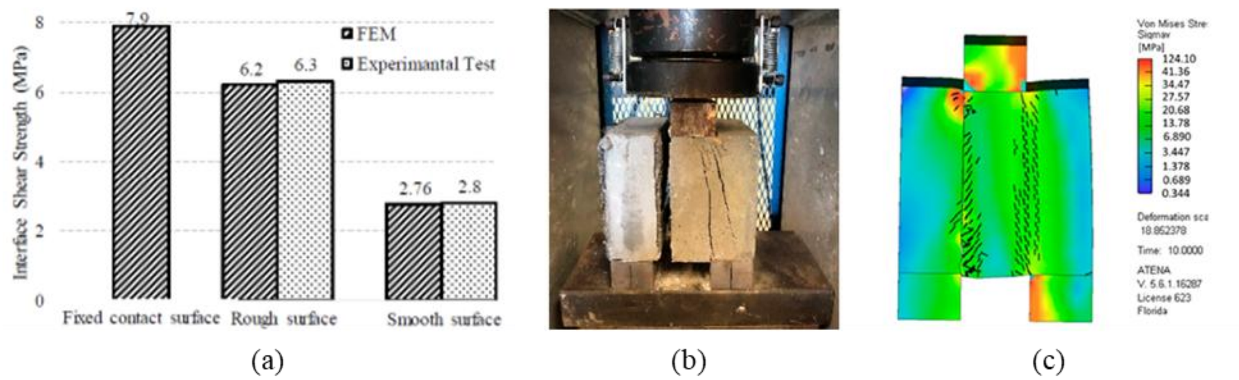

Figure 1.11. Sample of numerical modeling by Valikhani et al. [78].

A similar procedure was used to model joints between CC precast elements and UHPC joints, an example is by Chitty et al. [105] in Figure 1.12.

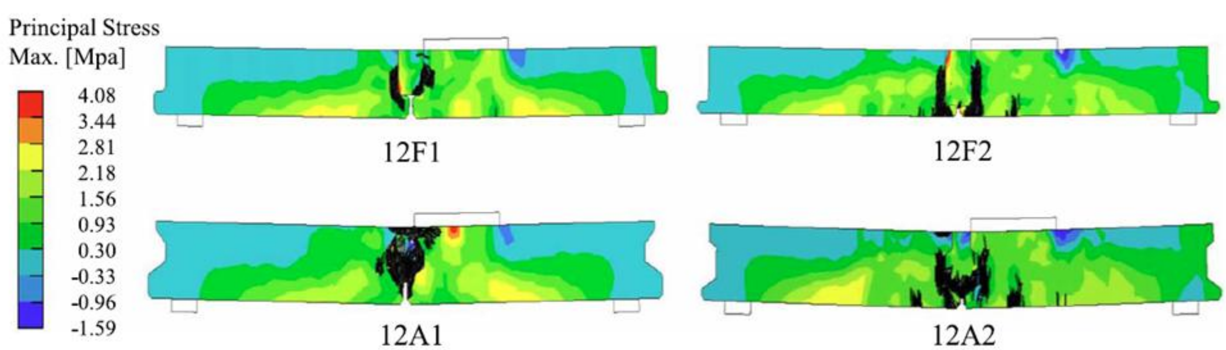

Figure 1.12. Sample model from Chitty et al. [105] of UHPC joint between precast CC slab beams.

1.6 UHPC-to-UHPC Bond

There have been several different research efforts investigating the bond between precast UHPC substrates and CIP UHPC. A summary of these studies is provided in this section.

Crane [97] performed pushoff tests with precast (substrate) UHPC and both CIP high-performance concrete (HPC) and UHPC. The specimens with a cold joint had a configuration as shown in Figure 1.13. Crane [97] investigated the following variables:

- Uncracked monolithic, pre-cracked monolithic, and smooth cold joints
- Different amounts of reinforcement crossing interface (clamping force), with $\rho_v f_y$ between 0 and around 450 psi
- Smooth cold joint, burlap cold joint, and fluted cold joint

Crane [97] found recommended friction (μ) and cohesion (c) factors by using linear regression of the shear stress versus clamping force ($\rho_v f_y$). The slope of the equation was assumed equal to the coefficient of friction (μ) and the intercept was assumed to be the cohesion factor (c), as shown in Equation 1-8 and Equation 1-9. Crane [97] suggested μ = 4.5 and c = 2,000 psi for monolithic uncracked UHPC interface and μ = 4.0 and c = 650 psi for monolithic cracked specimens.

Fang et al. [106] conducted UHPC substrate-to-CIP UHPC testing to simulate the bond between a UHPC girder and CIP UHPC shear pocket in a full-depth precast concrete deck panel. A schematic of their double-sided shear test specimen is shown in Figure 1.13. The specimen is built like there is a shear pocket on each side of the UHPC center portion. Reinforcement was crossing the UHPC-to-UHPC shear plane in all specimens. The researchers found that the amount of reinforcement crossing the interface had the largest effect on the shear strength.

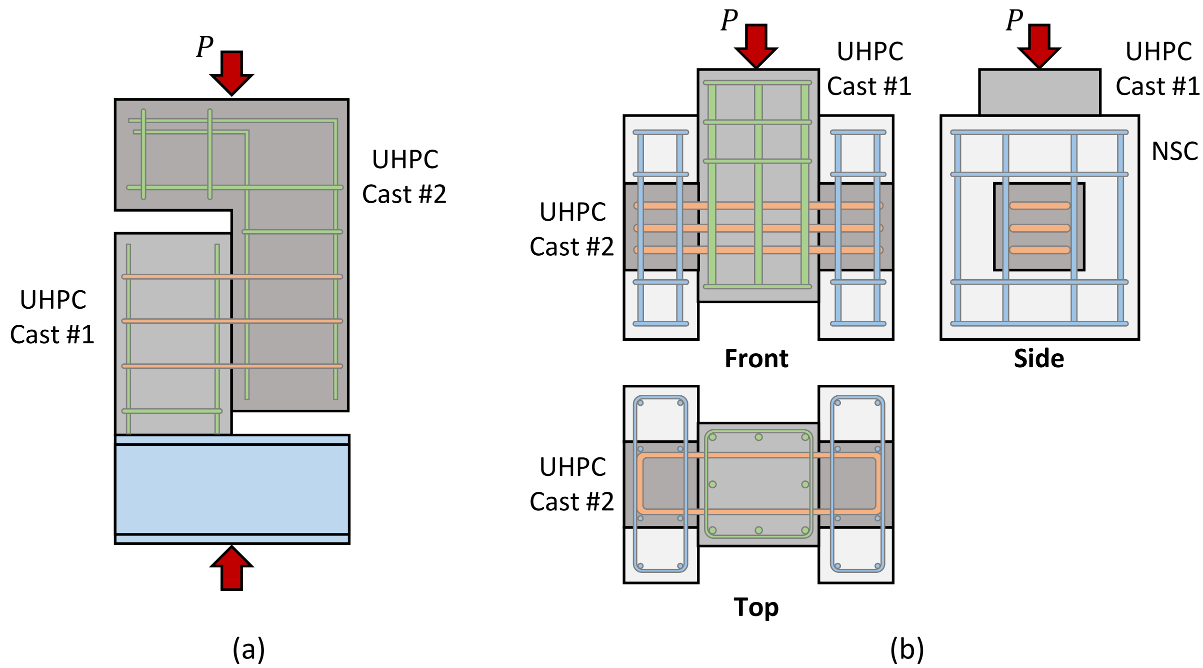

Figure 1.13. Shear tests for UHPC substrate-to-CIP UHPC boundary from (a) Crane [97] and (b) Fang et al. [106].

Graybeal [100] tested the direct tension pulloff capacity of a UHPC substrate and CIP UHPC overlay. A test setup like that shown in Figure 1.7 (d) was used for this testing. The UHPC substrate was prepared using scarification and hydro-demolition. Graybeal [100] found that the failure occurred at the interface between the precast and CIP UHPC for both the scarification and hydro-demolition surface preparation, although the hydro-demolition did result in a 31% increase in the pulloff tensile capacity compared to scarification.

Jang et al. [107] performed direct shear tests using pushoff specimens like those shown in Figure 1.14 (a). They looked at six different interface surface preparations: monolithic placement, smooth vertical construction joint, water jet treatment, construction joint with 0.4 by 0.4-inch grooves, construction joint with 0.8 by 0.8-inch grooves, and construction joint with 1.2 by 1.2-inch grooves. They found that the grooved specimens performed better than the water jetted surface with the 1.2 by 1.2-inch grooves providing 2.45 times the shear strength as water jetting.

Kim et al. [108] performed modified push-through tests with dry and wet UHPC-to-UHPC joints with varying levels of transverse stress and different numbers of shear keys. The dry joint specimens were created with two precast UHPC segments with different rib details. The wet joint specimens had two precast UHPC components with a narrow CIP UHPC portion between them. The failure load increased with increasing number of shear keys, increasing shear key height, and increasing confining stresses for both dry and wet joints. Using epoxy in the dry joint only slightly increased the capacity (less than 7%).

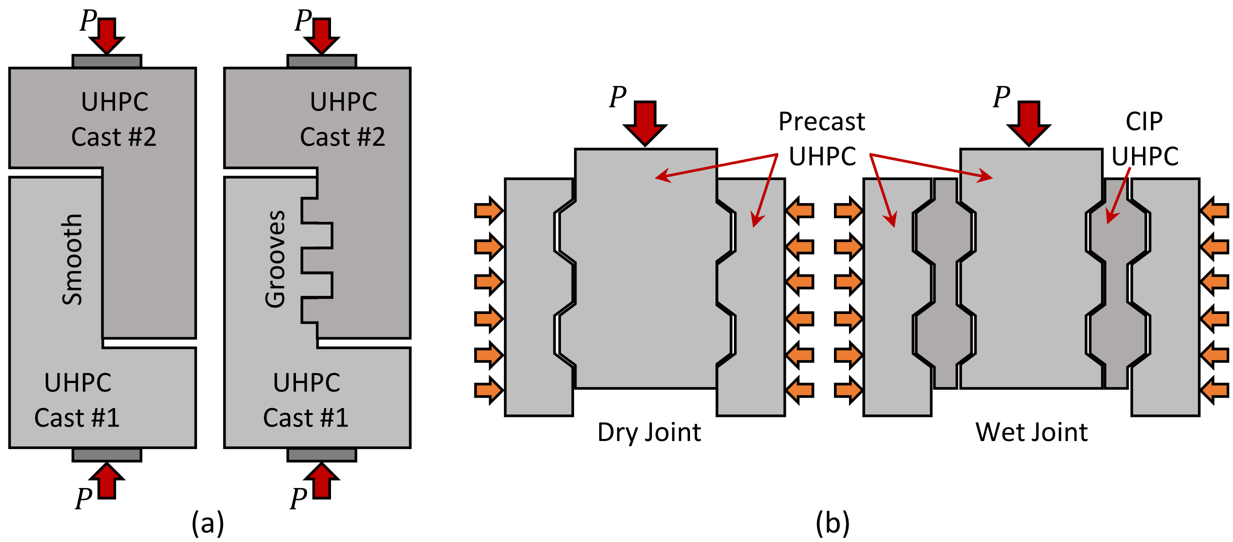

Figure 1.14. Sample of specimens used for shear testing by (a) Jang et al. [107] and (b) Kim et al. [108].

Li et al. [109] also investigated the direct shear capacity of UHPC-to-UHPC joint using a pushoff type test, as shown in Figure 1.15 (a). They tested monolithic UHPC specimens and specimens with a water-jetted cold joints with different fiber contents and types. They found that a waterjet treatment, which was able to expose fibers along the interface, was able to reach 42.5% of the shear strength of the monolithically cast specimens.

Qi et al. [110] performed flexural tests on a dove-tail joint detail proposed to connect UHPC deck panels, shown in Figure 1.15 (b). The connection between the precast UHPC deck panel and CIP UHPC joint included reinforcement crossing the interface and a dove-tail shaped joint detail. Prestressing strands were also used across the joint in some of the specimens. The researchers prepared the joint interface using a steel wire mesh (SWM) interface treatment procedure. A steel wire mesh was fixed to the mold side of the forms with staple gun; the steel wire mesh was removed from the precast component leaving some exposed steel fibers. This SWM treatment procedure may deserve additional investigation depending on the exposed fiber results obtainable with paste retarders.

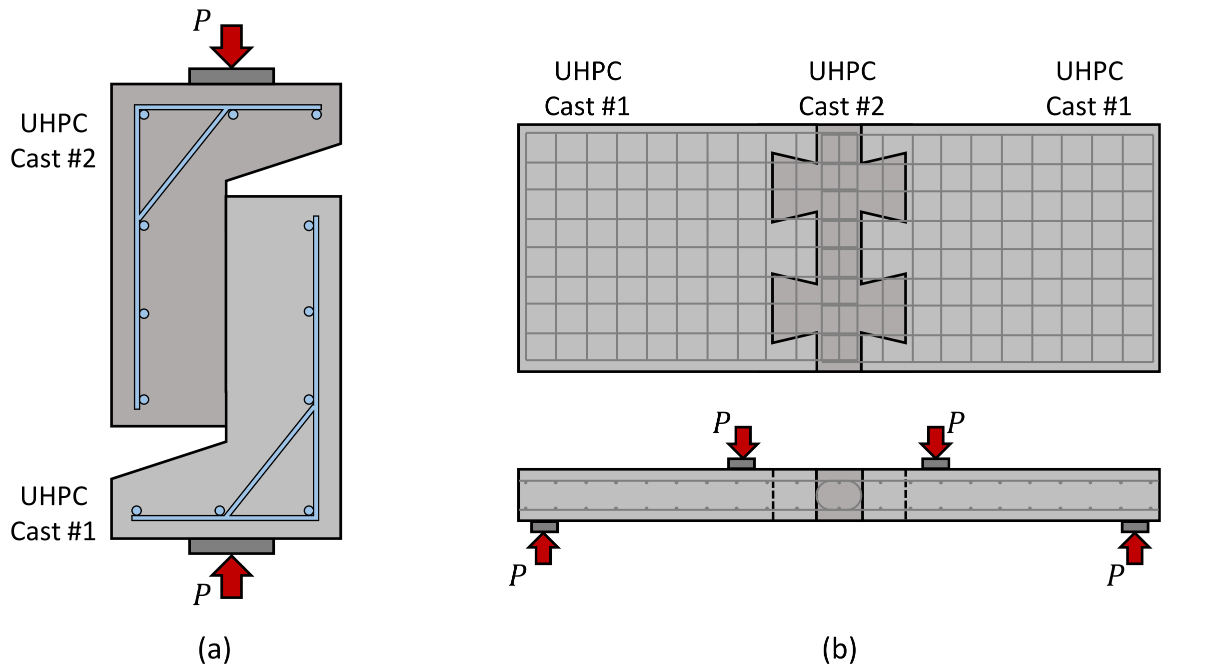

Figure 1.15. Sample specimens for UHPC-to-UHPC connections from (a) Li et al. [109] and (b) Qi et al. [110].

Semendary and Svecova [99] performed a more comprehensive investigation of precast UHPC-to-CIP UHPC bond. They investigated the bond performance using direct tension, bishear, and slant shear tests, shown in Figure 1.16, on six different interface surface textures. Semendary and Svecova [99] used a direct tension test on cylinders based on ASTM C1404 [111] as they state it was "proven by previous research to most consistently lead to interface failure" [45]. The six different surface roughnesses were one as-cast and five different form liners, based on those used by Aaleti and Sritharan [84]. They found that the bond was correlated to surface roughness.

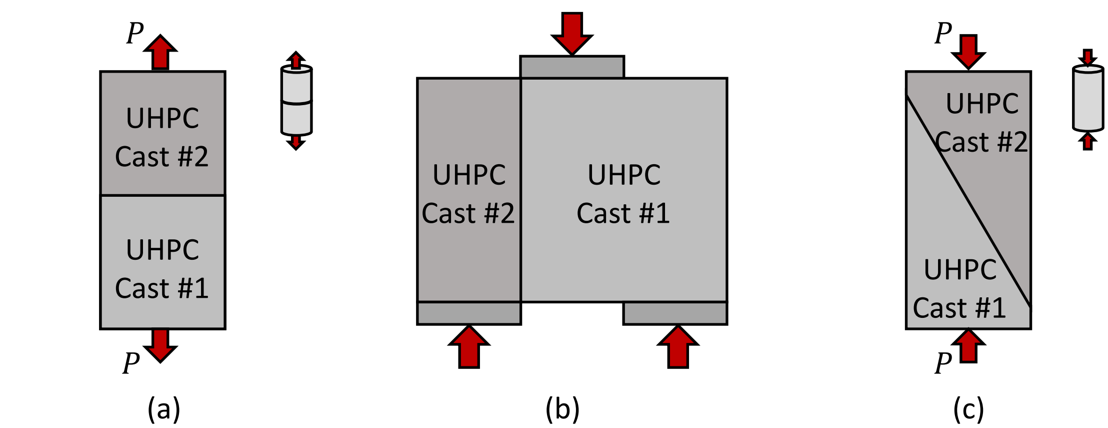

Figure 1.16. Testing performed by Semendary and Svecova [99]: (a) direct tension based on ASTM C1404 [111], (b) bishear, and (c) slant shear.

Semendary and Svecova [99] also found the friction coefficient and cohesion based on Equations 1-11 to 1-13Equation where the cohesion (c) is found based on the direct tension test and the friction (μ) from the slant shear test, where the normal stress (σ_n) is based on the applied stress and interface angle in the slant shear test. They found cohesion values between 50.7 and 127.6 psi and friction coefficients between 1.59 and 1.70. The internal friction angle (ϕ) was found using Equation 1-10 to be between 57.8° and 59.5°. They also used Carol's approach to find the cohesion and friction coefficients, which are described in other sources [55] and in the following section of this proposal.

Sturm et al. [112] also tested the shear friction material properties of UHPC, although their research was on monolithically cast UHPC. They developed a different shear test using a slotted cylinder, as shown in Figure 1.17. The researchers highlighted several advantages of their proposed shear test over other shear friction tests currently used.

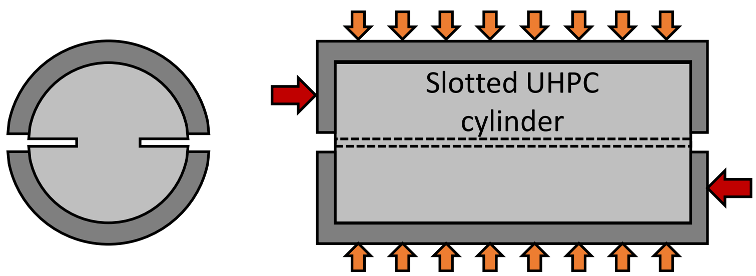

Figure 1.17. Alternate test for UHPC shear friction developed by Sturm et al. [112].

There are two additional on-going research efforts investigating the precast UHPC-to-CIP UHPC interface. One research effort is on-going with PCI, Tadros et al. [5], and the other at FHWA, Muzenski et al. [113].

Tadros et al. [5] proposed a fluted interface for UHPC-to-UHPC interfaces as shown in Figure 1.18 with a flute length of between 6 and 12 inches. This interface would be achieved using a formliner.

Figure 1.18. Fluted interface proposed by Tadros et al. [5] for UHPC-to-UHPC interfaces.

They proposed using the following design recommendations, shown in Equation 1-14 based on AASHTO LRFD BDS.

$$V_{ni} = cA_{cv} + \mu(A_{vf} f_y + P_c) \leq 0.3f'_c A_{cv}$$ Equation 1-14

The cohesion factors and coefficients of friction proposed by Tadros et al. [5] are shown in Table 1.10.

Table 1.10. Cohesion and friction factors proposed by Tadros et al. [5]

Interface Condition	**c (ksi)**	**μ**
For UHPC placed against a clean UHPC surface that is fluted	1.0	1.0
For CC placed against a clean UHPC surface that is fluted or roughened	0.4	1.4
For CC placed against a clean UHPC surface, free of laitance, but not intentionally roughened	0.075	0.6

Tadros et al. [5] did not perform any testing yet; the test specimens planned for testing are shown in Figure 1.19. The planned pushoff testing includes specimens with different CC-to-UHPC and UHPC-to-UHPC interfaces. The UHPC-to-UHPC connections have a focus on UHPC precast members and UHPC precast deck panels with CIP UHPC pocket connections. There are also several full-scale tests planned.

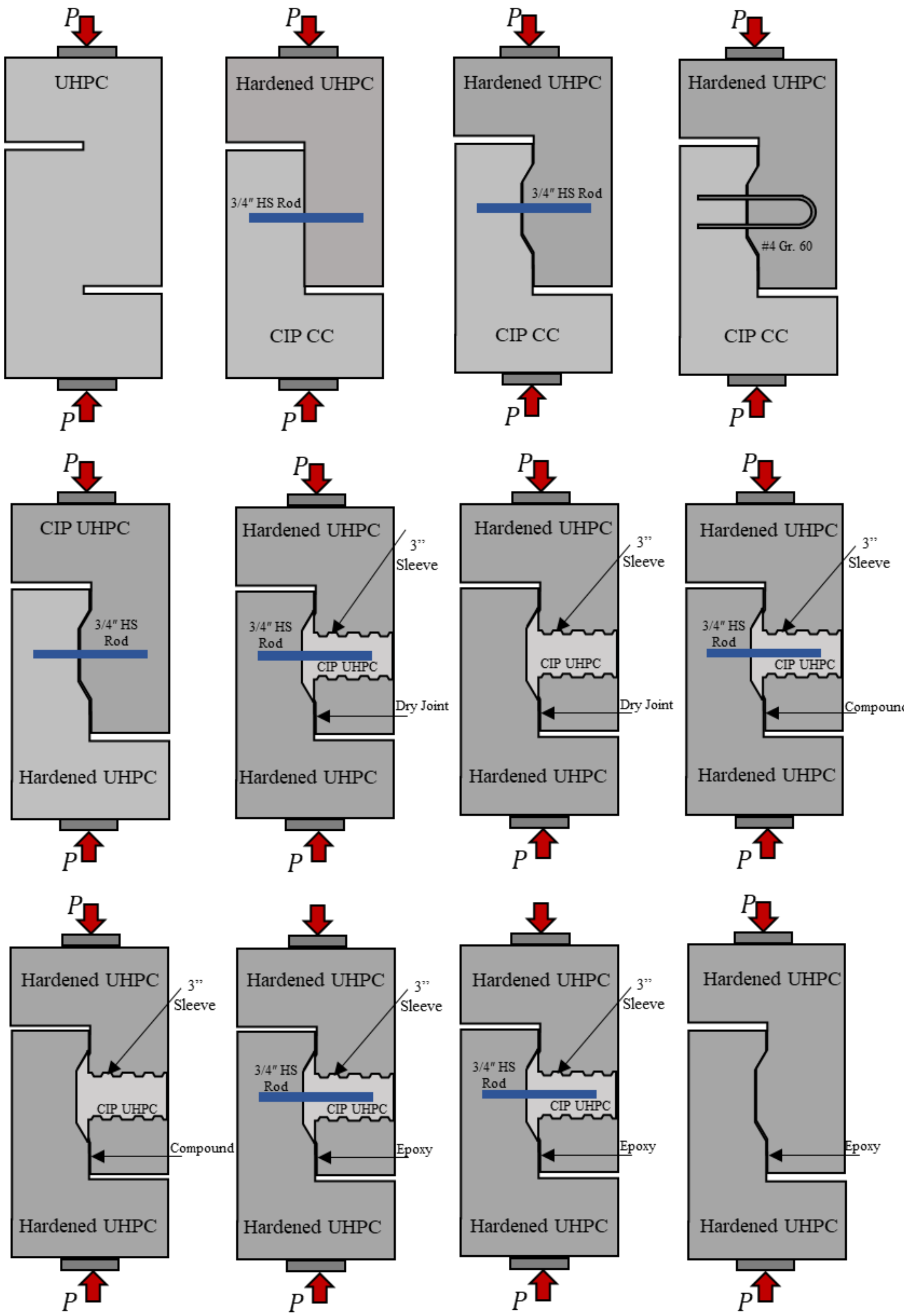

Figure 1.19. Test specimens planned for testing by Tadros et al. [5].

FHWA has been doing extensive research on UHPC for the past few decades. Some of their more recent testing is related to the interface shear behavior of UHPC [113], [114]. Muzenski et al. [113] reports on the monolithically cast specimens in the interface shear testing program. These pushoff test specimens had different amounts of reinforcement crossing the interface and different yield strengths for the reinforcement crossing the interface.

Muzenski et al. [113] used electrical resistance strain gauges on reinforcing bars and digital image correlation (DIC) to measure the strains in the reinforcement and on the surface. DIC was used to create virtual gauges as shown in Figure 1.20.

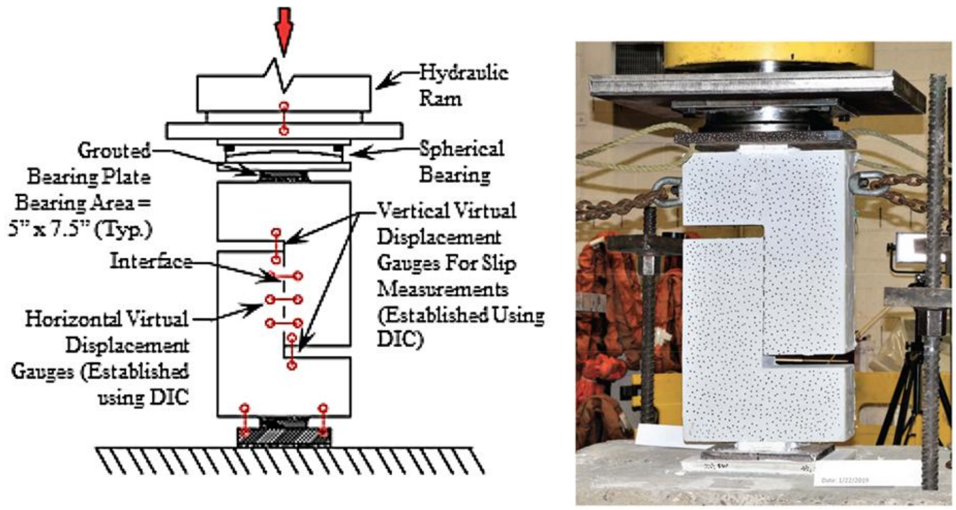

Figure 1.20. Instrumentation scheme and test setup for pushoff specimens from Muzenski et al. [113].

Muzenski et al. [113] proposed the equation shown in Equation 1-15.

$$V_{ni} = \left[\, \mu\left(A_{sv} f_s + A_{cv} \gamma f_{t,loc}\right) + A_{cv} c\right] \leq K \cdot A_{cv} \qquad \text{Equation 1-15}$$

They proposed the following values based on the results from the monolithic UHPC pushoff specimens.

μ = friction factor, 1.0 for monolithically cast UHPC

f_s = stress in steel, min [$E_s \cdot \varepsilon_{t,loc}$, f_y]

$f_{t,loc}$ = tensile strength of UHPC at localization; determined by direct tension testing, but not greater than 1.75 ksi

c = y-intercept for capacity model of monolithically cast UHPC, 1.4 ksi

γ = material reduction factor, 0.85

K = limiting shear stress capacity for monolithically cast concrete, 4.5 ksi

Muzenski [114] provided additional data with varying fiber contents to verify this equation proposed for monolithically cast UHPC. The performance of the proposed equation for all the monolically cast specimens is shown in Figure 1.21.

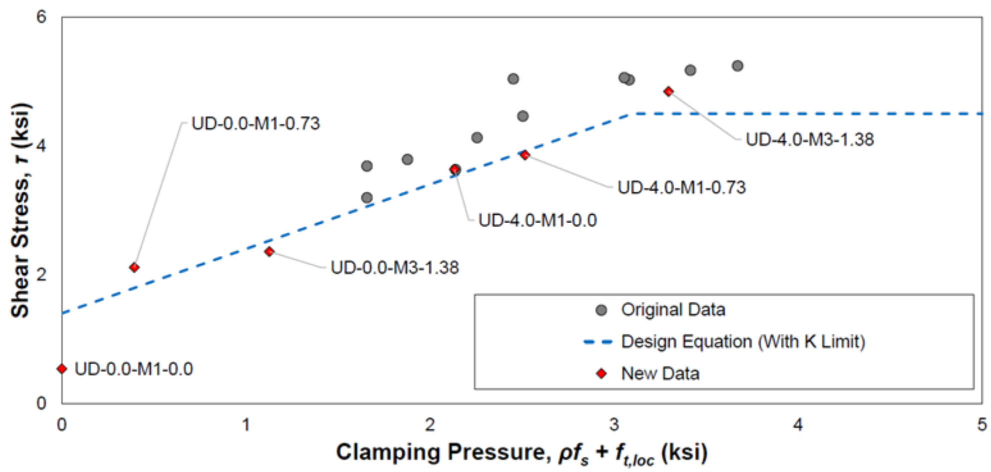

Figure 1.21. Performance of proposed interface shear equations for monolithically cast UHPC specimens from Muzenski [114].

Muzenski [114] also reported on three additional pushoff specimens with different surface conditions, shown in Figure 1.22.

(a) (b) (c)

Figure 1.22. Surface conditions tested by Muzenski [114]: (a) smooth surface, (b) plywood surface, and (c) roughened surface.

They proposed an alternate equation, Equation 1-16, for the interface capacity of the UHPC-to-UHPC cold joint.

$$V_{ni} = [\,\mu(C_1 + C_2 + P_C) + A_{cv}c] \leq K \cdot A_{cv} \qquad \text{Equation 1-16}$$

The recommended coefficients from Muzenski [114] are summarized in Table 1.11. The recommended value for C_1 ($C_1 = A_{vf}f_y$) makes Equation 1-16 essentially equivalent to Equation 1-14 proposed by Tadros et al. [5], with two primary differences. First, the cohesion term for UHPC against UHPC interface that is intentionally roughened proposed by Muzenski [114] (c =

0.075) is significantly less than the value proposed by Tadros et al. [5] (c = 1.0) shown in Table 1.10 above. Second, the limit in Equation 1-14 is based on the concrete strength ($0.3f'_cA_{cv}$), while the limit in Equation 1-16 is based on the interface condition ($1.8A_{cv}$ for intentionally roughened UHPC-to-UHPC interface). This limit ends up being significantly higher for a typical UHPC compressive strength (18 ksi) in Equation 1-14 (limit = $5.4A_{cv}$).

Table 1.11. Suggested values for non-monolithic design from Muzenski [114]

Interface Condition	Intentionally Roughened?	c (ksi)	μ	K (ksi)	C_1 (ksi)	C_2 (ksi)
UHPC against UHPC	Yes	0.075	1.0	1.8	$A_{vf}f_y$	0
UHPC against UHPC	No	0.075	0.6	0.8	$A_{vf}f_y$	0
UHPC against Concrete	Yes	0.24	1.0	1.8	$A_{vf}f_y$	0
UHPC against Concrete	No	0.075	0.6	0.8	$A_{vf}f_y$	0
Concrete against UHPC	Yes	0.075	1.0	1.8	$A_{vf}f_y$	0
Concrete against UHPC	No	0.075	0.6	0.8	$A_{vf}f_y$	0

The performance of the proposed equation and coefficients by Muzenski [114] based on test results of previous UHPC-to-UHPC joints is shown in Figure 1.23. The proposed equation and coefficients provided reasonable estimates for the limited number of tests performed to date.

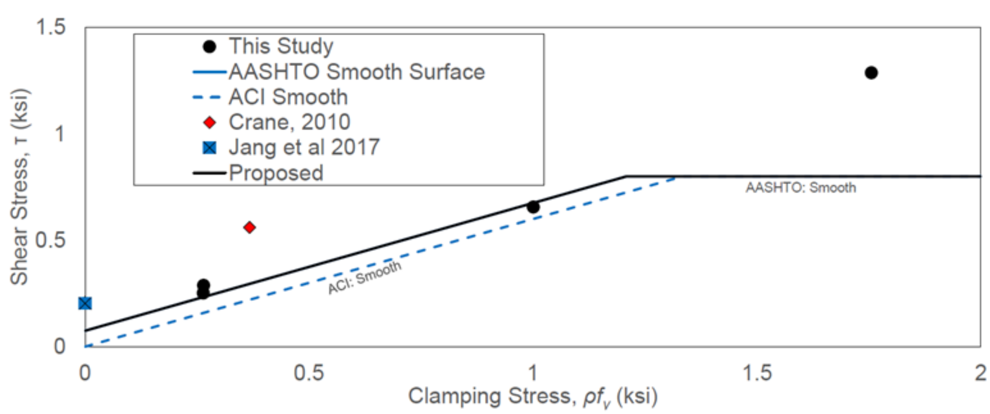

Figure 1.23. Performance of proposed equation and coefficients from Muzenski [114].

1.7 Measuring Surface Roughness

The bond strength between two different concrete surfaces depends on the surface preparation and surface roughness, as shown by the previous studies referenced above. As mentioned, many different surface preparation techniques have been used to create different levels of roughness of the interface, but a limited number of these studies measured or quantified the surface roughness of the interface.

The current provisions of ACI 318 and AASHTO LRFD BDS use a qualitative approach based on visual inspection of the surface roughness. This qualitative approach consists of comparing the interface surface to nine standard surface samples defined by the International Concrete Repair Institute [115]; this approach is dependent on technician's subjective assessment. Different ratings can lead to different estimated values, so it would be better to have an objective measure of surface roughness.

There are several different recognized methods for measuring surface roughness quantitatively. Different methods for evaluating surface roughness are summarized in Table 1.12.

Table 1.12. Comparison of roughness quantification methods, from Santos and Julio [116], [117]

Method	Non-Destructive?	Cost	Portability	Work Intensive	Contact with Surface?
Sand Patch Test	Yes	Low	Yes	No	Yes
PDI Method	No	Low	No	Yes	Yes
2D-LRA Method	Yes	Medium	Yes	No	No
3D Laser Scanning method	Yes	High	Yes	No	No
Outflow Meter	Yes	Low	Yes	No	Yes
Mechanical Stylus	No	Medium	No	Yes	Yes
Circular Track Meter	Yes	Medium	Yes	No	No
Digital Surface Roughness Meter	Yes	Medium	Yes	No	No
Microscopy	No	High	No	Yes	No
Slit-Island Method	No	Low	No	Yes	Yes
Roughness Gradient Method	No	Low	No	Yes	Yes
Photogrammetric Method	Yes	Medium	Yes	Yes	No
Shadow Profilometry	Yes	Low	Yes	Yes	Yes

There have also been several roughness parameters defined by previous researchers for quantifying surface roughness. The most frequently used roughness parameters are the average roughness (R_a), Equation 1-17; root-mean-square roughness (R_q), Equation 1-18; and the mean peak height (R_{pm}), Equation 1-19. The mean peak height can be used for considering the local variability of the surface profile not captured by R_a and R_q.

$$R_a \approx \frac{1}{n}\sum_{i=1}^{n}|z_i| \qquad \text{Equation 1-17}$$

$$R_q \approx \sqrt{\frac{1}{n}\sum_{i=1}^{n} {z_i}^2} \qquad \text{Equation 1-18}$$

$$R_{pm} = \frac{1}{5}\sum_{i=1}^{5} p_i \qquad \text{Equation 1-19}$$

Where:

z_i = the amplitude of each measurement

n = the number of discrete measurements

p_i = the maximum peak height in each sampling length

Brief summaries of the most frequently used methods for quantifying surface roughness are provided in the following section.

1.7.1 Sand Patch Method

The sand patch method, based on ASTM E965 [118], is the simplest method for quantifying surface roughness; it is the least expensive and easiest to use in both field and laboratory applications. This method is based on spreading a known volume of calibrated sand on top of the surface using a hockey puck and measuring the area of the surface that covered by sand. The mean texture depth (MTD) can be calculated according to Equation 1-20.

$$MTD = \frac{4V}{\pi D^2} \qquad \text{Equation 1-20}$$

Where:

V = the volume of sand dropped over the surface (in^3)

D = the average value of the diameter of the area covered by the sand (in)

Researchers have reported mixed results with respect to the sand patch test. Santos and Julio [116] reported issues with repeatability and differences between roughnesses measured with sand patch tests and other optical methods (2D-LRA and 3D-LS methods described later). They commented that the sand patch test is not an ideal test for distinguishing between smooth to slightly rough surfaces. Sample photographs of their sand patch test results are shown in Figure 1.24.

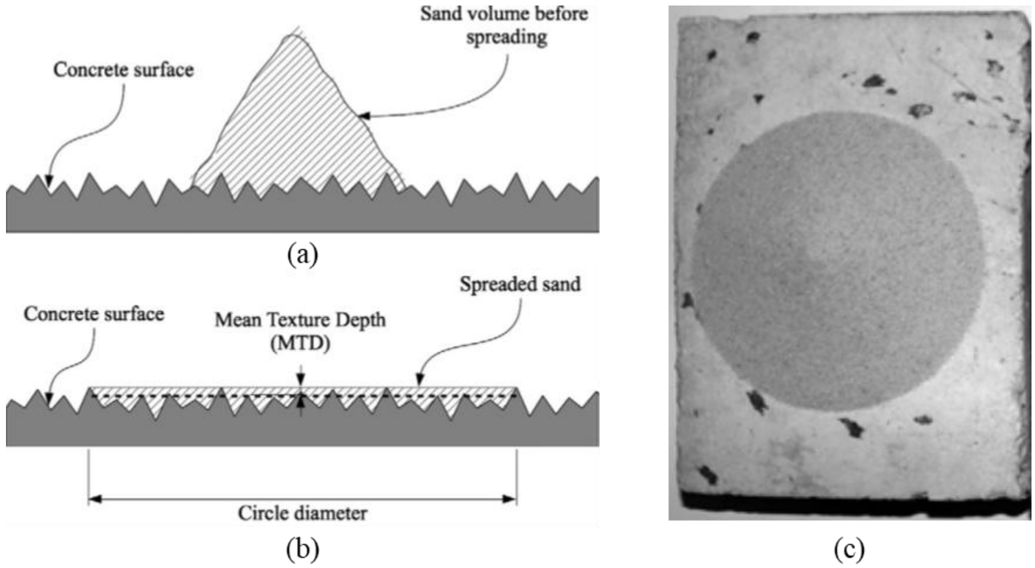

Figure 1.24. Sand pitch test, (a) before spreading, (b) after spreading, and (c) sample of sand after spreading from [116], [117].

This method was also used by several other researchers testing the bond behavior between concrete materials [84], [99]. Semendary and Svecova [99] found differences between the roughness parameter measured using a close proximity scanner (LS-40 Pavement Surface Analyzer) and the sand patch test results reported by Aaleti and Sritharan [84] for similar form liners.

1.7.2 Processing Digital Image (PDI Method)

The processing digital image (PDI) method was first introduced by Santos and Julio [119] for measuring surface roughness. This method is based on numerically processing a captured digital image of the profile of the surface roughness, shown in Figure 1.25 (a). The image of the side profile of the image is processed using a common software package, Figure 1.26 (b), to obtain the surface roughness profile along the length of the sample. The roughness profile is then used to determine the appropriate roughness parameters. This test is not completely in situ; a sample is prepared by putting epoxy over the surface and then sawing on a plane perpendicular to the interface. This process must be completed in a lab and is time consuming. While this method has been successfully used in past research, it is important to capture images with the same lighting condition, angle and constant distance from the concrete surface to get consistent results with high accuracy [120].

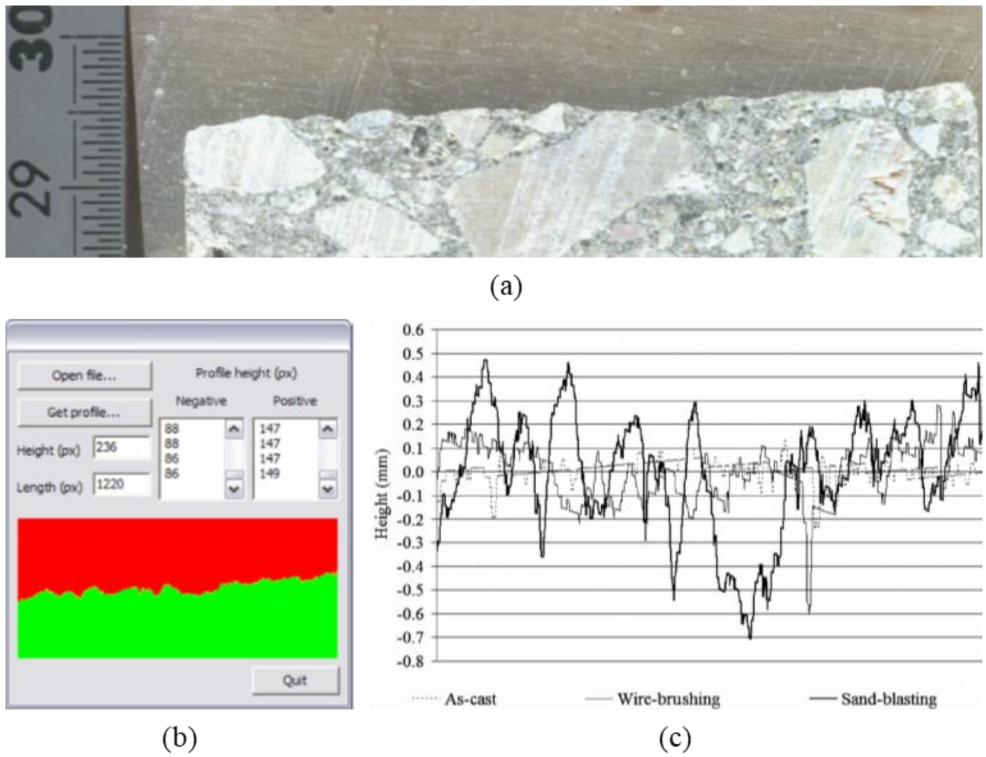

Figure 1.25. Processing digital image (PDI) method from Santos et al. [119]: (a) digital image of surface roughness, (b) 2D roughness profile, and (c) roughness profiles for different finishes.

Santos and Julio [117] further developed the PDI method and created a laser scanning device to create a 2D profile like that shown in Figure 1.25 (b). The authors called this the 2D laser roughness analyzer (2D-LRA) method.

1.7.3 3D Laser Scanning Method

The 3D laser scanning method captures a 3D sample of the concrete surface instead of a 2D profile. A sample 3D laser scanner and scanned surface are shown in Figure 1.26. The concept is generally similar to that of the PDI and 2D-LRA methods, where a laser scanner is used to create a digital surface profile that is then used to generate the desired roughness parameters. The accuracy and resolution of the scanner are important variables for choosing the right scanner for measuring the surface roughness. A 3D scanner with a maximum resolution of 0.0015 inches was previously used and shown to have adequate accuracy for smooth surfaces [116]. Higher resolution may be required depending on the roughness of the surface. 3D scanners have been used in several studies [95], [116], [120] to quantify the level of surface roughness of an interface.

(a) (b)

Figure 1.26. (a) 3D scanner from Santos and Julio [117] and (b) sample of 3D scan of exposed aggregate finish from Valikhani et al. [120].

1.8 UHPC Durability and Corrosion Resistance

UHPC is generally thought to mitigate the corrosion of reinforcing steel due to its low permeability. However, this characteristic pertains to uncracked, bulk UHPC; water and chlorides are still able to reach reinforcing steel at cracks in the UHPC or at interface cracks. This highlights the importance of having adequate bonding of CIP UHPC to the substrate concrete material to prevent the formation of interfaces where preferential transport of aggressive chemical species (such as chloride ions and water) as well as water retention can occur. In this case, steel corrosion in the bulk UHPC is expected to be low, but localized corrosion at the interface can still occur. Research by Lau et al. [121] showed that localized steel corrosion developed on rebar intersecting a crack on bridge piles constructed with high-performance concrete. Fast chloride penetration was observed through the concrete crack while very low chloride diffusion occurred on the adjacent concrete surfaces. Isolated incidences may not create severe corrosion conditions, but adverse orientation of the crack to the embedded rebar and fast chloride penetration can lead to more severe corrosion. The high concrete resistivity in UHPC was shown to beneficially minimize microcell and to some extent macrocell corrosion coupling of the steel [122]. Depending on the crack width, penetration, and exposure environments, concretes with a low water-to-cement ratio may have unreacted cement and binders that can allow for some level of self-healing [123].

In addition to the corrosion of embedded steel rebar, the metal fibers at the interface of UHPC can also corrode during construction, as well as due to exposure to the environment in service. The discontinuous distribution of fibers in UHPC can allow for stresses to be distributed and thus minimize large cracks, but as reported by Shin and Yoo [124], localized corrosion of steel fibers can occur at the microcracks (subject to fast chloride penetration). Fiber-reinforced concrete develops tensile capacity due to the pull out of the fibers rather than fracture. Yoo et al. [125] reported improved tensile performance for fibers with some level of corrosion if a pullout failure mode was dominant.

One solution for addressing the corrosion concern at interfaces would be satisfied by applying corrosion inhibitor material. There have been some studies that tried to evaluate the effectiveness of corrosion inhibitors. Anodic corrosion inhibitors like calcium nitrite were used in different conditions to assess their effectiveness [126]. The calcium nitrite reacts to facilitate stable oxide films on the steel interface to elevate the critical chloride threshold concentration and maintain passive conditions. The dosage level of nitrite to chloride ions was reported to be ~1 [127]. At higher chloride contamination levels, greater amounts of inhibitor are required. It was shown that such inhibitors are effective on non-carbonated concrete with a relatively low level of chloride or carbonated concrete without chloride. In other words, calcium nitrite is potentially helpful for places with no corrosion to fairly low corrosion conditions [126]. This outcome may be generalized for other available inhibitors as they are designed to prevent corrosion and not designed to treat or stop active corrosion. However, more studies are required for evaluating the effectiveness of available inhibitors like DCI® [128] that comes in liquid form and can be mixed with other constituents

2. TEST METHODOLOGY

The testing was made to evaluate the bond between precast UHPC and cast in place (CIP) UHPC by various test methods such as by tensile pulloff, flexural bond, and shear pushoff testing. An overview of these tests is provided in this section. All of these tests require UHPC to be cast at two separate times to create a cold joint at the interface.

2.1 Concrete Bond Tests

2.1.1 Tension Pulloff Test

Direct tension pulloff test is based on ASTM C1583, Standard Test Method for Tensile Strength of Concrete Surfaces and the Bond Strength or Tensile Strength of Concrete Repair and Overlay Materials by Direct Tension (Pulloff Method). This test provides conservative results compared with other test methods [50] and can be used for determining the cohesion factor at interface.

SRC has the James Bond Tensile Strength Test (P-C-7300) apparatus, as shown in Figure 2.1. This equipment can be used to determine the tensile strength of an interface using 2-inch diameter cores through the overlay and substrate materials.

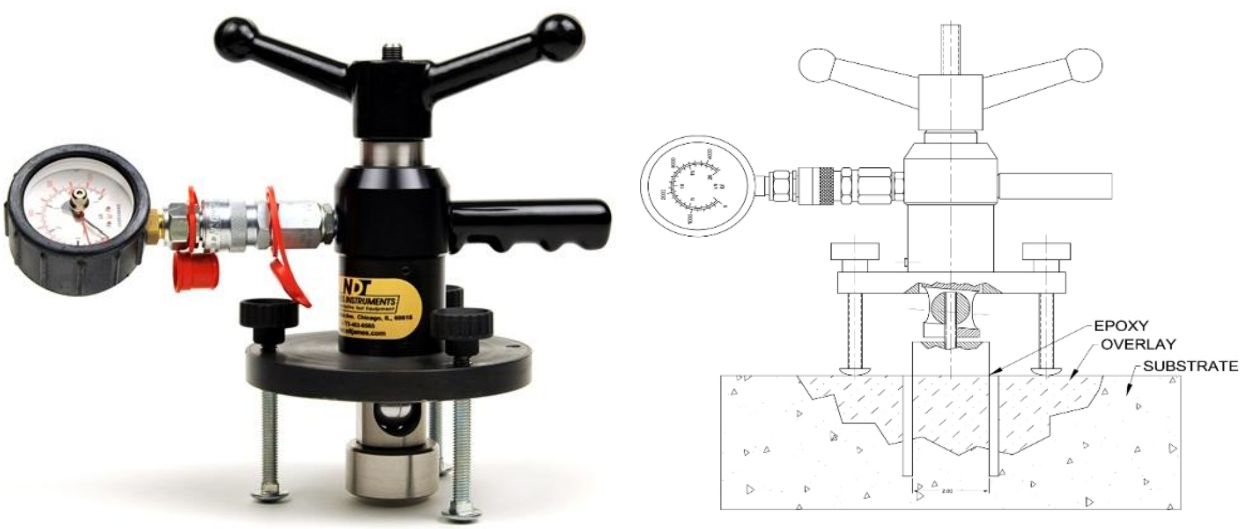

(a) (b)

Figure 2.1. The equipment for tensile strength of overlays; (a) P-C-7300 James Bond Test System and (b) tensile test core diagram [129].

This test has been used by previous researchers. The proposed specimen size for this study is shown in Figure 2.2 which is based on previous studies that used same test method [47] [50]-[52] [99], [130]. The three alignment plates (or leveling feet) of the James Bond Test™ MK III are spaced around the circumference of a 6-inch diameter circle; the 3-inch edge distance from center of the core will ensure all three alignments plates can rest on the specimen during testing.

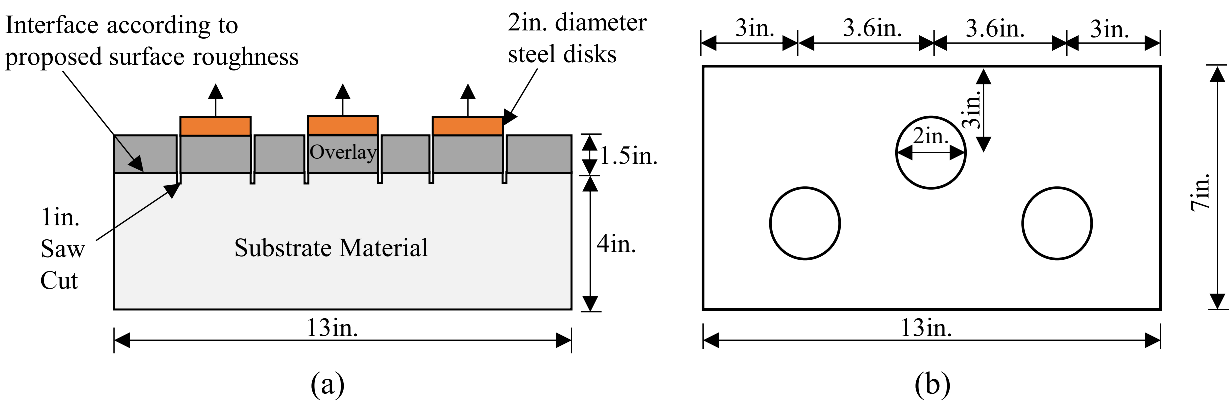

Figure 2.2. Specimen geometry for direct tension pulloff test, from Harris et al. [51].

The thickness of the overlay for this test was 1.5 inches, and the substrate thickness was 4 inches. Each test block provides three cores. The interface between overlay part and substrate will be according to the research text matrix without using any external bonding agent between two parts.

The lowest measured values by Semendary et al. [99] (0.051 ksi) are associated with an as-cast surface. Higher values by Graybeal [100] (0.651 ksi) were on a UHPC substrate prepared with hydro-demolition and failure at the interface. Semendary et al. [99] also measured the direct tensile strength of a monolithic UHPC using their test method and found the mean tensile strength to be 0.650 ksi.

2.1.2 Shear Pushoff Test

The shear pushoff test was used for this research as it measures direct shear at a reasonable scale and allows for easier inclusion of reinforcement crossing the interface and isolation of the effects of this reinforcement. The specimen size for pushoff tests is shown in Figure 2.3 and 2.4.

The size of the specimens used for pushoff tests has changed over time since the first tests by Hofbeck et al. [63] in 1969. The size of specimens has generally increased for different reasons including allowing for sufficient development lengths of larger internal steel reinforcement with larger required bend diameters [92] and to increase cover [113]. In general, however, the length of the interface plane is 12 inches and width of the specimens between 5 and 7.5 inches. The width of the specimens of Crane [92] was 7.25 inches, which corresponded to the width of typical 2x8 lumber. A size like that used by Crane [92], shown in Figure 2.4 was used for this testing. This is based primarily on the volume of UHPC available during one cast and the proposed number of specimens per cast.

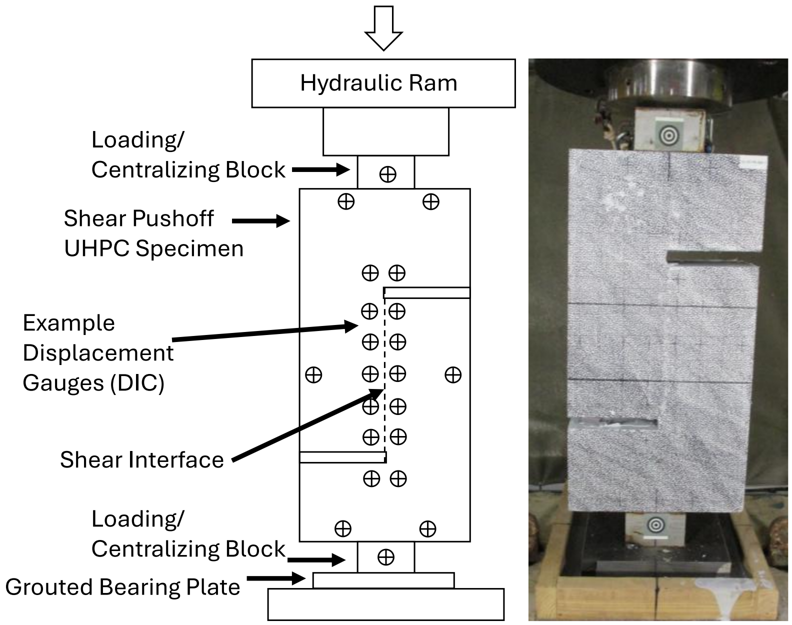

Figure 2.3. Example of pushoff test setup.

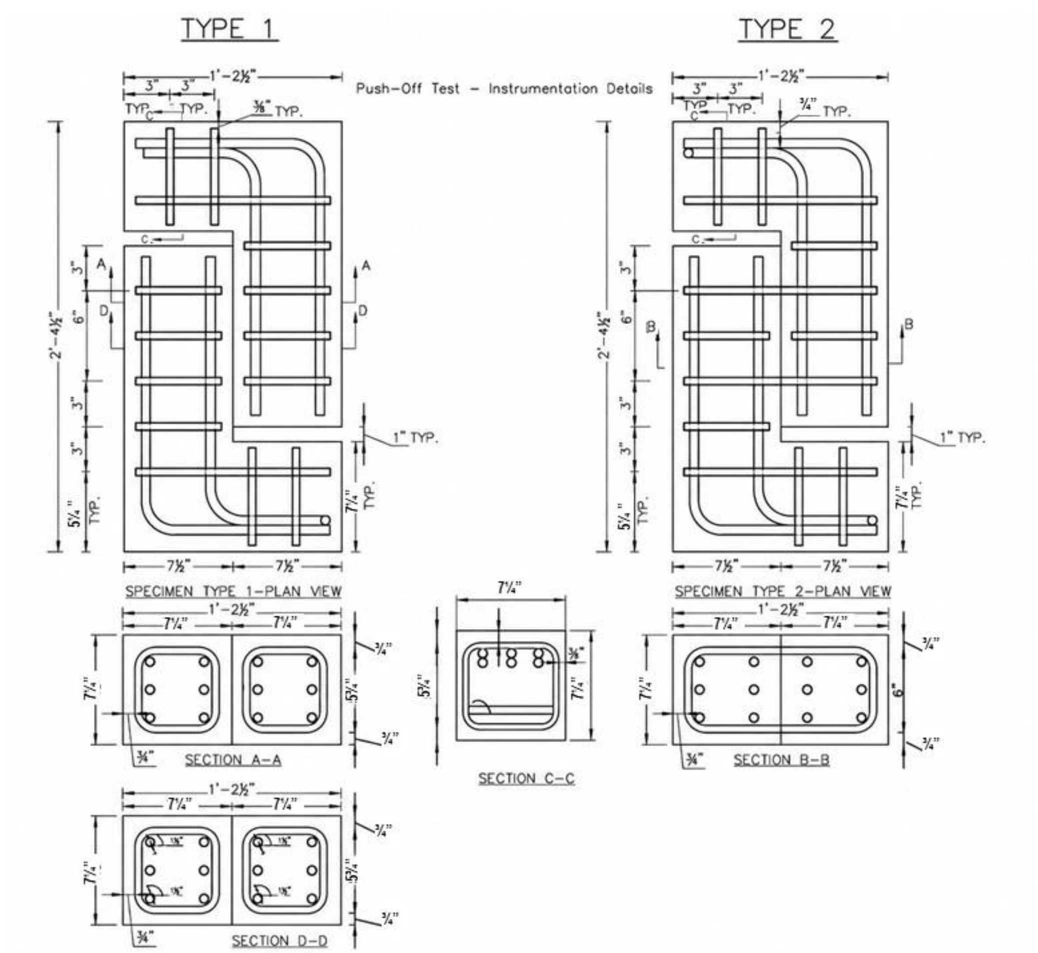

Figure 2.4. Example of shear pushoff specimen geometry and reinforcement.

2.1.3 Flexural Bond Test

The test that is typically used to evaluate the flexural bond strength is a modified modulus of rupture test with third point loading [131], shown in Figure 2.5. The flexural bond strength at the interface is considered sufficient (i.e., greater than the flexural strength of the surrounding materials) if the failure occurs in the substrate material and not at the interface [50]. The flexural bond strength of the interface can be found from the measured strength if failure occurs at the interface, which is the most likely outcome of the testing of UHPC-to-UHPC interfaces.

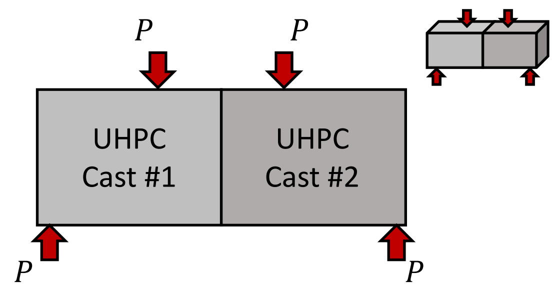

Figure 2.5. Modified modulus of rupture test to evaluate interface bond strength under flexural stresses.

The flexural tests were performed in accordance with ASTM C1609. The specimen size for the flexural bond tests will be the same as the modulus of rupture material testing performed on the substrate and cast-in-place (CIP) materials to allow for a direct comparison of the flexural bond strength with the flexural strength of the substrate and CIP materials.

Different prism sizes have been used previously by other researchers for modulus of rupture testing of UHPC. Prism specimens with 3 in. by 3 in. by 11 in. size and an effective span length of 9 in. were used to determine the flexural behavior of non-proprietary UHPC concrete [3]-[4], [24]. Prism specimens with 4 in. by 4 in. by 14 in. size and an effective span length of 12 in. were used by Tadros et al. [5]. Prism specimens with 6 in. by 6 in. by 20 in. or 24 in. size and an effective span length of 18in. were also used in previous studies [77]-[78]. The size of the prisms for the modulus of rupture material tests and flexural bond tests is 4 in. by 4 in. by 14 in. with 12-in. effective span length.

2.2 Experimental Variables

The variables initially proposed to be investigated are summarized in Table 2.1Table 2.1. These variables include UHPC mix design (both proprietary and non-proprietary), concrete strength and age (of both the precast and field-cast UHPC), surface (form) treatment method, mechanical surface roughness, pre-wetting procedures, and the condition of steel fibers at time of placement of the field-cast UHPC.

Table 2.1. Experimental variables

Experimental Variable	Values for Test Matrix
Type of UHPC Mixture	Proprietary (different producers), non-proprietary (different mixture designs and constituent materials)
Age of substrate UHPC at time of CIP UHPC placement	28 days[1], 90 days[2]
Age of CIP UHPC at time of testing	7 days[3], 28 days[4]
Substrate surface condition	Smooth (plywood), paste retarder, different form liners
Prewetting procedure	None, spraying, wet burlap, water ponding (SSD)
Condition of steel fibers	Clean fibers, pre-corroded
Reinforcement crossing the interface plane	Different amounts of reinforcement and/or other mechanical connectors crossing the interface

1. Actual age ranged from 21-34 days, with extended times for Set 5. 2. Actual age 91 days. 3. Actual age ranged from 6-8 days 4. Actual age ranged from 27-62 days, with extended times for Set 5. See Table 2.8 for schedule.

The type of UHPC and age of the UHPC at time of testing will dictate the strength of the UHPC, so the UHPC strength is not included as a variable in Table 2.1. Additionally, reinforcement crossing the interface plane will be an experimental variable only investigated in one type of test (pushoff). These factors were considered when developing the proposed experimental matrix.

The UHPC type, age, strength, and other related properties will affect the bond performance of the interface between UHPC substrates and CIP UHPC materials. This section summarizes the different considerations and options related to proprietary, prebagged UHPC mixtures and non-proprietary UHPC mixtures.

2.2.1 Proprietary UHPC

Prebagged UHPC materials are available from several different suppliers. Additionally, each supplier typically has several different mixtures based on application. The research considered a prebagged UHPC option, referred throughout as UHPC Material A.

Table 2.2 shows a summary of specified mechanical properties for proprietary UHPC mixtures considered.

Table 2.2. UHPC Material A characteristics reported by manufacturer

Material	**Fiber%**	**Compressive Strength (ksi)**		**Flexural Tensile Strength (ksi)**		**Ultimate direct tensile strength(ksi)**
		7-day	28-day	7-day	28-day	28-day
UHPC Material A	2	15.8	21.5ksi	6.121	>6.527	2.582

2.2.2 Non-Proprietary UHPC Options

A commercially available non-proprietary UHPC, referred to as UHPC material B, was used for this research. Strengths provided by the manufacturer are shown in Table 2.3 and 2.4.

Table 2.3. Compressive strength for UHPC Material B reported by manufacturer

Value	**Laboratory-Cured, End Ground**	**Match-Cured, End Ground**	**Match-Cured, Capped**
Average	19.0 ksi	19.8 ksi	21.8 ksi
St. Dev.[1]	0.150 ksi	0.060 ksi	0.530 ksi

[1]standard deviation from 3 test samples

Table 2.4. Flexural properties at 28 days for UHPC Material B reported by manufacturer

Value	**First-Peak Flexural Strength (psi)**	**Peak Flexural Strength (psi)**	**Peak Flexural Strength (% of first-peak)**	**Residual Flexural Strength at L/300 (% of first-peak)**	**Residual Strength at L/150 (% of first peak)**
Target Min.	1,500	2,000	125%	90%	75%
Average	1,960	3,170	162%	160%	137%
St. Dev.[1]	160	165	7%	5%	8%

[1]standard deviation from 3 test samples

2.2.3 Age of UHPC Substrate at Time of Placement of CIP Material

The age of the UHPC is one factor that will dictate the extent of cement hydration that has occurred, which correlates to the concrete strength. The age of the UHPC substrate at time of casting for the CIP UHPC and the age of the CIP UHPC at time of testing will both likely affect the bond performance. The time between casting of the substrate and joint UHPC may be several months or more in the field. Substrate age of 28 and 90 days were considered

2.2.4 Surface Roughness

The surface roughness or surface texture is an important parameter for the bond strength. The effect of different surface conditions on bond strengths was studied in several previous experimental studies by intentionally roughened surfaces. Different methods for roughening a surface included formliners and surface paste retarders. Pressure water cleaning to remove concrete laitance from the use of paste retardants was used. Considering the high compressive strength and hardness of UHPC, some methods like wire brushing or grooving may require more effort compared to conventional concrete and can damage and break exposed steel fibers.

***Paste Retarders*:** Paste retarders are commonly used for conventional concrete to achieve exposed aggregate finishes. Paste retarders are painted on forms within 24 hours before casting, following manufacturer instructions. A pressure washer is used within 24 hours after casting to wash away the wet paste and leave the exposed aggregate finish. Different grade paste retarders can be used to achieve different magnitudes of surface roughness for conventional concrete.

Paste retarders have been used for UHPC with varying degrees of success. MasterBuilders HV Grey paste retarder [132] left a roughened surface with exposed fibers. Two different paste retarders were used including a solvent based MFinish HV78 and a water based MFinish XR48 Pink. The HV78 grey paste retarder was described by the manufacturer to provide a deep etch greater than 3/4 inch. The XR48 pink paste retarder was described by the manufacturer to provide a medium light etch of 3/8 to ½ inch.

***Formliners*:** Formliners are primarily designed to create architectural finish on concrete surfaces. These forms are usually made using plastic or urethane. There have been a few previous studies where formliners were used to create different concrete surface roughness for bond strength evaluations [92] [133]. There are several different formliner manufacturers that typically provide single use formliner made from styrene and multi-use plastic base formliners. Two formliners from US Formliner were used (Figure 2.6): 2/92 RIO BRAVO (granulation 0.15 inch) and 2/76 NIL (granulation 0.31 inch).

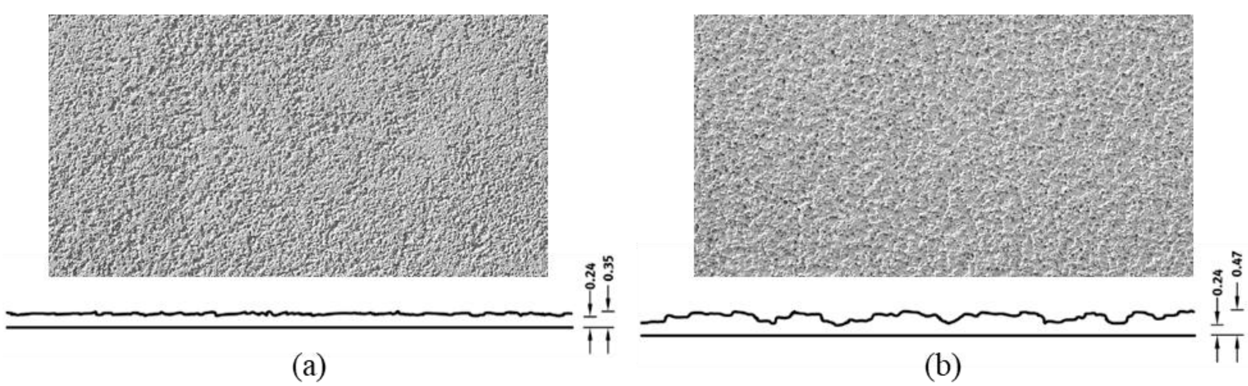

Figure 2.6. Formliners to be used from US Formliner: (a) 2/92 Rio Bravo and (b) 2/76 Nil.

2.2.5 Prewetting Condition

The surface preparation of the substrate UHPC prior to casting of the CIP UHPC may also affect the bond between the two materials. Previous researchers [50] have found that the interface moisture (e.g., dry, water spraying, wet burlap, and water ponding) affects the bond between CC substrate and CIP UHPC.

Prewetting conditions have been studied in several previous studies on bond interface. One study on bond behavior between two conventional concrete surfaces found that pre-wetting the substrate surface did not show significant change in bond strength [47]. A second study by Graybeal [50] investigating the effect of prewetting on the interface between CC and UHPC found that both wet burlap and saturated surface dry (SSD) conditions enhance the tensile bond strength. Graybeal [50] investigated four different conditions:

Control:	No surface preparation performed
Water spraying:	Sprayed water on concrete substrate immediately before joint casting
Wet burlap:	Place wet burlap on the substrate 2 to 3 hours before joint casting
Water ponding:	SSD was achieved by ponding water for 24 hours prior to casting and drying the surface with a paper towel right before joint casting

In an additional study investigating bond between UHPC and conventional concrete, it was shown that saturated substrate concrete provides some moisture to help hydration of UHPC during the curing time which increases the cohesion at interface and increases the bond strength [77], [134].

Surface wetting is often prescribed for conventional concrete to promote wetting of coarse aggregate and promote cement hydration at the interface surface. However, UHPC does not contain coarse aggregate and is expected to develop a highly impermeable bulk material. It was thought that wetting regimes just prior to matchcasting would simply create a surface wet condition similar to a surface spray condition. Instead, the burlap and water immersion regimes were made immediately after demolding of the substrate concrete 1-5 days after casting. The prolonged wetting would affect the degree of cement hydration of the interface surface layer. For this research program, a 'dry' condition was considered by maintaining demolded specimens in ambient indoor sheltered laboratory conditons, a'spray' condition where tap water was sprayed onto the concrete interface surface just prior to casting, a 'wet burlap' condition where a prolonged wetting condition was maintained after demolding up to the time of casting, and a 'wet ponding' condition where a saturated calcium hydroxide solution was ponded on the interface surface ~1 week after demolding up to the time of casting.

2.2.6 Pre-corroded Exposed Steel Fibers

The next variable investigated is the condition of exposed steel fibers at the time of casting of the CIP UHPC portion of the specimens. Initial research plans were ambitious to consider various fiber corrosion conditions: (1) clean, (2) naturally conditioned, (3) salt fog, and (4) water ponding. The salt fog condition was intended to create an accelerated rust layer around all the exposed fibers to assess the influence of accumulated corrosion products on fiber slip and development length. The water ponding will create localized pitting corrosion at the base of the fibers to identify role of possible loss of tensile strength. However, the number and size of specimens made this effort prohibitive. Also, the exposed steel fibers were found to not extend out of the interface surface plane. Instead, corrosion of exposed steel fibers was made by prolonged wetting under burlap saturated with a 5% NaCl solution. Some test conditions where the specimens were ponded, used a 5% NaCl calcium hydroxide solution to promote corrosion.

Paste retarders were used on the UHPC substrate to attempt to create a surface condition with exposed steel fibers.

Several modes of corrosion conditioning were made depending on the incorporation of surface wetting. These conditions include:

Clean Fibers**:** Specimens that were used for the 'Dry' and 'Spray' surface wetting conditions were left in ambient dry indoor laboratory conditions, where rust development was mitigated. Specimens that were used in the 'Wet Burlap' wetting condition were maintained in a sealed container with application of a vapor-phase corrosion inhibitor. Specimens that were used in 'Wet Ponding' wetting conditions had its interface ponded with a saturated calcium hydroxide solution to promote steel corrosion passivation.

Pre-Corroded Fibers**:** Specimens that were used for the 'Dry' and 'Spray' surface wetting conditions were initially subjected to a 5% NaCl solution wetted burlap placed on its interface surface that was periodically manually maintained and inspected until observation of rust development on the exposed fibers. At that time, the specimens were allowed to dry in the ambient dry indoor laboratory environment until time of matchcasting. Due to the low permeability of the UHPC, this drying process was considered to be sufficient.

Specimens that were used for the 'Wet Burlap' surface wetting condition were maintained in the wet burlap containing the chloride solution until the time of resetting the formwork for the matchcast. A wet burlap was placed on the interface surface until the time of the matchcast.

Specimens that were used for the 'Wet Ponding' surface condition had its ponding solution made of a 5% NaCl saturated calcium hydroxide solution. The salt concentration exceeded the chloride threshold concentration in the pH~12.6 solution. Specimen interface surfaces were subjected to the salt solution until the time of resetting the formwork; at which time, a wet burlap was placed on the interface surface until matchcasting.

Carbonation-induced corrosion of the steel at the concrete-to-air interface and corrosion of fibers embedded below the interface surface was not expected to be significant, so the surface rusting of the exposed fiber was expected to be the dominant corrosion characteristic.

Evaporation of solution was minimized by the development of an irrigation system where a slow-drip nozzle was used to introduce small amounts of tap water onto the surface of the wetted specimens enclosed within plastic bins. This exposure condition helped to assess the effects of localized fiber cross-section loss on promoting fiber rupture during loading.

It is anticipated that the mode of fiber corrosion at the UHPC-to-UHPC interface can have different effects on the mechanical behavior. If excessive surface corrosion and localized cross-section loss does indeed have significant impact on the mechanical behavior of the joint, corrosion mitigation techniques may be employed. One test case considered washing of corrosion products. Vapor phase inhibitors can dissipate upon exposure of the surface to the open atmosphere and additional surface cleaning prior to matchcasting. The efficacy of a vapor phase corrosion inhibitor was explored and its effects on bond will be considered.

2.2.7 Reinforcement Crossing the Interface Plane

The shear friction capacity of an interface is partially governed by the normal force across the interface. The normal force crossing the interface is also required to determine the cohesion coefficient and coefficient of friction. Shear friction interfaces often do not have an actively applied normal force; however, a normal force is created as the plane begins to slide if there is reinforcement crossing the interface. Codes and specifications will typically determine the normal force from the reinforcement by taking the area of reinforcement crossing the interface times the yield strength of the reinforcement. At least two reinforcement ratios for the reinforcement crossing the interface were tested in the shear pushoff tests to determine the cohesion coefficient and coefficient of friction.

Different reinforcement ratios have been tested by various researchers [62] [92] [113] [135]. In general, research results have always shown a linear relationship between shear stress (v_u) and clamping pressure or clamping stress (τ_n), where clamping stress is the reinforcement ratio times stress in reinforcement. Early shear pushoff tests on conventional concrete specimens used reinforcement ratios between 0.002 and 0.0248, which would correspond to clamping stresses between 0.100 and 1.25 ksi (with stirrup yield stresses around 50 ksi) [62] [135]. Kahn and Mitchell [64] later used eight legs of stirrups across the interface at 2-inch spacing, which resulted in a reinforcement ratio of 0.0147, which corresponds to clamping stress of 0.882 ksi.

Muzenski et al. [113] investigated monolithic UHPC-to-UHPC interfaces with clamping pressures between 0 and 3.31 ksi (2.76% reinforcement), assuming reinforcement yielded with three different grade steels. They measured the stress in the reinforcement crossing the interface and found the reinforcement to not reach yield for most specimens above a 0.83 ksi clamping stress (1.38% reinforcement). They found a linear relationship between shear stress and clamping pressure for this large range of clamping stresses, where the actual stress in the reinforcement was used to calculate clamping stress at peak loads. Two other researchers investigating different clamping stresses on UHPC pushoff specimens were Crane [92] and Wu et al. [136]. Crane [92] tested two different clamping stresses, 0 ksi and 0.30 ksi (0.50% reinforcement). Wu et al. [43] tested four different clamping stresses between 0 ksi and 2.5 ksi (3.1% reinforcement). Wu et al. [136] also found a linear relationship between shear stress and stirrup ratio. Reinforcement across the shear plane is usually in the form of closed stirrups around longitudinal reinforcement, so an even number of reinforcing bars is generally provided. Some examples of using cross reinforcement in shear plane are shown in Photo 2.1. Examples of the placement of rebar (foil) strain gages and fiber optic strain gages are shown in Photo 2.2.

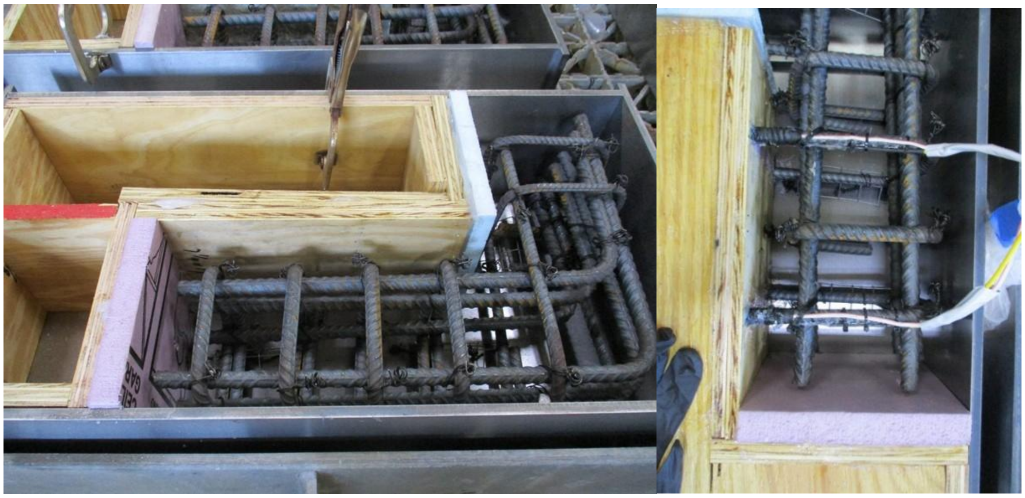

Photo 2.1. Reinforcement crossing shear plane on shear pushoff test (left: ρv=0 and right: ρv=9.2e-3).

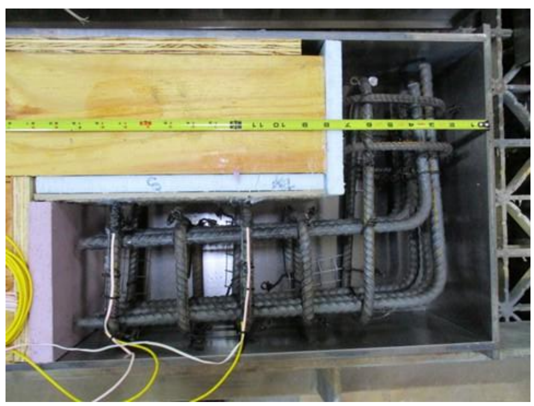

a)

b)

Photo 2.2. Placement of rebar strain gage and fiber optic strain gages on a) matchcast pushoff specimens and b) monolithically cast specimens.

Several different options for shear pushoff specimen size and interface reinforcement are shown in Table 2.5.

Table 2.5. Reported research reinforcement crossing the shear interface in pushoff test specimens

#	Pushoff Test Size	A_{cv} (in^2)	Rebar Details	A_{sv} (in^2)	ρ_v	f_y (ksi)	τ_n (ksi)
1	Crane (2010)	87	2 - U.S. No. 3	0.22	0.0025	60	0.152
2	Crane (2010)	87	4 - U.S. No. 3	0.44	0.0051	60	0.303
3	Crane (2010)	87	6 - U.S. No. 3	0.66	0.0076	60	0.455
4	Crane (2010)	87	2 - U.S. No. 4	0.40	0.0046	60	0.276
5	Crane (2010)	87	4 - U.S. No. 4	0.80	0.0092	60	0.552
6	Crane (2010)	87	6 - U.S. No. 4	1.20	0.0138	60	0.828
7	Tadros et al. (2021)	60	2 - U.S. No. 3	0.22	0.0037	60	0.220
8	Tadros et al. (2021)	60	4 - U.S. No. 3	0.44	0.0073	60	0.440
9	Tadros et al. (2021)	60	6 - U.S. No. 3	0.66	0.0110	60	0.660
10	Tadros et al. (2021)	60	2 - U.S. No. 4	0.40	0.0067	60	0.400
11	Tadros et al. (2021)	60	4 - U.S. No. 4	0.80	0.0133	60	0.800
12	Tadros et al. (2021)	60	6 - U.S. No. 4	1.20	0.0200	60	1.200

Testing here used a specimen size similar to Crane [92] with a clamping stress close to 0.5 ksi, which can be achieved with four #4 bars across the interface.

2.3 Experimental Matrix

2.3.1 Testing

The experimental matrix is introduced in this section. The experimental matrix was developed based on the experimental variables discussed in Section 2.2 and logistical limitations (e.g., mixer capacity, timeframe, budget). All of the UHPC mixing was conducted at FDOT's Structures Research Center (SRC). The SRC has two different high-shear mixers available that have previously been used to successfully mix UHPC [105].

***Mixer System Horizontal Shaft Mixer*:** This mixer, shown in Figure 2.7 (a), has been used for Lafarge Ductal supersack mixes with volume of 0.665 cubic yards (18.0 cubic feet) [34]. SRC staff later communicated a maximum volume of 0.550 cubic yards (14.9 cubic feet).

***Imer Mortarman 750 Vertical Shaft Mixer*:** This mixer, shown in Figure 2.7(b), has been used to mix UHPC with volume up to 4.0 cubic feet. SRC staff commented that the mixer struggles to mix the maximum capacity, so it is preferred to mix smaller quantities.

(a) (b)

Figure 2.7. Available mixers for UHPC at SRC; (a) Mixer System Horizontal Shaft Mixer with 0.55 yd^3 capacity for UHPC [45] and (b) Imer Mortarman mixer with maximum of about 3 ft^3 capacity for UHPC [46].

The basic UHPC material properties were characterized using three different tests:

Compressive Strength**:** This test should be conducted according to ASTM C39 (Compressive Strength of Cylindrical Concrete Specimens) and ASTM C1856 (Standard Practice for Fabricating and Testing Specimens of Ultra-High Performance Concrete) [8] [137] at different ages including 7, 28 and 56 days and the approximate day of the tests. All cylinder samples should be capped, stored with the samples or in similar conditions, and be demolded 24 hours before testing. No special curing methods are required for compressive strength samples. After demolding and before compressive tests, all samples need to be ground on both ends using an automatic cylinder end grinder machine, to satisfy the planeness required by ASTM C39 and ASTM C1856.

Direct Tension Test**:** The direct tensile characteristics of the material should be measured using the direct tension test on 2in. by 2in. by 12in. prisms. This test should be conducted according to Graybeal [138] at 28 days. This test is driven from the direct tension test that is used commonly for mechanical testing of rectangular steel plate according to ASTM E8/E8M [139].

Modulus of Rupture/Flexural Bond Test**:** The rupture strength of the concrete should be measured using the modulus of rupture test in accordance with ASTM C78/C78M – 18, Flexural Strength of Concrete (Using Simple Beam with Third-Point Loading) [131]. Use ASTM C1609 [140] to measure the rupture strength of the UHPC. Specimen size should be 4-inch by 4-inch by 14-inch to allow for a 1-inch overhang on each side of the 12-inch span. Load and deflection should be measured during testing. Deflection-controlled load should be applied based on ASTM C1609 [140].

Direct Tension Pulloff Test**:** Tension pulloff test should be conducted according to ASTM C1583 [141] and ASTM D7234 [142] using the James Bond Test™ MK III. All three locations need to be cored with 2.5 in diameter cores with a depth extending approximately 1 inch below the interface. The coring procedure on hardened concrete minimizes the stress concentration along the edges. The James Bond Tester™ MK III applies tension to a circular steel disk that is connected to the surface through structural grade epoxy. The controlled tensile force is applied until failure occurs at the weakest point. The tensile strength is found by taking the maximal force divided by the idealized area of the interface.

***Shear Pushoff Test*:** Shear pushoff tests were conducted with a vertical configuration that requires a load frame attached to a strong floor. Additional details on geometry, reinforcement, and instrumentation are shown in Figure 2.3 and 2.4. Foil and fiber optic strain gauges on reinforcing bars were used to measure strains during testing.

These material tests should be performed for the substrate and cast-in-place UHPC materials for each batch.

Table 2.6. Summary of proposed material tests and required specimens

Test type	**Specimen**	**Age of test**	**Total number of specimens (3 samples/age)**
Compressive strength	3"x6" cylinder	7, 28, 56 days and days of tests	12
Tensile Strength	2"x2"x10" prism	28 days	3
Flexural strength	4"x4"x14" prism	28 days	3

2.3.2 Naming Convention

The naming convention for specimens is included in the shop drawings for the specimens. The basic naming convention is shown in Figure 2.8. Specific labeling depends on experimental set and its variables. For instance, letters representing the cross reinforcement are used only for shear pushoff specimens. Preventing condition, surface condition and corrosion condition only appear in labeling if they are variable in that specific set.

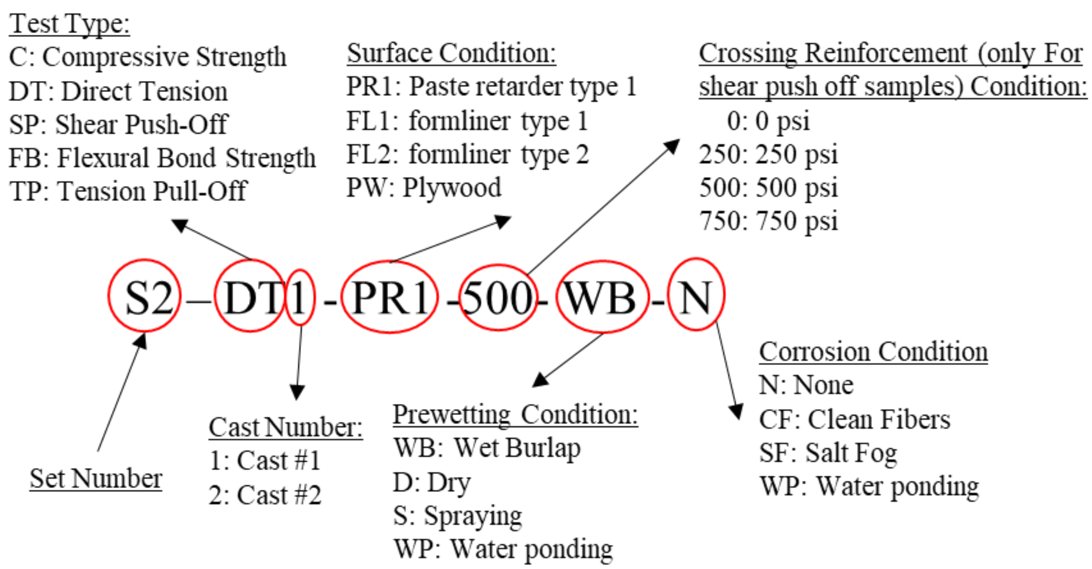

Figure 2.8. Specimen naming convention.

The following experimental matrix, shown in Table 2.7, is based on casting at FDOT SRC

The surface conditions used were:
Plywood: smooth, as-cast against unpainted plywood
PR1: roughened surface achieved using paste retarder, MasterFinish HV 78 Gray or MasterFinish XR48 Pink paste retarder from Master Builders
FL1: form liner with exposed aggregate-type finish and specified granulation of 0.15 inches (US Formliner 2/92 Rio Bravo), shown in Figure 2.6 (a)
FL2: form liner with exposed aggregate-type finish and specified granulation of 0.31 inches (US Formliner 2/76 Nil), shown in Figure 2.6 (b)

Table 2.7. Experimental matrix (variable highlighted and italicized for each mixture number)

Set #	Target Parameter	Substrate Material	Sub. Cast Location	CIP Material	CIP Cast Location	Sub. Age at CIP (days)	CIP Age (Test Day)	Surface Condition[1]	Reinforcement		Prewetting	Corrosion Cond.
0	Control (Monolithic)	*Proprietary #1*	SRC	--	--	--	28	--	0 psi	250 psi	--	--
		Proprietary #1	SRC	--	--	--	28	--	500 psi	750 psi	--	--
1	Surface condition	Proprietary #1	SRC	Proprietary #1	SRC	*28*	28	*Plywood*	0 psi	500 psi	Dry	None
		Proprietary #1	SRC	Proprietary #1	SRC	*28*	28	*PR1*	0 psi	500 psi	Dry	None
		Proprietary #1	SRC	Proprietary #1	SRC	*28*	28	*FL1*	0 psi	500 psi	Dry	None
		Proprietary #1	SRC	Proprietary #1	SRC	*28*	28	*FL2*	0 psi	500 psi	Dry	None
2	Surface condition, w/older substrate	Proprietary #1	SRC	Proprietary #1	SRC	*90*	28	*Plywood*	0 psi	500 psi	Dry	None
		Proprietary #1	SRC	Proprietary #1	SRC	*90*	28	*PR1*	0 psi	500 psi	Dry	None
		Proprietary #1	SRC	Proprietary #1	SRC	*90*	28	*FL1*	0 psi	500 psi	Dry	None
		Proprietary #1	SRC	Proprietary #1	SRC	*90*	28	*FL2*	0 psi	500 psi	Dry	None
3	Prewetting/ Surface Roughness	Proprietary #1	SRC	Proprietary #1	SRC	28	28	*Base Cond. (FL2)*	0 psi	500 psi	*Dry*	None
		Proprietary #1	SRC	Proprietary #1	SRC	28	28	*Base Cond. (FL2)*	0 psi	500 psi	*Spraying*	None
		Proprietary #1	SRC	Proprietary #1	SRC	28	28	*Base Cond. (FL2)*	0 psi	500 psi	*Wet burlap*	None
		Proprietary #1	SRC	Proprietary #1	SRC	28	28	*Base Cond. (FL2)*	0 psi	500 psi	*Water ponding*	None

Set #	Target Parameter	Substrate Material	Sub. Cast Location	CIP Material	CIP Cast Location	Sub. Age at CIP (days)	CIP Age (Test Day)	Surface Condition[1]	Reinforcement		Prewetting	Corrosion Cond.
5	Prewetting w/ Corroded Fibers	*Proprietary #1*	SRC	Proprietary #1	SRC	28	28	PR	0 psi	500 psi	*Dry*	*Salt burlap*
		Proprietary #1	SRC	Proprietary #1	SRC	28	28	PR	0 psi	500 psi	*Spraying*	*Salt burlap*
		Proprietary #1	SRC	Proprietary #1	SRC	28	28	PR	0 psi	500 psi	*Wet burlap*	*Salt burlap*
		Proprietary #1	SRC	Proprietary #1	SRC	28	28	PR	0 psi	500 psi	*Water ponding*	*Salt ponding*
4	Prewetting/ Exposed Fibers	Proprietary #1	SRC	Proprietary #1	SRC	28	28	PR	0 psi	500 psi	*Dry*	*None*
		Proprietary #1	SRC	Proprietary #1	SRC	28	28	PR	0 psi	500 psi	*Spraying*	*None*
		Proprietary #1	SRC	Proprietary #1	SRC	28	28	PR	0 psi	500 psi	*Wet burlap*	*Inhibitor VPI*
		Proprietary #1	SRC	Proprietary #1	SRC	28	28	PR	0 psi	500 psi	*Water ponding*	*Inhibitor CH ponding*
6	Prewetting w/non-prop.	*Non-Prop. #1*	SRC	Proprietary #1	SRC	28	28	PR	0 psi	500 psi	*Dry*	*Salt burlap*
		Non-Prop. #1	SRC	Proprietary #1	SRC	28	28	PR	0 psi	500 psi	*Spraying*	*Salt burlap*
		Non-Prop. #1	SRC	Proprietary #1	SRC	28	28	PR.	0 psi	500 psi	*Wet burlap*	*Salt burlap*
		Non-Prop. #1	SRC	Proprietary #1	SRC	28	28	PR	0 psi	500 psi	*Water ponding*	*Salt ponding*
7	Prewetting w/non-prop. and prop./surface rougjness (Early strength)	Non-Prop. #1	SRC	Proprietary #1	SRC	28	*7*	*PR*	0 psi	500 psi	Wet burlap	None
		Non-Prop. #1	SRC	Proprietary #1	SRC	28	*7*	*PR*	0 psi	500 psi	Dry	None
		Non-Prop. #1	SRC	Proprietary #1	SRC	28	*7*	*FL1*	0 psi	500 psi	Wet burlap	None
		Non-Prop. #1	SRC	Proprietary #1	SRC	28	*7*	*FL1*	0 psi	500 psi	Dry	None

Set #	Target Parameter	Substrate Material	Sub. Cast Location	CIP Material	CIP Cast Location	Sub. Age at CIP (days)	CIP Age (Test Day)	Surface Condition[1]	Reinforcement		Prewetting	Corrosion Cond.
8	Surface condition w/non-prop. and prop. [3] Monolithic	*Non-Prop. #1*	SRC				7		0 psi	250 psi	Wet burlap	None
		Non-Prop. #1	SRC				7		500 psi	750 psi	Wet burlap	None
		Non-Prop. #1	SRC				28		0 psi	250 psi	Wet burlap	None
		Non-Prop. #1	SRC				28		500 psi	750 psi	Wet burlap	None
9	Corrosion w/non-prop.[3]	Non-Prop. #1	SRC	Proprietary #1	SRC	28	28	PR (Corr)			Wet burlap	*Salt burlap*
		Non-Prop. #1	SRC	Proprietary #1	SRC	28	28	PR (No Corr)			Wet burlap	*None*
		Non-Prop. #1	SRC	Proprietary #1	SRC	28	28	PR Cleaned fibers			Wet burlap	*Pressure Wash Clean*

2.4 Summary of Testing

Laboratory work for the project was intensive in terms of scheduling, space management, and labor due to the research approach to cast and environmentally condition the separate components of the shear pushoff UHPC specimen, concrete curing, and physical testing. Table 2.8 lists activities at the FDOT Structural Research Center.

Table 2.8 Laboratory Research Activity

Date	UHPC Cast Activity	Testing Activity
8/1/23	Cast Set 2-1	
10/3/23	Cast Set 1-1	
10/31/23	Cast Set 2-2	
11/6/23	Cast Set 1-2	
12/3/23		Test Set 1
12/10/23		Test Set 2
4/22/24	Cast Set 3-1	
5/19/24	Cast Set 3-2	
7/22/24	Cast Set 4-1	
7/25/24		Test Set 3
8/12/24	Cast Set 4-2	
9/9/24	Cast Set 5-1	
9/12/24		Test Set 4
3/17/25	Cast Set 5-2	
6/2/25	Cast Set 0 and Set 5b	
6/9/25	Cast Set 0b	
6/10/25		Test Set 5
7/15/25		Test Set 0 and Set 5b
10/13/25	Cast Set 6-1	
11/16/25	Cast Set 6-2	
1/5/26	Cast Set 7-1	
1/7/26		Test Set 6
1/29/26	Cast Set 7-2	
2/4/26		Test Set 7
3/8/26	Cast Set 8	
3/16/26		Test Set 8a
3/30/26		Test Set 8b
4/2/26	Cast Set 9	

The following section with a photo montage gives a general synopsis of the level of work required in the fabrication and testing phases of the research.

UHPC Material Acquisition**:** UHPC materials from two commercial sources were used. Materials typically come in components including cementitious materials, admixtures, and fibers. The cementitious materials typically arrive in pre-weighed large sacks.

Photo 2.3. UHPC materials from two sources.

Storage and Space Management: The large sacs of cementitious materials were stored in sheltered indoor conditions and required significant space for storage. Handling required a crane or forklift.

Photo 2.4. Large orders of material included large supersacks of cementitious materials.

Rebar, Formwork, and Mold Preparation**:** Steel rebar was fabricated by a local producer. The rebar cage and much of the formwork with plywood and foam, were fabricated by the FDOT SRC staff. Form liners were commercially available. Steel formwork for the shear pushoff test was fabricated by an external shop and standard forms for the flexural bond test and direct tension test were purchased.

Photo 2.5. Large order of Gr60 rebar, steel formwork, lumber, foam, and associated hardware.

***Rebar Cage Fabrication and Sensor Installation*:** The rebar cage assembly and installation of foil and fiber optic strain gages were completed by FDOT SRC staff.

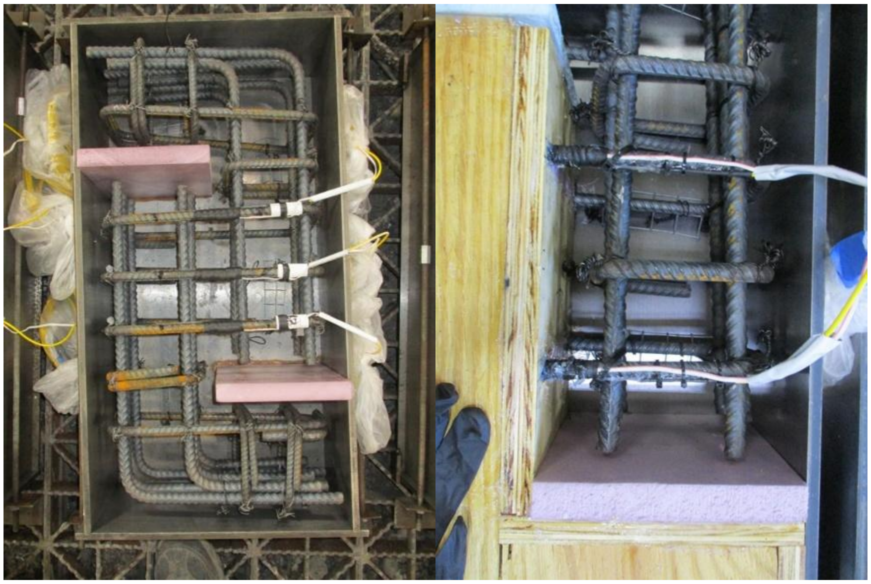

Photo 2.6. Several designs for reinforcing steel for shear pushoff testing. Connection of surface mounted strain gages and fiber optic gages.

Weighing, Mixing, Testing: Prior to casting, raw UHPC ingredients were pre-weighed. Eight of the nine test sets utilized a horizontal shaft concrete mixer. The smaller test Set 9 used a planetary mortar mixer. Liquid components and water were typically added during mixing using a commercially available dispenser. Fresh UHPC material was dispensed into the larger formwork using a concrete bucket or manually poured into smaller molds with scoops or pitchers. UHPC temperature was monitored during various stages of mixing. The UHPC was poured typically from one end of the formwork such that the flow allowed for the steel fibers to align in a consistent manner. After careful placement of the UHPC at the desired height and at a point near initial setting, the top surface of the UHPC was tamped by a steel roller to remove excess trapped air and create a uniform surface texture. The poured UHPC was covered with tarp typically for 24 hours prior to demolding.

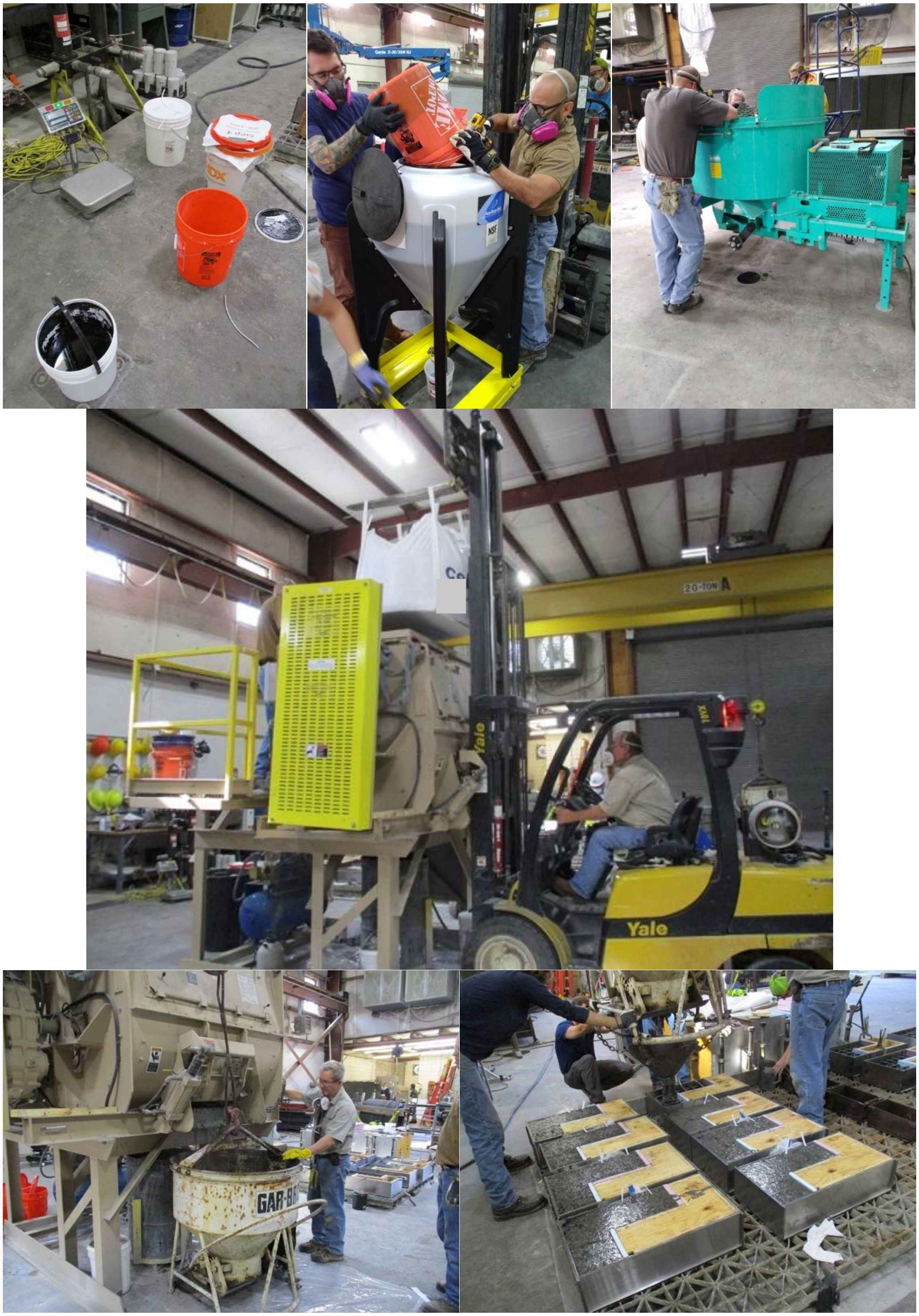

Photo 2.7. Two different UHPC mix designs, large order batching and mixing, and pouring.

***QC Testing*:** Quality control for workability included visual inspection for consistency of the UHPC during mixing and flow table test. Three-inch diameter concrete cylinders were cast for compressive strength testing.

Photo 2.8. UHPC flow table test.

***Demolding, Cleaning*:** Demolding was typically made 24 hours after casting. Standard molds for prisms were easier to demold. Shear pushoff specimens were more complicated due to their complex geometry, rebar placement, internal formwork components, and sensor placement. Some internal wood and foam formwork was reusable but often was damaged during the demolding process. Steel formwork was cleaned to remove excess hardened UHPC and reoiled for storage and later use.

Photo 2.9 Large quantity and size of various moldwork, disassembly, cleaning, and rebuild.

Sample Preparation**:** After demolding, the various test specimens were prepared for testing or prepared for placement of the matchcast UHPC. Surface preparation included pressure washing the surface of specimens with concrete laitance developed from the paste retarder, grinding outer UHPC surfaces or edges for attachment of pulloff test dolleys or to flatten surfaces edges to attach acrylic plates for ponding, pre-drilling and dolley attachment for pulloff tests.

Photo 2.10. Preparation of specimens for pulloff testing and matchcast testing.

Environmental Exposure System and Surface Conditioning**:** Test specimens subjected to extended time surface wetting were placed in sealed plastic containers that were fitted with a timed irrigation system that maintained moisture levels. Specimens requiring dry conditions were left in sheltered indoor laboratory conditions.

Specimens that were wetted by burlap were placed into the plastic containers with the joint surface facing upwards. In some test conditions, a dosage of a vapor-phase inhibitor was placed in the plastic containers prior to placement of the burlap. A slow drip nozzle was placed over the specimen surface to periodically rewet the burlap. Specimens that were ponded had either their joint surface placed face down (elevated with spacers) in a shallow pool of saturated calcium hydroxide solution placed in its container or were placed face up with acrylic plates attached to form a ponding pool filled with the saturated calcium hydroxide solution. When specimens required pre-corroded exposed steel fibers, the burlap was wet with salt-laden burlap (5% NaCl) or the ponding solution included 5% NaCl. The slow drip irrigation system typically was timed to drip tap water for a few minutes each day to compensate for evaporation.

Specimens that required pre-corroded steel fibers but not extended wetting had salt laden burlap placed on its surface and sealed under cling wrap (periodically manually rewet with salt solution) for several weeks until the fibers throughout the joint surface exhibited rust. At that time, the burlap was removed and the specimen left to dry out in sheltered indoor lab conditions prior to the matchcasting.

Photo 2.11. Development of irrigation system to maintain moisture or prolonged wet burlap and bonding wetting conditions and corrosion conditions for exposed steel fibers.

***Equipment Setup, Installation and Testing*:** Flexural bond test specimens were shipped to FDOT State Material Office for testing. Direct tension specimens were shipped to FIU for testing. Compressive strength, tensile pulloff and shear pushoff testing were conducted at FDOT SRC. Early shear pushoff test specimens had their front surface painted with a spectral pattern for digital image correlation measurements. Results from that effort are not reported here but the data has been archived for future dissemination. The test specimens were mounted and centered on a leveled platform under an actuator mounted to a reaction frame for testing. Handling of the test specimens required a crane and forklift with a custom-made collar developed at FDOT SRC. Load and displacement were recorded as well as the interface rebar strain from foil and fiber optic strain gages.

Photo 2.12. Handling of large UHPC pushoff test specimen by forklift and crane.

Photo 2.13. Sophisticated shear pushoff testing including test frame, mechanical actuators, sensors, data acquisitions, DIC high speed cameras and lighting.

3. CORROSION MITIGATION CONSIDERATION

Corrosion control of steel structural components in the physical civil infrastructure can be a challenge [143]. Steel and reinforced concrete bridge elements subjected to aggressive exposure environments (during construction and in service), including in coastal marine environments where saltwater exposure to bridge substructural elements and salt air exposure to the superstructure, can cause premature material degradation. The effectiveness of mitigation can vary depending on material defects, presence and accumulation of salts, pollution levels, fluctuating humidity and temperature, amongst other design and construction factors [144]. Durability of UHPC is expected to be good due to its low permeability characteristics [145], but atmospheric exposure of structural elements during the manufacturing process can cause early corrosion of exposed fibers. This can be visually unappealing, and there may be mechanical degradation as well for various systems including cases where element sections require match concrete casting with interfaces with exposed fibers [146-147]. Only a few studies have investigated different methods to protect the steel fibers from corrosion.

The study by Yoo, 2022 [146] showed testing of steel fibers treated with ethylenediaminetetraacetic acid (EDTA) solution and a nano-SiO_2 coating for use in ultra-high-performance concrete (UHPC). The treatment improved fiber bonding and strength; however, some treatments led to higher susceptibility to corrosion and deterioration of tensile performance. Fen et al., 2019 [147], studied the electrochemical behavior of steel bars embedded in UHPC with galvanized steel fibers exposed in 3.5 wt % NaCl solution. Results showed an increase in the charge transfer resistance of the steel bars with time, indicating corrosion protection. The study by Yoo, Gim, and Chun, 2020 [148], investigated the effect of steel fiber corrosion on ultra-high-performance fiber-reinforced concrete tensile behavior. Fibers with corrosion levels from 0 to 15% by weight (from average measurements of fiber bundles) were tested, including both unwashed and washed fibers. Results showed that moderate corrosion (up to 2–5%) increased surface roughness and improved fiber bridging, enhancing tensile performance. Beyond this level, excessive corrosion caused fiber ruptures and reduced performance. Washed fibers gave higher bond strengths than the unwashed corroded fibers.

Vapor-phase corrosion inhibitors (VCIs) have been promoted as an effective and cost-efficient method for controlling corrosion. Sodium carboxylates, aliphatic amines, cyclohexylamines, benzoates, and nitrobenzoates are commonly used VCIs [149]. VCI in the form of powders, papers, and coatings can be advantageous for its application in various manufacturing and construction environments [150]. For example, VCIs have been promoted for use for post-tensioned tendons. Case studies and research have shown corrosion degradation of post-tensioned strand [151-154].

The material volatilizes to form an inhibiting corrosion compound on steel surfaces within an enclosed space. The VCI molecules can saturate that space, and ideally occluded surfaces can also be protected [155]. The protective layer (stable bond) on the metal surface would prevent the ingress of corrosive agents and influence the rate of electrochemical reactions such as metal dissolution or oxygen reduction to mitigate corrosion [156-157]. Parameters that affect the efficacy of the material include the vapor pressure saturation levels, molecular structural characteristics, availability of reactive groups for surface physical or chemical binding, and contamination [150].

Bavarian et al, 2015 [156], studied corrosion behavior of carbon and galvanized steel samples in a 200 ppm chloride environment for over six months to evaluate corrosion. One setup used 10% vapor-phase inhibitor, while the other used dry air at low humidity (<40% RH). Results showed that the inhibitor provided excellent protection, keeping corrosion rates below 0.08 mpy, whereas samples in dry air developed red rust after 21 days, with corrosion rates up to 1.6 mpy. It was noted that the vapor phase corrosion inhibitors provided effective corrosion protection for short term storage.

Supplemental research described here focused on characterizing the corrosion behavior of carbon steel under controlled atmospheric conditions. Laboratory testing to identify corrosion development of carbon steel in various relative humidities (10%, 75%, 85%, and 99%) and with various amounts of surface salt contamination were conducted with and without the use of vapor-phase inhibitor. Results of the findings can inform the implementation of VCI to mitigate corrosion in various environmental conditions [158].

Laboratory testing was conducted on 48 steel coupons (3 inch by 2.5 inch (7.6 cm by 6.4 cm)). Specimen identification was engraved on the coupons prior to testing. The coupon specimens were cleaned with acetone and weighed prior to testing. Eight glass environmental chambers with a controlled nominal relative humidity (dry (<15%), 75%, 85%, and 97% RH) were constructed. The humidities were maintained with desiccant rock or a saturated salt solution. Sodium chloride, potassium chloride and potassium sulfate solutions were used for the 75%, 85% and 97% RH, respectively. The saturated salt solution depth was 1 inch (2.54 cm), and the test coupons were elevated so they had no contact with the solution. Humidity and temperature gauge were placed in each chamber to monitor the parameters. Six steel and six galvanized coupons were placed in each chamber.

Salt was deposited on the surface of the coupons by placing four separate 1 mL drops of salt solution using a pipette. The deposited water droplet was ~10 mm in diameter. The test solutions were plain DI water, 0.05% NaCl and 0.5% NaCl. Figure 3.1 shows an example of how the water drops were deposited on the surface of the coupons. After depositing the water drop, the solutions were allowed to evaporate by heating in an oven, leaving a thin layer of salt.

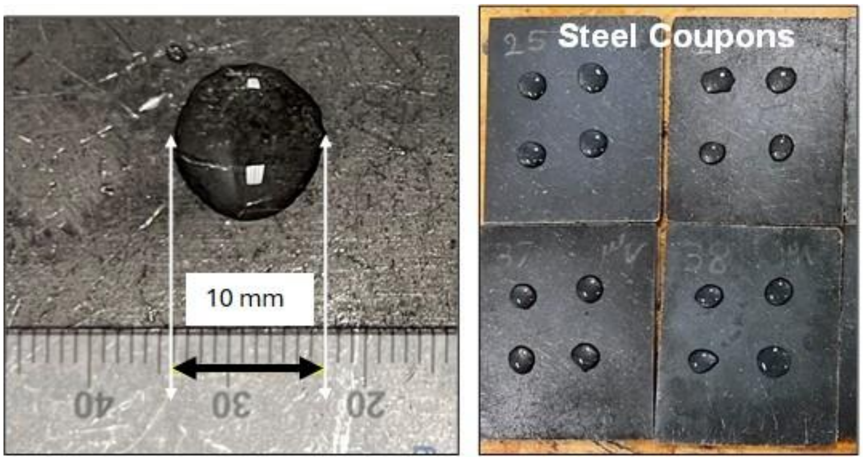

Photo 3.1. Example photos of sodium chloride deposition on steel coupons.

After placing the test specimens in the chambers, a commercially available vapor phase corrosion inhibitor was placed in each specified chamber. Mass loss on the specimens (the difference in mass before and after testing) was calculated after 7, 23, 70-90 days of exposure. The specimens were cleaned of corrosion products using acetone, and their mass was then recorded each time. Photo 3.2 shows a picture of the chambers with coupons.

Photo 3.2. Photos of corrosion test setup.

Temperature and humidity of the environmental chambers were monitored over 30 days. As Figure 3.1 shows, the temperature for all chambers was (~69ºF to 75ºF). The relative humidity of dry conditions was maintained at 10%. There were fluctuations for nominal 75% and 85% RH (due to temperature fluctuations). Despite the fluctuations, the relative differences between the test cases remained distinct to allow for comparisons by moisture availability.

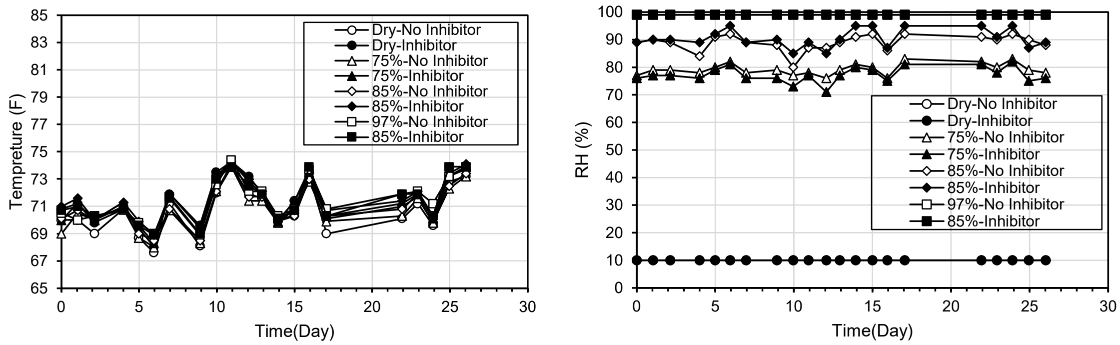

Figure 3.1. Temperature and relative humidity measurement in the chambers.

Figure 3.2 shows the mass loss for the steel coupons placed in the dry condition through time with and without the use of vapor phase inhibitor. As expected, the mass loss was low in the dry condition in all salt deposition cases. The upper limit 0.01% mass loss is low and values below these values may be considered negligible and can be attributed to the minor rust formation during the salt solution deposition and drying step. There was a slight increase in mass loss with time for the unprotected specimens with the high level of salt deposition (0.5% case). The high level of salt contamination may provide hygroscopic conditions that allow some moisture to be retained at the steel surface under the rust products. This was apparently mitigated by the presence of the inhibitor in the dry environment.

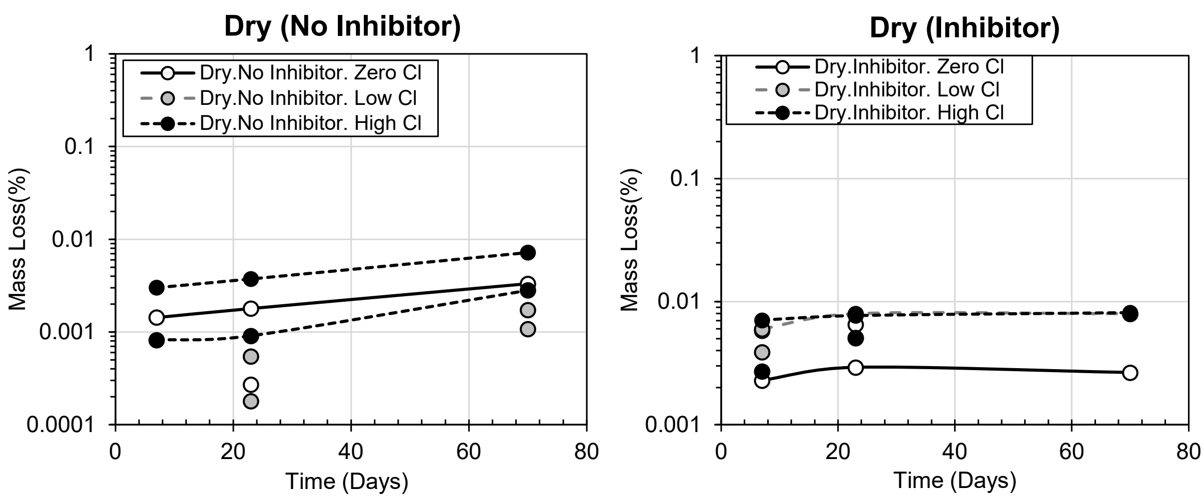

Figure 3.2. Mass loss of steel coupons (Dry). Replicate data shown.

Mass loss is shown in Figure 3.3 for the steel specimens placed in higher moisture environments (75-99% RH). In the 75%RH environment, the mass loss for the first 20 days was not dissimilar from the base dry condition case. The mass loss was below 0.01% except for the conditions with the high chloride deposition. The deposited salt allowed for hygroscopic conditions at the metal surface under the rust to form, allowing greater moisture presence that elevated the corrosion rate. Comparatively, the rate of mass loss with time (visually identified as the slope of the curves) was lower with the presence of the inhibitor. However, it was evident that regardless of inhibitor presence, significant corrosion developed by day 70.

Similar trends were observed at the higher humidity test conditions. As expected, the mass loss was greater in the environments with higher relative humidity and was most severe with the specimens with greater salt deposition. Notably, the general trend of lower rates of corrosion (lower slopes in the mass loss with time graph) for up to 20 days was maintained for the specimens with the VCI at the higher relative humidities. Later stages all show an increase in corrosion rate. This trend was most evident in the 97% RH case.

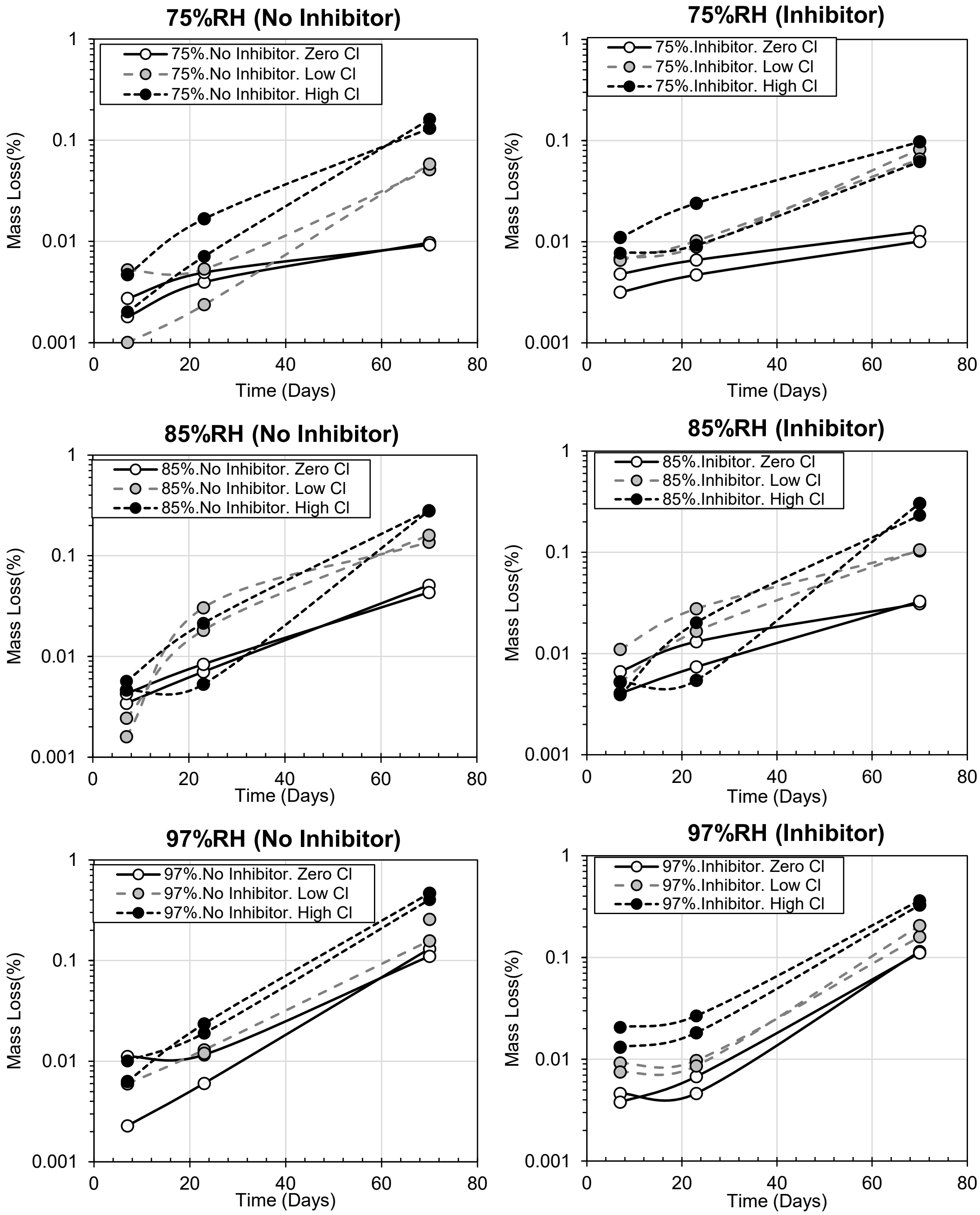

Figure 3.3. Mass loss of steel coupons (Moisture). Replicate data shown.

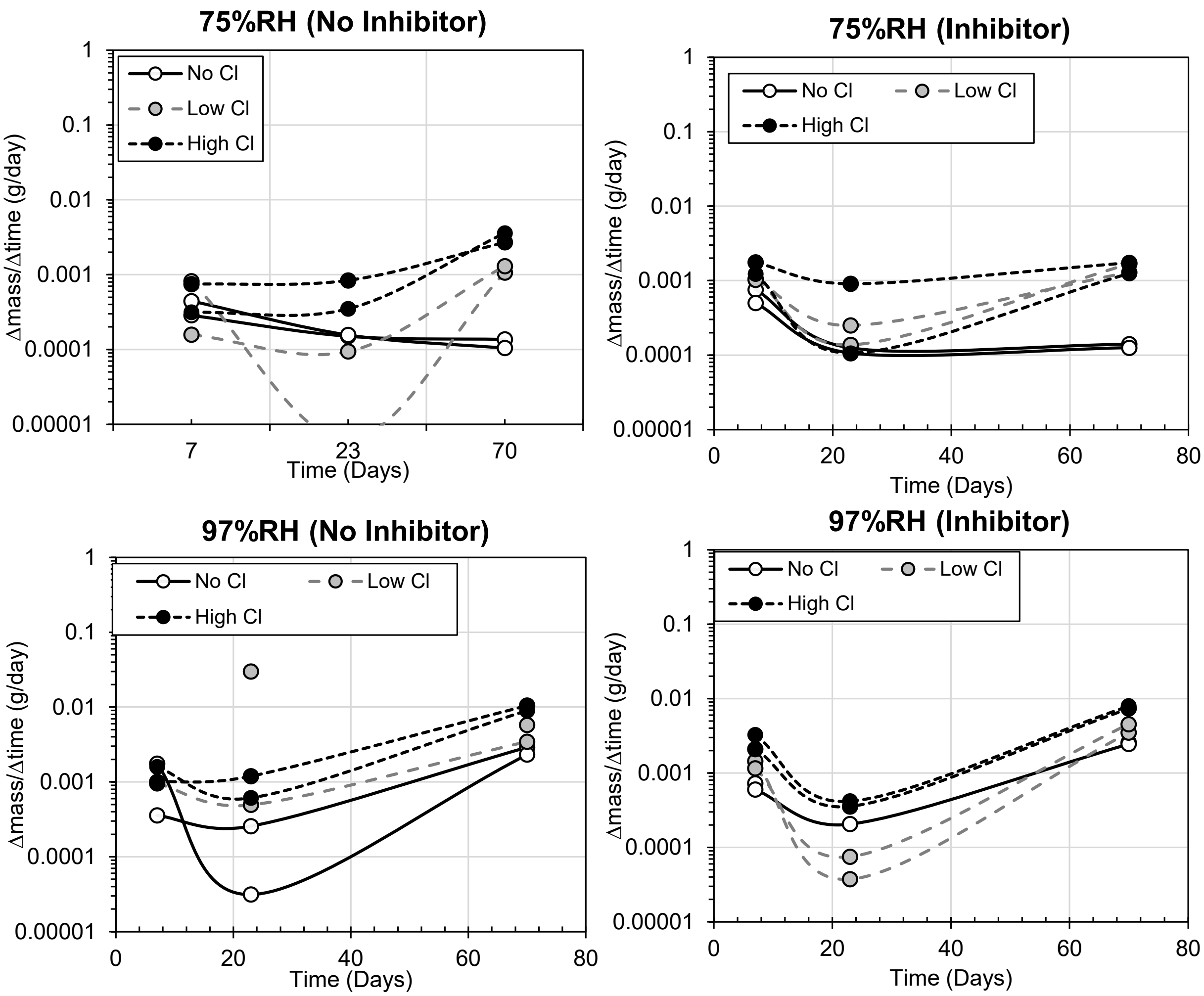

Figure 3.4. Apparent mass loss rate. Replicate data shown.

There was general observation of an increase in corrosion rate that continued through times of exposure in the absence of the inhibitor; but in the presence of the inhibitor, there was a bimodal behavior of mass loss rate for the first 20 days that was then followed by a more substantial increase rate in mass loss afterwards. To further elucidate this observation, the apparent corrosion rate was calculated as the change in mass divided by exposure time between day 0-7, 7-23, and 23-70. Results for the 75% and 97% RH cases are shown in Figure 3.4. There was a greater drop in mass loss rates for early exposures with the presence of the inhibitor in comparison to the non-protected cases, indicating the beneficial effect of the VCI at early times. By day 70, the inhibitive effect significantly weakened albeit in some cases still relatively better than the non-protected condition. In general, for the early stages of testing, the inhibitor appeared to allow for a lower corrosion rate to develop but its efficacy drops with longer exposure times.

Photo 3.3 shows photographs of select sets of steel coupons after 70 days of exposure. Superficial surface rust developed for the coupons in the dry condition regardless of salt deposition and inhibitor presence. Significant steel corrosion developed on coupons with greater salt deposition and placed at higher relative humidities. The initial dosing of the inhibitors lost efficacy after longer term exposure. Additional dosage of the inhibitor with time to maintain conditions to allow the protective film to form would be beneficial as the chambers were evidently inadequate to maintain a closed environment.

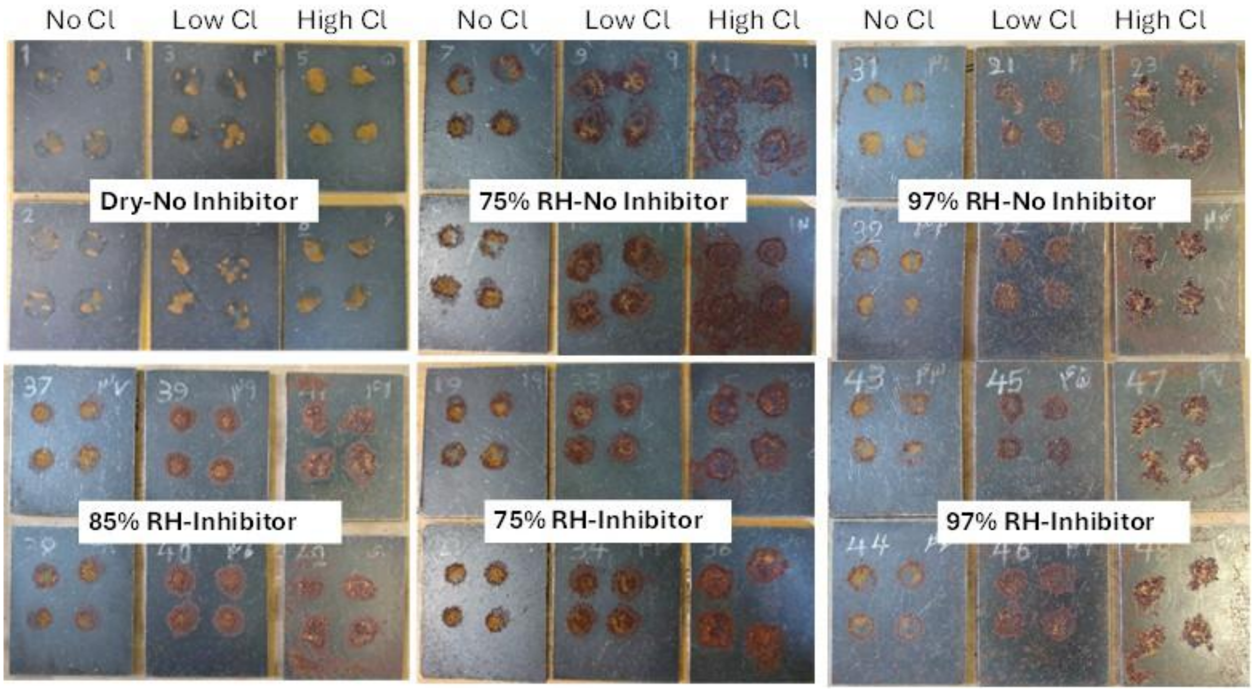

Photo 3.3. Photos of steel coupons after 70-day of exposure.

The performance of the VCI depends on environmental conditions, particularly humidity levels and salt contamination levels. The inhibitor showed beneficial effects to mitigate corrosion relative to untreated steel, but its efficacy can diminish with time if left without interval maintenance. Steel developed the greatest amount of corrosion in the cases with salt contamination, even in environments above 75% RH where mass loss was ten times greater than on non-contaminated surfaces.

4. RESULTS AND DISCUSSION

This chapter was subdivided into sections to separate test variables relating to surface condition and wetting conditions.

4.1 Monolithic (Bulk) UHPC

4.1.1 Compression, Direct Tension and Flexural Bond

Compiled results from compressive strength, direct tension, and flexural strength testing for monolithically cast prisms and cylinders are shown in Figure 4.1 and 4.2. Values were in the magnitude expected for UHPC materials. Some low values from direct tension and flexural bond testing of monolithically cast specimens were considered as outliers without any specific remarks from its testing. The larger median tensile strength for UHPC Material B shown in Figure 4.2 was assumed to be due to the smaller test population compared to that of UHPC Material A. Some UHPC Material A and B also have compressive strengths less than 17,500 psi after 28 days.

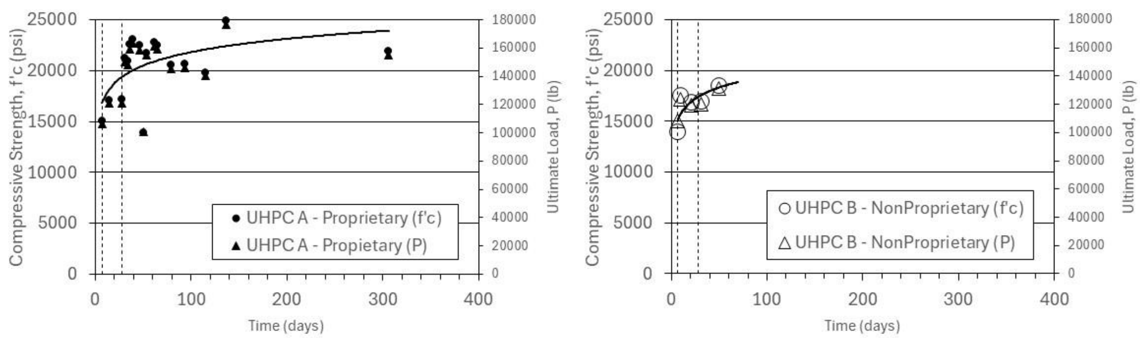

Figure 4.1. UHPC compressive strength.
Left: UHPC Material A. Right: UHPC Material B.

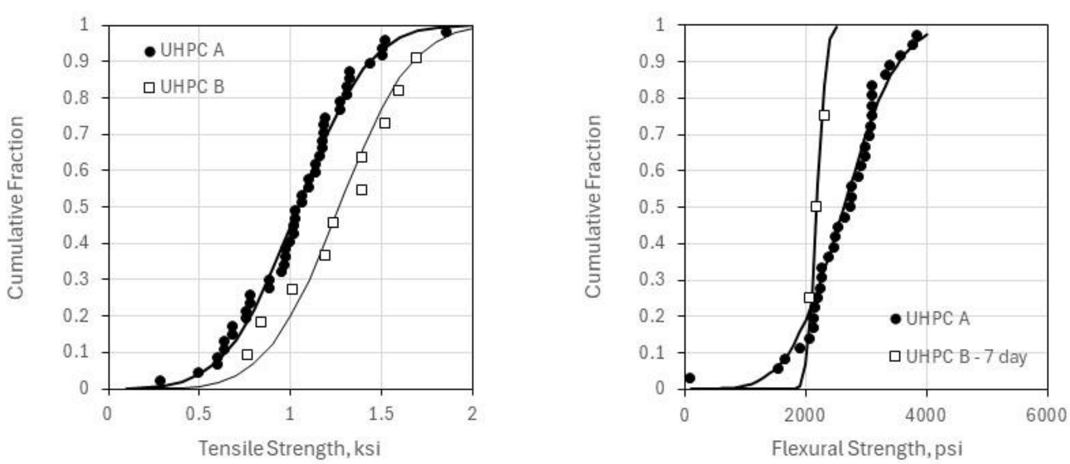

Figure 4.2. Bond strength characterized by direct tension (left) and flexural bond (right) test.

4.1.2 Tension Pulloff

Tension pulloff testing was made using a commercially available device, Photo 4.1 (that conformed to ASTM C1583) that measures the tensile stresses developed from axially pulling a steel cylindrical dolly epoxied to the outer surface of the UHPC. Testing was made in triplicate by coring three separate test locations on each UHPC cast test block and was considered to be adequate for test replication. It is understood that the errors due to the stochastic nature of concrete material testing for the various test conditions were limited to the domain from singly cast test blocks.

Photo 4.1. Pulloff test device.

Figure 4.3 shows the results for the bulk monolithic UHPC Materials A and B (Set 0 and 8). Testing was made for UHPC Material A after 28 days and for Material B at 7 days and 21 days after casting. All testing of the monolithically cast materials resulted in failure of the bulk material with fibers engaged. Pulloff strengths were similar and ranged from ~600 to 1,030 psi regardless of age. Similar results were obtained from direct tension tests that ranged from 500 to 1,800 psi for UHPC Material A and 770 to 1,700 psi for UHPC Material B.

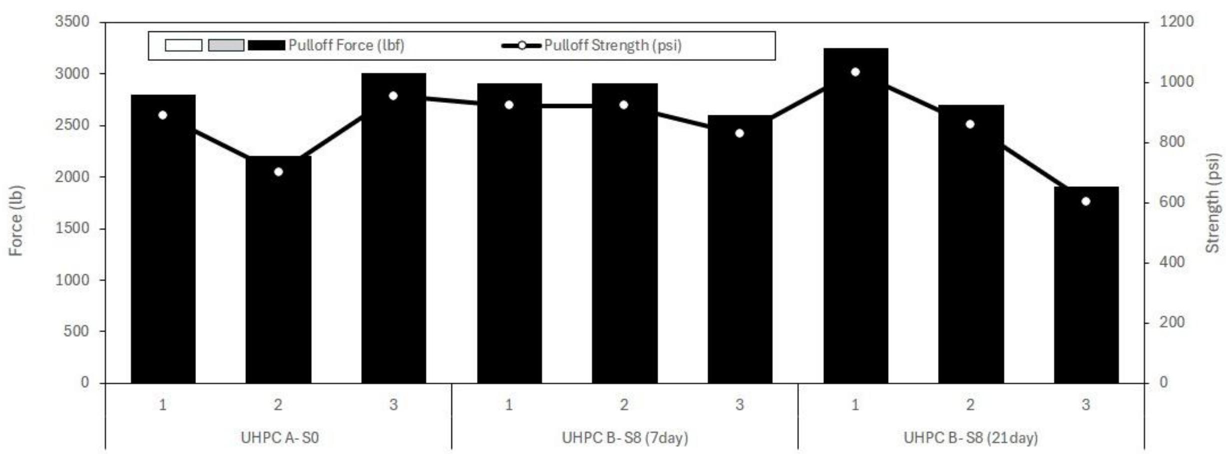

Figure 4.3. Pulloff force and strength of bulk monolithic UHPC Material A and B. White (-): Adhesive failure, Grey (x): Interface failure, Black (○): Substrate failure.

4.1.3 Flexural Bond

Compiled results of flexural bond testing conforming to ASTM C1609 for monolithically cast UHPC materials are shown in Figure 4.4. The bulk monolithically cast material was tested as a control for comparison of flexural behavior of matchcast concrete with various cast interface surface conditions and surface wetting conditions.

Flexural strength, f, values were calculated from the equation $f = PL/bd^2$ per ASTM C1609 where P is the load and L, b, and d are beam dimensions. The toughness was calculated as the area under the load-deflection curve by trapezoidal rule approximation up to a deflected depth of L/150.

First peak strengths, f_1, were 1,100 to 1,900 psi and peak strengths, f_P, was between 1,500 to 3,800 psi for UHPC Material A. Deflections at first peak, d_1, and peak, d_P ranged from 0.0002 to 0.004 inch and 0.002 and 0.08 inch, respectively. Residual strength at L/600, f^D_{600} and at L/150, f^D_{150}, ranged from 1,200 to 3,500 psi and 350 to 2,800 psi. Fracture toughness, T^D_{150} ranged from 400 to 1,400 lb-in.

There was no distinct differentiation for UHPC Material A bulk flexural behavior during early testing (sets 1-3) from later sets. Also, there was no differentiation in residual strength of set 5 and set 5B specimens (where misdosage of water was made in set 5), and trends were unclear in the flexural strength, residual strength, and toughness. Replicate testing in S5B-FB1 showed greater strengths than S5 but replicate testing in S5B-FB2 was lower. Lower water-to-cement ratio (such as in set 5) can provide improved strengths; but again, differentiation in the change of f_1 to f_P as well as residual strengths were not clear between sets 5 and 5B.

For UHPC Material B at 7 days, f_1 ranged from 1,400 to 1,600 psi, f_P ranged from 2,000 to 2,300, d_1 ranged from 0.002 to 0.004 inch, d_P ranged from 0.022 to 0.039 inch, f^D_{600} ranged from 1,600 to 2,100 psi, and f^D_{150} ranged from 1,000 to 1,400 psi. At early times, flexural behavior was marginally weaker but on par with Material A behavior after 28 days.

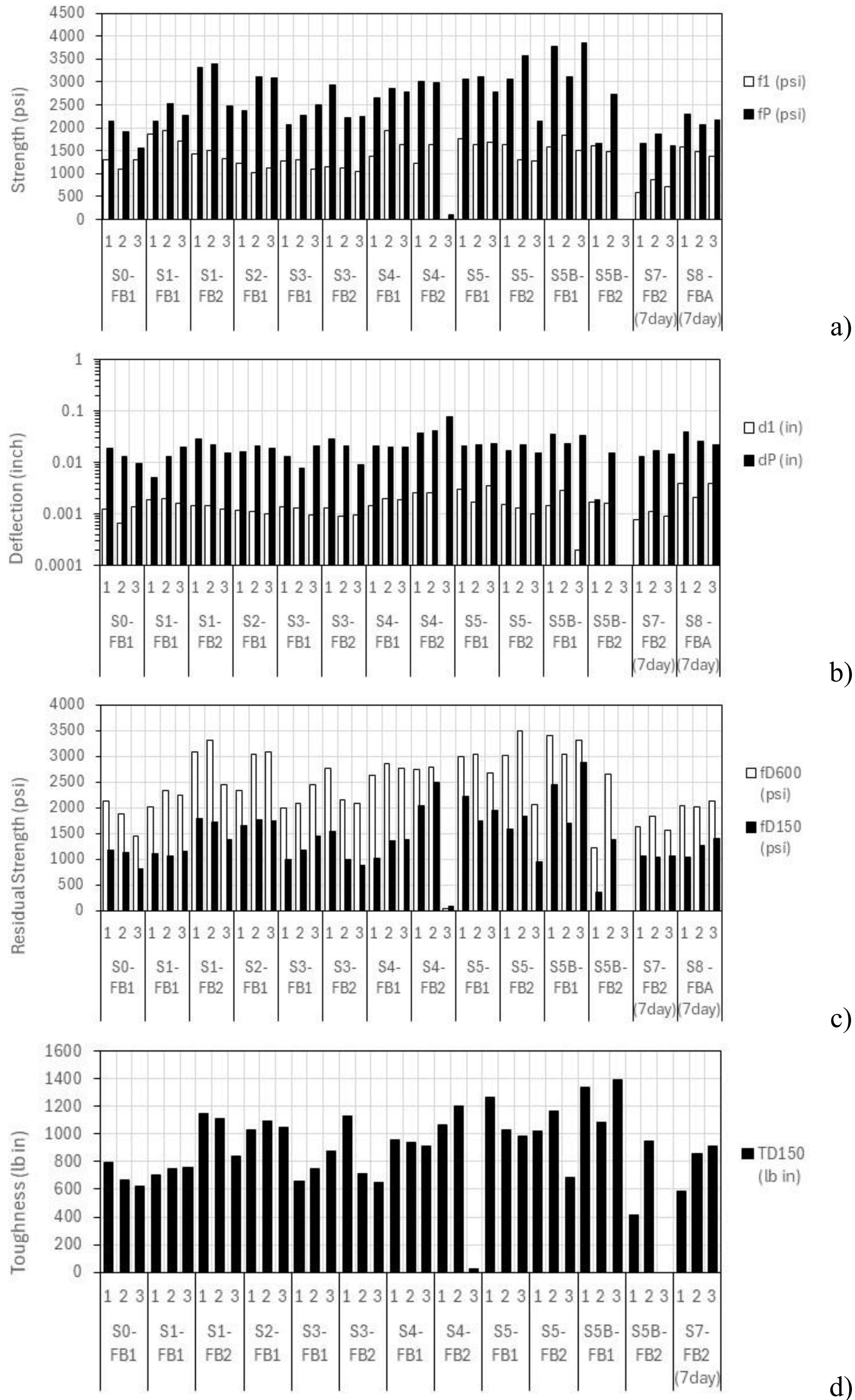

Figure 4.4. Flexural performance of monolithically cast UHPC.
a) Peak strength f_P and first peak load f_1. b) Peak deflection d_P and first peak deflection d_1.
c) Residual strength f^D_{600} and f^D_{600} , d) Toughness T^D_{150}
(Set No.-Cast No. (S#-FB#)).

4.1.4 Shear Pushoff

General Results: The results of shear pushoff testing for the control monolithically cast (Set 0) test specimen with UHPC Material A and (Set 8) with UHPC Material B is presented. Figure 4.5 and Figure 4.6 shows a composite graph for testing of Set 0 and Set 8 specimens with reinforcement ratio ρ_v=0, 4.6e-3 (0.46%), 9.2e-3 (0.92%), 13.8e-3 (1.38%), corresponding to 0, 2, 4, and 6 #4 rebars placed across the shear interface plane. The curves from testing of the specimens with the varying reinforcements levels showed consistent loading response up to peak stress. The order of plotting the replicate data in the figure besides ρ_v was arbitrarily made simply referring to specimen labels. The general shape of the response of shear stress versus the vertical slip of the specimen at the interface followed expected behavior typically observed for concrete and UHPC. Specifically, the increase in shear stress up to a peak stress, f_P showed a decrease in positive strength growth (softening) (especially at higher reinforcement ratios) as the tensile capacity of the rebar (and embedded fibers) engages. Upon reaching f_P, a large drop in the developed stress levels resulted as the initial concrete crack and fiber pullout extended to where the reinforcing steel is solely carrying the applied load. Further loading shown at extended slip ranges exhibits further failure and rupture of the reinforcing of steel. Results from replicate testing for UHPC Materials A and B are shown in Figures 4.7 and 4.10.

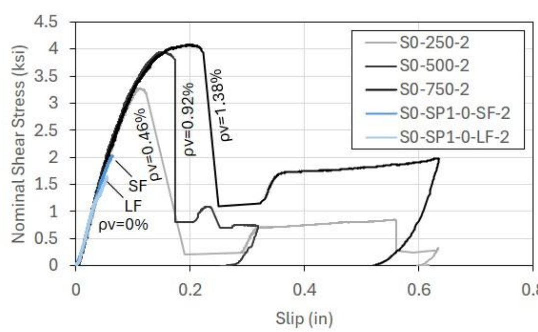

Figure 4.5. Shear stress vs slip for UHPC Material A.

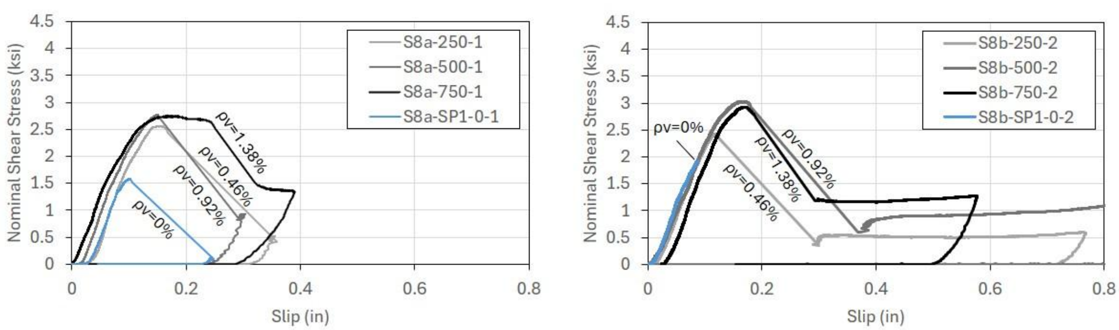

b)

Figure 4.6. Shear stress vs slip for UHPC Material B (Left: 7-day hydration. Right: 21-day hydration).

***UHPC Material A*:** Replicate data for the UHPC Material A is shown organized by reinforcement ratio in Figure 4.7. It is noted that the supplemental testing accounting for misplaced fiber type for UHPC material A showed similar load responses, comparing the 'SF' and ‘LF’ data (referring to short and long fibers, respectively) in Figure 4.7a. ‘SF’ refers to 0.2x13 mm fibers and ‘LF’ refers to the misplaced 0.3x20 mm fibers. The supplemental testing was only conducted for the ρ_v=0 case as any influence of the fiber type would be observable here. Photo 4.2 shows an example of cases with ‘LF’ where there was fiber segregation to the bottom of the cast UHPC. As can be seen in the photo, there was only fiber engagement and pulling on one side of the shear interface during the loading. Pushoff strengths in this case were lower; but otherwise, the effect of the misplaced fiber was not considered further.

Photo 4.2. Segregated fibers in Set 0 pushoff specimens.

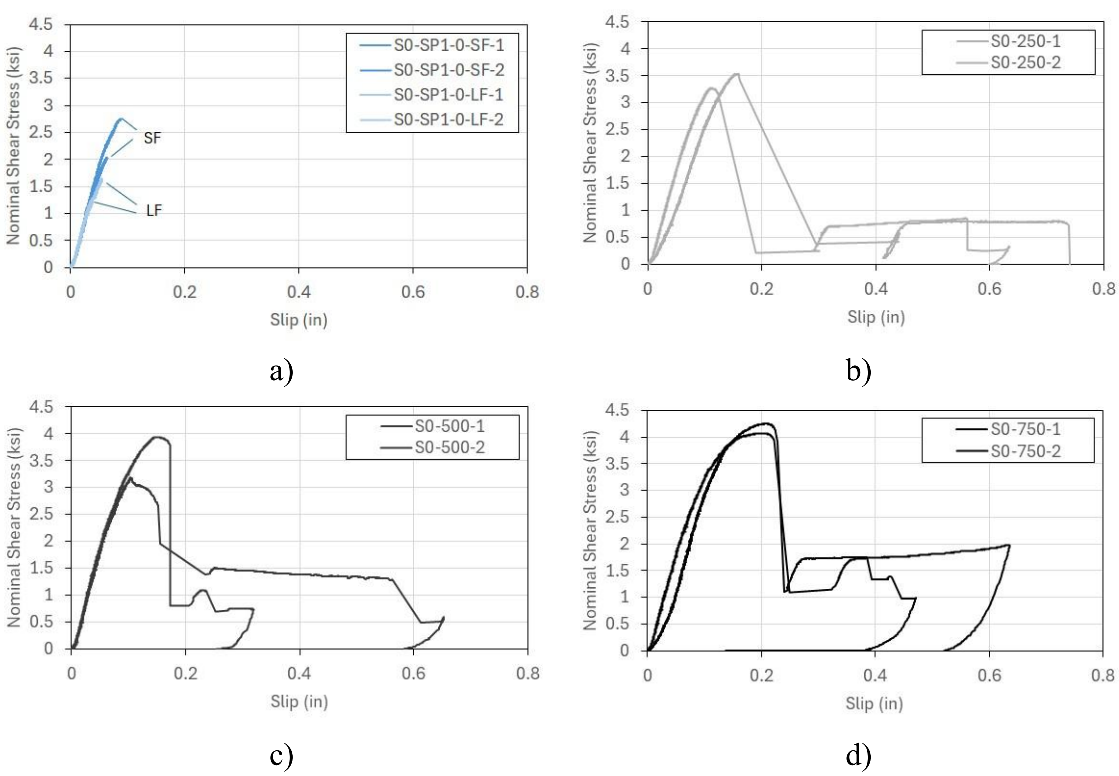

Figure 4.7. Shear stress vs slip for replicate UHPC Material A.
a) ρ_v=0, b) ρ_v=4.6e-3 (0.46%) , c) ρ_v=9.2e-3 (0.92%), d) ρ_v=13.8e-3 (1.38%).
Replicate data shown.

The corresponding stress-strain curves for the replicate specimens are shown in Figure 4.8, where the strain corresponds to the horizontal strain measured for the reinforcing steel placed across the shear interface. Data from foil and fiber optic strain gages were reviewed. Fiber optic strain data from locations corresponding to quarter points and mid points were considered when available; however, as some of the data set often showed excess noise, the graphs were plotted using data from the foil strain gages. The strain response was truncated at the peak stress, f_P for clarity of presentation. Prior to reaching f_P, the responses typically exhibited an instantaneous increase in strain (referred to as f_{crack}, followed by a bilinear increase. Initial concrete cracking was assumed to occur at or prior to f_{crack}. The bilinear increase in strain up to f_P has often been associated with post-cracking behavior with engagement of the embedded fibers. Consequently, the fibers continue to debond with increased load and the crack widens to where the reinforcing steel solely engages the load post f_P. Development of f_{crack} occurred below 2 ksi and was assumed to be associated with initial cracking.

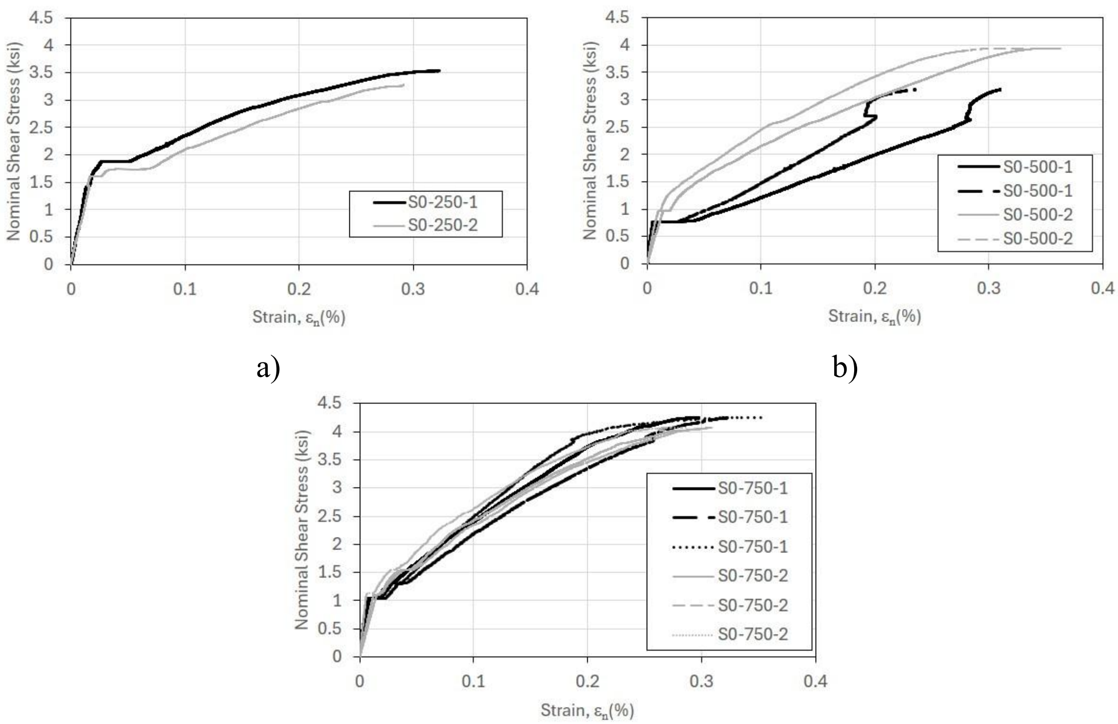

a) b)

c)

Figure 4.8. Control monolithically cast UHPC Material A stress-strain curve.
a) ρ_v=0.46%, b) ρ_v=0.92%, c) ρ_v=1.38%.

UHPC Material B**:** Similar monolithically cast pushoff testing for UHPC material B was conducted. Two test sets included testing after 7-day of concrete curing and 21-day of concrete curing in ambient laboratory environmental conditions. The compressive strength, f'c at 7 days was approximately 13,900 psi and f'c at 21 days was approximately 16,900 psi. Similar values were observed for UHPC material A where $f'c_{7day}$~15,000 psi. For later discussion, f'c for UHPC material A at the time of pushoff testing exceeded 20,000 psi.

The general response to loading as described previously for UHPC material A was similarly observed for the UHPC material B here (Figure 4.7 and 4.8), with the observable difference in f_P at the earlier testing times at 7 and 21 days for Material B compared to over 28 day hydration for Material A.

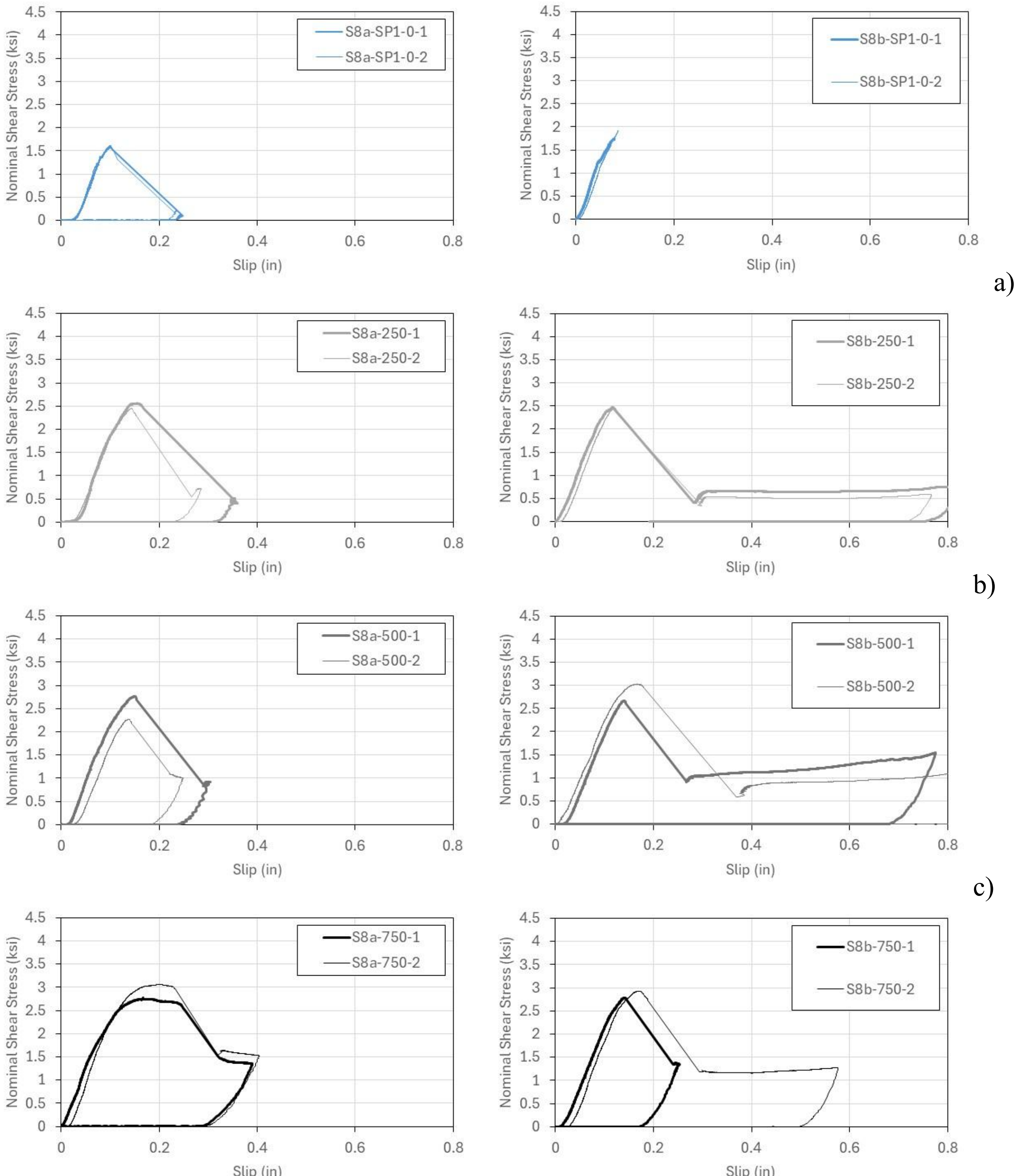

Figure 4.9. Shear stress vs slip for replicate UHPC Material B.
a) ρ_v=0%, b) ρ_v=0.46%, c) ρ_v=0.92%, d) ρ_v=1.38%
Left: 7-day. Right: 21-day. Replicate data shown.

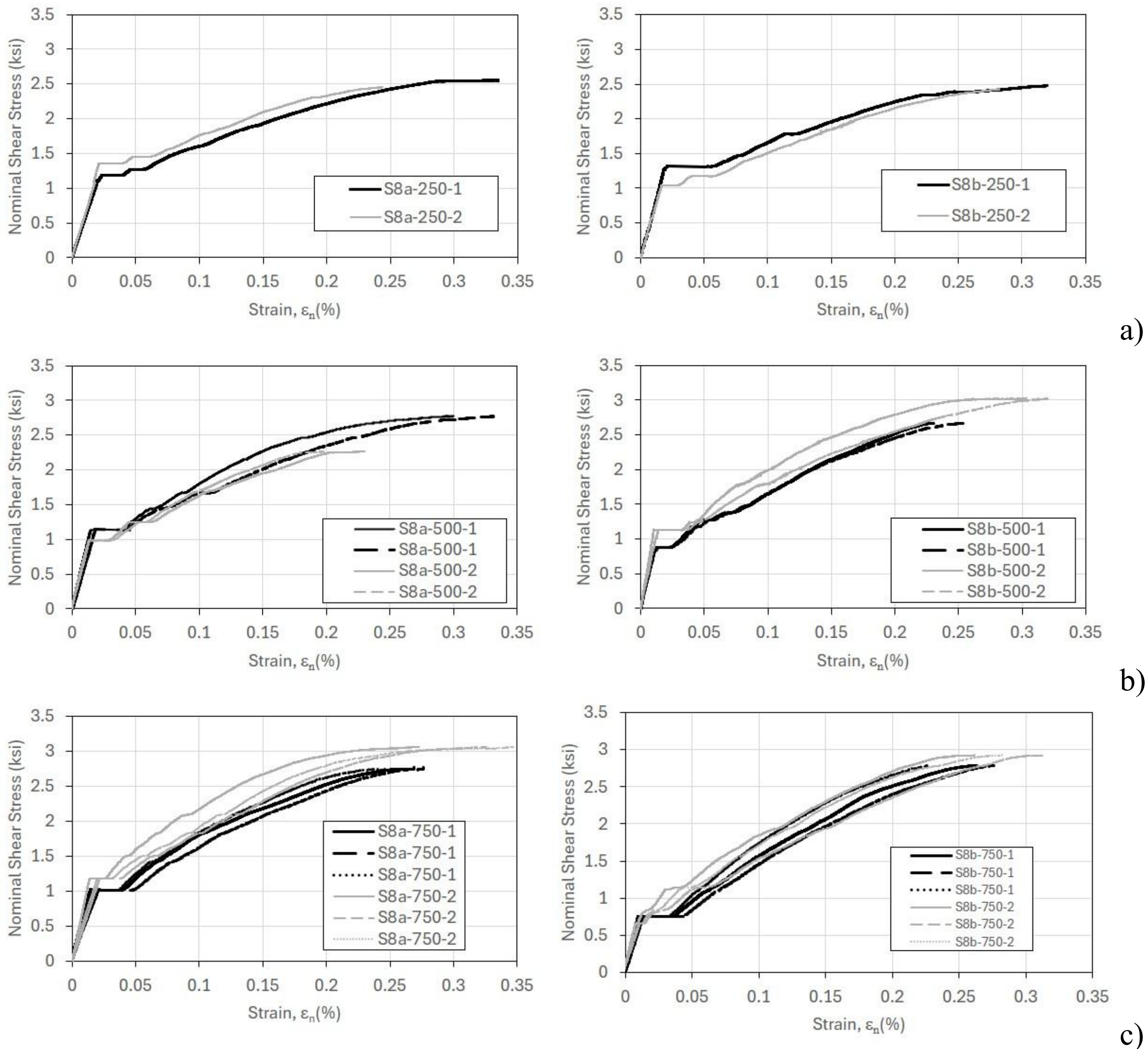

Figure 4.10. Monolithically cast UHPC Material B stress-strain curve.
a) ρ_v=0.46%, b) ρ_v= 0.92%, c) ρ_v=1.38%
Left) 7-day hydration, Right) 21-day hydration. Replicate data shown.

***Shear Stress vs Clamping Pressure*:** The shear stress vs clamping pressure for the monolithically cast UHPC Material A and B is shown in Figure 4.11. The clamping pressure is the reinforcement ratio, ρ_v, times the stress in the interface reinforcing steel at peak load, $f_{s,peak}$ calculated by Hooke's Law from the larger strain measured from either the foil or fiber optic strain gages. In cases where the reinforcing steel yielded prior to peak load, $f_{s,peak}$ was taken as f_y. As expected, greater shear strength developed with greater amount of reinforcing steel at the shear interface. As shown in the figure, the y-intercept at ρf_s=0 (interpreted as the cohesion coefficient) was greater as the concrete strengthens by cement hydration with time. The older tested concrete for UHPC Material A also showed a larger slope interpreted as the friction factor, μ. For UHPC Material B at 7 and 21 days, μ was similar. Values calculated here (c~1.8-2 ksi and μ~1.2-2.1) were greater than that proposed by Muzenski et al, 2002 for capacity calculations for UHPC.

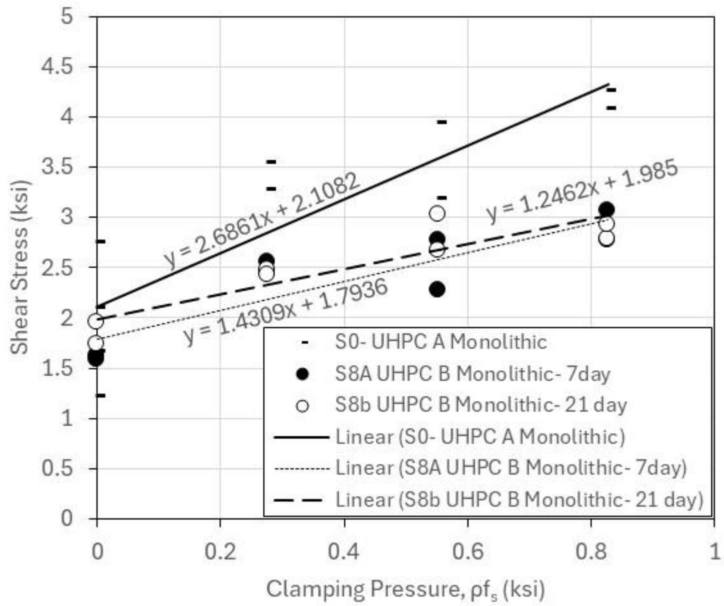

Figure 4.11. Shear stress versus clamping pressure of monolithically cast UHPC Material A and B.

4.2 Matchcast UHPC- Surface Roughness

Early testing with UHPC Material A showed that the material can form a skin of weak porous materials. The effect did not appear to affect bulk concrete behavior, as described in the previous section. It is suggested and as a recuring discussion in this section, that test sets 1-2 using UHPC Material A had conditions where there developed locally weaker materials at surfaces, observed as sometimes significant concrete laitance at the outer cast surface and porous material (from 'bugholes' to larger air bubbles) at molded interfaces in contact with porous formwork. This effect was thought to be due to differential water evaporation and high surface tension of UHPC that can affect movement of entrapped air. At the shear interface surface, interaction of air and water (especially when UHPC inherently has low pore water content) with the molding material (including plywood, foam, and even porous cement paste due to the past retardant) may create non-uniform moisture and air transport conditions. This effect was less in later mixes of the material (possibly in part due to newer raw material, adjustment of accelerator admixture, temperature and greater experience handling the material.

Testing described in this section was intended to differentiate behavior of joint surfaces with various surfaces textures, but the effects of deficient materials that formed at the interface created conflicting outcomes. Results are nevertheless presented in the following sections with discussion on the influence of the effects of deficient interface material.

4.2.1 Tension Pulloff

Tension pulloff testing was conducted on the specimens with a matchcast UHPC overlayed on a substrate UHPC subjected to various surface conditions and preparation (including roughness and exposed steel fibers). Photo 4.3 show examples of pulloff failures.

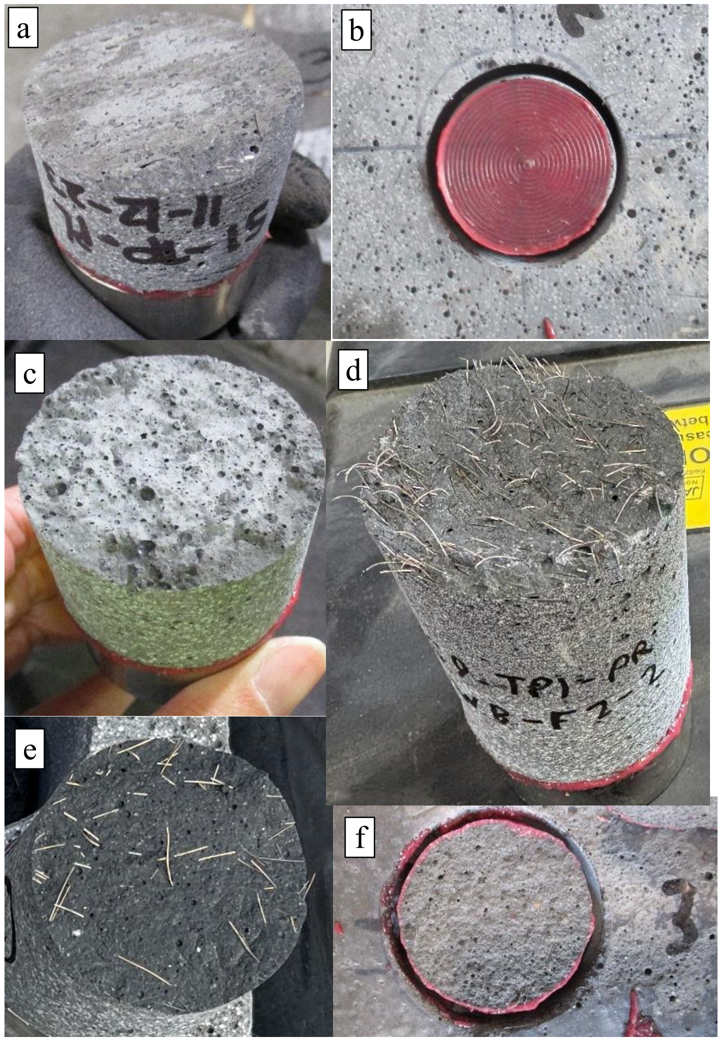

Photo 4.3. Examples of tensile pulloff failure modalities.

A smooth surface was created by using plywood formwork (Photo 4.2a). Roughened surfaces were created using two formliners (Photo 4.3c). Steel fibers were exposed at the interface surface by pressure washing concrete laitance that formed from fresh UHPC cast on formwork coated with paste retardant. The pressure washing produced some surface striations on the interface surface but was otherwise smooth. Failures occurred as adhesive failure of the epoxy (Figure 4.3b) where values were taken as a minimum, at the joint interface (Photo 4.3a,c,e), or the substrate (Photo 4.3d) where fibers were pulled.

Due to the development of the weak skin on the outer upward surface of UHPC Material A in sets 1-2, the outer surface of the matchcast overlay material was mechanically ground in later sets so that the mechanical dolly could be epoxied to higher quality material beneath the skin layer. Photo 4.2f shows an example of a failed test where the mechanical dolly separated at the weak skin material. No other treatments relating to the effects on the concrete surfaces due to internal moisture and air movement during concrete curing were made except for pressure washing of the concrete laitance produced by paste retardants.

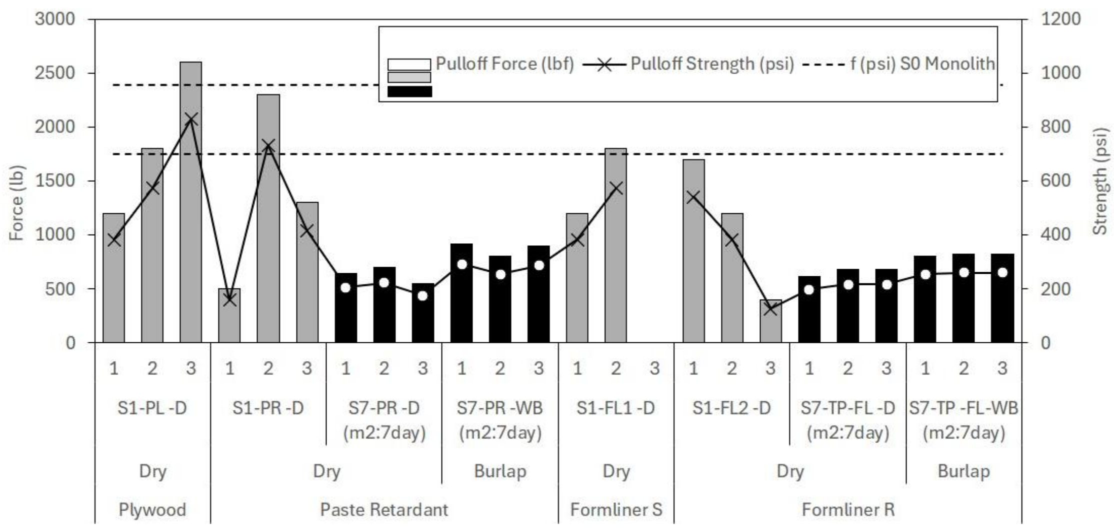

Figure 4.12. Pulloff force and strength of matchcast UHPC with various surface conditions. White (-): Adhesive failure, Grey (x): Interface failure, Black (○): Substrate failure.

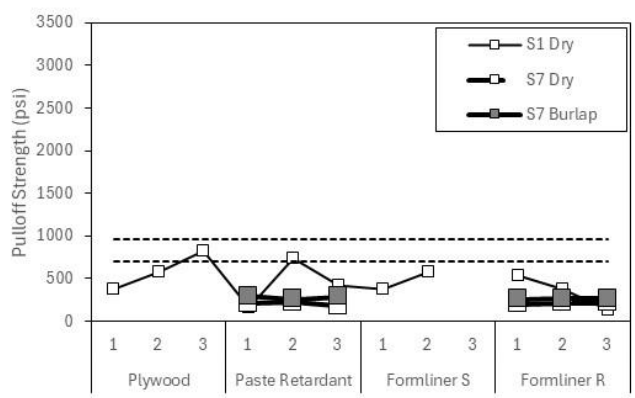

Figure 4.13. Comparison of Set 1 and Set 7 pulloff strength of matchcast UHPC with various surface conditions. Dotted lines shown as reference to monolithically cast Set 0.

Figures 4.12 and 4.13 shows the results of pulloff tests for specimens with their matchcast interface that was created with various textures (such as smooth surfaces by plywood, roughened surfaces with two formliners, exposed fibers by pressure washing concrete laitance from paste retardant). Set 1 utilized UHPC Material A for both substrate and overlay. Set 7 utilized UHPC Material B in the substrate cured for ~28 days and UHPC material A in the overlay, tested at ~7 days. On first review, there was marginal differentiation in strength comparing testing UHPC materials from set 1 and set 7.

Set 1 materials with either smooth interfaces without exposed fiber or smooth interfaces with exposed fibers when cured in ambient dry conditions resulted in elevated pulloff strengths (that sometimes were in the order of its monolithic control specimens) that resulted in bond failure at the interface. The relatively larger strengths were considered to be due to the longer hydration time at the time of testing than for Set 7. Set 1 materials with the two grades of roughened surface texture formed from form liners, had somewhat lower bond strengths (below values measured for the monolithic specimens) than the surfaces with exposed fibers. Testing with the smooth surface produced by plywood resulted in somewhat higher values but had failure that occurred at the interface. This would at least be consistent with the expectation that the smooth interface should provide a weaker plane than the bulk material. Set 7 materials with smooth interfaces with exposed fibers and the rougher texture form liner were not well differentiated but resulted in lower pulloff strengths at 7-day than the Set 1 specimens; but importantly, the failure of the Set 7 specimens occurred in the substrate Material B and not at the cast interface. The failure in the substrate Material B occurred at stresses in the order of 300 psi even though testing of the monolithically cast Material B had pulloff strengths 2-3 times greater.

UHPC B material after 28 days had a compressive strength, f'c, greater than 16,900 psi and UHPC A after 7 days had f'c~15,000 psi. UHPC Materials A and B showed similar tensile strength from direct tension tests (if not median values slightly higher for Material B). The similar bulk material mechanical behavior would indicate similar conditions despite the age difference and the differentiation in strength and failure modality would not intuitively be expected. Rather, it would seem that the distinct difference in the failure behavior observed in this series of testing would be related to the local interface material anomalies.

The failure of Set 1 materials at the interface (for plywood, paste retardant, and two formliner conditions) indicate that a weak plane at the cast interface developed (in part due to the deficient skin material at the interface introduced earlier) regardless of surface condition (including exposed fiber). Although the substrate concrete with the cast interface surface was on the bottom face of the mold for the first casting, porous formwork materials (including the plywood and formliners as well as cement laitance caused by the paste retardant) could conceivably affect moisture and air movement. Photo 4.4 shows a bond failure at the porous material developed at the joint interface.

Photo 4.4. Comparison of porous interface (left) to typical interface appearance (right).

It was thought that placement of the UHPC on porous molding materials and the transport of internal moisture and air created the heterogeneous conditions. This anomaly brings to discussion the possible effect of accumulated air and moisture gradients at the interface and its effect on near surface UHPC hydration. Excess prolonged moisture presence during the curing stage could affect the homogeneity of concrete by depth as UHPC has inherently low water to cement ratio. As to why of all conditions, the smooth plywood conditions cast in dry conditions (failing at the interface) obtained the high strength associated with chemical cohesion; the conjecture of differential water transport may be considered in another way. Whereas the poor-quality skin may develop (due to evaporative processes and the lack of residual pore water to hydrate the cement rich material) at the outer concrete surface, casting on plywood may retain displaced moisture that becomes available later. This would presumably result in greater strength but would nevertheless create heterogeneity on the surface. The extent of the heterogeneity and its effect when placed in contact with cast-in-place UHPC may either create a locally weak interface (relative to the bulk material) as observed in the skin layer or possibly stronger cohesion due to greater moisture availability in its small pore network. This may follow the line of inquisition relating to the difference in behavior between wetting by burlap and prolonged wetting by ponding. Testing on the role of surface wetting is later discussed in Section 4.3.

4.2.2. Flexural Bond

The compiled results of flexural bond tests for the matchcast UHPC specimens are shown in Figures 4.14 to 4.16. The figures were separated by strength, P, and deflection, d, at peak and first peak denoted by subscript P and 1, respectively; followed by residual strength at L/600 f^D_{600} and L/150 f^D_{150} and toughness T^D_{150}, Test conditions included various surface conditions including surface roughness (smooth texture formed against plywood formwork, roughened surfaces made by two formliners, exposed steel fibers produced by pressure washing concrete laitance formed from casting fresh UHPC on formwork with paste retardant).

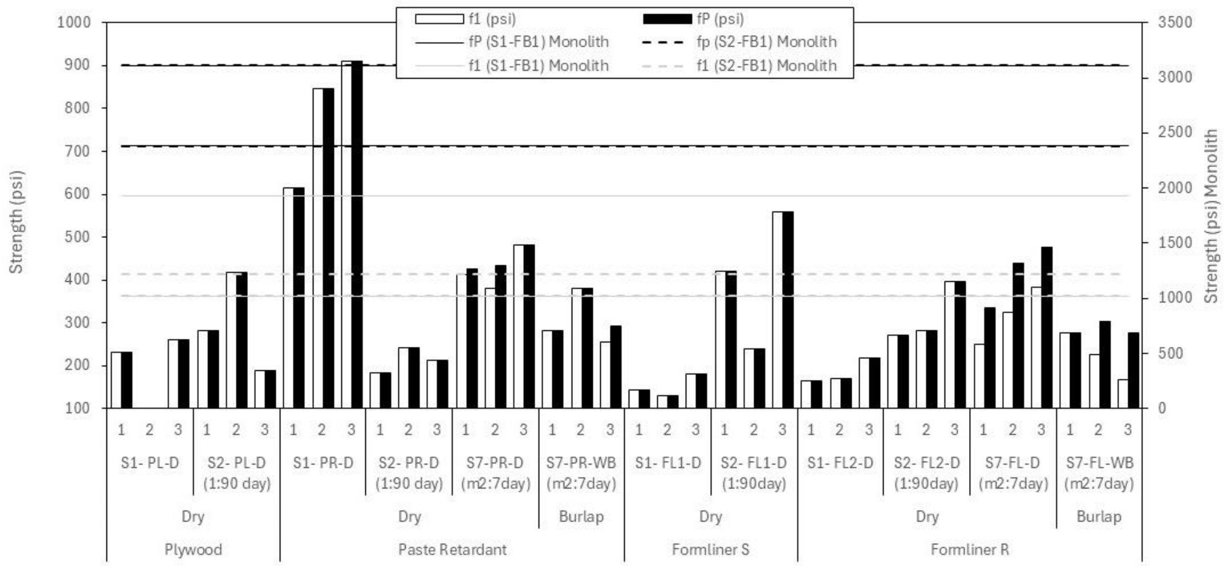

a)

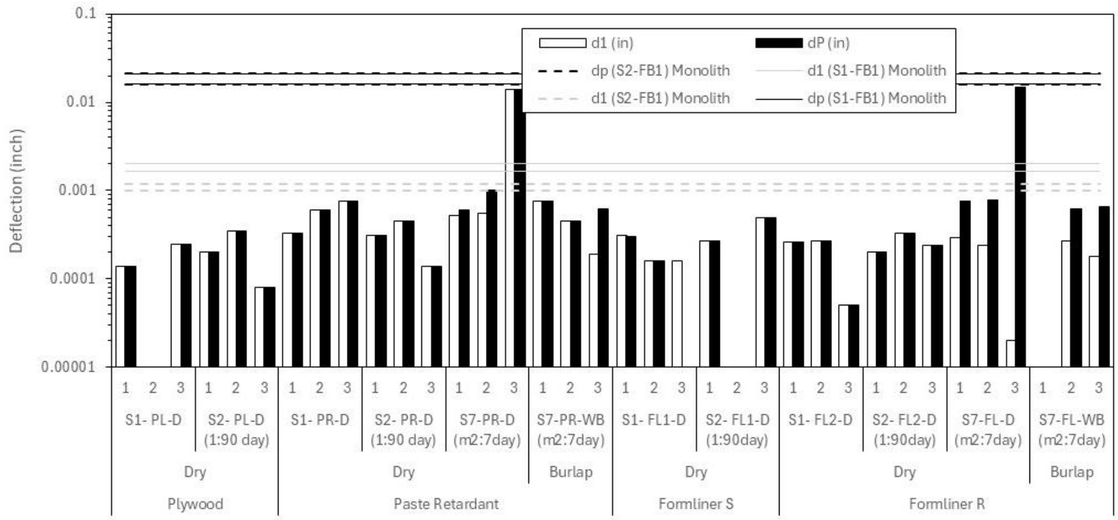

b)

Figure 4.14. Flexural performance of matchcast UHPC with various surface conditions: Plywood, Paste Retardant, and Formliners. a) Peak load and first peak load. b) Peak deflection and first peak deflection.

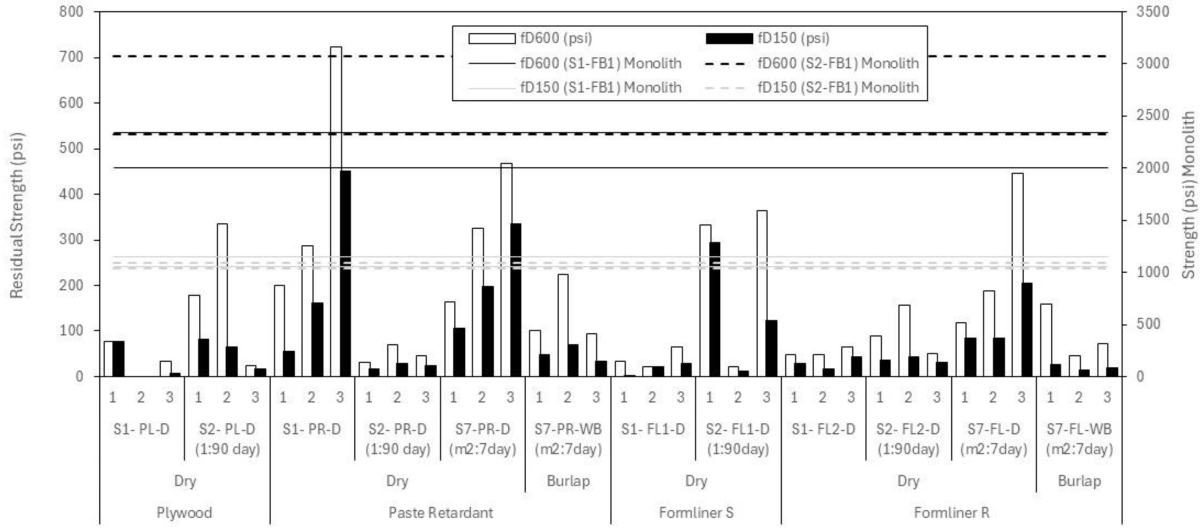

c)

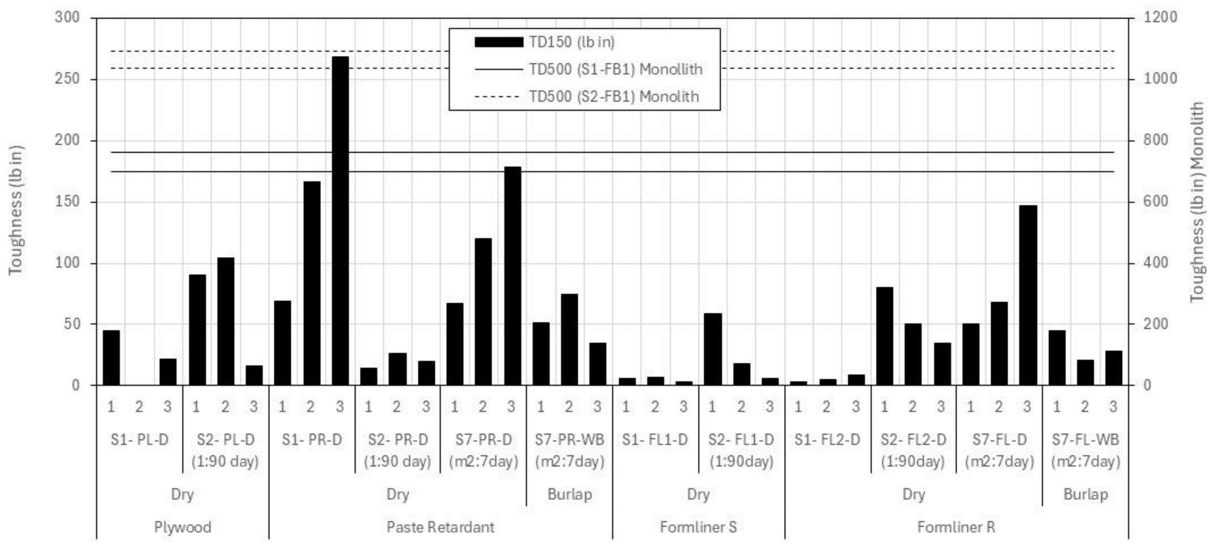

d)

Figure 4.15. Flexural performance of matchcast UHPC with various surface conditions: Plywood, Paste Retardant, and Formliners. a) Residual strength, b) Toughness.

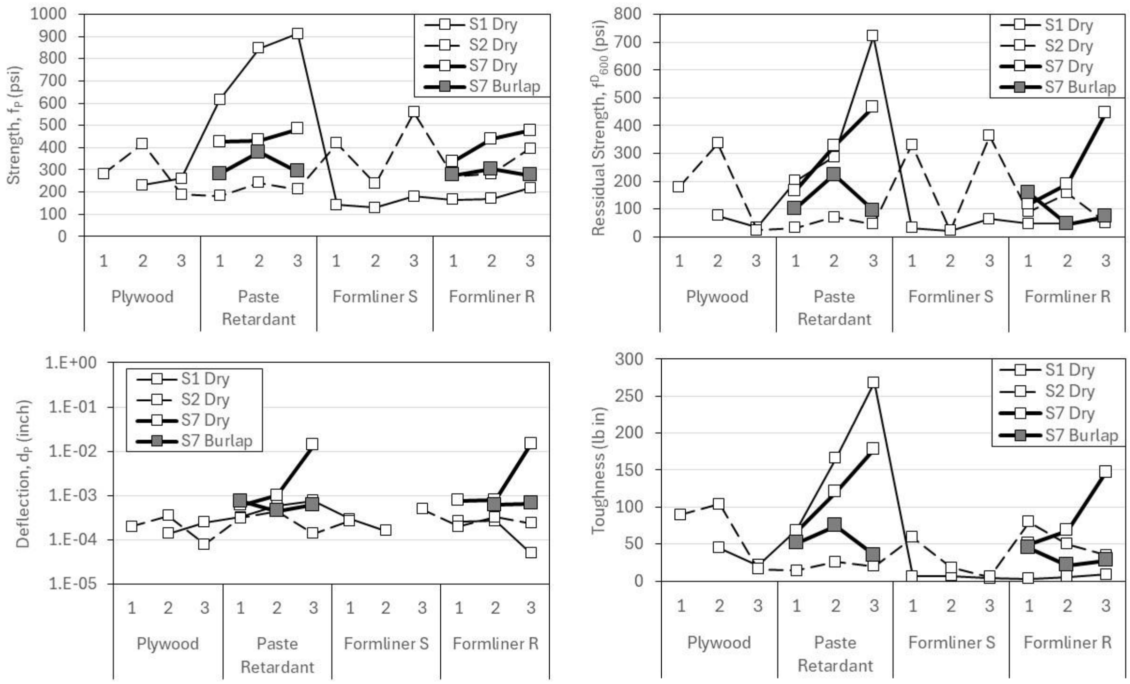

Figure 4.16. Flexural performance of matchcast UHPC with various surface conditions.

In Figure 4.14, it was evident that the flexural strength to first cracking at f_1 for the matchcast specimens was significantly smaller than the monolithically cast complementary specimens, regardless of surface condition. Correspondingly, peak strength f_P for the matchcast specimens were lower than the bulk material behavior as well. Indeed, the majority of cases, f_1 and f_P were similar if not identical. Strengthening post cracking was indicated in only a few conditions.

Prefacing the discussion, referring to development of compressive strengths, UHPC Material A in the early test sets developed f'c ~20,000 psi after day 30. In composite material beams in Set 7, the UHPC Material B developed f'c~17,500 psi by the time of testing. Since Modulus of Rupture is often correlated to compressive strength, Set 7 materials could then be expected to be lower than Set 1 materials. Indeed, this is reflected in the monolithically cast specimens.

Figure 4.16 redraws data for the flexural strength f_P and toughness T^D_{150} for easier visual comparison of data. With the exception of Set 1 Paste Retardant, Dry cast specimens (S1-PR-D), similar bifurcation of outcomes between Set 1-2 UHPC Material A and Set 7 UHPC materials. It can be observed that the early set 1 and 2 material resulted in lower strength than the Set 7 material, even though Set 7 materials contained Material B with lower f'c due to the testing at 7 days. This would indicate that even though the set 1 and 2 data have greater f'c and flexural strength than Set 7, the presence of the interface anomalies and its conditions allowed development of a weaker bond between sections. This would correspond to the lower calculated residual flexural strengths after cracking and lower toughness.

The S1-PR-D specimens showed the highest flexural bond strength, highest residual strengths, and highest toughness values; even though similar Set 2 specimens (with the difference being that the substrate concrete was allowed to cure 3 times longer) had amongst the lowest flexural response.

Head-to-head comparison of the different surface roughness conditions becomes complicated. Clear trends are also not seen within the individual test sets. The high tensile pulloff strength for the specimens cast on smooth surfaces formed from plywood presented earlier was not commensurate with the flexural strengths, residual strengths, and toughness of the flexural bond test specimens cast for that set. The stochastic nature of concrete material testing continues to make experimental work challenging.

4.2.3 Shear Pushoff

The following section shows the results of shear pushoff testing on matchcast test specimens with various surface conditions, conditioning (including wetting and fiber corrosion), and dissimilar substrate and matchcast UHPC materials. Groupings of test results from complementary test sets are presented for each figure in Figures 4.17-4.18.

Figure 4.17 and 4.18 shows results from test sets 1 and 2. Comparisons on the effect of various surface conditions (roughness) are presented, including a smooth interface using plywood, textured surface with two forms of formliner, and exposed steel fibers at the interface with the use of a paste retarder. Set 2 replicated the testing in Set 1 with the additional test condition where the UHPC material A substrate was allowed to cure for 90 days instead of 28 days before casting of the matchcast UHPC material A. UHPC material A developed a compressive strength, f'c exceeding 20,000 psi at 90 days. At the time of testing the substrate developed f'c exceeding 24,000 psi and the matchcast concrete exceeded 22,000 psi at the time of testing at ~120 days. For sets 1 and 2, an alcohol-based compound was used that resulted in both exposed fibers and significant surface roughening due to an unintended reaction of the compound and foam formwork material used for the shear pushoff test.

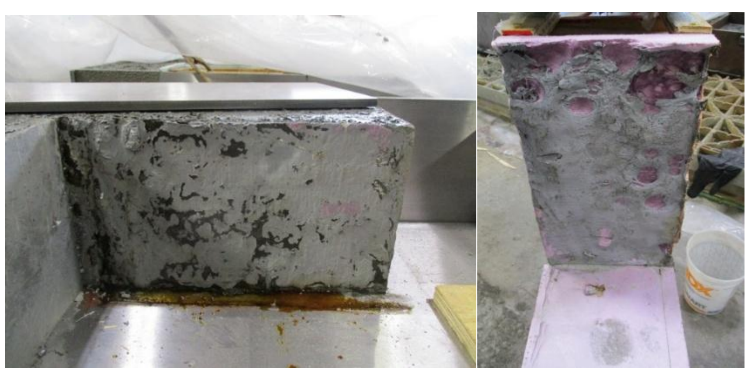

Photo 4.5. Roughened concrete laitance prior to pressure washing (left) and reaction of paste retarder with foam molding material (right).

Photo 4.5 shows an example of the resulting effect. This effect was not developed for the flexural bond test, and pulloff testing presented earlier as the foam formwork was not used. After set 1 and 2, a water-based paste retardant was used, and the dual presence (although of interest albeit without good control) of exposed steel fibers and surface roughening combined with exposed fibers was not further tested. Details of the paste retarders are described in Section 2.2.4.

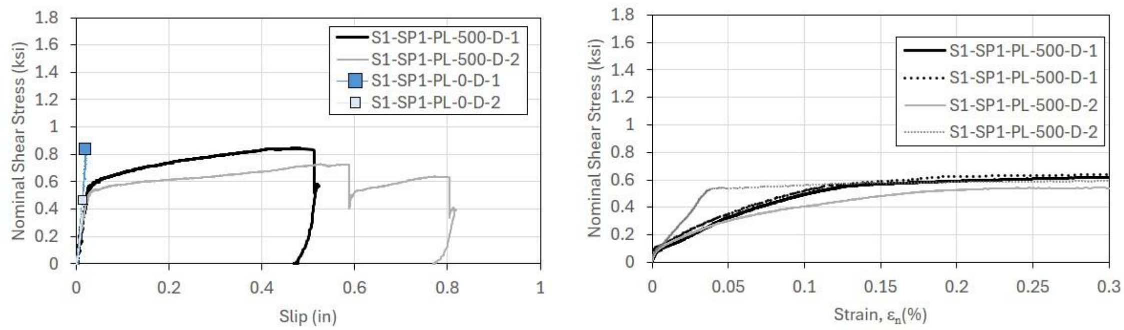

a)

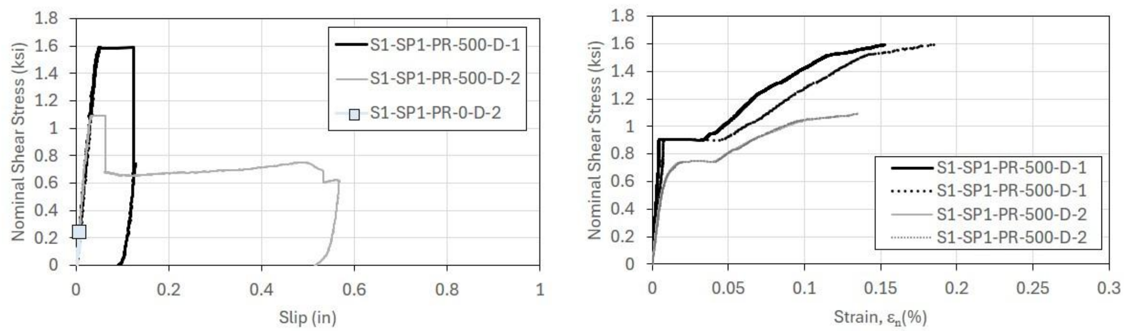

b)

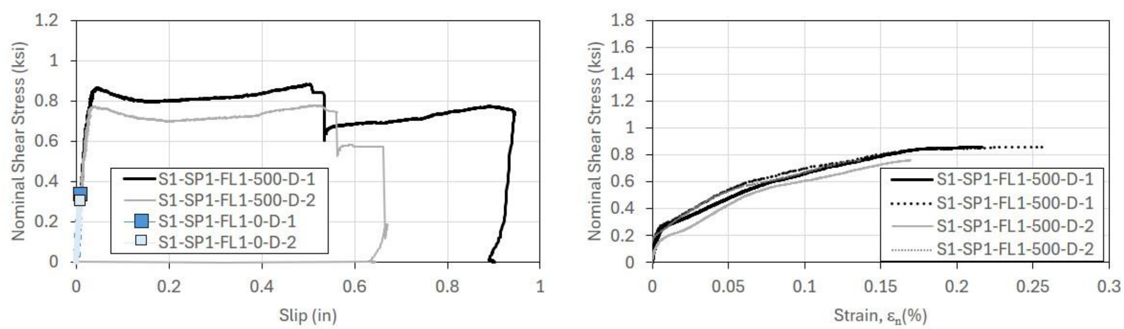

c)

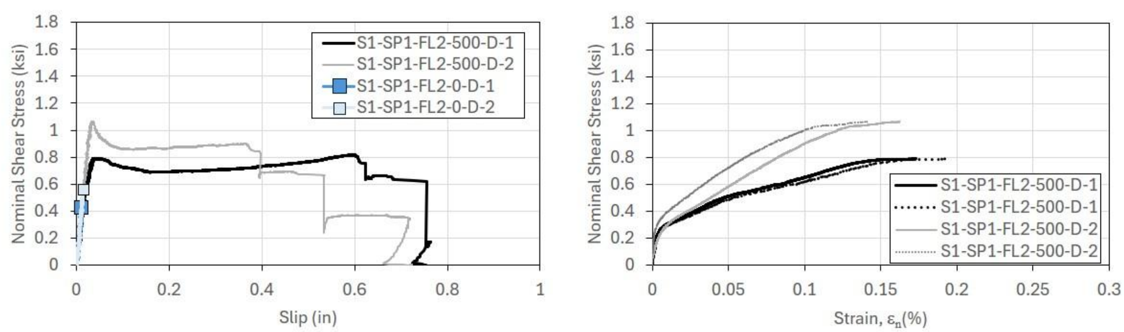

d)

Figure 4.17. Shear pushoff comparison of cast concrete surface roughness (Dry surface condition)- Plywood, Paste Retardant, and Formliners (S1 Data). Top to Bottom: a) Plywood, b) Paste retardant at 28 day, c) Formliner 1 at 28 day, d) Formliner 2 at 28 day. Strain data for top and bottom rebar. Replicate data shown.

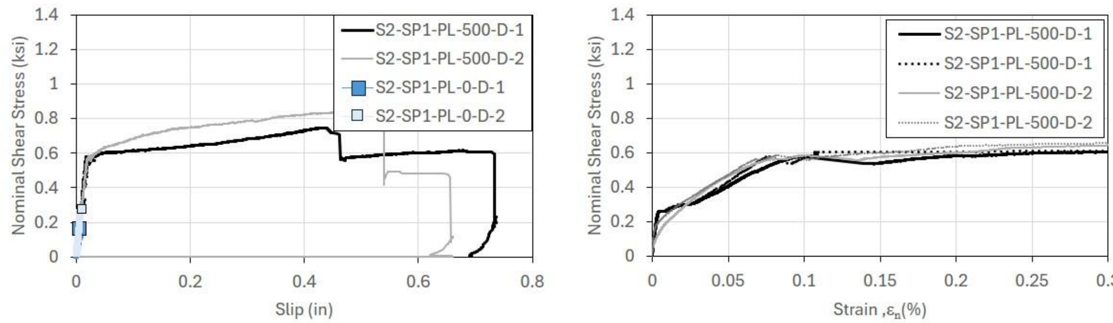

a)

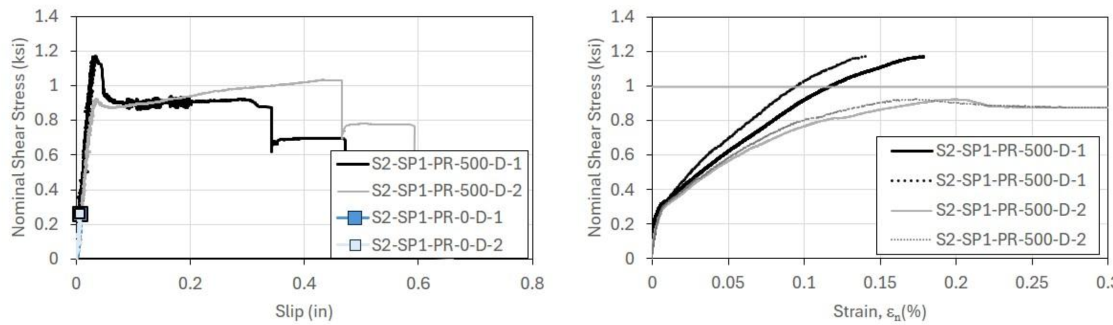

b)

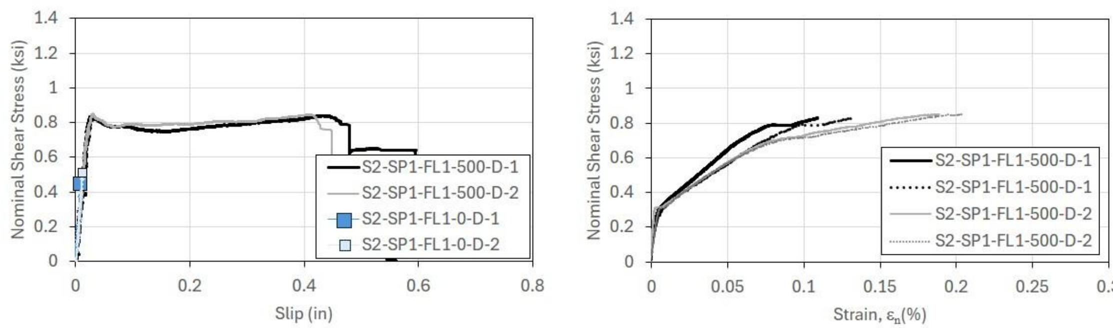

c)

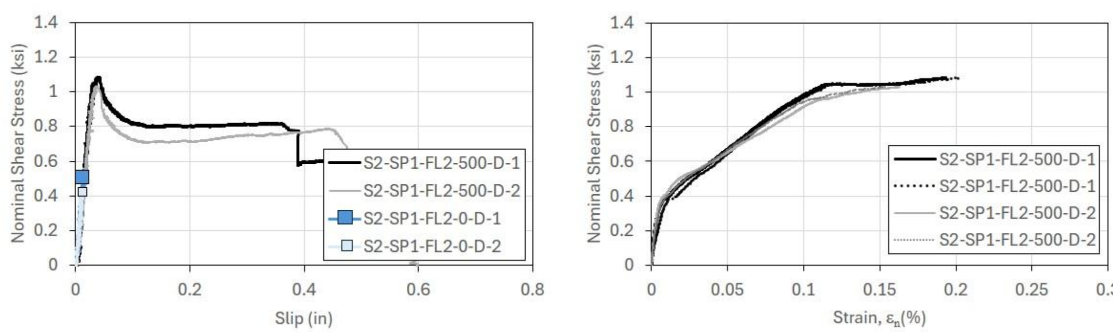

d)

Figure 4.18. Shear pushoff comparison of cast concrete surface roughness (Dry surface condition)- Plywood, Paste Retardant, and Formliners (S2 Data). Top to Bottom: a) Plywood at 90 day b) Paste retardant at 90 day, c) Formliner 1 at 90 day, d) Formliner 2 at 90 day. Strain data for top and bottom rebar. Replicate data shown.

Further discussion on the effect of the surface condition on shear performance is presented in Chapter 5.

4.3 Matchcast UHPC- Surface Wetting and Exposed Steel Fiber

Surface wetting is often prescribed for conventional concrete to promote wetting of coarse aggregate and promote cement hydration at the interface surface. However, UHPC does not contain coarse aggregate and is expected to develop a highly impermeable bulk material. It was thought that wetting regimes just prior to matchcasting would simply create a surface wet condition similar to a surface spray condition.

In these test sets, surface wetting conditions included prolonged ponding in calcium hydroxide solution, prolonged wet burlap exposure, surface wet by spray just prior to matchcasting, or maintained in a dry ambient sheltered indoor environment (Table 4.1).

Table 4.1. Surface wetting conditions

<table>
<tr><th colspan="3">Wetting Condition</th><th>Conditioning</th></tr>
<tr><td colspan="3">Surface Dry</td><td>Indoor Storage</td></tr>
<tr><td rowspan="3">Surface Wet</td><td colspan="2">Spray</td><td>Indoor Storage. Surface sprayed with tapwater ~15 min prior to casting</td></tr>
<tr><td rowspan="2">Continuous Moisture</td><td>Burlap</td><td>Burlap placed on surface and wet by irrigation system or manual routine wetting</td></tr>
<tr><td>Ponding</td><td>Saturated calcium hydroxide solution</td></tr>
</table>

The burlap and water immersion regimes were made immediately after demolding of the substrate concrete 1-5 days after casting and the specimens were maintained in sealed containers where moisture was maintained by a slow drip irrigation system.

Prolonged wetting during this time can result in corrosion of the steel fibers. For test conditions requiring non-corroded fibers, the concrete within the containers stored outdoors was treated with a vapor-phase inhibitor to mitigate surface rusting. Supplemental testing on the use of the vapor phase inhibitor was described in Chapter 3. Specimens that were wet by ponding had a saturated calcium hydroxide solution to both create an alkaline solution to prevent steel corrosion and also mitigate any leaching effects of the concrete pore water into the external ponding solution.

In some test sets, the exposed steel fibers were pre-corroded by retaining 5% NaCl solution in burlap or immersed in 5% NaCl calcium hydroxide solution for an extended period of time until iron rust was observed. Rust typically appeared as globular rusticles that remained attached to the fiber surface.

When dry or surface spray wetting conditions were needed, the interface surface was allowed to dry. Since UHPC is highly impermeable, the drying of the surface in ambient indoor environments was considered adequate. Specimens that required ponding or burlap wetting were maintained in those conditions.

4.3.1 Tension Pulloff

Figures 4.19 and 4.20 compiles results of testing from sets that compare the effects of surface wetting conditions prior to casting on a) roughened joint surfaces made with a form liner and b) exposed steel fibers made with a paste retarder. Figure 20 reproduces data from Figure 19 but redrawn to clarity of individual test cases. UHPC Material A used in these sets appear to have been less impacted by material surface anomalies than those previously presented in Section 4.2. The compiled results show consistent trends on the effect of the two surface conditions and also when the exposed fibers were pre-corroded prior to matchcasting. The results also provide evidence on the effect of moisture availability and the influence of prolonged exposure to free water on surface conditions.

Within each surface wetting regime (ponding, burlap, spray, and dry), there was consistent differentiation in the tensile pulloff strength between specimens with roughened interfaces and specimens with clean exposed fibers. Figure 4.20 replots the data for easier visual side-by-side comparisons. The pulloff strength for the specimens with the roughened surfaces by form liner (from Set 3) was consistently comparatively lower than the specimens with the exposed clean steel fibers. The specimens with the roughened surfaces also exhibited failure typically occurring at the interface.

Pulloff strength for the paste retardant cast specimens with non-corroded fibers (for Set 4) consistently had high pulloff strength on par with monolithically cast bulk UHPC, in the order of 700-1,000 psi if not greater. Failures typically occurred in the substrate. This would be expected as the fibers at the interface could engage to provide elevated tensile capacity.

However, when the fibers were pre-corroded, the tensile pulloff strength was generally lower (with some exceptions with outlying data points and conditions with non-prescribed water dosage in the matchcast, where Set 5 had lower water content in the overlay UHPC coincidently resulted in higher pulloff strengths)). The exposed clean fibers created sufficient connection to the substrate that failure typically occurred as cohesive failure of the substrate. Surfaces wet under burlap showed substrate failure in 15 of 21 cases, surfaces ponded in solution 3-6 of 15 cases, surfaces water sprayed 7-10 of 15, and surfaces in ambient dry conditions 11 of 15 cases. This general trend appears throughout various tests described later in this section.

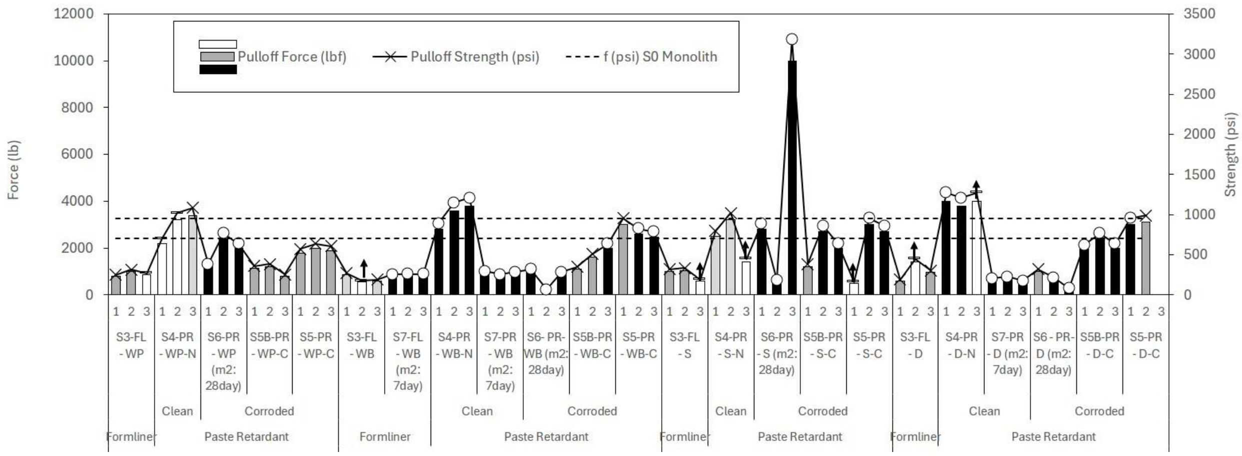

Figure 4.19. Pulloff force and strength of matchcast UHPC Material A and B with various surface wetting conditions. White (-): Adhesive failure, Grey (x): Interface failure, Black (○): Substrate failure.

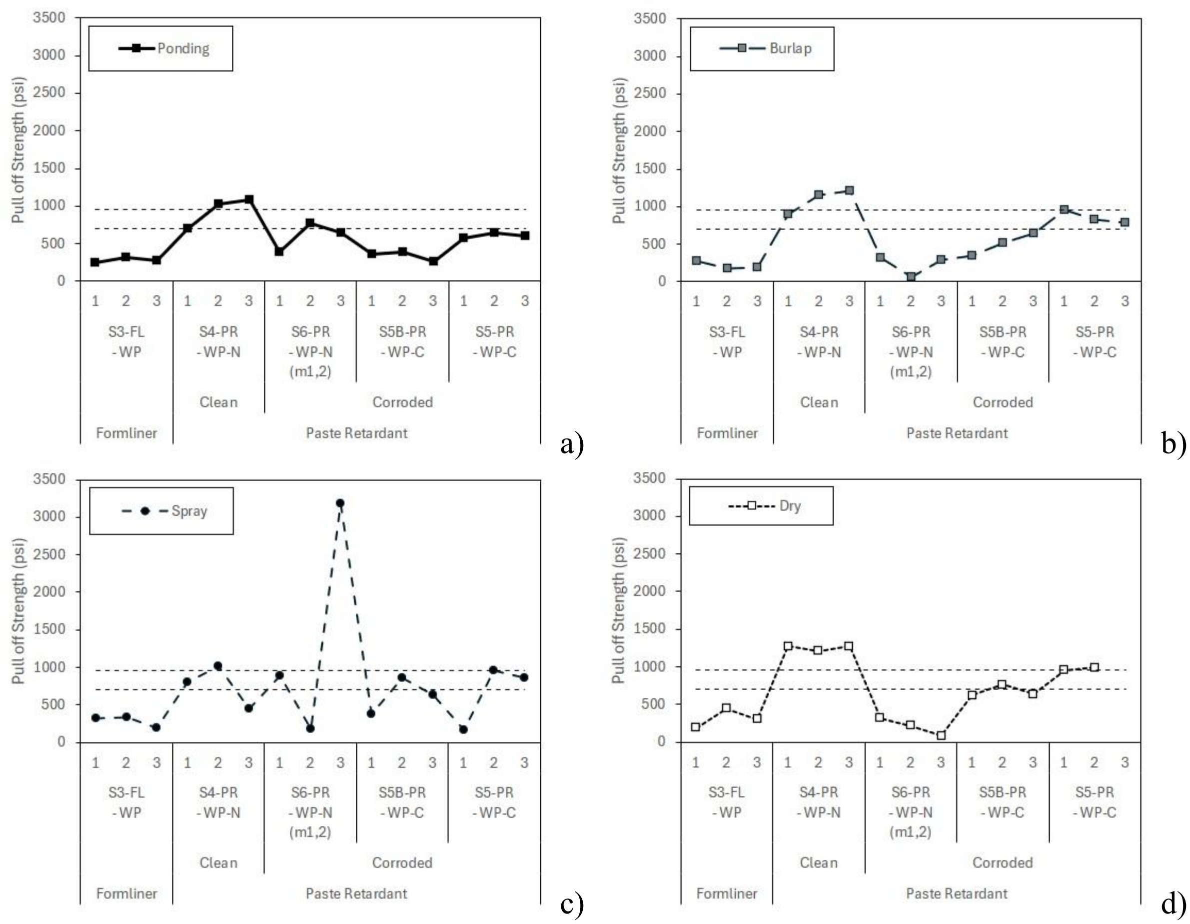

Figure 4.20. Pulloff strength of matchcast UHPC material with various surface wetting conditions. a) ponding, b) burlap, c) spray, d) dry.

Additional testing in Set 9 continued to assess the effect the pre-corroded exposed steel fibers as an extension to Set 6 with the dissimilar substrate and overlay material (UHPC Material B in the substrate and UHPC Material A in the overlay). Similar to methodologies for fiber exposure and burlap wetting described earlier were made; however, the vapor-phase inhibitor was not used. The indoor setting where the conditioning was made here was less aggressive than outdoor temperature cycling conditions utilized in earlier sets. Fiber corrosion was observed to be minimal. In addition to a non-corroded and corroded fiber condition, a third condition included pressure washing the joint surface with pre-corroded fibers to remove loose rust from the fiber surface.

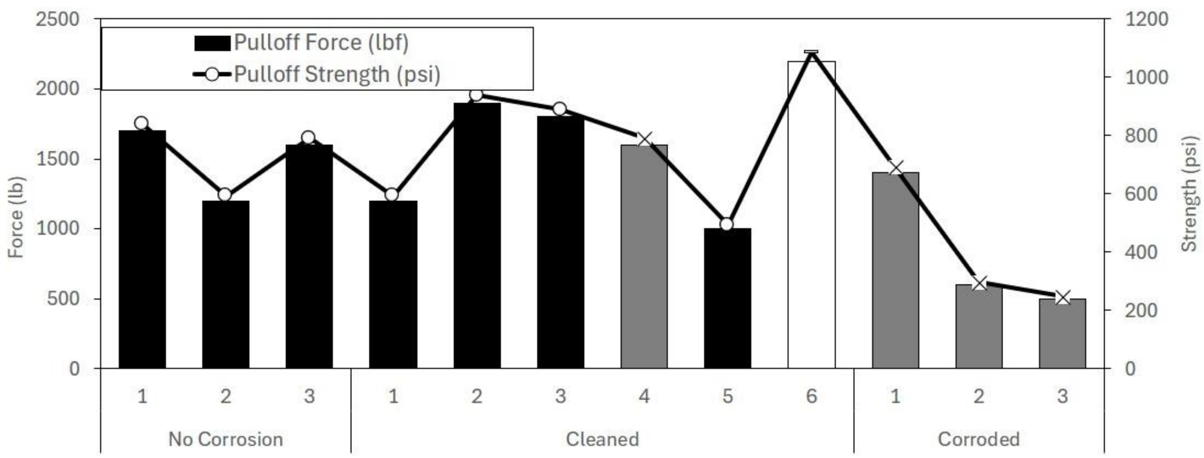

Figure 4.21. Pulloff force and strength of matchcast UHPC with cleaned and corroded exposed steel fibers.
White (-): Adhesive failure, Grey (x): Interface failure, Black (○): Substrate failure.

a)


b)


c)

Photo 4.6. Surface interface of pulloff specimens with a) non-corroded, b) cleaned, and c) corroded fibers.

As shown in Figure 4.21, the pre-corroded fibers created conditions for lower pulloff strengths with failure developing at the interface and the non-corroded fibers allowed for larger pulloff strengths and failures occurring in the substrate. Importantly, it was observed that pulloff strengths were higher when the rust was cleaned from the fiber surface. In 4 of 6 tests, the failure occurred at the substrate with one test resulting in failure of the epoxy at a high strength above 1 ksi. One of the six tests resulted in failure at the interface. Photo 4.6 shows examples of the failure modes for the non-corroded, cleaned, and corroded fiber conditions, where substrate failure occurred in the first two cases and interface bond failure occurred for the corroded case. Engaged and pulled fibers were clearly observed when failure at the substrate occurred. Little fiber engagement developed and the surface rust on the fibers were still visible after testing for the corroded fiber case. This test indicated that cleaning of the interface to remove loose rust allows for the fibers to have better development to improve their tensile performance. The test did not consider the effect of more compact forms of corrosion products and the effect of reduced cross-sectional area on bond and tensile performance.

Cleaning of the pre-corroded fibers to remove loose surface rust can be made with beneficial effect for the joint surface bonding; however, the results do not represent more severe corrosion conditions. In conditions where prolonged outdoor exposure or delayed field construction is necessary, the extent of loss of exposed fibers or significant loss of fiber cross-section should be reviewed for approval. Corrosion protection should be considered as well. Furthermore, the cleaning should be made sufficiently close to the time of the matchcast so that additional surface rust does not form and flash rusting of the bare fibers should be avoided. Damage to the exposed fibers should be avoided during the cleaning process. Wire brush was shown in trials to not be an effective means of cleaning and resulted in the removal of fibers from the surface.

4.3.2 Flexural Bond

Figures 4.22 and 4.23 shows details of test results from the flexural bond test. Figure 4.24 shows an abbreviated version of the graphs replotted for better visual comparison of test conditions. The compiled data show clear evidence that exposed clean steel fibers at the interface have positive attributes to the interface bond and more so than surface roughness alone. Similar to the outcomes from the pulloff testing, the flexural strength, residual strength, and toughness all show improved bond and mechanical performance in flexure for the exposed fibers than the roughened surface using form liner. Similar to the pulloff testing, the testing here also revealed that pre-corroded fibers negate that effect and have reduced performance. The high flexural strength, residual strength, and toughness would be consistent with the notion that exposed fibers at the interface would engage to provide elevated tensile strength.

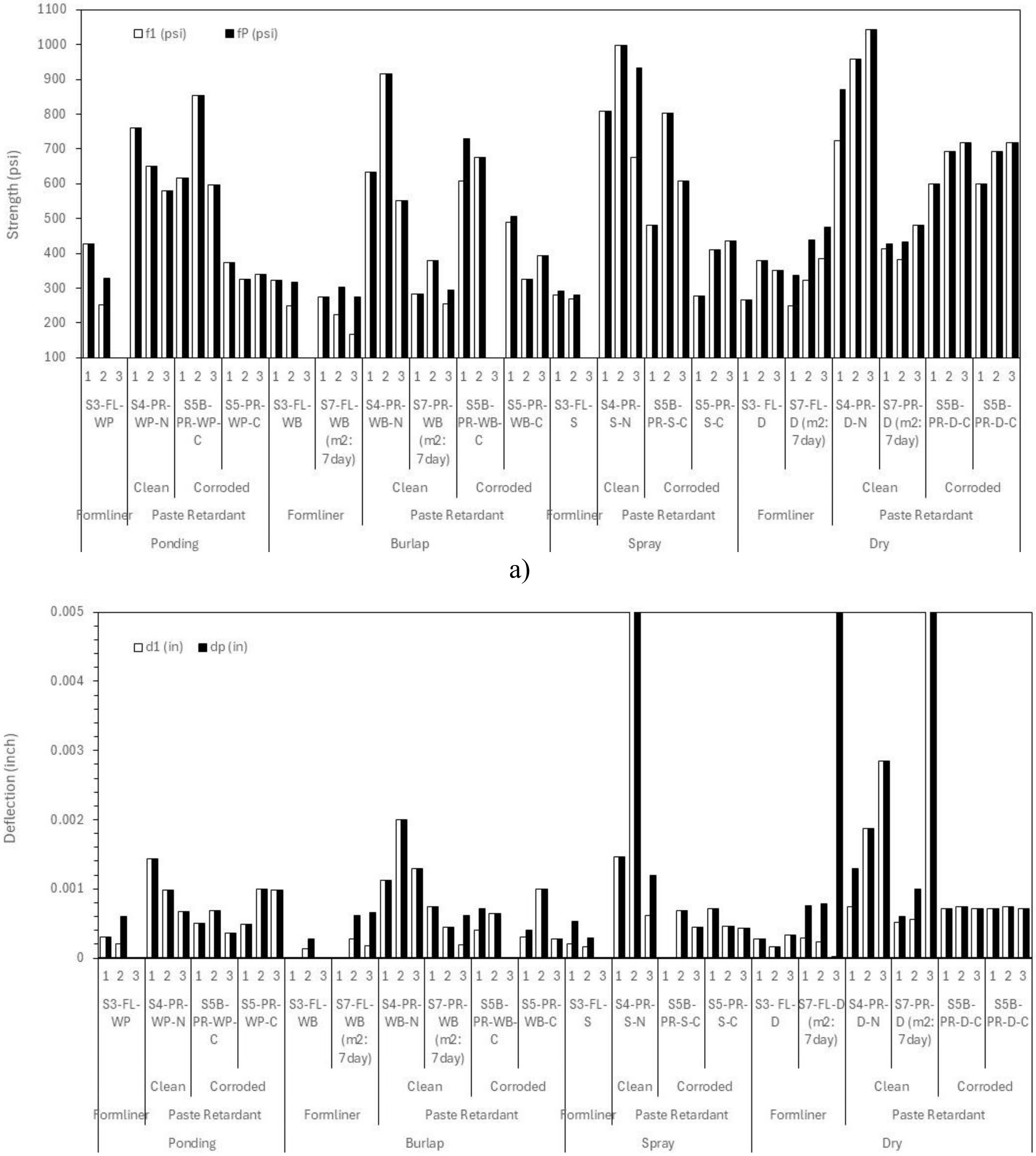

a)

b)

Figure 4.22. Flexural performance of matchcast UHPC with various surface wetting: Dry, Spray, Burlap, Ponding. a) Peak strength and first peak strength. b) Peak deflection and first peak deflection. Deflection exceeding 0.005 inch was capped for graphical clarity.

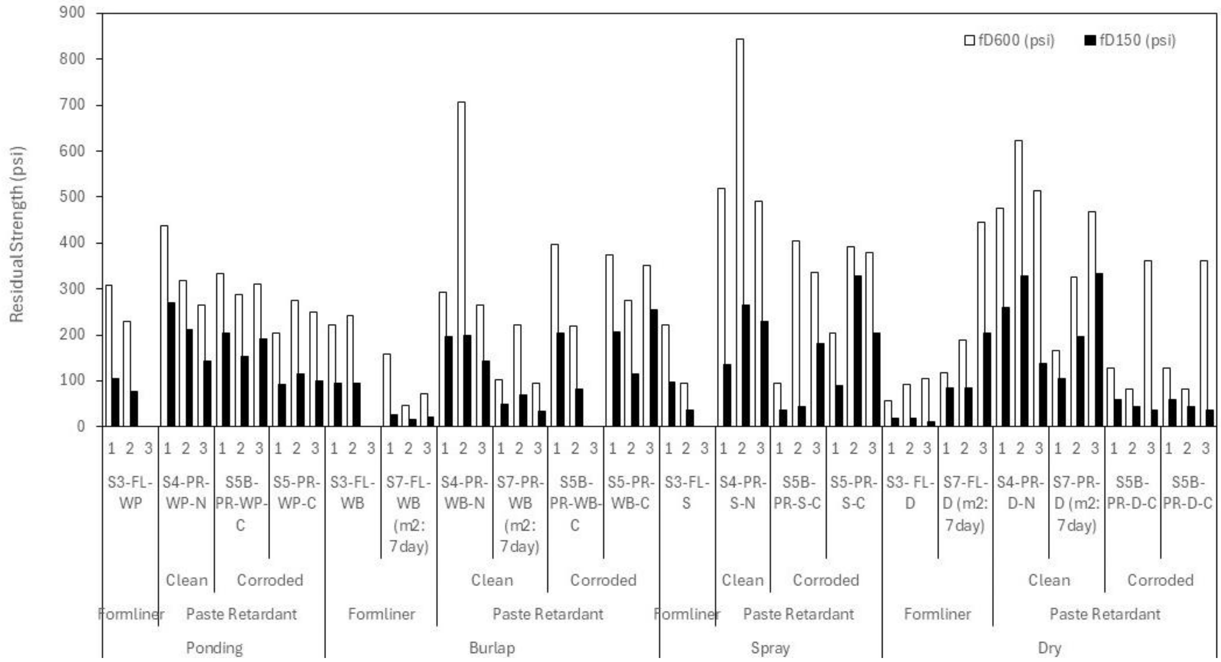

a)

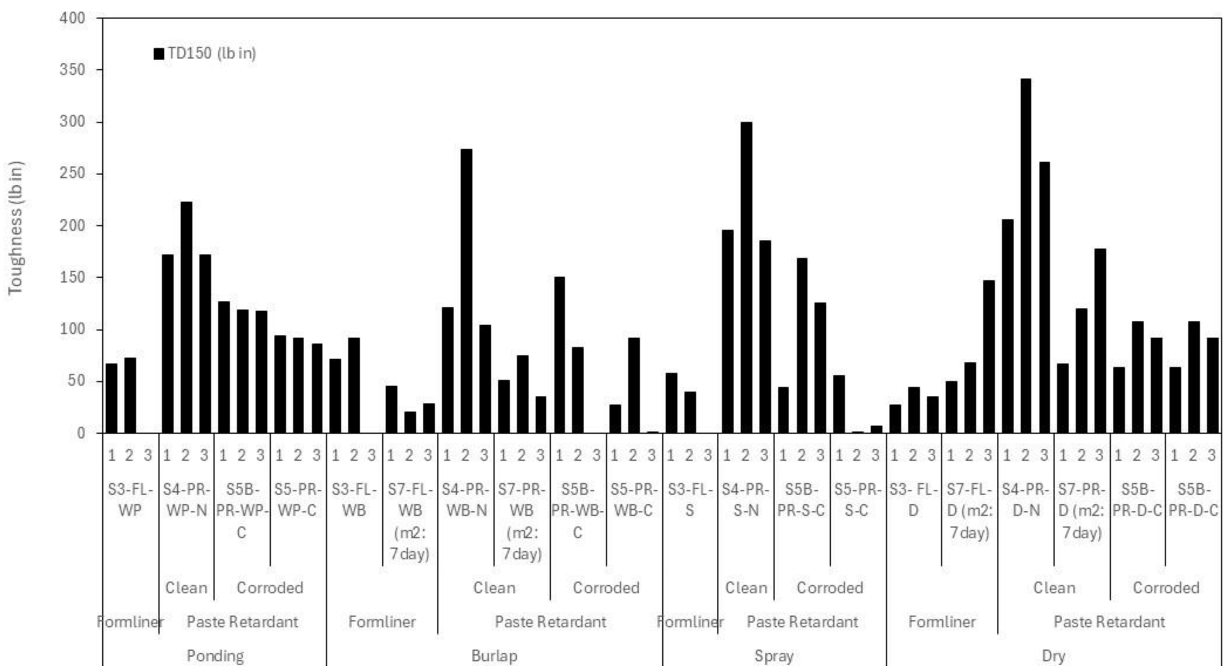

b)

Figure 4.23. Flexural performance of matchcast UHPC with various surface wetting conditions: Dry, Spray, Burlap, Ponding. a) Residual strength, b) Toughness.

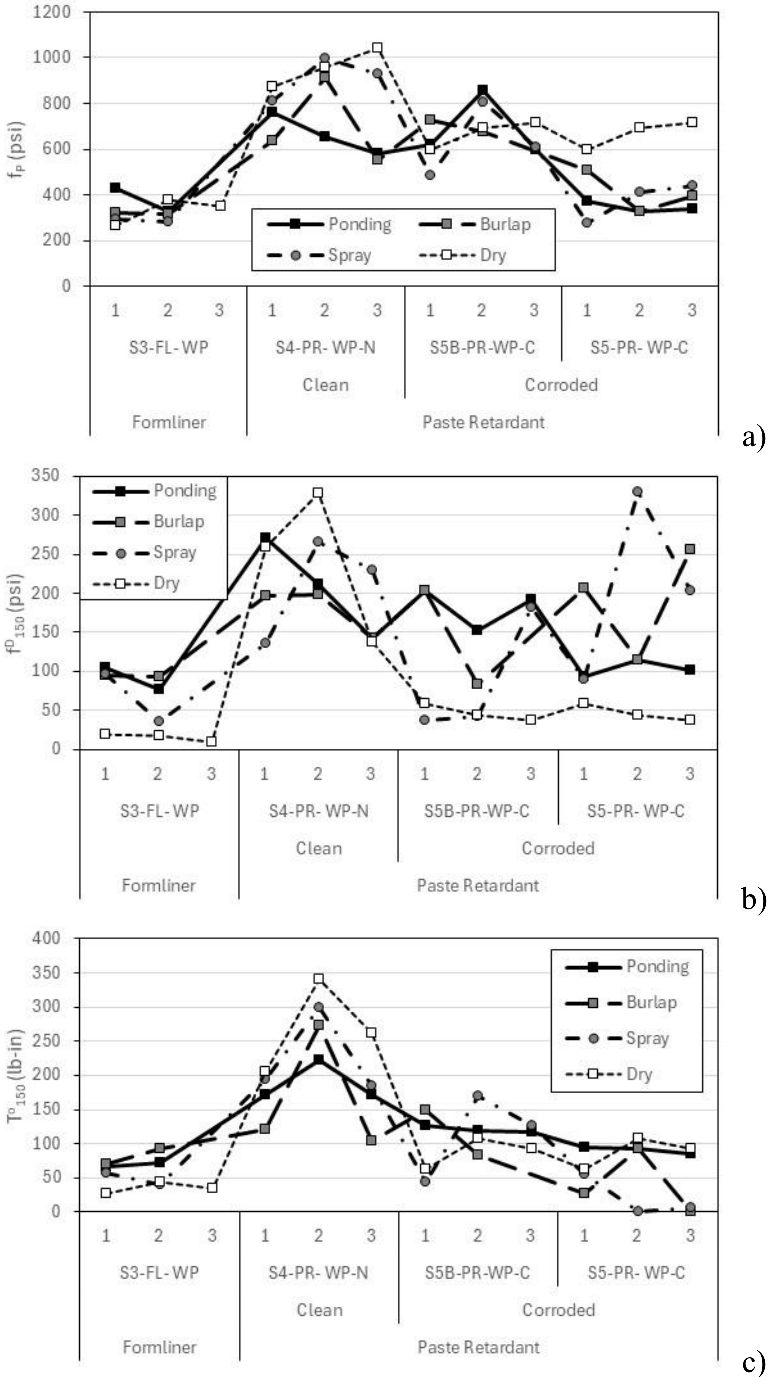

Figure 4.24. Flexural performance of matchcast UHPC with various surface wetting conditions. a) Peak strength. b) Residual strength at L/150 deflection. c) Toughness.

In terms of the role of surface wetting, it was purported that prolonged wetting in ponding conditions resulted in the lowest flexural strength and toughness, although residual strength did not show reduced values. This observation was considered to be related to how a cement-rich but low available moisture in UHPC materials cures with available internal and external moisture at various stages of development. Delayed external moisture presence such as by internal curing would conceivably allow additional hydration of remnant Portland cement clinker. But, as inquired here, excess early moisture content may be incorporated in the moisture-poor material at its cast surfaces, resulting in locally higher water-to-cement mixes. This is what is being considered as heterogeneous conditions at the interface that could affect cohesion and interface interactions. Further deliberation is made from shear pushoff testing described next.

4.3.3 Shear Pushoff

The shear stress versus slip and shear stress versus strain data are compiled in Figures 4.25-4.31 for test sets 3-7, ordered by surface wetting conditions within each figure. Representative curves were selected for abridged representation of the data in Figure 4.32. In the following, references to the full and abridged figures are presented in the discussion of data.

As presented earlier, the effect of surface wetting was of interest in these sets of experiments. The prolonged moisture exposure for some specimens— starting at early times (1-day after casting)— would likely have effects on the concrete condition at the near surface of the shear interface area. Presumably, prolonged moisture presence would promote cement hydration at the near surface and possibly create nonhomogeneous concrete strength through the bulk material. It was also posited that effects resulting in elevated levels of cement hydration would affect the cohesion of the matchcast interface. For example, considering that the f'c for UHPC is inherently high, would greater presence of unhydrated cement at the UHPC surface in the dry condition promote chemical cohesion upon wetting by the matchcast material greater than that of elevated hydration of the substrate surface? Or would the heterogeneity create local weaker planes allowing fracture to develop away from the cast interface?

Figure 4.32a (and Fig. 4.25 and 4.26) show the results of complementary data from sets 3 and 4. Test specimens had either a roughened surface (without exposed steel fibers at the interface) developed by casting with a formliner or a generally smooth surface with exposed steel fibers developed by moderate high-pressure water removal of concrete laitance produced by the water-based paste retardant.

Figure 4.32b (and Fig. 4.27 and 4-28) showing data from Set 7 further compares the effect of moisture, contrasting prolonged wetting with burlap and dry, for roughened surfaces created using form liners and exposed steel fibers as described earlier. In this set, the test specimens were maintained in a sheltered indoor environment, and the burlap wetness was manually maintained. The indoor setting was less aggressive than the conditions for sets 3 and 4 with the daily outdoor temperature cycling. The vapor-phase inhibitor was not utilized, and steel rusting of the steel fibers was minimal.

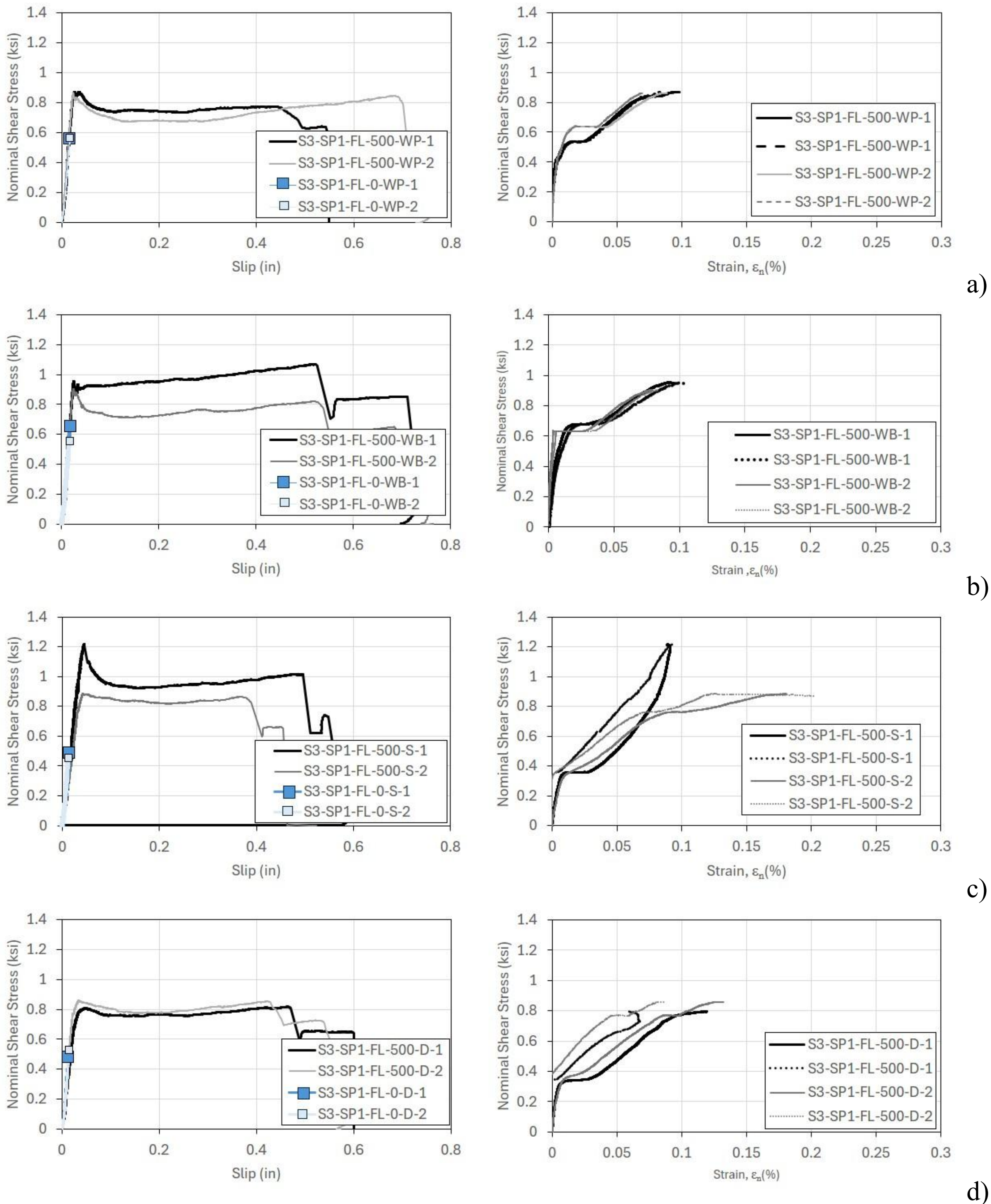

Figure 4.25. Form liner shear pushoff comparison of various surface wetting conditions: Dry, Spray, Burlap, Ponding (S3 Data). Top to Bottom: a) Ponding, b) Burlap, c) Surface spray, d) Dry conditioning. Replicate data shown.

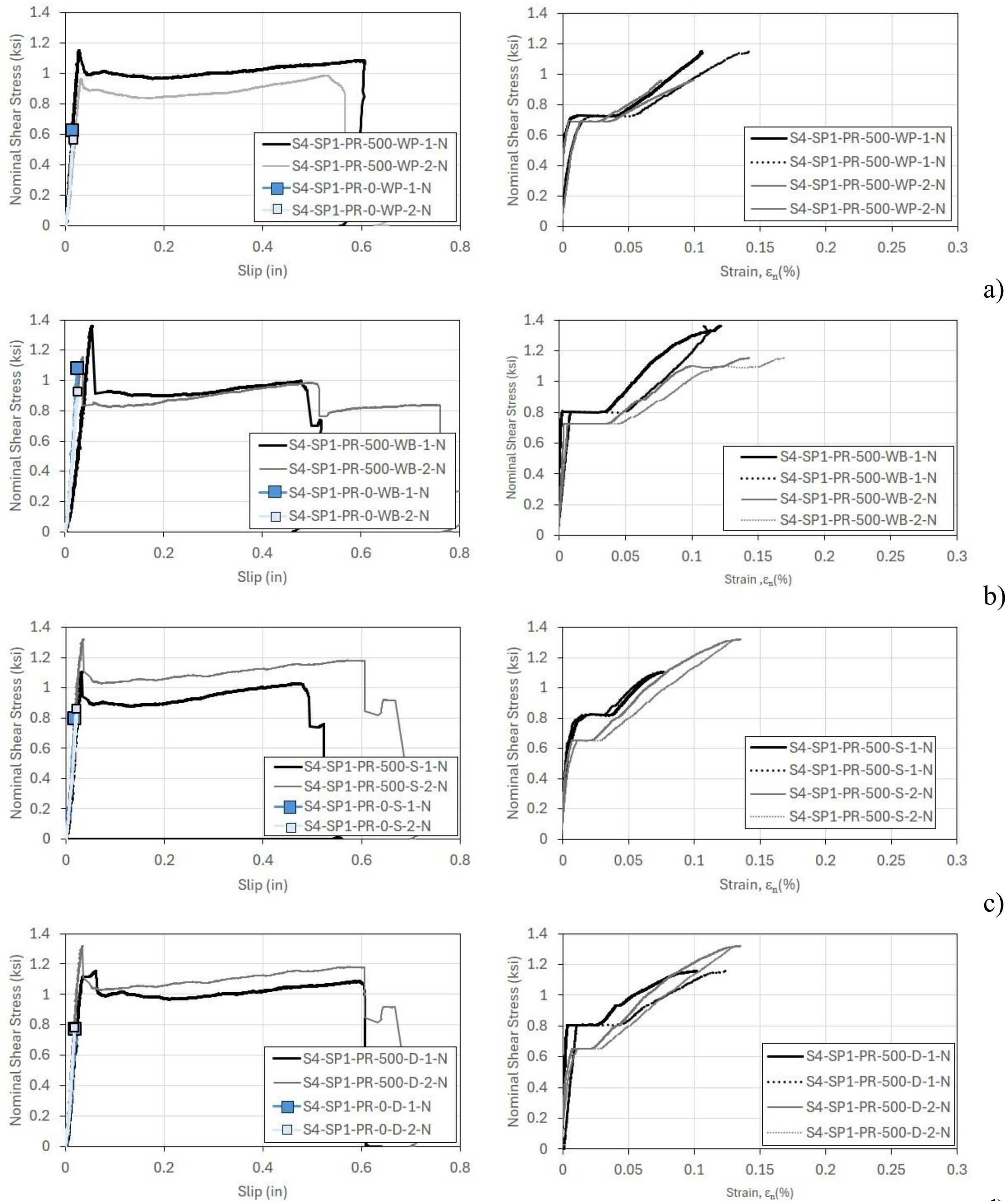

Figure 4.26. Paste retarder shear pushoff comparison of various surface wetting conditions: Dry, Spray, Burlap, Ponding (S4 Data). Top to Bottom: a) Ponding, b) Burlap, c) Surface spray, d) Dry conditioning. Replicate data shown.

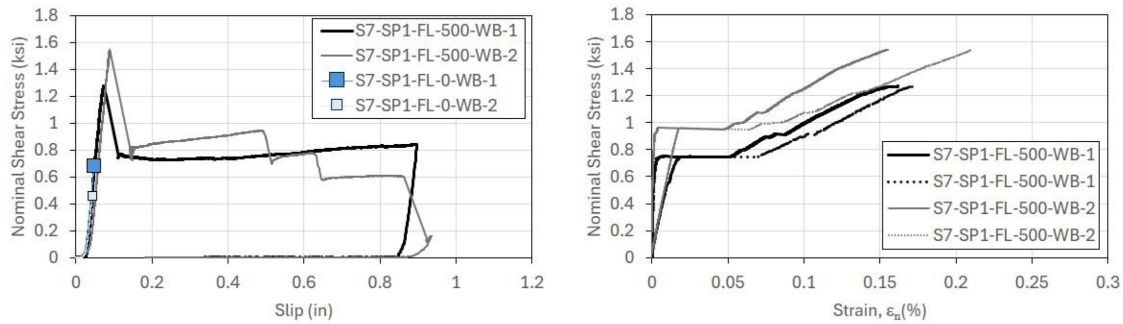

a)

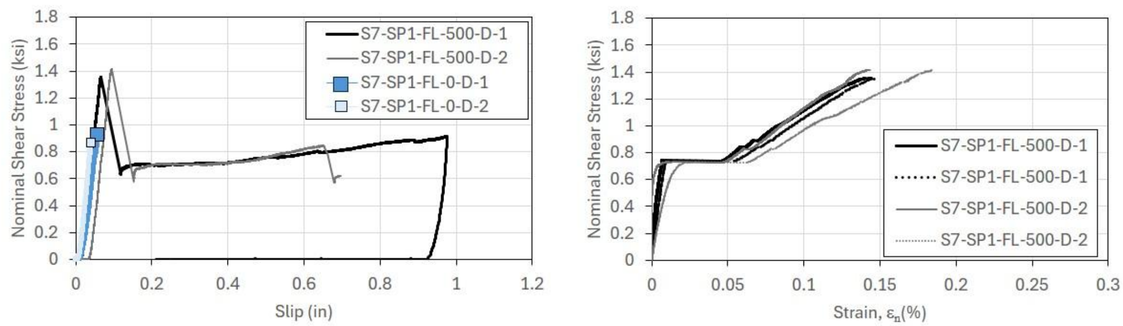

b)

Figure 4.27. Shear pushoff comparison of form liner with dry and burlap surface wetting for mixed UHPC Materials A and B (Set 7 data). Top to Bottom: a) Burlap, b) Dry. Replicate data shown.

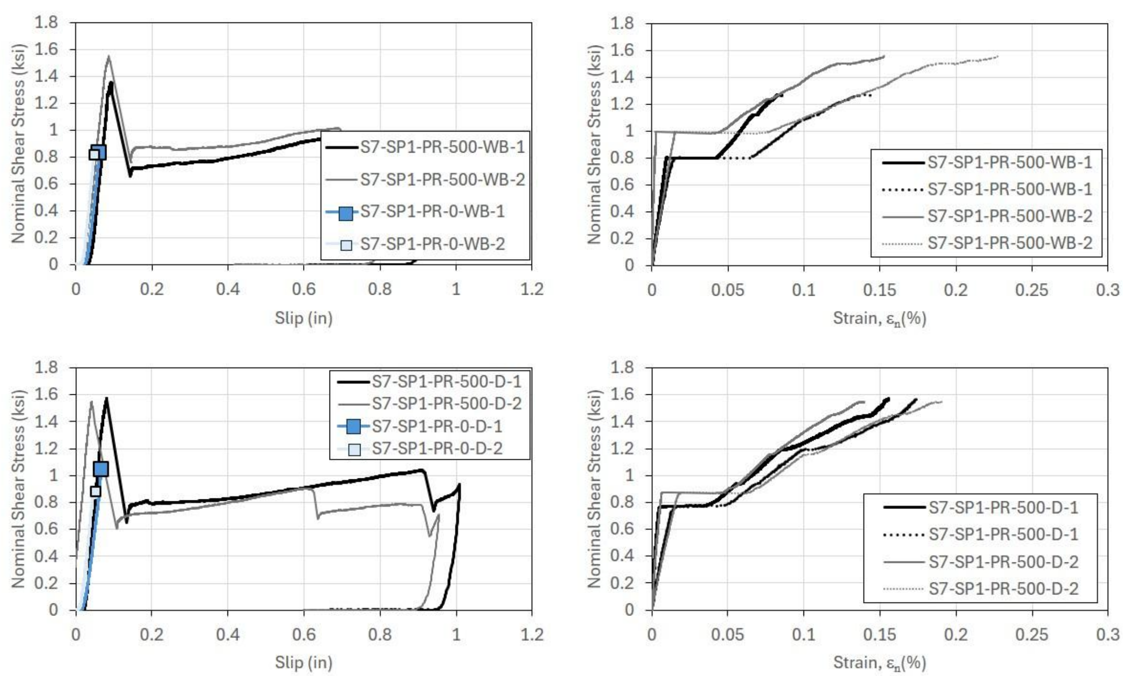

Figure 4.28. Shear pushoff comparison of paste retarder with dry and burlap surface wetting for mixed UHPC Materials A and B (Set 7 data). Top to Bottom: a) Burlap, b) Dry. Replicate data shown.

Figure 4.32c (and Fig. 4.29 and 4.30) shows results of pushoff testing from sets 4 and 5. In these test sets, steel fibers at the shear interface area were exposed by use of the water-based paste retardant. The steel fibers were either maintained with minimal corrosion with the vapor phase inhibitor or use of the saturated calcium hydroxide solution as described earlier, or pre-corroded. The steel fibers were corroded either by wetting with salt water under burlap or ponded in a 5% NaCl calcium hydroxide solution. After corrosion development (typically observed by rusticles on the exposed steel fiber surface (Photo 4.7)), the concrete surface was subjected to the various wetting regimes prior to the matchcasting.

Photo 4.7. Rust on exposed steel fibers.

Specimens intended to be cast in the dry or surface wet condition were allowed to dry out while wet burlap or ponding continued for specimens for those respective test conditions. Since the UHPC is highly impermeable, it was assumed that the drying was adequate for the concrete near surface. The extent of fiber rusting was not deliberated further than visual observations of the aforementioned rusticles. Control of metal loss (and change in cross-sectional area) was not possible as the fiber distribution was variable and ability to extend the length of the fibers out of plane from the surface was not possible without unintended fiber damage and breakage. Early anticipated research approach to address the effect of corrosion-induced fiber cross-section could not be assessed for these tests. Further deliberation was made for an additional test set (Set 9) described earlier, for the effect of the presence of the loose corrosion product on the steel surface is discussed elsewhere. The influence of surface rusting on the fiber body on the tensile capacity at the interface (such as reduced mechanical behavior during pulling and debondong) ideally could be addressed by the testing described next.

Figure 4.32d (and Figure 4.31) shows the results from Set 6. Additional testing of pre-corroded fibers was made to provide additional data and to identify behavior in dissimilar UHPC substrate (UHPC Material B) and matchcast (UHPC Material A) materials.

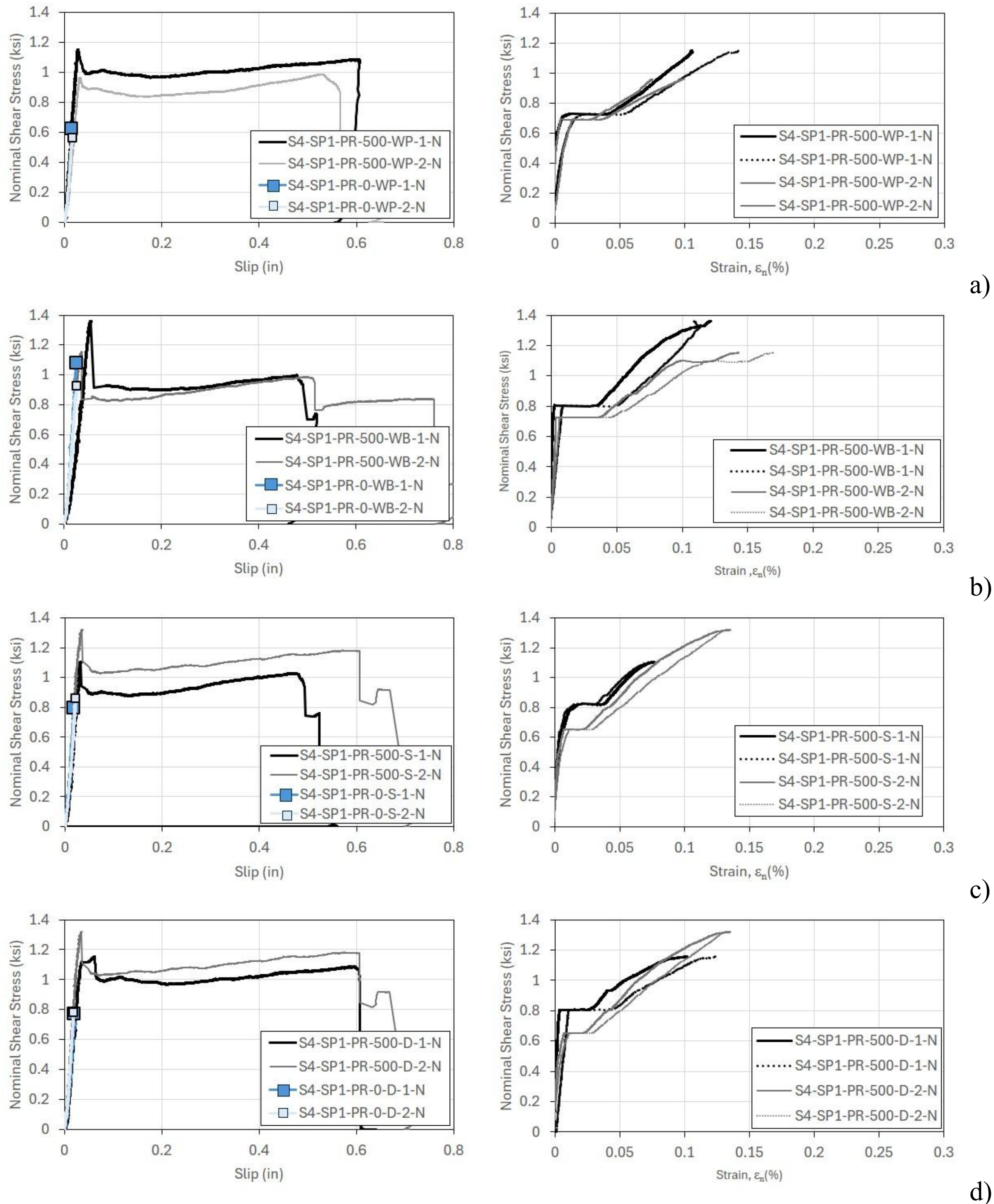

Figure 4.29. Shear pushoff comparison of non-corroded surface fibers with various surface wetting: Dry, Spray, Burlap, Ponding (S4 Data- Reproduced from Fig. 4.26). Top to Bottom: a) Ponding, b) Burlap, c) Spray, d) Dry. Replicate data shown.

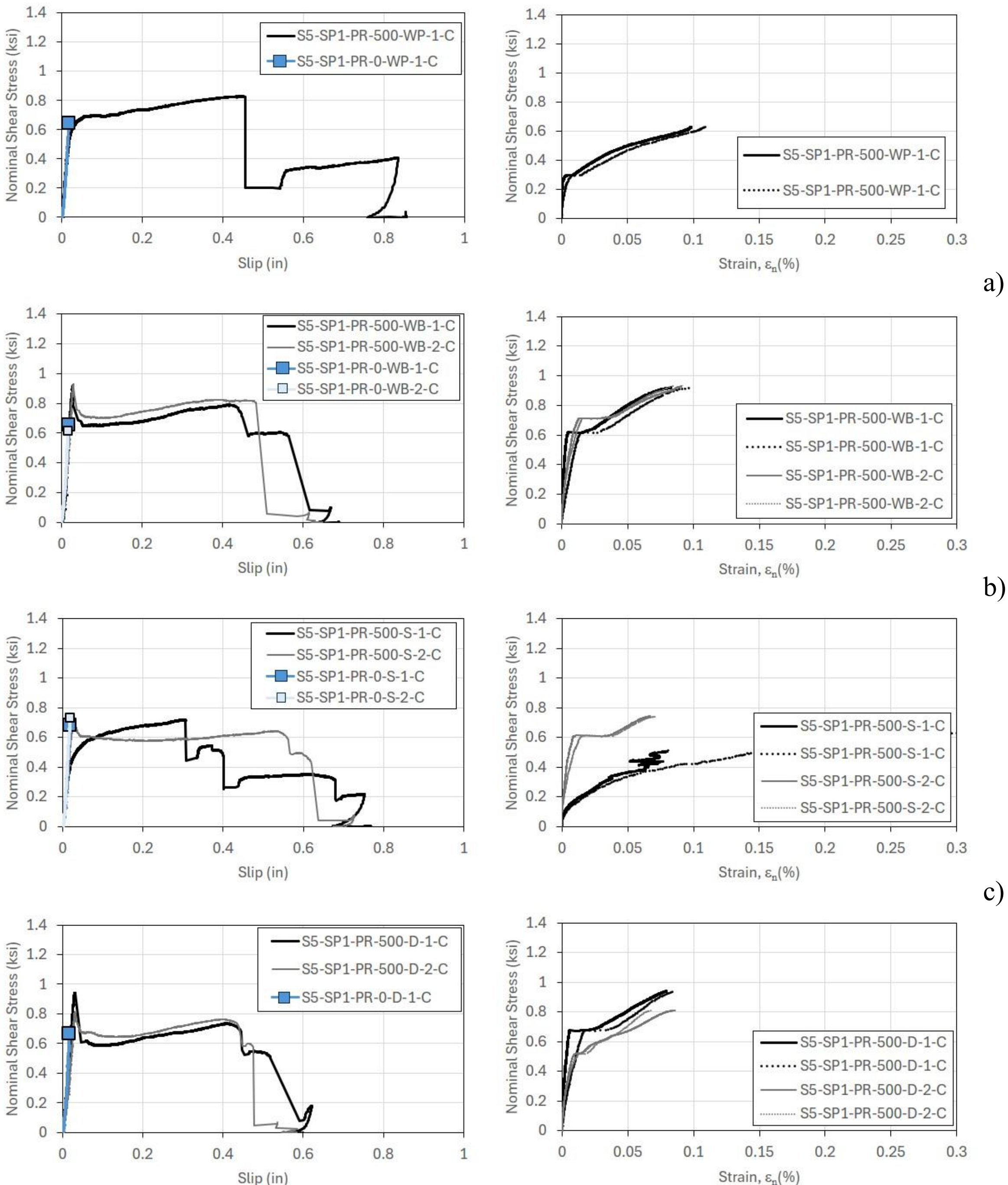

Figure 4.30. Shear pushoff comparison of pre-corroded surface fibers with various surface wetting: Dry, Spray, Burlap, Ponding (S5 Data). Top to Bottom: a) Ponding, b) Burlap, c) Spray, d) Dry. Replicate data shown.

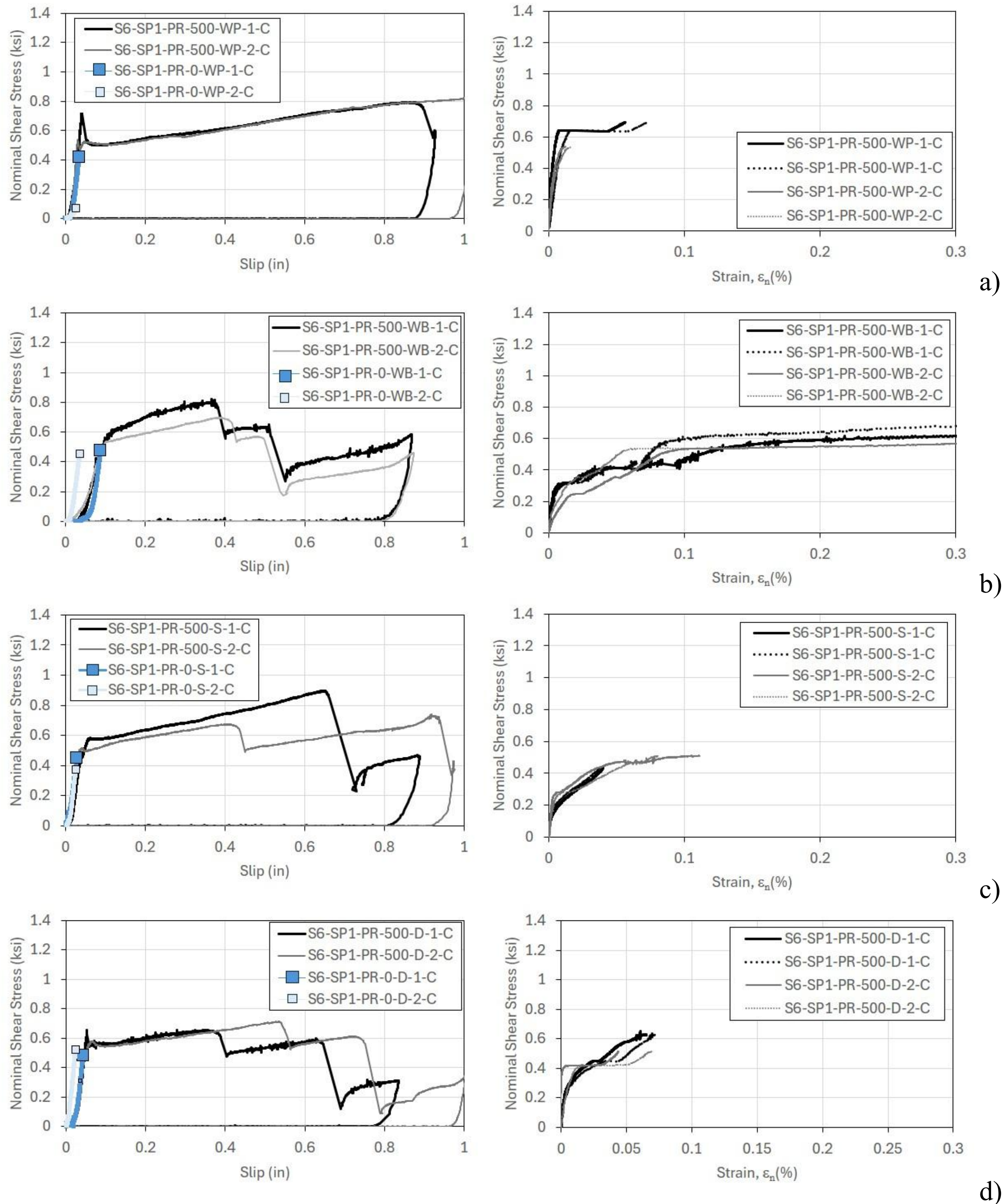

Figure 4.31. Shear pushoff comparison of pre-corroded surface fibers in dissimilar cast UHPC materials with various surface wetting: Dry, Spray, Burlap, Ponding (S6 Data). Top to Bottom: a) Ponding, b) Burlap, c) Spray, d) Dry.

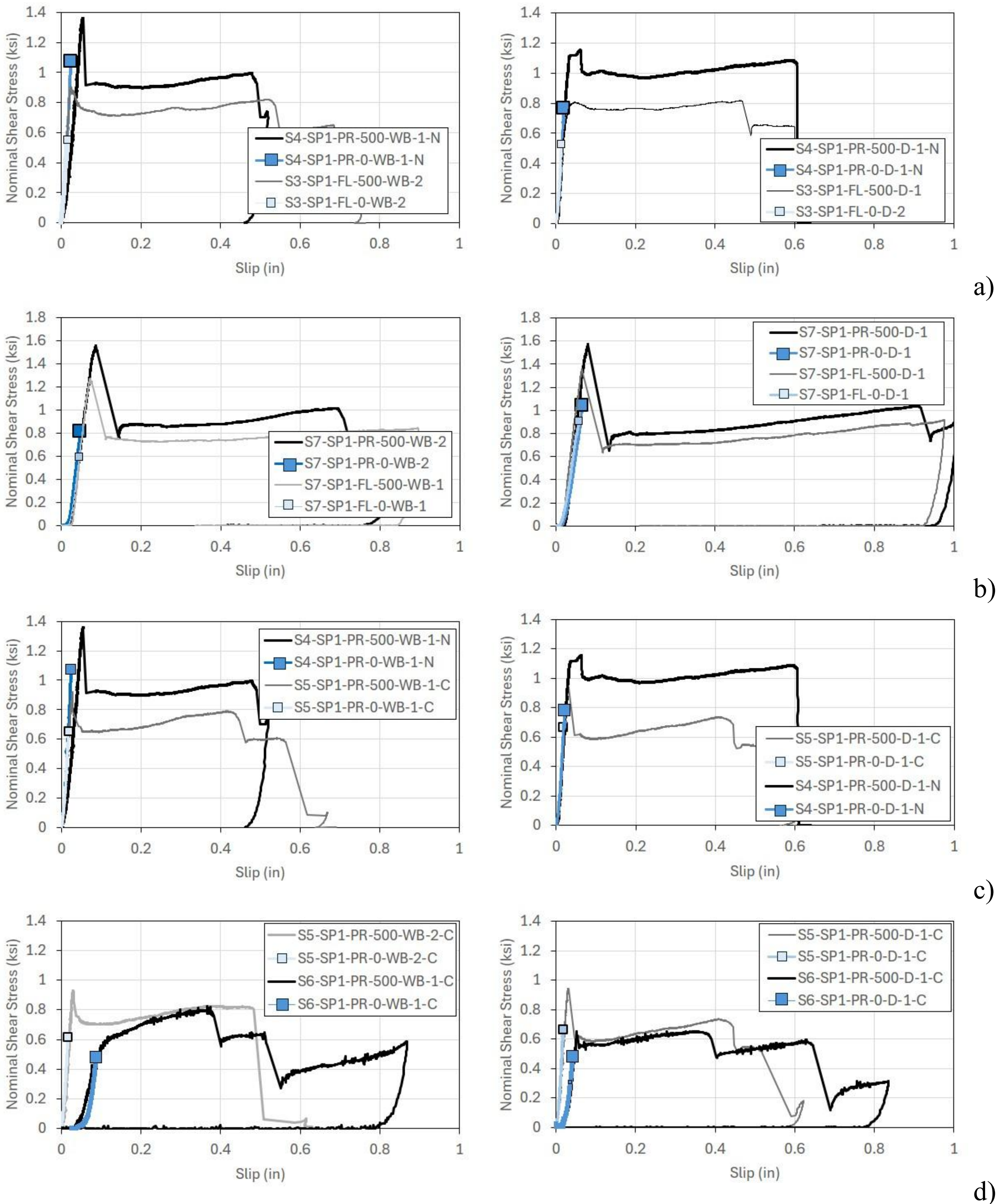

Figure 4.32. Overview of shear pushoff performance with joint interface with exposed steel fiber. a) Comparison of form liner and paster retardant. b) with dissimilar UHPC. c) Effect of pre-corroded fibers. d) Comparison of corroded fiber cast dissimilar and homogeneous UHPC matchcast. Left) Burlap. Right) Dry.

Side by side comparisons of the curves in Figures 4.23 to 4.29 are difficult to make, so extracted parameters were directly compared in Figures 5.1 to 5.4 presented in the next section.

5 EFFECTS OF SURFACE CONDITIONS ON COHESION AND FRICTION

5.1 Exploration on Effect of Cast Surface Conditions and Surface Preparation

The shear stress versus slip and the stress-strain curves for the matchcast test specimens presented in Sections 4.2.3 and 4.3.3 show similar overall characteristics as the monolithically-cast specimen. Notable features include greater f_P values for the rebar reinforced specimens (ρ_v=9.2e-3) than the unreinforced specimens (ρ_v=0) associated with the elevated capacity due to the post-crack clamping pressure, interface friction and fiber contributions. Due to the lower f_p values for the matchcast specimens than the monolithically cast specimens, the crack widening of the interface occurred with a quicker transition to post peak behavior sustained by the reinforcing steel, that was able to retain some capacity with additional loading until rebar rupture. In some cases, there was some strengthening that may be attributed to strain hardening of the rebar. For structural considerations, these effects post f_p would not be dependable as the effect would not necessarily be reproducible. In the stress-strain curve, the specimens show approximate linear behavior until transition to a plateau that was nominally attributed to UHPC cracking, f_{crack}, although the actual formation of the first crack may develop earlier. The increase in strain at f_{crack} was not necessarily expected if the fibers in the UHPC engage to prevent significant crack widening. The initial observation was initially attributed to less effective fiber engagement at the shear interface for the matchcast specimens in comparison to monolithically cast conditions. However, similar behavior was observed for the control monolithically cast specimens described earlier. After f_{crack}, there was a bilinear behavior in the stress-strain curve associated with engagement of the fibers up to f_P where the capacity of the fibers is exceeded and the crack widens to a point where the reinforcing steel solely carries the load.

Some specimens had some deviation to these general characteristics. Some cases, such as for the matchcast specimens on a smooth interface cast with plywood, did not show the distinct f_P peak at earlier strains (relating to a clear transition from fiber-loaded to rebar-loaded conditions), and instead showed a continued increase up to rebar fracture. Strain in the following figures was capped at 0.5% for clarity. Evidently the strain at these maximum values would well exceed the strain capacity of the rebar, fy (equivalent to ~0.2% in the graphs). For the typical conditions, the rebar strain at f_P was near or below fy.

Figures 5.1 and 5.2 have shear pushoff test parameters sorted by surface conditions such as roughness, (including smooth interface cast by plywood, roughened surface made by two formliners, and exposed steel fibers at the shear interface created by a paste retardant). It is reminded that specimens in sets 1 and 2 had a mixed roughened and exposed fiber condition. Figures 5.3 and 5.4 have shear pushoff test parameters sorted by surface preparation conditions such as wetting conditions, including dry, surface spray, and prolonged wetting by burlap and ponding.

Due to the large variable set in the experiments, limited test population, and the stochastic nature of concrete testing where exact control of all parameters is not possible (ranging from variations in raw material, casting conditions, strength development, fiber orientation and distribution, environmental and temperature effects), discussion of the test results will be made relating to general gleaned trends that incorporate multiple test sets with remark on the effects of the variable test parameters for the sets. When direct trends are obscured, conjecture of possible mechanisms is presented for discussion with the caveat that additional testing would be needed for resolution.

Crack stress, f_{crack}: The approximation of the shear stress at first crack of the matchcast specimens was made by assuming the value at failure for the non-reinforced (ρ_v=0) specimens (labeled as '0') and the value obtained at f_{crack} from the stress-strain curves for the reinforced (ρ_v=9.2e-3) specimens (labeled as '500'). The stress-strain curves often did show indication of the beginning of the transition to f_{crack} at earlier loads. This value was difficult to isolate without additional data treatment, and the f_{crack} characteristic was considered as a useful marker due to its distinct display.

Of note and for further persuasion of its consideration, f_{crack} was in the order of values typically associated with UHPC 1st cracking. As shown in Figures 5.1 and 5.3, the resolved values of f_{crack} for each test condition (for both '0' and '500' ksi reinforcement levels) were similar. As such, comparisons of the various surface conditions and preparation and their effect on interface chemical cohesion may be gleaned. After a general discussion of the results, details on the cohesion coefficient, c is presented later.

Figure 5.1 shows two distinct f_{crack} value ranges, (0.2< f_{crack}<0.5 ksi and 0.6< f_{crack}<1 ksi) for the many test parameters presented. The most prominent distinction between these two ranges is associated with UHPC material. Set 1and 2 utilized UHPC Material A and Set 7 utilized UHPC Material B in the substrate and Material A in the matchcast. This provides indicators that the material itself affects contribution to strength by its chemical cohesion. There are various reasons for this effect including concrete surface physical conditions, amount and degree of hydration of Portland cement in UHPC materials that have low water availability, and the effect of wetting conditions that affect the level of hydration at the interface surface. Indeed, early testing of UHPC material A (such as for sets 1-2) showed a surface skin layer on the outer cast surface area (Photo 5.1 and Photo 5.2) that was porous and sometimes friable.

Photo 5.1. Porous friable UHPC skin material.

Photo 5.2. Pores at surface of deficient interface concrete.

As previously introduced, this effect was thought to be due to differential water evaporation and high surface tension of UHPC that can affect movement of entrapped air. This effect was less in later mixes of the material (possibly in part due to newer raw material, adjustment of accelerator admixture, and greater experience handling the material. Indeed, as shown in Figure 5.3, the higher range of f_{crack} was resolved for UHPC Material A in test sets 4 and 5.

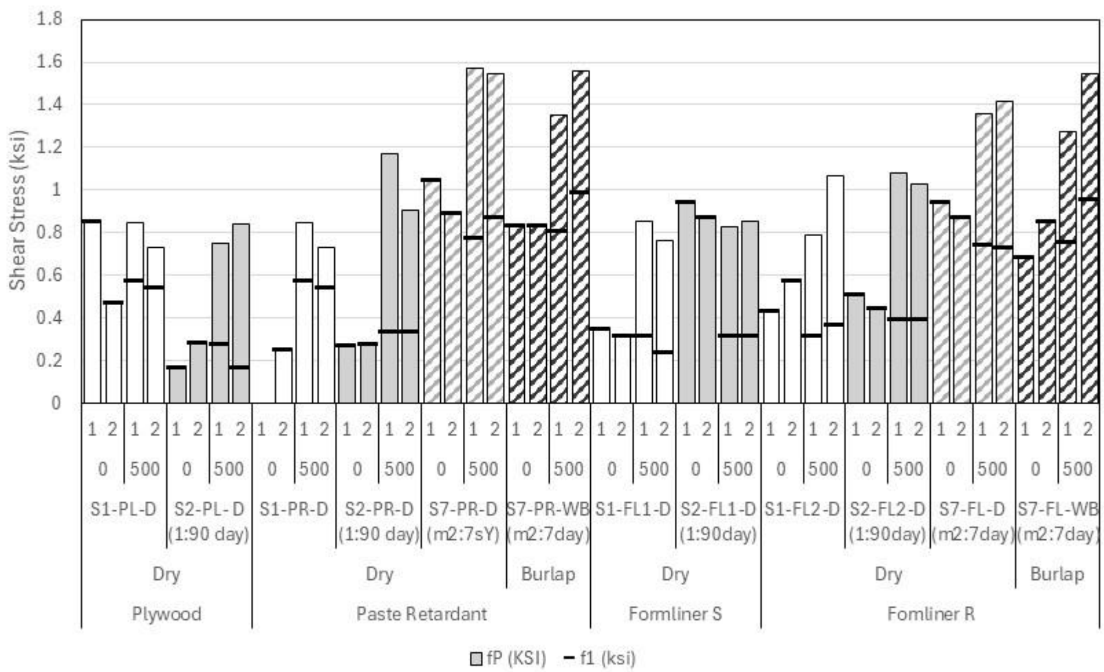

Figure 5.1. Comparison of peak shear stress, f_P and stress near 1st crack, f_{crack} for shear pushoff testing with various surface conditions: Plywood, Paste Retardant, and Form Liners.

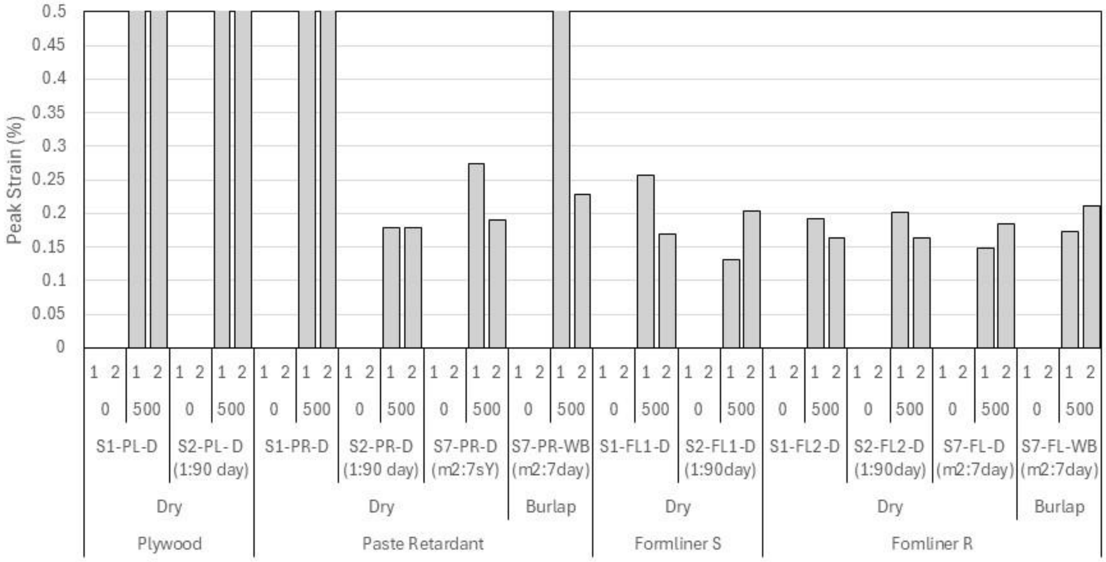

Figure 5.2. Comparison of peak strain for shear pushoff testing with various surface conditions: Plywood, Paste Retardant, and Form Liners. Peak strain was capped at 0.5% in the graph for clarity.

Figure 5.3 shows data that provide supporting evidence on the effect of the surface condition and preparation, although complete description of behavior from these complex systems is difficult. For the four surface wetting conditions (ponding, burlap, spray, and dry), comparisons of f_{crack} for specimens with roughened interfaces made with form liner and specimens with smooth interfaces with exposed fibers created by pressure-water cleaning of concrete laitance from use of a water-based paste retardant can be made. For each wetting condition, f_{crack} for the specimens with the roughened surface was lower than that of the specimens with exposed clean fibers. This effect is not necessarily intuitive for f_{crack} and both surface roughness and exposed fibers were thought to have a more prominent role post cracking where the rougher surface would provide greater friction for the slipping at the interface and the exposed fiber would engage to provide elevated post-cracking capacity. Furthermore, there was a consistent drop in f_{crack} for the specimens (generally even lower than the roughened surface condition) when the steel fibers were pre-corroded. As will be discussed next, similar trends relating to greater strengths with exposed fibers were observed for f_P. Also, similar trends were observed in tensile pulloff and flexural bond testing described in the last section. The trend is self-consistent with the expected role of surface roughness and the fibers in the presence of tensile loads that provide greater contact surface area in the former and engage the fiber in the latter. By conjecture, bonding of the matchcast material onto a substrate may be enhanced with exposed steel fibers that provide interlock akin to mechanical devices and studs at a smaller scale. Cement hydration on the steel surface may create a cement paste rich zone elevating local strength and any amount of concrete volume change during the curing stage (ie shrinkage) may create local compressive forces around the exposed fiber surface. The negative effect of surface heterogeneities, that may develop due to the incorporation of available moisture from the fresh matchcast concrete to the already low pore water content in the UHPC substrate, may be lessened by better anchorage provided by the steel fibers.

The general trends comparing the effect of wetting further provides explanation of possible role of water on the chemical cohesion of the matchcast sections. In the case with the roughened surface without exposed steel fibers, f_{crack} was generally higher in the presence of extended moisture availability (such as when comparing the uniform data set in Set 3 (Figure 5.3)), although higher strength was obtained under burlap than under prolonged ponding. Per conjecture provided above concerning prolonged excessive moisture availability to a cement system with well short of moisture content for complete hydration, another influence of the heterogeneous conditions developed by the differential water availability to the hardened substrate concrete and fresh matchcast concrete may be present. The long term wetting that promotes cement hydration at the near surface of the substrate UHPC would also conceivably provide a greater amount of pore water albeit in low porosity conditions, to the fresh substrate concrete again creating local heterogeneity at the interface surface, resulting in lower strengths in the ponded condition. These concepts are difficult to be held to account heuristically without more refined material testing.

Values were generally similar for the various wetting regimes for the specimens with exposed clean fibers (f_{crack}~0.8 ksi), indicating benefit of the fiber presence, although was somewhat lower (f_{crack}~0.6 ksi) when fully exposed to water by ponding—indicating some negative effect of prolonged excess water presence. The decrease in apparent cohesion in the pre-corroded condition may corroborate these conjectures, where the loose rust products on the fibers would negate those benefits. Another simpler conjecture relating to surface roughness may be that minor striations on the specimens with the exposed fiber caused by pressure washing may afford better mechanical keys for adhesion than the pattern created by the form liner.

Peak Stress, f_P: As alluded to earlier, the figures show f_P values greater than f_{crack} values in the presence of reinforcing steel across the shear interface. This is expected as there would be a clamping force upon initial concrete cracking, as the bulk UHPC material no longer solely governs the strength. The surface condition such as roughness would affect the friction of the interface and the presence of fibers would contribute to the capacity of the section prior to mechanical loss as the load exceeds capacity. Therefore, general comparisons of the peak shear strength may provide characterization of the post-cracking shear behavior with the various variables in surface condition and preparation.

The test specimens with the smooth interface made with plywood had comparable f_P values to its complementary test specimens with roughness formed by formliner and with exposed steel fiber in both test sets 1 and 2 (Figure 5.1). This trend was not expected as the smooth surface of the cast interface would be expected to have a lower friction coefficient and no enhancement in the absence of exposed steel fibers at the cast interface. There were similar trends in the tension pulloff and flexural bond test for some test conditions described earlier. For example, tensile pulloff strength for the smooth interface made with plywood was unexpectedly amongst the strongest. Fracture toughness was also higher than some roughened surface conditions. The results further indicate difficulty to gage the bond at the matchcast interface and the actual crack propagation in complex concrete and UHPC material systems.

As mentioned earlier, these plywood cast specimens did not show the distinct f_P peak at earlier strains (relating to a distinct transition from fiber-loaded to rebar-loaded conditions) and instead showed a continued increase to rebar fracture. Evidently the strain at these maximum values would well exceed the yield strain of the rebar, fy (equivalent to ~0.2% in the graphs). For the typical conditions of the other test parameters, the rebar strain at f_P was near or below fy.

Figure 5.3 does show results with stronger differentiation in behavior between test variables. As mentioned earlier, the chemical cohesion behavior estimated by f_{crack} was similar for the test materials within each wetting condition. The f_P however was expectedly and consistently greater in the presence of the shear reinforcing steel where the effects of friction and steel fiber engagement can be assessed. Furthermore, the results show that f_P was consistently greater with the presence of exposed steel fibers than when compared to the roughened interface surface using form liner. Strain was typically near or below yield limits for the steel except for some cases (notably the smooth surface plywood case) where the largest stress developed beyond opening of the crack and at rupture of the steel.

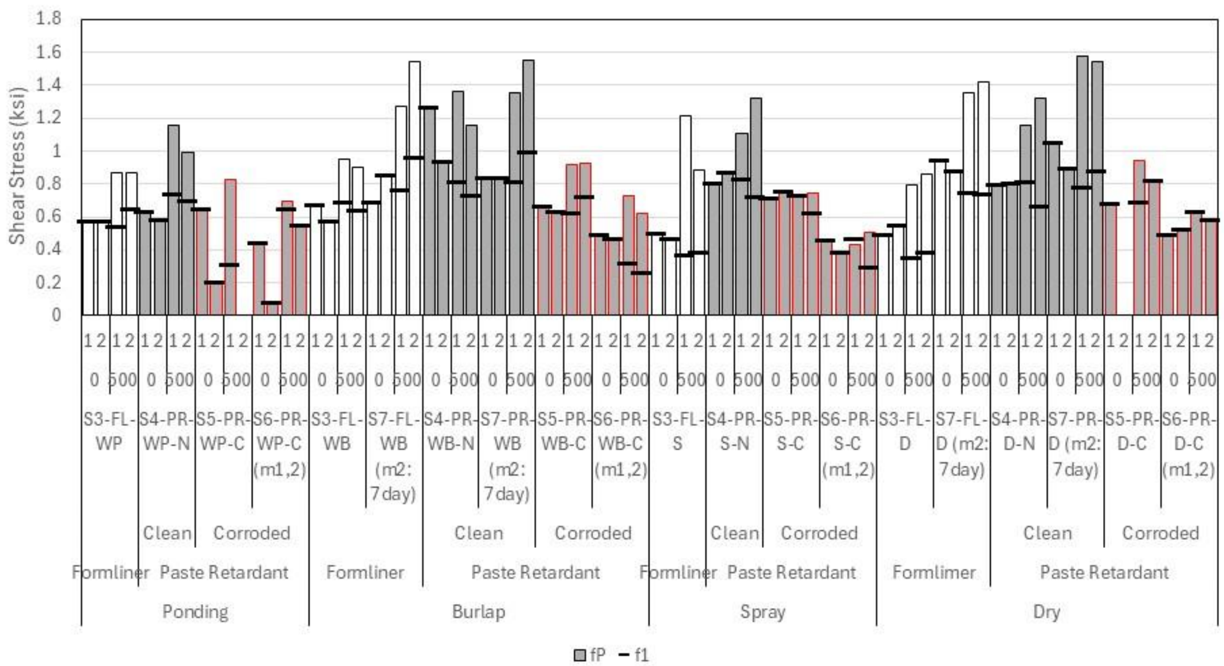

Figure 5.3. Comparison of peak shear stress, f_P and stress near 1st crack, f_{crack} for shear pushoff testing with various surface wetting: Dry, Spray, Burlap, Ponding.

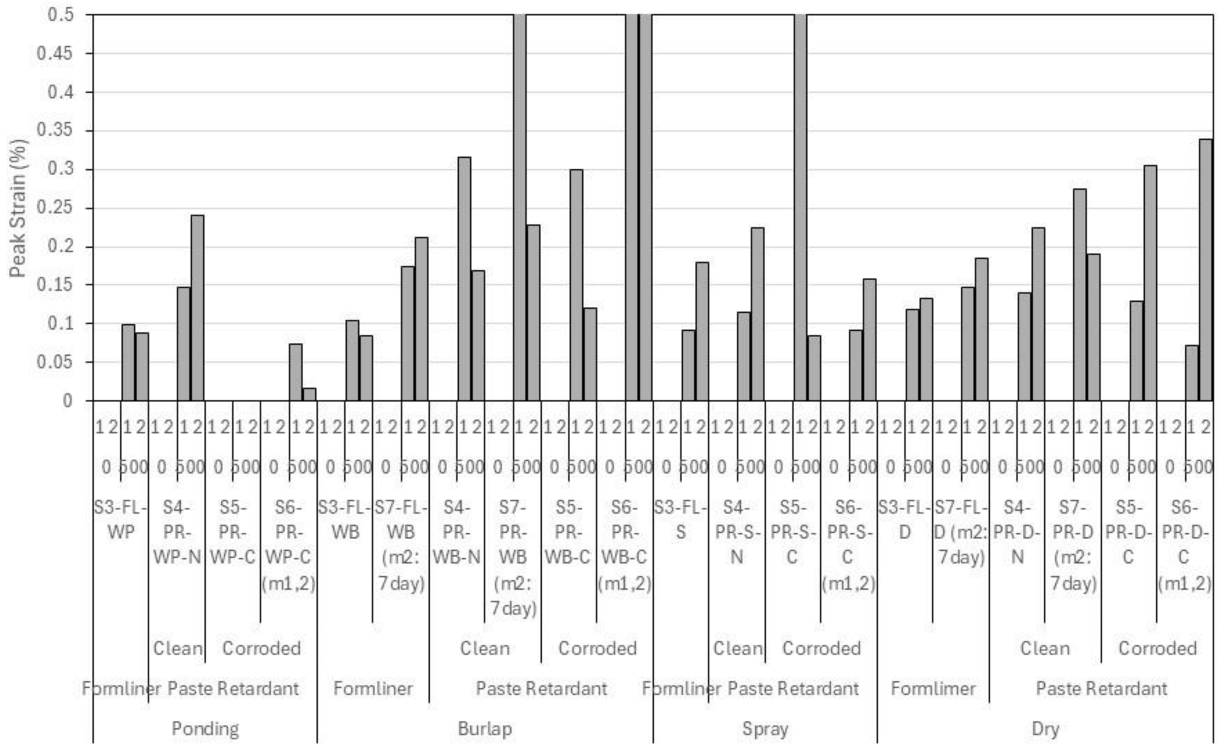

Figure 5.4. Comparison of peak strain for shear pushoff testing with various surface wetting: Dry, Spray, Burlap, Ponding. Peak strain was capped at 0.5% in the graph for clarity.

5.2 Summary of Major Test Outcomes for Surface Conditions and Wetting

5.2.1 Plywood

Precasting UHPC on untreated plywood resulted in a smooth surface with no steel fibers exposed at the surface. The joint surface bond between cast-in-place and precast UHPC materials resulted in failure at the interface. Tensile pulloff and flexural testing resulted in inconsistent mechanical performance, in part due to development of material surface anomalies in early test sets. Shear pushoff testing consistently showed no clear transition from fiber-loading conditions to rebar-loading conditions as typically observed for fiber-reinforced concrete.

5.2.2 Formliner

The form liner that provided granulation of 0.31 inch provided consistent and reproducable surface roughness. It is noted that usage should follow manufacturer's recommendations for reuse of the form liner. The roughened surface did not have exposed fibers. Pulloff and flexural testing did not reveal strong differentiation in mechanical performance between the smoother form liner (0.15 inch granulation) and coarser material (0.31 inch granulation), in part due to development of material surface anomalies in early test sets. Pulloff testing resulted in failure at the interface for said early test sets for the two roughnesses but resulted in failure in the substrate in latter testing of the rougher form liner. Pushoff testing also yielded similar results between surface roughnesses, although as will be presented later, the differences in roughness were reflected in the resolved friction coefficients. Pushoff testing resulted in typical stress-slip curves for fiber-reinforced concrete showing a distinct f_P upon opening of the crack, followed by drop and sustained strength when the shear reinforcing rebar engages.

5.2.3 Paste Retarder

Paste retarders that can provide 3/8 to 1/2 inch etching were sufficient to remove surface materials to reveal steel fibers after cleaning of concrete laitance by water pressure washing. Similar to the testing with the form liners, material surface anomalies in early testing obscurred the test outcomes; however, later testing revealed elevated mechanical performance afforded by the exposed steel fibers. Pulloff strength with non-corroded fibers were similar to bulk monolithic UHPC materials where the failure typically occurred in the substrate UHPC. Flexural response was likewise elevated, with higher peak strength, residual strength, and toughness. Pushoff testing also resulted in typical stress-slip curves for fiber-reinforced concrete showing a distinct f_P upon opening of the crack, followed by drop and sustained strength when the shear reinforcing rebar engages.

5.2.4 Fiber Corrosion

Pre-corroded fibers on the surface of joint interface showed reduced mechanical performance than when the fibers were uncorroded. Pulloff, flexural, and pushoff testing all consistently showed lower strengths in the presence of corrosion. Pushoff testing also resulted in typical stress-slip curves for fiber-reinforced concrete showing a distinct f_P upon opening of the crack; albeit at lower strengths. The surface rust apparently reduced the bond of the matchcast UHPC to the joint surface and was thought to result in lower pre-crack cohesion and post-crack fiber engagement.

5.2.5 Surface Wetting

Although there was variability in the pulloff and flexural testing, overall behavior including in pushoff testing showed emerging trends in pre-crack concrete strength in relation to the surface wetting. For both the formliner and paste retarder, there were higher interface strengths when the surface was kept wet by burlap. Wet burlap provded elevated strength compared to dry casting. Surface wetting by spray just prior to matchcast did not indicate improvement. Also, prolonged wetting by ponding in saturated calcium hydroxide solution did not provide enhancement.

5.3 Cohesion Coefficient, c and Friction Factor, μ

The shear stress versus clamping pressure graphs for the various test sets are shown in Figure 5.5 and 5.6. The individual data points in the graphs were from the various test sets. In the former, data introduced in Section 4.2.3 and monolithically cast Set 0 specimens are shown. In the latter, compiled data from the various matchcast pushoff specimens introduced in Section 4.3.3, excluding pre-corroded exposed fiber test cases are shown. The shear stress was the applied force divided by the concrete interface area. Data points show the peak values from the testing. The clamping pressure was the interface reinforcement ration multiplied by the stress in the reinforcement at the peak load. Test sub variables were disregarded to give a general sense of behavior regarding surface physical conditions and surface wetting conditions. The scatter of individual data points shows the separate effects of the test variables from each set. The shear stress versus clamping pressure curve for the individual test cases was made to calculate the y-intercept at $\rho f_s=0$, representing the cohesion coefficient, c and the slope of the line, representing the friction factor, μ by simple linear regression conforming to the shear provision for nominal resistance V_n,

$$V_n=cA_{cV}+\mu(A_{sV}f_y) \qquad \text{Equation 5-1}$$

Where c is the cohesion coefficient, μ is the friction factor, A_{cV} is the concrete interface area, A_{sV} is the interface reinforcement cross-sectional area, and f_y is the reinforcement yield stress. Due to initial research design approach, only two reinforcement ratios were tested (ρ_V=0 and 9.2e-3) in duplicate. Due to errors often associated with the stochastic nature of concrete materials, the data are often not ideal. The errors were only considered by representation of the r^2 coefficient of determination value from the linear regression. The strain for the first crack condition was assumed to be zero, although some nominal value would be present such as in the reinforced test specimens. The strain was calculated from the maximum strain value extracted from the various rebar strain gages and fiber optic strain gages at f_P when below fy for the grade 60 steel by Hooke's Law assuming a modulus value of 29,000 ksi or assigned a value of fy=60 ksi if the bar yielded before f_P. A comprehensive approach to differentiate strain and rebar tensile stress at the interface and away from the interface was not considered here, but the data is available for further study, especially for the particularly interesting concept of crack localization away from the cast interface. Further assessment will be reported in future dissemination of data. In Figure 5.5, data from the monolithically cast specimen is shown as well for comparison. As expected, the interface shear of the matchcast specimens is significantly lower than the monolithic condiiton. Furthermore, values conforming to AASHTO LRFD 6th edition are shown for reference in the figure. Cases for a monolithically cast and matchcast with 0.25 inch roughness and unroughened are shown. In all three cases, the measured values for UHPC exceeded the design provisions.

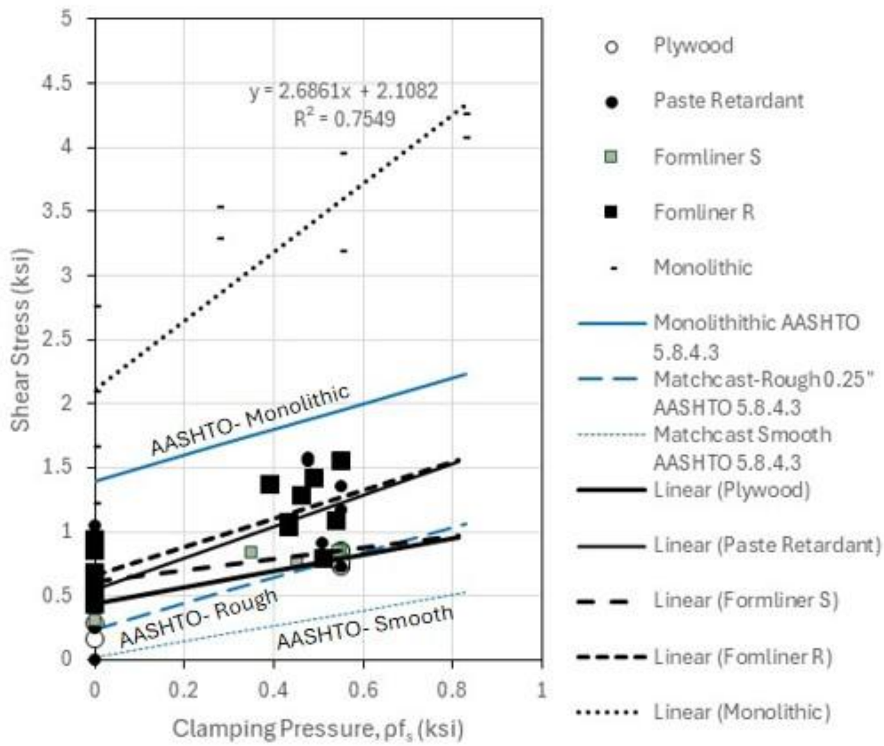

Figure 5.5. Shear versus clamping pressure for pushoff specimens with various cast interface conditions.

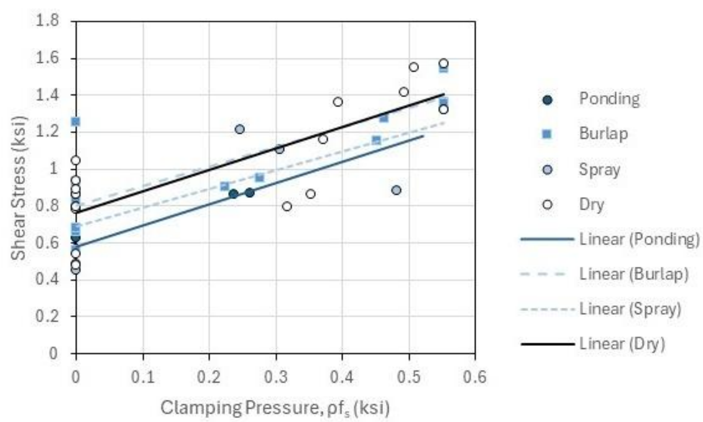

Figure 5.6. Shear versus clamping pressure for pushoff specimens with various surface wetting conditions.

Compilation of resolved cohesion coefficient and friction factor from the individually fit shear stress versus curves is shown in Figure 5.7 and 5. 8. Figure 5.7 compiles test cases relating to the various cast interface conditions such as roughness and exposed fiber (data presented in Section 4.2.3). Figure 5.8 compiles data from test cases relating to the effects of surface wetting conditions (data presented in Section 4.3.3). The linear regression coefficient of determination value representing errors are also given as reference, although these errors would not capture the stochastic errors between different test sets such as variability in UHPC response between sets either by casting or by material behavior as discussed earlier.

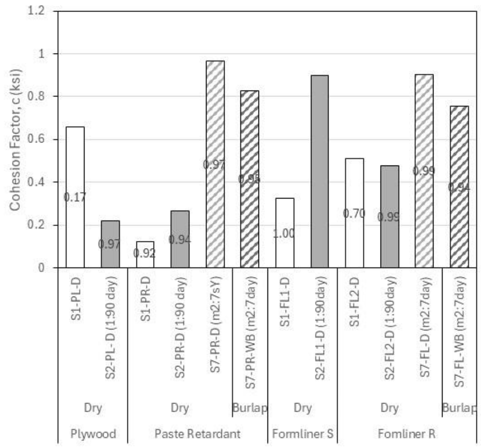

a)

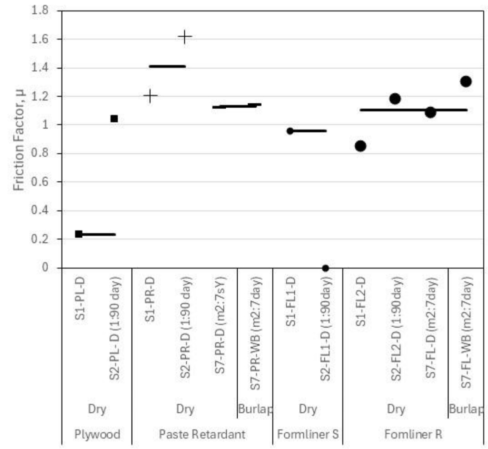

b)

Figure 5.7. Comparison of a) cohesion coefficient and b) friction factor for pushoff specimens with various cast interface conditions. + represents condition with combined rough surface with exposed clean fibers.

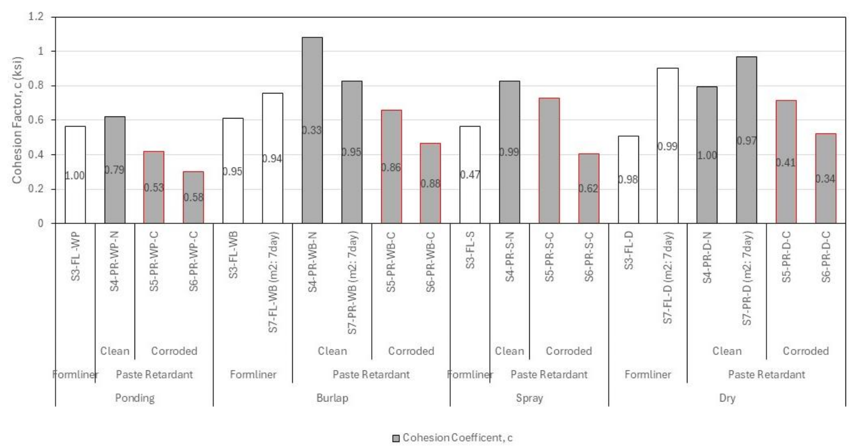

a)

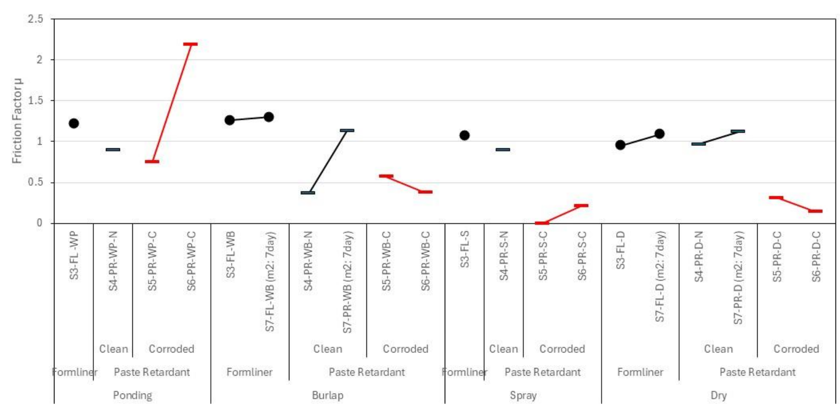

b)

Figure 5.8. Comparison of a) cohesion coefficient and b) friction factor for pushoff specimens with various surface wetting conditions.

The cohesion coefficient for the various cast interface conditions ranged from 0.12 to 1.08 ksi and the friction factor ranged from 0 to 2.19. However, as presented before, compilation of test results shown in Figure 5.8 provides clearer differentiation in behavior. As discussed before, conditions with exposed steel fibers provide greater strength associated with pre-cracking cohesion than conditions with roughened surfaces created with formliner. However, corrosion of the fibers reduces that benefit to levels below formliner. Wetting by burlap provides greater cohesion; followed by dry and superficial prewetting; and lowest cohesion developed when subjected to prolonged ponding in solution.

The friction factor was generally elevated with the roughened surface, followed by exposed clean fiber, and lowest for the corroded fiber. There was a case where a high friction factor was observed for corroded fibers. The type of corrosion product, its compactness on the metal surface, and degree of corrosion can affect development of the fiber as it engages upon cracking. Corrosion of the fibers due to preferential transport of moisture and aggressive ionic species at cracked sections could reduce the interface shear capacity of a section.

Table 5.1. Resolved cohesion coefficient, c and friction factor, μ

Interface Condition	Surface Wetting	Cohesion Coefficient, c (ksi)	Friction Factor, μ
Smooth Interface (Plywood)	Dry	0.22-0.66	0.23-1.04
Smooth Formliner	Dry	0.33-0.9	0-0.96
Rough Formliner	Ponding	0.56	1.22
	Burlap	0.61	1.26
	Spray	0.57	1.08
	Dry	0.48-0.90	0.85-1.18
Rough, Laitance surface, Exposed Clean Fiber (Paste Retardant)	Dry	0.12-0.27	1.21-1.62
Smooth, Exposed Clean Fiber (Paste Retardant)	Ponding	0.62	0.9
	Burlap	0.83-1.08	0.36-1.13
	Spray	0.83	0.89
	Dry	0.79-0.97	0.96-1.12
Smooth, Exposed Corroded Fiber (Paste Retardant)	Ponding	0.30-0.42	0.75-2.19
	Burlap	0.47-0.66	0.38-0.57
	Spray	0.41-0.73	0-0.22
	Dry	0.52-0.71	0.34-0.41

Table 5.1 shows a tabulation of the resolved cohesion and friction parameters without prejudice to the errors associated with the testing between sets. Some values appear to be outlying. Even when compiled with all testing, the general trends discussed from Figure 5.8 still hold. Higher friction factors characterize roughened surfaces with $0.85<\mu<1.62$. Smooth surfaces with clean exposed steel fibers have friction factors in the range of $0.36<\mu<1.13$. Although some friction may be developed at local 'keys' at individual fiber site, this parameter reflects the additional post-crack capacity due to the development of the fiber as it engages across the crack interface.

The smoother formliner and the plywood-cast smooth interface was characterized by $0<\mu<1.04$. Smooth interfaces with exposed steel fibers also develop good bond of the matchcast UHPC where the cohesion coefficient was $0.62<c<1.08$ ksi. However, corroded fibers reduce it benefit of the fibers to promote cohesion where $0.30<c<0.73$. The smooth interface surface created with plywood forms had $0.22<c<0.66$, and specimens where a surface layer of weaker UHPC was observed had the lowest cohesion coefficient, $0.12<c<0.27$. Importantly, prolonged surface wetting with burlap promoted cohesion of the matchcast UHPC, but excess moisture availability from ponding had effect to reduce that bond. It is emphasized that although the prolonged moisture presence by burlap provided benefit on the bond, cases where there is exposed steel fiber can corrode and negate that benefit. Corrosion mitigation may be considered. As described in detail Chapter 3, the use of vapor-phase inhibitor can provide benefit as long as its dosing remains adequate prior to the matchcast, that there are no surface chloride contaminants, and that efficacy is lower in high humidity conditions. Optimal conditions can be difficult as the volume around the treated concrete needs to be well sealed and that the cement hydration and temperature cycling and condensation can maintain relative humidity within the container can reach 100%. Further consideration on the magnitude of corrosion, corrosion product type and its compactness and adherence to the steel surface, and local cross-sectional loss may be made to better understand its role to reduce the interface shear capacity.

6. INTERFACE SHEAR CAPACITY

AASHTO LRFD Bridge Design Specifications provide stipulation for interface shear capacity V_{ni} (kip) as

$$V_{ni} = cA_{cv} + \mu(A_{vf}f_y + P_c) \quad \text{Equation 6-1}$$

where,

- c — is the cohesion coefficient incorporating chemical cohesion and interlock, established from empirical data,
- μ — is the friction factor of a naturally developed cracked plane of bulk concrete or the interface of matchcast concrete,
- A_{cv} — is the surface area of the concrete interface shear plane
- A_{vf} — is the area of the interface shear reinforcement across the shear plane
- fy — is the yield stress of the reinforcing steel
- P_c — is other compressive forces normal to the shear plane.

Two limit states are given. $V_{ni} \leq K_1 f'cA_{cv}$ to prevent crushing of the concrete/aggregate and $V_{ni} \leq K_2 A_{cv}$ as a limit state of interface shear force within bounds of available empirical data.

AASHTO LRFD indicates limitation of available data to normal weight $3.5 < f'c < 18$ ksi and light weight concrete $4 < f'c < 5.2$ ksi and matchcast normal weight concrete $2.5 < f'c < 16.5$ ksi. UHPC materials at 7 day can exceed these values.

For a normal weight, monolithically-cast concrete,
$c = 0.40$ ksi, $\mu = 1.4$, $K_1 = 0.25$, $K_2 = 1.5$ ksi

For a normal weight, matchcast concrete with surface roughness of 0.25 inch,
$c = 0.24$ ksi, $\mu = 1.0$, $K_1 = 0.25$, $K_2 = 1.5$ ksi

For a normal weight, matchcast concrete without roughening,
$c = 0.075$ ksi, $\mu = 0.6$, $K_1 = 0.2$, $K_2 = 0.8$ ksi

Resolved c and μ values presented earlier can exceed these values. As a heuristic approach, additional c and μ values may be proposed for the various surface conditions and preparation. The fit values from the data could successfully capture the data points from which it was derived, as shown in Figure 6.1 as examples. Selection of the lower bound values would provide strength estimates below observed behavior, albeit that existing AASHTO provisions appear to be adequate for conditions where steel fibers are not exposed at the interface. Improvements to avoid over-conservatism for the fiber-exposed interfaces could be made; however, the sampling size of testing would need to be extended for higher confidence.

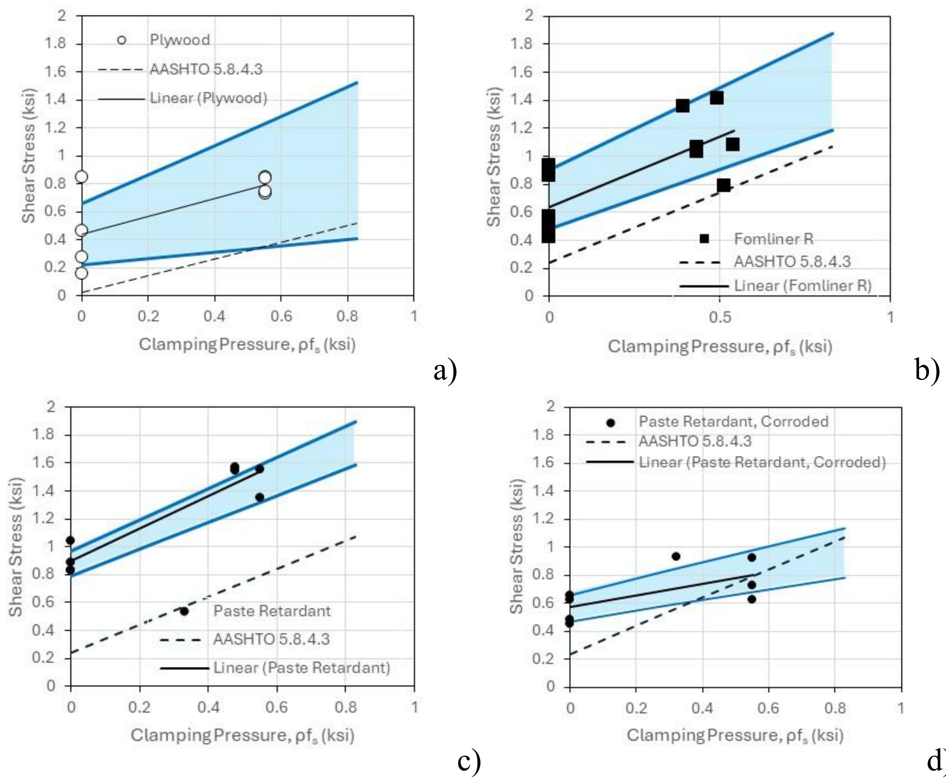

Figure 6.1. Presentation of fit c and μ values with original test data.
Blue lines represent bounds from fitted c and μ values. a) plywood, b) formliner, c) paste retarder: non-corroded fibers, d) paste retarder: corroded fibers. Reference AASHTO c and μ values: for a) unroughened ssurface c=0.075, μ=0.6; b-d) roughened 0.25 inch surface c=0.24, μ=1.

Furthermore, the lack of coarse aggregate but the presence of steel fibers as presented earlier affect the bond cohesion characteristic and post-cracking behavior, such that direct application to Eq. 6.1 would be oversimplified. Muzenski et al., 2022 proposed another term to the post-cracking component of Equation 6.2 for monolithically cast concrete. The clamping force provided by the reinforcing steel post cracking remains, but a term to address the tensile contribution provided by the UHPC and fibers that engage after initial cracking prior to loss of capacity at the peak stress was proposed. When the stress values at peak exceed fy, the rebar would have evidently yielded, resulting in the additional stresses being exerted to the UHPC fiber and its debonding. Then, fy would be limiting. When strain values at peak are less than fy, the UHPC and fiber can provide capacity prior to transitioning to the rebar, and the stress $f_{t,loc}$ at $\varepsilon_{t,loc}$ would be limiting until reaching fy.

$$V_n = cA_{cv} + \mu(A_{vf}f_s + A_{cv}\gamma f_{t,loc}) \qquad \text{Equation 6-2}$$

with a limit state $V_n < KA_{cv}$, and $f_{t,loc} < 1.75$ ksi,

where,

f_s is the minimum of $E_s\varepsilon_{t,loc}$ or fy depending whether the strain is below fy at ultimate capacity. E_s is the Young's Modulus for steel and $\varepsilon_{t,loc}$ is the strain

$f_{t,loc}$ is the tensile strength of the UHPC upon crack initiation
γ is a reduction factor
K is an upperbound of 4.5 ksi observed in testing with larger reinforcement ratios

For monolithically cast UHPC,
c = 1.4 ksi, μ = 1.0, γ =0.85, K = 4.5 ksi,

Similar concepts may be considered for matchcast UHPC to incorporate the effect of the fibers on strength. The cohesive bond component would intuitively be similar; albeit with expectation for lower strengths. The combined post cracking tensile component of the friction term with the clamping force from the rebar and engagement of the fiber that contribute to the ultimate interface shear strength have physical sense for a matchcast system, but the $\gamma f_{t,loc}$ component is not easily translated to the matchcast system. $f_{t,loc}$ was derived from direct tension test of UHPC where fiber engagement would occur at the naturally developed crack plane. In the matchcast system, there is less confidence in the mechanism on how the fibers can develop. For example, one would presume that the test specimens without exposed steel fibers at the cast interface would crack at the initial interface plane and that the absence of fibers would thus not have significant contribution. However, testing from pulloff testing and pushoff testing sometimes resulted in fracture and shearing at an interface immediately adjacent to the initial plane (Photo 6.1). In the photo, failure resulted in removal of material adjacent to the initial roughened surface cast on formliner and locally engaging steel fibers.

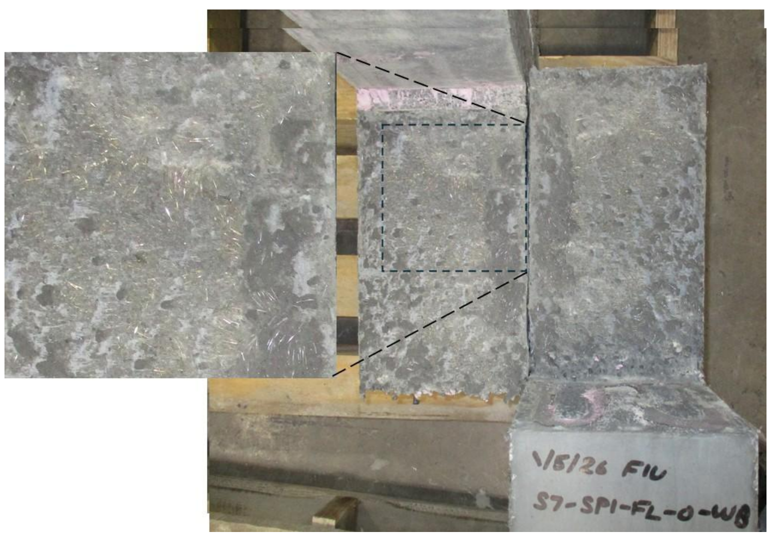

Photo 6.1. Interface shear failure resulting in removal of material adjacent to cast interface. Detail showing engaged steel for interface cast on formliner.

It was presumed that the side with the weaker concrete developed this adjacent plane. There, it was observed that indeed fibers could be engaged. This was consistent with the observation of pulloff failure sometimes occurring at the substrate (engaging fibers in substrate) rather than the interface. Other conditions had premature failure at the cast interface at lower stress. Generally, conditions with lower cohesion (such as the plywood, smooth form liner, and corroded fiber), resulted in bond failure without fiber engagement. This complicates expectation and estimation of $f_{t,loc}$ for matchcast systems. It would seem that the component associated with fiber presence can relate to the friction component of the shear strength as well as cohesion. The cA_{cv} term in part numerically accounts for chemical cohesion in the conventional sense; but in the presence of fibers. the $f_{t,loc}A_{cv}$ term would additionally account for the cohesion component. This can be envisioned in the shear resistance formulation when A_{vf} is zero and the remaining terms are summed up as the y-intercept of the stress-clamping pressure curve. The work presented by Muzenski et al., 2022 presents this confluence of the shear behavior afforded by the $f_{t,loc}$ term by presenting the shear stress vs clamping pressure graph with the combined clamping pressure from the rebar and the fibers in the x-axis. In the presentation here, the y-axis is instead translated to where the $f_{t,loc}$ term associated with the exposed fibers can be considered to contribute to behavior associated with cohesion as well. This was presented in part due to convention on how cohesion may be nominally assessed in Equation 6.1 with the direct tension or tensile pulloff testing as well as test observations. Pulloff testing revealed that bond at the joint interface prior to cracking in the presence of exposed clean fibers was elevated and fracture developed offset form the interface and in the substrate.

It was evident that fibers present at the cast interface have a positive effect on bond prior to cracking and ultimate shear strength post-cracking. Further assessment and testing for the accounting of the cA_{cv} and $\mu A_{cv}f_{t,loc}$ in the interface shear resistance equation may be considered in the future. As a more generic approach, the results from tensile pulloff and other testing are considered to provide a framework for correlating observed trends on failure modality and tensile strength to surface condition and preparation.

Data from the tensile pulloff testing when the failure mode occurred at the substrate with engaged fibers was reconsidered here. When bond failure occurred, it was considered that there would be less confidence in fiber engagement and additional benefit would be less. This imposed criterion is discussed in assessment for the formliner, paste retardant, and pre-corroded conditions. Conservative approach would apply existing guidelines for non-fiber-reinforced materials for the plywood case.

The average pulloff strength for specimens with a smooth surface with exposed steel fibers was ~1,000 psi (similar to direct tension strengths). In the presence of pre-corroded fibers, average pulloff strengths were ~600 psi and indicated about a 40% reduction but was as low as 80 psi. When two dissimilar materials were used for the substrate and matchcast (even though f'c values of the two materials were similar at the time of testing), pulloff strengths were ~240 psi, resulting in a 76% reduction. With a roughened surface with no exposed fibers, the pulloff strength was 90-450 psi and average ~270 psi (average ~70% reduction).

For discussion, these reductions were applied to the $f_{t,loc}$ term to see if a simple reduction factor κ (as shown in Eq. 6-3) could account for the observed behavior accounting for improved tensile capacity from engaged fibers (Case 1). The use of the κ term will then be compared to the use of a simple modified μ term (Case 2) from test results as described earlier. The κ term in this convention, however, would not be inter-related with the friction μ term. Modification, such as possible improvement relating to anchor provided by the exposed fibers or decrease in the presence of loose corrosion products, to the interface friction would not be accounted contiguously.

By resolution from experimental data and inference from Eq. 6.2, there is an apparent connection on the overall interface shear strength provided by the fibers relating to both cohesive and tensile behavior. To this end, c and μ values were selected such that their combined effect relates to experimental pulloff strengths. As first approach, c values for smooth and rough interfaces and μ values for roughened surfaces were selected from existing AASHTO provisions. Although for convenience, μ was selected as 1 as general trends observed in Figure 6.1 (and Figure 6.2b) with superimposed composite data showed similar slopes in the stress-clamping pressure graphs.

The analysis included modification to the cohesion coefficient, c (as shown in Eq. 6-3 and 6-4) to account for trends observed with UHPC for all of the experimental outcomes including a) simple general baseline for all conditions and b) accounting for wetting conditions on cohesion by a factor, λ. Figure 6.2 reproduces resolved c and μ values presented in Table 5.1 as general guidance for the selection of c and μ terms in the analysis.

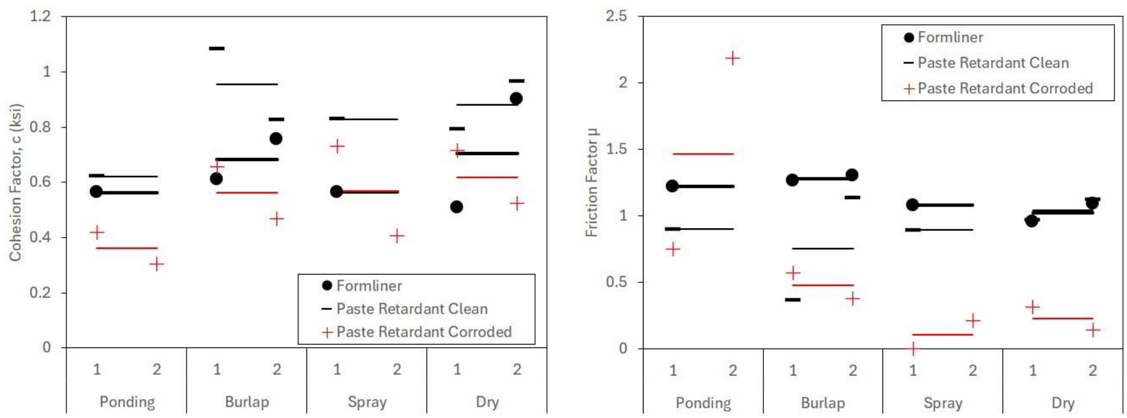

Figure 6.2. Abstracted cohesion coefficient and friction factor.

This simple exercise is made solely to identify if the friction associated with the engaged fibers can be identified for matchcast sections such as that proposed by Muzenski for monolithically cast UHPC.

Case 1:

$$V_n = \lambda c A_{cv} + \mu(A_{vf} f_s + A_{cv} \kappa f_{t,loc}) \qquad \text{Equation 6-3}$$

a) Smooth, Exposed Fiber

$f_{t,loc}$=1 ksi

μ= 1

c=0.075 (baseline), λ=1 (dry), 0.7 (ponding), 1.3 (burlap);

κ= 1 (exposed clean fiber), 0.2 (exposed pre-corroded fibers),

b) Roughened, Formliner

$f_{t,loc}$=1 ksi

μ= 1

κ= 0.3 (roughened, no exposed fiber),

$c = 0.24$ (baseline), $\lambda = 1$ (dry), 0.7 (ponding), 1.3 (burlap);

Case 2:

$$V_n = \lambda c A_{cv} + \mu(A_{vf} f_s) \qquad \text{Equation 6-4}$$

$c = 0.6$ (baseline), $\lambda = 1$ (dry), 0.7 (ponding), 1.3 (burlap)
$\mu = 1$ (exposed clean fiber), 0.3 (exposed pre-corroded fibers),
$\mu = 1$ (roughened, no exposed fiber),

Figures 6.3 to 6.5 shows comparisons of the numerical output for the Case 1 and Case 2 demonstration to estimate interface shear behavior with various surface conditions and wetting conditions. The compiled calculation outputs for matchcatch specimens with roughened surface made by formliner show that the approach outlined by AASHTO provisions but with modified c and μ values derived from experimental cases as well as approach presented by Muzenski et al., 2022 can both describe the behavior observed in experimental work. The modification to the cohesion coefficient by a scaling factor λ, can account for differences due to wetting.

Presentation of calculation outputs for cases with matchcasting on smooth surfaces with exposed steel fibers for both clean and pre-corroded conditions give interesting insight on the cohesion and tensile attributions of the fiber. Case 1 calculations allow for attribution of the effect of fiber conditions on both its contribution to cohesion as well as contribution to post crack clamping pressure. In terms of the graphical output, modification of terms associated with the fibers results in both changes in the y-intercept (associated with pre-cracking cohesion) and the post-crack shear stress without need for extra consideration to modify the cohesion coefficient and friction factor when interface condition is not different. The equation allows accommodation of the effect of wetting that only affect c (with the λ term) and modifiers that can capture the effect of interface conditions such as fiber, fiber corrosion, and roughness (with the κ term) while maintaining base c and μ terms to values already associated with matchcast and UHPC materials. Case 2 calculations do not combine the effect of fibers on both cohesion and friction; but as shown in Figure 6.4, provide different characterization of experimental behavior. In the condition with the formliner (Figure 6.5), the experimental observations were well characterized in both computational cases. Additional testing would be ideal to determine which case better captures the shear behavior.

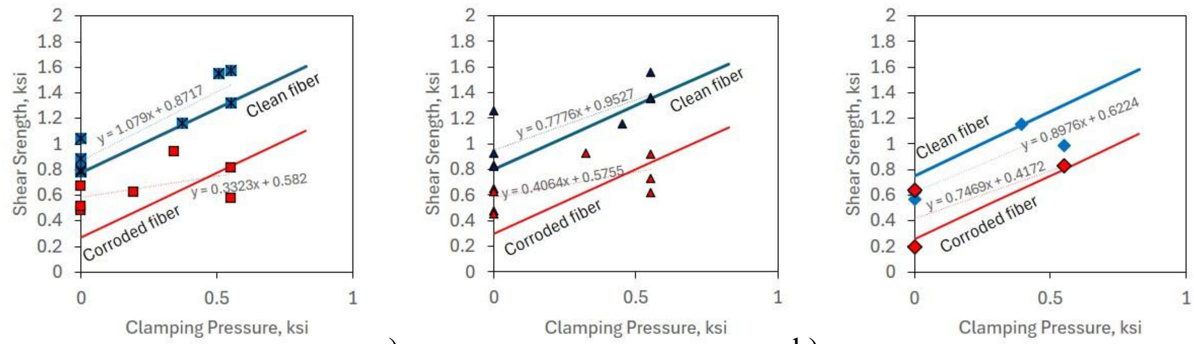

a) b)

c)

Figure 6.3. Presentation of Case 1 interface shear approximations for exposed fiber.

$V_n/A_{cv} = (\lambda c A_{cv} + \mu(A_{vf}f_s + A_{cv}\kappa f_{t,loc}))/ A_{cv}$

a) Ponding, b) Burlap, c) Dry

Blue: Clean Fiber. Red: Corroded Fiber.

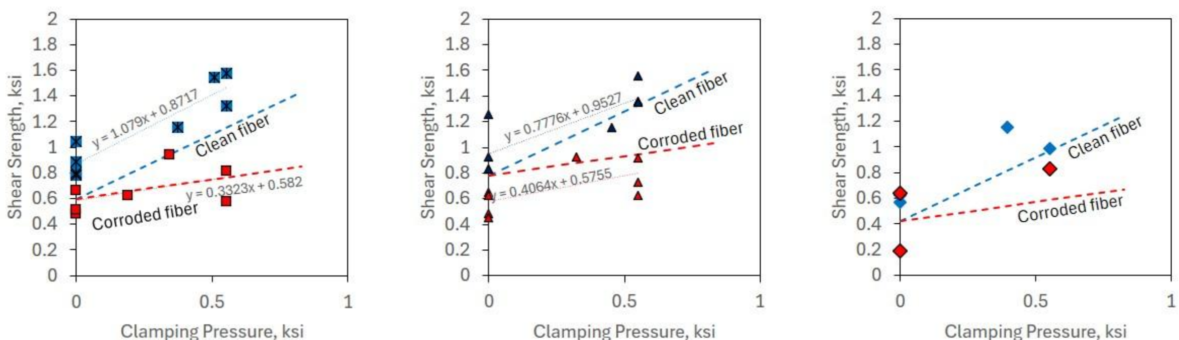

a) b) c)

Figure 6.4. Presentation of Case 2 interface shear approximations for exposed fiber.

$V_n/A_{cv} = (\lambda c A_{cv} + \mu(A_{vf}f_{s,loc}))/ A_{cv}$

a) Ponding, b) Burlap, c) Dry

Blue: Clean Fiber. Red: Corroded Fiber.

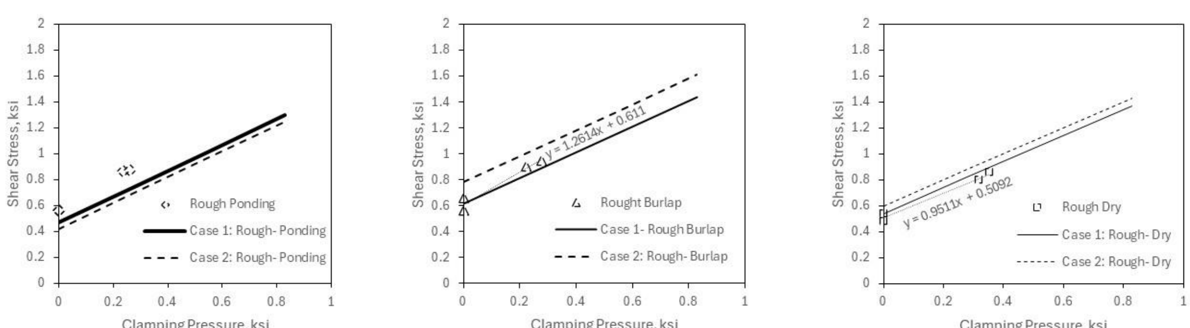

a) b) c)

Figure 6.5. Presentation of Case 2 interface shear approximations for roughened surfaces.

a) Ponding, b) Burlap, c) Dry.

Further development following this consideration with larger test sets is warranted and provide an exciting means to assess the behavior of the fibers. Optimization of coefficients is warranted. However, this was not completed as the data set in this initial work was not as robust as may be needed, especially when there are still outlying phenomena associated with heterogenous concrete strength and apparent differentiation in material batches from early testing. Additional numerical work will be disseminated when available. More detailed assessment should continue the arguments for consideration of rebar strain and other limit conditions.

7 CONSIDERATIONS FOR CONSTRUCTION

Based on the practical experiences from the physical work in the research to prepare the test specimens and the outcomes of the tests, perspective for construction practices is discussed. This includes components for UHPC mixing, material quality control, mold preparation, interface preparation, surface conditioning, and general observations.

There are several sources for UHPC materials in the market, and each has its own unique requirements for material preparation and mixing. It is imperative that technical support from those vendors is available and that constructors consult with those industry representatives to review nuances with the mix design and its appropriate mixing instructions. Items that should be reviewed prior to initializing activities at the plant or on site are presented followed by recommendations for construction specifications.

7.1 UHPC Mixing

Development of a standardized mix sheet that clearly identifies the individual components of the UHPC mix design, especially when prepackaged and preblended components are offered by various manufacturers. These components may have different raw materials combined and are given trade names without necessarily marking actual content in its packaging.

Packages from commercially available materials that have preblended and premixed components should be clearly labeled. Changes in products (including their contents, proportions, and weight) should be identified so that inadvertent misapplication of materials is prevented.

Appropriate storage conditions, especially in field conditions, for large material packages should be made to prevent material loss and component degradation. The date of delivery should be clearly stated on the storage container as some materials have expiration dates. Pre-hydrated cementitious materials should identified and discarded. Corroded fibers should not be used.

Photo 7.1. Prehydrated cement.

Trial mixes should be considered before large scale production. Although specific mixing instructions are usually given, there will inevitably be challenges especially in field conditions.

Some components require additional steps to implement than others that require timed additions, such as premixing and incorporation in specific sequence that can affect the material response during the mixing. Trial mixes will allow practitioners to get experience on handling specific sophisticated mix design and mixing requirements, including the time period in which the fresh material is still workable.

Identify sensitivity of the precision in mixing components to the workability and strength of the material, especially when admixtures for workability are incorporated (such as accelerators and viscosity-modifying admixtures, etc). Different sized batches may have different responses to the precision of material dosage. Different mixer types and its size may cause the precision in material dosage to be compromised (ie internal mixer mechanical and structural elements may trap material from being incorporated into the batch, screens may not allow incorporation of UHPC components within specified mix times, etc.).

Photo 7.2. Poor workability material due to water underdosage

Identify material guidelines for adjustments in various components to account for temperature and if specific workability characteristics are needed for complicated structural component geometry or construction constraints.

Identify mixer capability for required batch sizes and if enough power is available to turn the UHPC material during initial mixing and when there are delays to release the material from the mixing tank.

7.2 Material Quality Control

Standard fresh material testing such as flowtable tests should be conducted and recorded to identify anomalies in the mixed material.

Identify if workability and flow characteristics are not within expectations by the material provider.

Variations in source material for generic UHPC mix designs need to be identified. Changes in production or even different material providers of raw materials can cause varied responses of the material during mixing and thus affect its workability and hardened properties.

The dense and low internal moisture content of UHPC may cause some non-ideal air and moisture transport (such as evaporative processes) that may create a surface skin that can be detrimental to the strength of the matchcast interface surface. Use of spike rollers for example may alleviate excessive skin development. Consultation with the manufacturer technical support should be made.

Photo 7.3. Concrete surface deficiency.

Photo 7.4. Fiber segregation.

Uniform fiber distribution and prevention of fiber segregation and clumping is necessary.

7.3 Mold and Formwork Preparation

Formwork and molding materials should be compatible with any chemical components required to create designed surface conditions and use of the UHPC material. This may include compatibility of formwork materials with different paste retardants. For example, solvent based paste retarders such as those using toluene had caused polystyrene formwork to dissolve. Consultation with manufacturers for products should be conducted. Areas of concern can include absorption into the formwork material and adverse chemical reactions.

Materials that may alter moisture content of the cast fresh UHPC should be identified for compatibility with the UHPC material. For example, porous absorbent formwork materials may lower moisture content at surfaces in contact with the fresh UHPC material.

Photo 7.5. Incompatibility of materials.

The quality of formlining materials needs to be considered if repeat use is made. Various materials may have different robustness and wear resistance. Also, cleaning methods that don't degrade those materials should be considered for repeat use.

7.4 Interface Preparation and Conditioning

The strength development of the cast UHPC surface should be identified if pressure washing is considered for surface preparation.

Interfaces with exposed steel fibers should not be in direct contact with corrosive media that can include marine salts and industrial corrosive agents.

Interfaces with exposed steel fibers that require prolonged wetting should be protected from excessive rust development.

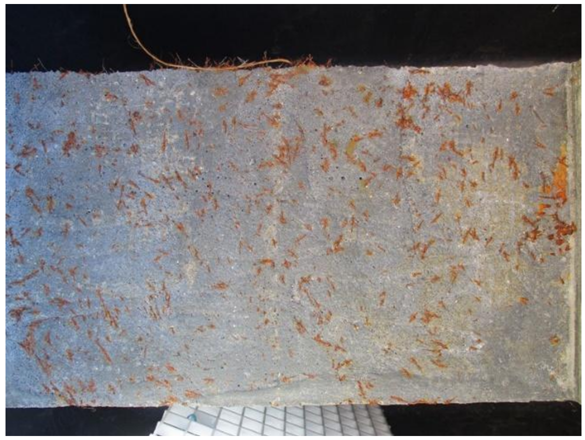

Photo 7.6. Exposed fiber corrosion.

Use of corrosion mitigation technologies (such as vapor phase inhibitors) require consultation with the material providers. Information such as dosing quantity, dosage rates, effect of relative humidity should be gathered. Appropriate containment is required.

Interfaces should be clean of any residual compounds and precipitated chemicals.

7.5 Draft Construction Specifications

JOINT SURFACE PREPARATION OF PRECAST UHPC

SECTION x
JOINT SURFACE PREPARATION OF PRECAST UHPC

x-1 Description.

Prepare formwork for casting and condition joint surface of precast UHPC in accordance with the requirements with Contract Documents following procedures herein.

The joint surface must conform to either surface roughness requirements or steel fiber exposure in accordance with this Section

Refer to Section 400 for Concrete Structures and Section 450 for concrete and precast concrete construction requirements additional to the requirements of this Section.

x-2 Materials.

x-2.1 Form Liners: Use form liners of durable, abrasion resistant materials that are unaffected by water and cementitious materials. Use form liners that can create a coarse rough cast texture featuring a continuous pattern of peaks and valleys of varying heights. In profile, the liner features a textured surface that rises up as high as 0.25 inch, and a urethane backing of about 0.25”, for a total thickness of approximately 0.5" inch. The cast concrete texture shall meet ICRI CSP grade 10. Use form liner materials withing its application usage prescribed by its Manufacturer and replace the form liner material as necessary to produce consistent coarse surface texture. Use form liner materials in one continuous layer. Do not use damaged or repaired form liner materials. Form liner material should conform to Section 400-5.3.2.

x-2.2 Plywood: Plywood not less than 5/8 inch in thickness manufactured with waterproof glue. Do not use pieces with bulged plies or raveled, untrue edges. Plywood formwork should conform to Section 400-5.3.3

x-2-3 Polystyrene Rigid Foam: Use polystyrene rigid foam comprised of expanded polystyrene manufactured from virgin resin of sufficient density to support the weight of concrete without deformation. Use polystyrene foam that has water absorption less than 0.3% by volume when tested according to ASTM C272. Provide a written certification from the manufacturer stating product meets the requirements of this Specification along with the delivery of the product. Reference to 400-5.7.4

x-2.4 Paste Retarder: Use a paster retarder that develops a medium light etch of 3/8 to ½ inch for conventional concrete. Use paste retarder on the formwork face for joint surface following manufacturer instructions and recommendations. Plywood or polystyrene rigid foam prescribed in x-2.2 and x-2.3, or metal formwork must be used such that the material is chemically compatible with the selected paste retarder. Follow manufacturer's instructions concerning absorption into the formwork material.

x-3 Finishing Concrete

x-3.1 General: Immediately after removing form work from the joint surface, remove all fins and irregular projections that can cause improper fit of the cast element for future formwork for CIP UHPC. In addition to the general surface work, additional surface work prescribed in Contract Documents for one of the conditions listed below.

x-3.2 Roughened Surface: Where the roughed surface was created using form liners prescribed in x-2.1, removed any remnant form lining material or debris that have remained adhered to the UHPC joint surface. Any observation of concrete laitance, skin, or excessive air voids on the joint surface should be identified and recorded for review by the Engineer for acceptance. Methodologies to remove the laitance without decreasing the specified roughness prescribed in x-2.1 shall be decided by the Engineer adoption and final acceptance.

x-3.3 Exposed Steel Fiber: Where exposed steel fibers were required in Contract Documents, formwork should be removed at a sufficient early time, no sooner than 12 hours after casting and not until the concrete strength is sufficient to avoid structural damage, to remove concrete laitance. The cement laitance developed on the joint surface due to reaction of the UHPC with the paste retarder prescribed in x-2.4 shall be removed by water pressure washing. The pressure washing shall be done so that complete removal of the paste retarder and cement laitance is made. Pressure washing shall be conducted so that excessive scoring of the joint surface and breakage of the exposed steel fibers is avoided. The exposed steel fibers shall be uniformly distributed throughout the joint surface area. Elements with surfaces with segregated fibers shall not be approved.

x-3.3.1 Cleaning Equipment: Use approved water blasting equipment to remove concrete laitance. Use equipment which is specifically manufactured to clean concrete surfaces. Use equipment that has a minimum rated nozzle capacity of 6,000 psi using the spray head.

x-3.3.2 Water for Cleaning: Use water meeting the requirements of Section 923.

x-3.3.3 Surface Cleaning Operation: During the cleaning operation, exercise caution to minimize the removal of UHPC material and breakage of the exposed steel fibers. Limit the duration of water blasting to remove remnant paste retarder and concrete laitance and provide a light abraded surface. Do not allow surface abrasion to exceed 0.016 inch.

x-4 Curing Concrete

x-4.1 General: Concrete curing of the precast UHPC section shall be made in accordance to Section 450. Where exposed steel fibers were required in Contract Documents and surface finishes prescribed in x-3.3 were made, additional curin conditions prescribed by Contract Documents shall conform to procedures described herein:

x-4.2 Continuous Moisture: In addition to curing requirements in x-4.1, curing of the exposed concrete surfaces shall be expanded by continuous moist cure for the 72 hour curing period. Place burlap on the joint surface and keep it continuously saturated by means of soil soakers, leaking pipes, or automatic sprinklers. Alternatively, the joint surface may be wet by ponding with a saturated calcium hydroxide solution.

x-4.3 Alternative Curing Methods: Alternative curing methods prescribed in Section 450 must be approved by the Engineer.

x-5 Surface Wetting

x-5.1 General: The joint surface shall be kept wet to a saturated surface dry condition prior to placement of caste-in-place (CIP) concrete by methods included herein. The surface shall be made to be in a saturated surface dry condition prior to placement of the CIP UHPC

x-5.2 Continuous Moisture: Maintain the joint surface wet at all times for at least 48 hours prior to placement of CIP UHPC. The joint surface shall not be allowed to dry out prior to placement of CIP UHPC. Place burlap on the joint surface and keep it continuously saturated by means of soil soakers, leaking pipes, or automatic sprinklers. Alternatively, the joint surface may be kept wet by ponding with a saturated calcium hydroxide solution. The ponding solution shall be periodically refreshed due to its carbonation with exposure to the atmosphere.

Prior to placement of CIP UHPC, the joint surface shall be clean of debris including burlap material snaggled on the roughened UHPC or exposed steel fibers and precipitated carbonation products from the ponding solution.

x-6 Protection of Joint Surface

x-6.1 General: Joint surfaces prescribed in Section x-3 shall be safely stored to prevent any physical damage, including surface texture and exposed steel fibers when prescribed. The joint surface shall be protected from adverse environmental exposure that degrades the UHPC or steel. The joint surface shall be protected from corrosive environments during storage, transportation, and erection until placement of CIP UHPC.

x-6.2 Corrosion Protection of Exposed Fiber: Protect the exposed steel fibers against corrosion at all times using materials and procedures described herein. The joint surface shall not be exposed to corrosive industrial or marine environments. Use corrosion protection materials with properties that are not detrimental to the steel fiber of the UHPC: Reference to 451-8

a) powder vapor-phase inhibitor

b) saturated calcium hydroxide solution

x-6.3 Powder Vapor-Phase Inhibitor: When storage or outdoor exposure for up to 1 month is required prior to CIP UHPC construction, use a powder vapor-phase inhibitor that does not affect the bond of the steel fiber when embedded in concrete. Use the material in accordance with manufacturer's instructions and recommendations, including its handling, storage, dosage content and reapplication. Vapor-phase inhibitors require dosage in a sealed closed environment. Selection of this containment space requires approval by the Engineer.

x-6.4 Calcium Hydroxide Solution Ponding: When prolonged storage or outdoor exposure greater than 1 month is necessary, use of a saturated calcium hydroxide solution shall be used. The solution shall be free of salts and avoid salt contamination. The solution shall be periodically replaced to maintain its pH to 12.0 to 12.6 and to remove excess carbonation products.

x-6.4 Cleanliness of Exposed Fiber: The exposed fibers shall be clean of contaminants introduced during its casting, storage, transport, and erection. Light surface rusting with coverage less than 10% of the joint surface concrete area may be removed by light pressure washing per x-3.3. Damage to the fibers by the washing shall be avoided. Excessive corrosion of steel fibers with fiber breakage require approval for acceptance by the Engineer.

8. SUMMARY AND CONCLUSIONS

The research provided insight into the effects of various material conditions for joint interfaces for matchcast UHPC that can be considered for practical application and implementation for design and construction. Major findings and conclusions from the work are listed below.

Mechanical Behavior

- Mechanical testing of matchcast UHPC (tension: pulloff testing, flexure: flexural bond testing, and shear: shear pushoff testing) resulted in lower strengths than bulk monolithically-cast UHPC.
- Failure of the joint interface of matchcast UHPC in tension (pulloff testing) and shear (pushoff testing) can occur at the interface plane or adjacent to the plane, indicating that the weakest failure plane is not necessarily at the joint interface. In pulloff testing, failure can occur in the substrate. In pushoff testing, failure can occur in a plane offset from the cast interface.
- Shear pushoff behavior of matchcast reinforced UHPC with roughened surfaces or with exposed steel fibers was characterized by typical stress-slip response showing early bilinear response, crack initiation, and post-crack strength. Results indicate that post-cracking fiber engagement can develop for matchcast UHPC.
- Shear pushoff behavior of matchcast reinforced UHPC with a smooth joint interface (cast on plywood); on the other hand, did not show clear transition from fiber-loading conditions to rebar-loading conditions as typically observed for fiber-reinforced concrete.
- Differential behavior due to different age substrate and matchcast UHPC were not clearly identified in testing.

Surface Roughness

- Form liners can provide reproducible and consistent surface roughness without exposed steel fibers. The roughened interface can improve the friction of the interface.
- Joint interfaces that have exposed steel fibers, but otherwise smooth surfaces improve shear resistance in both precrack cohesion and postcrack tensile strength. The improvement to post-cracking behavior was consistent with expectations for fiber engagement creating additional clamping pressures.
- Pre-corroded exposed steel fibers negate the positive effects of exposed fibers to improve shear strength.
- Washing or cleaning of surface rust on exposed steel fibers showed benefit to improve interface shear strength.

Surface Wetting

- Wet spray on the joint interface prior to UHPC matchcasting did not show improvement in strength over dry surface casting.
- Wetting of the joint interface by placement of burlap prior to UHPC matchcasting showed improved shear strength.
- Prolonged wetting of the joint interface by ponding in saturated calcium hydroxide solution resulted in lower interface shear strength.

Material Durability

- UHPC materials may form surface ‘skin’ layers (likely due to differential water evaporation and high surface tension of UHPC) that can create weaker materials at the joint interface.
- Powder vapor phase corrosion inhibitors can provide corrosion mitigation, but its effectiveness can vary depending on dosing levels and environmental aggressivity, including relative humidity and salt contamination. In lab testing, the inhibitor appeared to allow for a lower corrosion rate to develop but its efficacy drops with longer exposure times.

Shear Capacity

- Shear strength developed by matchcast UHPC generally exceed values prescribed by AASHTO 5.8.4.3.
- Resolved modified cohesion coefficient and friction factor from the testing was shown to describe shear behavior. An additional term representing the effect of surface wetting on the cohesion coefficient was presented.
- A modified shear equation to account for post-crack shear contributions from the steel fibers to the clamping pressure was presented to account for matchcast UHPC. An additional term to account for fiber condition at the joint interface and the negative effect of corroded fibers was presented. The term also can account for the observed increase in cohesion from mechanical testing with the presence of the exposed steel fiber at the joint interface.
- The presented modifications to the shear capacity equation allow for the accounting of the effect and condition of the exposed steel fibers without conflating their effects on cohesion and friction coefficients that have already been developed based on material and roughness factors.

Construction Considerations

- Recommended provisions for construction for the use of form liners, paste retarders, surface wetting, and fiber corrosion mitigation were presented.

REFERENCES

[1] A. Al. Semendary, E. P. Steinberg, K. K. Walsh, and E. Barnard, “Effects of Temperature Distributions on Thermally Induced Behavior of UHPC Shear Key Connections of an Adjacent Precast Prestressed Concrete Box Beam Bridge,” *J. Bridge Eng.*, vol. 24, no. 2, pp. 1–17, 2019, doi: https://doi.org/10.1061/(ASCE)BE.1943-5592.0001346.

[2] B. Graybeal, “Design and construction of field-cast UHPC Connections,” Federal Highway Administration (FHWA), FHWA-HRT-19-011, 2019.

[3] E. Shahrokhinasab and D. Garber, “Development of ‘ABC-UTC Non-Proprietary UHPC’ Mix,” Miami, Final Report ABC-UTC-2016-C2-FIU01-Final, May 2021.

[4] E. Shahrokhinasab, T. Looney, R. Floyd, and D. Garber, “Effect of Fiber, Cement, and Aggregate Type on Mechanical Properties of UHPC,” *Civ. Eng. J.*, vol. 7, no. 8, pp. 1290–1309, Aug. 2021, doi: http://dx.doi.org/10.28991/cej-2021-03091726.

[5] M. K. Tadros et al., “Implementation of Ultra-High-Performance Concrete in Long-Span Precast Pretensioned Elements for Concrete Buildings and Bridges,” Phase I Report to . Precast. Concr. Inst. PCI, Jan. 21, 2020.

[6] ACI Committee 239, “Ultra-High Performance Concrete: An Emerging Technology Report (ACI 239R-18),” *Farmington Hills MI Am. Concr. Inst.*, 2018.

[7] Association Francaise de Normalisation (AFNOR), “Concrete - Ultra-high performance fibre-reinforced concrete - Specifications, performance, production and conformity.,” *AFNOR Fr.*, pp. 18–470, France 2016.

[8] American Society for Testing and Materials (ASTM), “C1856/C1856M - 17 - Standard Practice for Fabricating and Testing Specimens of Ultra-High Performance Concrete,” 2017, doi: https://doi.org/10.1520/c1856_c1856m-17.

[9] Canadian Standards Association, “CSA A23.1 Concrete materials and methods of concrete construction, Annex U - Ultra-high Performance Concrete (UHPC).,” *Mississauga Ont. Can. Stand. Assoc.*, 2019.

[10] B. Graybeal, “Design and construction of field-cast UHPC connections.,” United States. Federal Highway Administration, 2014.

[11] Swiss Society of Engineers and Architects (SIA). (2016)., “SIA 2052 Béton fibré ultra-performant (BFUP) - Matériaux, dimensionnement et exécution (Ultra-High Performance Fibre Reinforced Cement-based Composites [UHPFRC]- Construction material, dimensioning and application).,” *Zurich SIA*, 2016.

[12] B. Graybeal, “Design and construction of field-cast UHPC connections.,” United States. Federal Highway Administration, 2019.

[13] P. Li, Q. Yu, and H. Brouwers, “Effect of coarse basalt aggregates on the properties of Ultra-high Performance Concrete (UHPC),” *Constr. Build. Mater.*, vol. 170, pp. 649–659, 2018.

[14] A. Arora, Y. Yao, B. Mobasher, and N. Neithalath, “Fundamental insights into the compressive and flexural response of binder-and aggregate-optimized ultra-high performance concrete (UHPC),” *Cem. Concr. Compos.*, vol. 98, pp. 1–13, 2019.

[15] M. S. Meddah, S. Zitouni, and S. Belâabes, “Effect of content and particle size distribution of coarse aggregate on the compressive strength of concrete,” *Constr. Build. Mater.*, vol. 24, no. 4, pp. 505–512, 2010, doi: https://doi.org/10.1016/j.conbuildmat.2009.10.009.

[16] M. Alkaysi and S. El-Tawil, "Effects of variations in the mix constituents of ultra high performance concrete (UHPC) on cost and performance," *Mater. Struct.*, vol. 49, no. 10, pp. 4185–4200, 2016, doi: https://doi.org/10.1617/s11527-015-0780-6.
[17] Z. B. Haber and B. A. Graybeal, "Experimental Evaluation of Prefabricated Deck Panel Connections," 2015.
[18] M. Berry, "Feasibility of Non-Proprietary Ultra-High Performance Concrete (UHPC) for Use in Highway Bridges in Montana: Phase II Field Application," 2018, [Online]. Available: https://scholarworks.montana.edu/xmlui/handle/1/15911
[19] S. El-Tawil, M. Alkaysi, A. E. Naaman, W. Hansen, and Z. Liu, "Development, Characterization and Applications of a Non Proprietary Ultra High Performance Concrete for Highway Bridges," Michigan Dept. of Transportation, 2016.
[20] J. S. Lawler, M. K. Tadros, M. Lampton, and E. N. Wagner, "Development of Non-Proprietary UHPC for Florida Precast Applications," 2019, vol. 2, no. 1. doi: https://doi.org/10.21838/uhpc.9689.
[21] M. A. Mosaberpanah and O. Eren, "Effect of quartz powder, quartz sand and water curing regimes on mechanical properties of UHPC using response surface modelling," *Adv. Concr. Constr.*, vol. 5, no. 5, p. 481, 2017.
[22] A. Neville and an O. M. C. Safari, *Properties of Concrete, Fifth Edition*. 2012. Accessed: Feb. 22, 2021. [Online]. Available: https://www.safaribooksonline.com/complete/auth0oauth2/&state=/library/view//9780273786337/?ar
[23] S. El-Tawil, Y.-S. Tai, J. A. Belcher II, and D. Rogers, "Open-Recipe Ultra-High-Performance Concrete," *Formwork*, p. 33, 2020.
[24] T. Looney, A. McDaniel, J. Volz, and R. Floyd, "Development and characterization of ultra-high performance concrete with slag cement for use as bridge joint material," *Development*, vol. 1, no. 02, 2019.
[25] M. Berry, R. Snidarich, and C. Wood, "Development of Non-Proprietary Ultra-High Performance Concrete," Montana Dept. of Transportation Research Programs, 2017.
[26] A. Tafraoui, G. Escadeillas, and T. Vidal, "Durability of the ultra high performances concrete containing metakaolin," *Constr. Build. Mater.*, vol. 112, pp. 980–987, 2016.
[27] A. Tafraoui, G. Escadeillas, S. Lebaili, and T. Vidal, "Metakaolin in the formulation of UHPC," *Constr. Build. Mater.*, vol. 23, no. 2, pp. 669–674, 2009.
[28] E. Shahrokhinasab, F. D. Chitty, M. Vahedi, and S. Zolfagharysaravi, "Improvement of Concrete Characterization Using Nanosilica," *Comput. Eng. Phys. Model.*, vol. 4, no. 2, pp. 39–52, 2021.
[29] A. Nasution, I. Imran, and M. Abdullah, "Improvement of concrete durability by nanomaterials," *Procedia Eng.*, vol. 125, pp. 608–612, 2015.
[30] A. Ehsani, M. Nili, and K. Shaabani, "Effect of nanosilica on the compressive strength development and water absorption properties of cement paste and concrete containing Fly Ash," *KSCE J. Civ. Eng.*, vol. 21, no. 5, pp. 1854–1865, 2017.
[31] "Ductal® | Innovative UHPC Solution," *Ductal*®, Jul. 27, 2015. https://www.ductal.com/en (accessed Feb. 25, 2021).
[32] L. Yang, C. Shi, and Z. Wu, "Mitigation techniques for autogenous shrinkage of ultra-high-performance concrete–A review," *Compos. Part B Eng.*, vol. 178, p. 107456, 2019.

[33] K. Liu *et al.*, "Mechanisms of autogenous shrinkage for Ultra-High Performance Concrete (UHPC) prepared with pre-wet porous fine aggregate (PFA)," *J. Build. Eng.*, vol. 54, p. 104622, 2022.
[34] A. J. Giesler, S. B. Applegate, and B. D. Weldon, "Implementing nonproprietary, ultra-high-performance concrete in a precasting plant," *PCI J.*, vol. 61, no. 6, pp. 68–80, 2016, doi: https://doi.org/10.15554/pcij61.6-03.
[35] B. A. Graybeal, "Development of Non-Proprietary Ultra-High-Performance Concrete for Use in the Highway Bridge Sector: TechBrief," United States. Federal Highway Administration, 2013.
[36] A. M. Matos, S. Nunes, C. Costa, and J. L. Barroso-Aguiar, "Characterization of non-proprietary UHPC for use in rehabilitation/strengthening applications," in *Rheology and Processing of Construction Materials*, Springer, 2019, pp. 552–559. doi: https://doi.org/10.1007/978-3-030-22566-7_64.
[37] R. Karim, M. Najimi, and B. Shafei, "Assessment of transport properties, volume stability, and frost resistance of non-proprietary ultra-high performance concrete," *Constr. Build. Mater.*, vol. 227, p. 117031, 2019, doi: https://doi.org/10.1016/j.conbuildmat.2019.117031.
[38] Y. Ohama, K. Demura, H. Nagao, and T. Ogi, "Adhesion of polymer-modified mortars to ordinary cement mortar by different test methods," in *Adhesion between polymers and concrete/Adhésion entre polymères et béton*, Springer, 1986, pp. 719–729.
[39] A. Abu-Tair, S. Rigden, and E. Burley, "Testing the bond between repair materials and concrete substrate," *Mater. J.*, vol. 93, no. 6, pp. 553–558, 1996.
[40] J. Wall, N. Shrive, and B. Gamble, "Testing of bond between fresh and hardened concrete," in *Adhesion between polymers and concrete/Adhésion entre polymères et béton*, Springer, 1986, pp. 335–344.
[41] M. Kunieda, N. Kurihara, Y. Uchida, and K. Rokugo, "Application of tension softening diagrams to evaluation of bond properties at concrete interfaces," *Eng. Fract. Mech.*, vol. 65, no. 2–3, pp. 299–315, 2000.
[42] T. Kamada and V. C. Li, "The effects of surface preparation on the fracture behavior of ECC/concrete repair system," *Cem. Concr. Compos.*, vol. 22, no. 6, pp. 423–431, 2000.
[43] K. H. Khayat and M. Valipour, "Design of Ultra High performance Concrete as an Overlay in Pavements and Bridge Decks," Aug. 2014.
[44] C. Zanotti and N. Randl, "Are concrete-concrete bond tests comparable?," *Cem. Concr. Compos.*, vol. 99, pp. 80–88, 2019.
[45] A. A. Semendary, W. Hamid, I. Khoury, E. P. Steinberg, and K. K. Walsh, "Experimental Investigation of Direct Tension Bond Performance of High-Strength Concrete and Ultrahigh-Performance Concrete Connections," *J. Mater. Civ. Eng.*, vol. 31, no. 9, pp. 1–13, 2019, doi: https://doi.org/10.1061/(ASCE)MT.1943-5533.0002800.
[46] Đ. Čairović *et al.*, "Suitability of different tests for characterization of the dimpled concrete-to-concrete interface," *Struct. Concr.*, vol. 22, no. 2, pp. 757–774, 2021.
[47] E. Julio, F. Branco, and V. Silva, "Concrete to Concrete Bond Strength. Infleunce of the Roughness of the Substrate Surface," *Constr. Build. Mater.*, vol. 18, no. 9, p. 675, 2004.
[48] A. Momayez, M. Ehsani, A. Ramezanianpour, and H. Rajaie, "Comparison of Methods for Evaluating Bond Strength Between Concrete Substrate and Repair Materials," *Cem. Concr. Res.*, vol. 35, p. 748, 2005.
[49] M. A. Carbonell Muñoz, D. K. Harris, T. M. Ahlborn, and D. C. Froster, "Bond Performance between Ultra-High Performance Concrete and Normal-Strength Concrete," *J.*

Mater. Civ. Eng., vol. 26, no. 8, pp. 1–9, 2014, doi: http://dx.doi.org/10.1061/(ASCE)MT.1943-5533.0000890.
[50] B. Graybeal, “Bond of Field-Cast Grouts to Precast Concrete Elements,” Federal Highway Administration (FHWA), Tech Note FHWA-HRT-16-081, Jan. 2017.
[51] D. K. Harris, M. A. C. Muñoz, A. Gheitasi, T. M. Ahlborn, and S. V. Rush, “The challenges related to interface bond characterization of ultra-high-performance concrete with implications for bridge rehabilitation practices,” *Adv. Civ. Eng. Mater.*, vol. 4, no. 2, pp. 75–101, 2014.
[52] P. Santos, E. Julio, and V. Silva, “Correlation Between Concrete to Concrete Bond Strength and the Roughness of the Substrate Surface,” *Constr. Build. Mater.*, vol. 21, no. 8, p. 1688, 2007.
[53] A. A. Semendary and D. Svecova, “Interfacial parameters for bridge connections at high-strength concrete–ultrahigh-performance concrete interface,” *J. Mater. Civ. Eng.*, vol. 32, no. 4, p. 04020060, 2020.
[54] Z. B. Haber, J. F. Munoz, I. D. la Varga, and B. A. Graybeal, “Bond characterization of UHPC overlays for concrete bridge decks: Laboratory and field testing,” *Constr. Build. Mater.*, vol. 190, pp. 1056–1068, 2018, doi: https://doi.org/10.1016/j.conbuildmat.2018.09.167.
[55] A. D. Espeche and J. León, “Estimation of bond strength envelopes for old-to-new concrete interfaces based on a cylinder splitting test,” *Constr. Build. Mater.*, vol. 25, no. 3, pp. 1222–1235, 2011.
[56] B. A. Tayeh, B. H. A. Bakar, M. A. M. Johari, and Y. L. Voo, “Mechanical and permeability properties of the interface between normal concrete substrate and ultra high performance fiber concrete overlay,” *Constr. Build. Mater.*, vol. 36, pp. 538–548, 2012, doi: http://dx.doi.org/10.1016/j.conbuildmat.2012.06.013.
[57] R. Saldanha, E. Júlio, D. Dias-da-Costa, and P. Santos, “A modified slant shear test designed to enforce adhesive failure,” *Constr. Build. Mater.*, vol. 41, pp. 673–680, 2013.
[58] C. Zanotti, N. Banthia, and G. Plizzari, “A study of some factors affecting bond in cementitious fiber reinforced repairs,” *Cem. Concr. Res.*, vol. 63, pp. 117–126, 2014.
[59] R. Bass, R. Carrasquillo, and J. Jirsa, “Shear Transfer Across New and Existing Concrete Interfaces,” *ACI J.*, vol. 86, no. 4, p. 383, 1989.
[60] D. Figueira, C. Sousa, R. Calcada, and A. NEves, “Push-Off Tests in the Study of Cyclic Behavior of Interfaces Between Concrete Cast at Different Times,” *J. Struct. Eng.*, vol. 142, no. 1, 2016.
[61] J. Frenay, “Shear Transfer Across a Single Crack In Reinforced Concrete Under Sustained Loading - Part I. Experiments,” 1985.
[62] N. Hanson, “Precast-Prestressed Concrete Bridges 2. Horizontal Shear Connections,” *PCA*, vol. 2, no. 2, p. 38, 1960.
[63] J. Hofbeck, O. Ibrahim, and A. Mattock, “Shear Transfer in Reinforced Concrete,” *ACI*, vol. 66, no. 2, p. 119, 1969.
[64] L. Kahn and A. Mitchell, “Shear Friction Tests with High-Strength Concrete,” *ACI Struct. J.*, vol. 99, no. 1, p. 98, 2002.
[65] A. Mattock and N. Hawkins, “Shear Transfer in Reinforced Concrete - Recent Research,” *PCI J.*, vol. 17, no. 2, p. 55, 1972.
[66] A. Mattock, W. Li, and T. Wang, “Shear transfer in lightweight reinforced concrete,” *PCI J.*, vol. 21, no. 1, p. 20, 1976.

[67] J. Myers, E. Sells, and J. Volz, “Aggregate Interlock Push-Off Test Results of Self-Consolodating Concrete (Scc) For Use in Infrastructure Elements,” presented at the New Developments in Structural Engineering and Construction, 2013.
[68] M. Mohamad, I. Ibrahim, R. Abdullah, A. Rahman, A. Kueh, and J. Usman, “Friction and Cohesion Coefficients of Composite Concrete to Concrete Bond,” *Cem. Concr. Compos.*, vol. 56, p. 1, 2015.
[69] A. Pruijssers and G. Lung, “Shear Transfer Across a Crack in Concrete Subjected to Repeated Loading,” 1985.
[70] J. Walraven and H. ReinHardt, “Theory and Experiments on the Mechanical Behaviour of Cracks in Plain and Reinforced Concrete Subjected to Shear Loading,” *Heron*, vol. 26, 1981.
[71] J. Walraven and J. Stroband, “Shear Friction in High-Strength Concrete,” *Spec. Publ.*, vol. 149, p. 311, 1994.
[72] J. Xu, C. Wu, Z.-X. Li, and C.-T. Ng, “Numerical Analysis of Shear Transfer Across an Initially Uncrack Reinforced Concrete Member,” *Eng. Struct.*, vol. 102, p. 296, 2015.
[73] T. E. Banta, “Horizontal Shear Transfer between Ultra-High Performance Concrete and Lightweight Concrete,” Virginia Polytechnic Institute and State University, Thesis, Feb. 2005.
[74] A. Long and A. Murray, “The ‘Pull-Off’ Partially Destructive Test for Concrete,” *ACI*, p. 327, 1984.
[75] C. Williams, J. Massey, O. Bayrak, and J. Jirsa, “Investigation of Interface Shear Transfer Using Push-Through Tests”.
[76] Y. Zhang, C. Zhang, Y. Zhu, J. Cao, and X. Shao, “An experimental study: various influence factors affecting interfacial shear performance of UHPC-NSC,” *Constr. Build. Mater.*, vol. 236, pp. 1–15, 2020, doi: https://doi.org/10.1016/j.conbuildmat.2019.117480.
[77] M. Farzad, M. Shafieifar, and A. Azizinamini, “Experimental and numerical study on bond strength between conventional concrete and Ultra High-Performance Concrete (UHPC),” *Eng. Struct.*, vol. 186, pp. 297–305, 2019, doi: https://doi.org/10.1016/j.engstruct.2019.02.030.
[78] A. Valikhani, A. J. Jahromi, I. M. Mantawy, and A. Azizinamini, “Numerical Modelling of Concrete-to-UHPC Bond Strength,” *Materials*, vol. 13, pp. 1–16, 2020, doi: http://dx.doi.org/10.3390/ma13061379.
[79] M. E. Mohamad and I. S. Ibrahim, “Interface shear strength of concrete-to-concrete bond with and without projecting steel reinforcement,” *J. Teknol.*, vol. 75, no. 1, 2015.
[80] Đ. Čairović, F. Girgle, V. Kostiha, J. Kadlec, and P. Stepanek, “Comparison and Review of Concrete-to-Concrete Interface Shear Resistance According to Major Design Codes,” 2016, vol. 249, pp. 166–172.
[81] M. Naderi, “New twist-off method for the evaluation of in-situ strength of concrete,” *J. Test. Eval.*, vol. 35, no. 6, pp. 602–608, 2007.
[82] J. Silfwerbrand, “Shear bond strength in repaired concrete structures,” *Mater. Struct.*, vol. 36, no. 6, pp. 419–424, 2003.
[83] C. Zanotti, N. Banthia, and G. Plizzari, “A study of some factors affecting bond in cementitious fiber reinforced repairs,” *Cem. Concr. Res.*, vol. 63, pp. 117–126, 2014.
[84] S. Aaleti and S. Sritharan, “Quantifying Bonding Characteristics between UHPC and Normal-Strength Concrete for Bridge Deck Application,” *J. Bridge Eng.*, vol. 24, no. 6, pp. 1–13, 2019, doi: https://doi.org/10.1061/(ASCE)BE.1943-5592.0001404.

[85] R. Loov and A. Patnaik, “Horizontal Shear Strength of Composite Concrete Beams With a Rough Interface,” *PCI J.*, p. 48, 1994.
[86] P. W. Birkeland and H. W. Birkeland, “Connections in precast concrete construction,” 1966, vol. 63, no. 3, pp. 345–368.
[87] American Concrete Institute, *Building Code Requirements for Structural Concrete (ACI 318-14): Commentary on Building Code Requirements for Structural Concrete (ACI 318R-14): an ACI Report*. American Concrete Institute. ACI, 2014.
[88] American Association of State Highway and Transportation Officials (AASHTO), “AASHTO LRFD Bridge Design Specification, Customary U.S. Units, 9th Edition,” Washington, D. C., 2020.
[89] A. H. Mattock, “Shear friction and high-strength concrete,” *Struct. J.*, vol. 98, no. 1, pp. 50–59, 2001.
[90] A. Mattock, W. Li, and T. Wang, “Shear transfer in lightweight reinforced concrete,” *PCI J.*, vol. 21, no. 1, p. 20, 1976.
[91] T. E. Banta, “Horizontal shear transfer between ultra high performance concrete and lightweight concrete,” 2005.
[92] C. K. Crane, *Shear and shear friction of ultra-high performance concrete bridge girders*. Georgia Institute of Technology, 2010.
[93] A. Valikhani, A. J. Jahromi, I. M. Mantawy, and A. Azizinamini, “Effect of mechanical connectors on interface shear strength between concrete substrates and UHPC: Experimental and numerical studies and proposed design equation,” *Constr. Build. Mater.*, vol. 267, p. 120587, 2021.
[94] Y.-J. Kim, W.-J. Chin, and S.-J. Jeon, “Interface shear strength at joints of ultra-high performance concrete structures,” *Int. J. Concr. Struct. Mater.*, vol. 12, no. 1, pp. 1–14, 2018.
[95] A. Valikhani, A. J. Jahromi, I. M. Mantawy, and A. Azizinamini, “Effect of mechanical connectors on interface shear strength between concrete substrates and UHPC: Experimental and numerical studies and proposed design equation,” *Constr. Build. Mater.*, vol. 267, pp. 1–17, 2021, doi: https://doi.org/10.1016/j.conbuildmat.2020.120587.
[96] S. Austin, P. Robins, and Y. Pan, “Shear bond testing of concrete repairs,” *Cem. Concr. Res.*, vol. 29, 1999.
[97] C. K. Crane, “Shear and Shear Friction of Ultra-High Performance Concrete Bridge Girders,” Georgia Institute of Technology, Dissertation, Aug. 2010.
[98] C. Zanotti and N. Randl, “Are concrete-concrete bond tests comparable?,” *Cem. Concr. Compos.*, vol. 99, pp. 80–88, 2019.
[99] A. A. Semendary and D. Svecova, “Bond Characterization and Interfacial Coefficients at Precast UHPC and Cast-in-Place UHPC Interface,” *J. Mater. Civ. Eng.*, vol. 33, no. 7, pp. 1–20, 2021, doi: https://doi.org/10.1061/(ASCE)MT.1943-5533.0003755.
[100] B. Graybeal, “Ultra-High Performance Concrete for Bridge Deck Overlays,” Federal Highway Administration (FHWA), Tech Note FHWA-HRT-17-097, Feb. 2018.
[101] A. Valikhani, A. J. Jahromi, I. M. Mantawy, and A. Azizinamini, “Experimental evaluation of concrete-to-UHPC bond strength with correlation to surface roughness for repair application,” *Constr. Build. Mater.*, vol. 238, pp. 1–12, 2020, doi: https://doi.org/10.1016/j.conbuildmat.2019.117753.

[102] American Association of State Highway and Transportation Officials (AASHTO), "AASHTO LRFD Bridge Design Specification, Customary U.S. Units, 3rd Edition," Washington, D. C., 2004.
[103] American Society for Testing and Materials (ASTM), "C1245/C1245M - Standard Test Method for Determining Relative Bond Strength Between Hardened Roller Compacted Concrete Lifts (Point Load Test)," p. 8, 2012.
[104] American Association of State Highway and Transportation Officials (AASHTO), "AASHTO LRFD Bridge Design Specification, Customary U.S. Units, 8th Edition," Washington, D. C., Sep. 2017.
[105] F. Chitty, C. Freeman, and D. Garber, "Joint design optimization for accelerated construction of slab beam bridges," *J. Bridge Eng.*, vol. 25, no. 7, p. 04020029, 2020.
[106] Z. Fang, H. Jiang, J. Xiao, X. Dong, and T. Shao, "Shear performance of UHPC-filled pocket connection between precast UHPC girders and full-depth precast concrete slabs," *Structures*, vol. 29, pp. 328–338, 2021, doi: https://doi.org/10.1016/j.istruc.2020.11.038.
[107] H.-O. Jang, H.-S. Lee, K. Cho, and J. Kim, "Experimental study on shear performance of plain construction joints integrated with ultra-high performance concrete (UHPC)," *Constr. Build. Mater.*, vol. 152, pp. 16–23, 2017, doi: http://dx.doi.org/10.1016/j.conbuildmat.2017.06.156.
[108] Y.-J. Kim, W.-J. Chin, and S.-J. Jeon, "Interface Shear Strength at Joints of Ultra-High Performance Concrete Structures," *Int. J. Concr. Struct. Mater.*, vol. 12, no. 59, pp. 1–14, 2018, doi: https://doi.org/10.1186/s40069-018-0298-8.
[109] C. Li, Z. Feng, L. Ke, R. Pan, and J. Nie, "Experimental Study on Shear Performance of Cast-In-Place Ultra-High Performance Concrete Structures," *Materials*, vol. 12, pp. 1–16, 2019, doi: http://dx.doi.org/10.3390/ma12193254.
[110] J. Qi, J. Wang, Z. Zhang, W. Li, and Y. Hu, "Flexural behavior of an innovative dovetail ultra-high performance concrete joint using steel wire mesh interface treatment in composite bridges," *Adv. Struct. Eng.*, vol. 23, no. 6, pp. 1142–1153, 2020, doi: https://doi.org/10.1177/1369433219891531.
[111] American Society for Testing and Materials (ASTM), "C1404/C1404M - Standard Test Method for Bond Strength of Adhesive Systems Used With Concrete as Measured by Direct Tension," 2003.
[112] A. B. Sturm, P. Visintin, K. Farries, and D. J. Oehlers, "New Testing Approach for Extracting the Shear Friction Material Properties of Ultra-High-Performance Fiber-Reinforced Concrete," *J. Mater. Civ. Eng.*, vol. 30, no. 10, pp. 1–13, 2018, doi: https://doi.org/10.1061/(ASCE)MT.1943-5533.0002427.
[113] S. Muzenski, Z. B. Haber, and B. Graybeal, "Interface Shear of Ultra-High-Performance Concrete," *ACI Struct. J.*, vol. 119, no. 1, pp. 267–280, Jan. 2022.
[114] S. Muzenski, "Interface Shear Behavior of Ultra-High Performance Concrete," presented at the International Accelerated Bridge Construction Conference, Virtual, Dec. 08, 2021.
[115] International Concrete Repair Institute, "Guide Specifications for Structural Concrete Repair." 2016. [Online]. Available: http://www.icri.org
[116] P. M. D. Santos and E. N. B. S. Júlio, "Comparison of Methods for Texture Assessment of Concrete Surfaces.," *ACI Mater. J.*, vol. 107, no. 5, 2010.
[117] P. M. Santos and E. N. Júlio, "A state-of-the-art review on roughness quantification methods for concrete surfaces," *Constr. Build. Mater.*, vol. 38, pp. 912–923, 2013.

[118] American Society for Testing and Materials (ASTM), "E965-15 - Standard Test Method for Measuring Pavement Macrotexture Depth Using a Volumetric Technique," 2019.
[119] P. M. Santos, E. N. Julio, and V. D. Silva, "Correlation between concrete-to-concrete bond strength and the roughness of the substrate surface," *Constr. Build. Mater.*, vol. 21, no. 8, pp. 1688–1695, 2007.
[120] A. Valikhani, A. Jaberi Jahromi, S. Pouyanfar, I. M. Mantawy, and A. Azizinamini, "Machine learning and image processing approaches for estimating concrete surface roughness using basic cameras," *Comput. Civ. Infrastruct. Eng.*, vol. 36, no. 2, pp. 213–226, 2021.
[121] K. Lau, A. A. Sagüés, and R. G. Powers, "Corrosion of epoxy-coated rebar in marine bridges—Part 2: Corrosion in cracked concrete," *Corrosion*, vol. 66, no. 6, pp. 065002-065002–16, 2010.
[122] M. Farzad, D. Garber, A. Azizinamini, and K. Lau, "Corrosion macrocell development in reinforced concrete with repair UHPC," presented at the CORROSION 2018, 2018.
[123] X. Huang and S. Kaewunruen, "Self-healing concrete," in *New Materials in Civil Engineering*, Elsevier, 2020, pp. 825–856.
[124] W. Shin and D.-Y. Yoo, "Influence of steel fibers corroded through multiple microcracks on the tensile behavior of ultra-high-performance concrete," *Constr. Build. Mater.*, vol. 259, p. 120428, 2020.
[125] D.-Y. Yoo, W. Shin, and B. Chun, "Corrosion effect on tensile behavior of ultra-high-performance concrete reinforced with straight steel fibers," *Cem. Concr. Compos.*, vol. 109, p. 103566, 2020.
[126] V. Ngala, C. Page, and M. Page, "Corrosion inhibitor systems for remedial treatment of reinforced concrete. Part 1: calcium nitrite," *Corros. Sci.*, vol. 44, no. 9, pp. 2073–2087, 2002.
[127] K.-Y. Ann, H. Jung, H. Kim, S. Kim, and H. Y. Moon, "Effect of calcium nitrite-based corrosion inhibitor in preventing corrosion of embedded steel in concrete," *Cem. Concr. Res.*, vol. 36, no. 3, pp. 530–535, 2006.
[128] gcp, "DCI® Corrosion Inhibitor." 2022. [Online]. Available: https://gcpat.com/en/solutions/products/dci-corrosion-inhibitor/dci-s
[129] "James Bond Test MK III." https://www.ndtjames.com/James_Bond_Tester_p/p-c-7300.htm (accessed Jun. 28, 2022)
[130] A. Momayez, M. Ehsani, A. Ramezanianpour, and H. Rajaie, "Comparison of methods for evaluating bond strength between concrete substrate and repair materials," *Cem. Concr. Res.*, vol. 35, no. 4, pp. 748–757, 2005.
[131] American Society for Testing and Materials (ASTM), "C78/C78M-21 - Standard Test Method for Flexure Strength of Concrete (Using Simple Beam with Third-Point Loading)," 2021.
[132] "Master Builders Solutions Construction Products," *North America*. https://www.master-builders-solutions.com/en-us (accessed Jun. 28, 2022).
[133] S. Aaleti, B. Petersen, and S. Sritharan, "Design guide for precast UHPC waffle deck panel system, including connections," 2013.
[134] M. A. Carbonell Muñoz, D. K. Harris, T. M. Ahlborn, and D. C. Froster, "Bond performance between ultrahigh-performance concrete and normal-strength concrete," *J. Mater. Civ. Eng.*, vol. 26, no. 8, p. 04014031, 2013.

[135] A. Anderson, “Composite designs in precast and cast-in-place concrete,” *Prog. Archit.*, vol. 41, no. 9, pp. 172–179, 1960.
[136] P. Wu, C. Wu, Z. Liu, and H. Hao, “Investigation of shear performance of UHPC by direct shear tests,” *Eng. Struct.*, vol. 183, pp. 780–790, 2019, doi: https://doi.org/10.1016/j.engstruct.2019.01.055.
[137] American Society for Testing and Materials (ASTM), “C39/C39M-21 - Standard Test Method forCompressive Strength of Cylindrical Concrete Specimens,” 2021.
[138] B. A. Graybeal and F. Baby, “Development of direct tension test method for ultra-high-performance fiber-reinforced concrete,” *ACI Mater. J.*, vol. 110, no. 2, p. 177, 2013.
[139] Astm, “ASTM E8/E8M-16a: Standard Test Methods for Tension Testing of Metallic Materials,” *West Conshohocken PA USA ASTM Int.*, 2016.
[140] American Society for Testing and Materials (ASTM), “C1609/C1609M - 19a - Standard Test Method for Flexural Performance of Fiber-Reinforced Concrete (Using Beam with Third-Point Loading),” 2019.
[141] American Society for Testing and Materials (ASTM), “C1583/C1583M-13 - Standard Test Method of Concrete Surfaces and the Bond Strength or Tensile Strength of Concrete Repair and Overlay Materials by Direct Tension (Pull-off Method),” 2013.
[142] D. ASTM, “7234; Standard Test Method for Pull-Off Adhesion Strength of Coatings on Concrete Using Portable Pull-Off Adhesion Testers,” *ASTM Int. West Conshohocken PA USA*, 2019.
[143] G. H. Koch, M. P. Brongers, N.G. Thompson, Y.P. Virmani, J.H. Payer, “Corrosion cost and preventive strategies in the United States” (No. FHWA-RD-01-156,, R315-01). United States. Federal Highway Administration. (2002).
[144] Tullmin and P.R. Roberge, Chapter 18: Atmospheric Corrosion, Uhlig's Corrosion Handbook, 2nd Ed., John Wiley & Sons, March 2000, pp. 305-321.
[145] N.A. Soliman, A. Tagnit-Hamou, “ Partial substitution of silica fume with fine glass powder in UHPC: Filling the micro gap”. Construction and Building Materials, 139, 374-383.(2017)
[146] D.Y. Yoo, Y.S. Jang, T. Oh, N. Banthia, “ Use of engineered steel fibers as reinforcements in ultra-high-performance concrete considering corrosion effect”. Cement and Concrete Composites, 133, 104692, (2022).
[147] L. Fan, W. Meng, L. Teng, K.H. Khayat, “Effect of steel fibers with galvanized coatings on corrosion of steel bars embedded in UHPC.” Composites Part B: Engineering, 177, 107445, (2017).
[148] D.Y. Yoo, J. Y. Gim, and B. Chun., “Effects of rust layer and corrosion degree on the pullout behavior of stel fibers from ultra-high-performance concrete”, J. Materials Research and Technology, 9(3). (2020).
[149] A. Pelesk, H. Otmačić Ćurković, “ Comparative study of volatile corrosion inhibitors in various electrochemical setups.” Coatings, 15(1), 94, (2025)
[150] B. Miksic, R.H. Miller, “ Fundamental principles of corrosion protection with vapor phase inhibitors.” Corrosion Inhibitors, Fifth., 1, 217-236, (1980).
[151] K. Lau, S. Permeh, I. Lasa, “Corrosion of prestress and posttension reinforced concrete bridges.” In Corrosion of steel in concrete structures (pp. 81-105). Woodhead Publishing. (2023)

[152] K. Lau, S. Permeh, " Assessment of durability and zinc activity of zinc-rich primer coatings by electrochemical noise technique." Progress in Organic Coatings, 167, p.106840, (2022).
[153] S. Permeh, K. Lau, M.E. Boan, B. Tansel, & M. Duncan, "Cathodic polarization behavior of steel with different marine fouling morphologies on submerged bridge elements with cathodic protection." Journal of Materials in Civil Engineering, 32(7), 04020184, (2020).
[154] S. Permeh, K. Lau, "Corrosion of galvanized steel in alkaline solution associated with sulfate and chloride ions." Construction and Building Materials, 392, p.131889.(2023)
[155] X. Wang, J. Ren, Z. Li, Y. Li, " Research progress of vapor phase corrosion inhibitors in marine environment." Environmental Science and Pollution Research, 29(59), 88432-88439.(2022)
[156] B. Bavarian, Y. Ikder, B. Samimi, L. Reiner, B. Miksic, " Comparison of the corrosion protection effectiveness of vapor corrosion inhibitors and dry air system." In NACE CORROSION (pp. NACE-2015). NACE.
[157] B. Boyle, I. Solutions, " A look at developments in vapor phase corrosion inhibitors. Metal finishing," 102(5), 37-41, (2024).
[158] S. Permeh, R. Armas, K. Lau., "Effectiveness of Vapor-Phase Inhibitor to Mitigate Corrosion of Highway Bridge Steel Elements Exposed to Aggressive Environments." In CONFERENCE 2026 (pp. 1-13). Association for Materials Protection and Performance. (2026, March).